Titre: Title:	Planar Functional Leaky-Wave Antenna Engineering : Concepts, Structures, and Techniques for Radar Sensing Systems
Auteur: Author:	Dongze Zheng
Date:	2021
Type:	Mémoire ou thèse / Dissertation or Thesis
Référence: Citation:	Zheng, D. (2021). Planar Functional Leaky-Wave Antenna Engineering : Concepts, Structures, and Techniques for Radar Sensing Systems [Thèse de doctorat, Polytechnique Montréal]. PolyPublie. https://publications.polymtl.ca/9905/

POLYTECHNIQUE MONTRÉAL

affiliée à l'Université de Montréal

Planar functional leaky-wave antenna engineering : concepts, structures, and techniques for radar sensing systems

DONGZE ZHENG

Département de génie électrique

Thèse présentée en vue de l'obtention du diplôme de *Philosophiæ Doctor*

Génie électrique

Décembre 2021

POLYTECHNIQUE MONTRÉAL

affiliée à l'Université de Montréal

Cette thèse intitulée:

Planar functional leaky-wave antenna engineering : concepts, structures, and techniques for radar sensing systems

présentée par **Dongze ZHENG**

en vue de l'obtention du diplôme de *Philosophiæ Doctor*

a été dûment acceptée par le jury d'examen constitué de :

Mohammad S. SHARAWI, présidente
Ke WU, membre et directeur de recherche
Halim BOUTAYEB, membre
Yang HAO, membre externe

DEDICATION

To my beloved parents and sister

To the memory of my grandparents

ACKNOWLEDGEMENTS

I would like to express my sincere gratitude to my supervisor Prof. Ke Wu, for giving me this precious opportunity to join his research group at Poly-Grames Research Center, for providing me with valuable guidance and help during my Ph. D. studies, and for exemplifying me about what a great scholar and scientist should be. Prof. Wu lets me know that doing research can be an attitude of life and exploring the unknown can be the ultimate goal of life. Here, I would like to quote a well-known saying that widely spreads through the river of long history of China— "A teacher for a day is a father for life", to one more express my respect and appreciation to Prof. Wu.

I would like to thank Prof. Mohammad S. Sharawi, Prof. Halim Boutayeb, and Prof. Yang Hao for serving as jury members of my Ph. D. defense.

I also would like to express my thanks to all the technicians at Poly-Grames Research Center, especially Mr. Traian Antonescu, Mr. Maxime Thibault, and Mr. Jules Gauthier, for their continuous efforts on fabrications and measurements through my Ph. D. studies.

Pursuing a Ph. D. degree is not an easy task. During this process, I have also received numerous helps and supports from my colleagues and friends. I still clearly remember that the first day when I arrived at Montreal 4 years ago and Mr. Wentao Lin invited me to his home to have the dinner. I still clearly remember that Dr. Desong Wang and his wife often invited me to their home to celebrate some festivals within the past 4 years. I also cannot forget Dr. Yue-Long Lyu who gave me a big help in the understanding and design of LWAs as well as in the paper written, and Mr. Ben You who usually acted as a life mentor and with whom I often discussed about what a normal life should be. It seems that I cannot mention all of my colleagues and friends and narrate our related unforgettable stories, but I still would like to thank Dr. Xiaoqiang Gu, Dr. Chunmei Liu, Dr. Jun Xu, Dr. Xiaoyi Wang, Dr. Yifan Yin, Dr. Kang Zhou, Dr. Qingtao Chen, Mr. MuhibUr Rahman, Dr. Yang Cao, and Dr. Peiyong Qiu for their company during my Ph. D. studies.

I am extremely grateful to my parents and elder sister for their unconditional love, supports, and encouragements. Special appreciation should be dedicated to my ex-girlfriend whose name once appeared in my master's thesis 4 years ago while still being mentioned in this Ph. D. thesis. I would like to give my heartfelt gratitude to her for her several-year company in my life although we all got lost eventually in the world of each other.

RÉSUMÉ

Les antennes à ondes de fuite (LWA) sont des structures guidées particulières caractérisées par la propagation des ondes et le rayonnement. Les LWAs ont attiré beaucoup d'attention depuis ses premières créations dans les années 1940 grâce aux nombreuses caractéristiques attrayantes telles qu'une directivité élevée, un faisceau directif étroit, un mécanisme d'alimentation simple, une configuration simple et une capacité particulière de balayage de faisceau fréquentiel (ou cartographie espace-fréquence). En plus, grâce à ses capacités de balayage spatial en fréquence, les LWAs ont été exploités par la partie académique ainsi que la partie industrielle dans plusieurs applications, notamment les applications de radar. De nos jours, les LWAs présentant multiples fonctionnalités/caractéristiques électriques ainsi que les applications de LWAs au niveau de systèmes sont à la mode. Dans ce contexte, cette thèse propose plusieurs nouveaux techniques et concepts pour développer des LWAs avec des fonctionnalités/comportements électriques élégants. En outre, cette thèse présente également une solution frontale de LWA à large bande pour des systèmes radar.

Concernant les fonctionnalités/comportements électriques des LWAs, chapitre 3 est dédié à une LWA en SIW basé sur le mode TE_{20} à fente longitudinale qui est caractérisée par les faibles niveaux de lobe secondaire et de polarisation croisée. Dans ce travail, une paire de longues fentes sinueuses sont gravées symétriquement sur le bord supérieur d'un SIW en mode TE_{20}. Des formes sinueuses visent à réduire le niveau de lobe secondaire, tandis que la symétrie impaire du mode TE_{20} et les longues fentes symétriques contribuent à diminuer la polarisation croisée. Dans le chapitre 4, les effets de charge des rayonnements discontinuités (RDs) ont été explorés pour augmenter la dispersion ou le taux de balayage des LWAs. Basé sur cela, une LWA à fentes transversales quasi-uniforme en SIW avec la capabilité de balayage rapide et son réseau hexagonal ont été proposés et étudiés pour des applications à ondes millimétriques. Le mécanisme du balayage rapide est basé sur les cellules unitaires à courte période et la longue fente transversale avec une réactance inductive forte. Dans le chapitre 5, le concept de filtre passe-bande radiatif (RBPF) est proposé et étudié pour développer une classe de LWA filtrante multifonctionnel qui présente simultanément un balayage de faisceau rapide en fréquence et une caractéristique sélective en fréquence. Un BPF à bande étroite qui est délibérément rendu radiatif à l'aide de RD supplémentaires et dont la bande passante est de nature à ondes rapides est spécialement conçu pour fonctionner comme un LWA.

Basé sur ce concept, les caractéristiques de filtrage/dispersion et de rayonnement des LWAs peuvent être contrôlées indépendamment par différents modules. Dans chapitre 6, le concept de résonateur multimode (MMR) est proposé et démontré pour développer une classe de LWA ayant un rayonnement stable (une efficacité de rayonnement et un gain stables). La condition pour un rayonnement stable est dérivée, sur la base de laquelle le concept MMR est naturellement proposé comme une solution pour la stabilité de rayonnement. En plus, une classe de LWA multifonctionnels monocouches avec des caractéristiques de rayonnement et de filtrage flexibles est proposée et démontrée au chapitre 7. Les RD présentant des résonances multiples tout en possédant particulièrement une capacité de contrôle de modèle flexible sont exploités pour accomplir ces libertés de conception et multifonctionnalités des LWA. Pour un système large bande, un réseau frontal de LWA basé sur le banc de filtres (FB) est proposé au chapitre 8, et est particulièrement étudiée pour les applications de radar caractérisées par un domaine fréquence-espace cousu de fonctionnement des radars. Les détails techniques demandés de l'assemblage fréquence-espace sont présentés et la procédure de conception détaillé d'un réseau LWA basé sur FB est également développé pour faciliter la mise en place. La technique de réseau LWA basé sur FB peut être déployée dans des systèmes radar sans décalage, en tant qu'une solution complémentaire de l'antenne réseau à commande de phase. Pour conclure, les contributions et les perspectives de la thèse sont présentées dans chapitre 9 et 10.

ABSTRACT

Leaky-wave antennas (LWAs), as a special kind of guiding structures characterized by both wave guidance and wave radiation, have received much attention since the inception of the first LWA in 1940s, thanks to their many appealing features such as high directivity, narrow directive beam, easy feeding mechanism, simple configuration, and particular frequency-driven beam-scanning (or space-frequency mapping) capability. LWAs have been in the spotlight of both academics and industries since their unique frequency-scanning can be exploited for a wide variety of practical applications among which the radar sensing system is of particular importance to our practical world. The development of various kinds of LWAs featuring multifarious functionalities/electrical characteristics and the exploration of possible system-level applications using LWAs constitute such two research mainstreams in the recent development of leaky-wave R&D communities, which presents a prevailing trend in our RF/microwave realm. Under this context, this thesis proposes and investigates several novel concepts and techniques to design and decorate LWAs with elegant functionalities and electrical behaviors. Besides, this thesis also furnishes a feasible antenna front-end solution enabling LWAs to be used for wideband operation in radar sensing systems.

When it comes to the functionalities and electrical behaviors of LWAs that the thesis mainly focuses on, Chapter 3 is dedicated to a longitudinally slotted TE_{20} mode-driven SIW (substrate-integrated waveguide) LWA characterized simultaneously by low side-lobe and low cross-polarization behaviors. In this work, a pair of meandering long slots are etched symmetrically on the top broadside of a TE_{20}-mode SIW. Specially designed meandering shapes imposed on the long slots are set to realize low side-lobe properties, whereas the odd-symmetry of TE_{20} mode along with the even-symmetrically etched long slots results in an effective radiation particularly possessing low cross-polarization. In Chapter 4, loading effects of radiating discontinuities (RDs) have been explored to increase the dispersion or beam-scanning rate of LWAs, based on which a quasi-uniform transversely slotted SIW LWA featuring rapid beam-scanning and its hexagonal array have been proposed and investigated for millimeter-wave applications. The design concept or technicalities of the rapid beam-scanning property is simply based on the use of a short period of unit-cells and a long transverse slot with a sharp inductive reactance. In Chapter 5, the concept of radiative bandpass filter (RBPF) is proposed and investigated for developing a class of multifunctional filtering LWAs which exhibit simultaneous rapid frequency-dependent beam-

scanning and frequency-selective characteristics. A narrowband BPF that is deliberately made radiative using additional RDs and whose passband is fast-wave-natured is specially designed to operate as an LWA. With this concept, both filtering/dispersion and radiation tasks can be independently managed by different modules for LWAs. In Chapter 6, a scheme based on the multimode resonator (MMR) concept is proposed and demonstrated for the design and development of a class of LWAs to realize stable radiation properties (i.e., stable radiation efficiency and gain). The condition for LWAs to realize stable radiation properties is derived, based on which the MMR concept is naturally proposed as a solution for the radiation stability. Further, a class of single-layered multifunctional LWAs with flexibly engineered radiation and filtering characteristics are proposed and demonstrated in Chapter 7. RDs exhibiting multiple resonances while particularly possessing flexible model-control capability are exploited to accomplish such design freedoms and multifunctionalities of LWAs. For possible practical wideband system applications, a front-end array technique of LWAs on the basis of a filter bank (FB) concept is devised in Chapter 8 and is particularly studied for prospective radar sensing applications characterized by a stitched frequency-space domain of radar operation. Technicalities of the required frequency-space stitching are presented and a detailed design flow regarding a generalized FB-enabled LWA array is also developed to facilitate a practical implementation. The proposed FB-enabled LWA array technique may be potentially deployed in shifterless beam-scanning radar systems, as a complementary solution to the current phased array counterpart. Finally, some discussions and conclusions about the thesis's contributions while some future works that will be conducted are presented in Chapter 9 and 10 to complete this thesis work.

TABLE OF CONTENTS

LIST OF TABLES

LIST OF FIGURES

LIST OF SYMBOLS AND ABBREVIATIONS

ACPA	Aperture-Coupled Patch Antenna
ALSSP	Asymmetrically Longitudinal Shunt-Slot-Pair
AoT	Angle-of-Target
BSF	Beam-Scanning Function
CPI	Coherent Processing Interval
CPS	Coplanar Stripline
CPW	Coplanar Waveguide
CW	Continuous Wave
DSP	Digital Signal Processing
EBG	Electromagnetic Bandgap
EIRP	Effective Isotropically Radiated Power
FB	Filter Bank
FFT	Fast Fourier Transform
FMCW	Frequency-Modulated Continuous-Wave
FoV	Field of View
GCPW	Grounded Coplanar Waveguide
GD	Group Delay
GDD	Group Delay Dispersion
HIS	High Impedance Surface
IF	Intermediate Frequency
IoTs	Internet of Things
IoV	Internet of Vehicle
LFM	Linear Frequency Modulation

LWA	Leaky-Wave Antenna
MED	Magneto-Electric Dipole
MMR	Multi-Mode Resonator
NRLSP	Non-Radiative Longitudinal Slot-Pair
OCSLR	Open-Circuited Stub-Loaded-Resonator
OCUIR	Open-Circuited Uniform-Impedance-Resonator
PRS	Partially Reflective Surface
RBPF	Radiative Band-Pass Filter
RCS	Radar Cross Section
RD	Radiating Discontinuity
RF	Radio Frequency
RWG	Rectangular Waveguide
Rx	Receiving
SIW	Substrate-Integrated Waveguide
SLL	Side-Lobe Level
SLR	Stub-Loaded Resonator
SMR	Single-Mode Resonator
SSPP	Spoof Surface Plasmon Polariton
TL	Transmission Line
ToF	Time-of-Flight
TS	Transverse Slot
Tx	Transmitting
V2X	Vehicle-to-Everything

LIST OF APPENDICES

CHAPTER 1 INTRODUCTION

1.1 Background: A Historical Perspective

Radar techniques can date back to about one hundred years ago, and they have significantly burst into bloom and played their critical roles during the *Word War II*, and continued to evolve rapidly across the *Cold War* period [1][2]. Although various radar systems have been mainly developed for military and national defense purposes in the initial stages since they were invented, their influences have been expanded to civil and commercial applications and they have gradually and increasingly become an essential part of our daily life in recent decades. Representative application scenarios of radars can be found in Figure 1.1. As an electromagnetic system, the radar is used for the detection, localization, and characterization of surrounding objects such as aircrafts, ships, spacecraft, vehicles, people, and the natural environment. However, just like those human beings have to turn and move their heads or eyeballs to search, sense, and detect their ambient environment, the early-stage radars also need to rotate their antennas to scout potential targets around them. This is the so-called "mechanical beam-scanning" [as shown in Figure 1.2(a)], where normally a fixed-beam antenna (e.g., parabolic reflector antenna) is employed along with electric motors and rotors used to scan the antenna beam mechanically. Although this beam-scanning scheme is straightforward for implementation and has played a predominant role in the initial stage of radar development history, it has to tolerate obvious drawbacks such the use of bulky and heavy inertial devices (i.e., motors and rotors), slow beam-scanning/data-update rate, beam inflexibility, and short mean time between failures [1].

Generally speaking, the radar antenna beam of a typical mechanical beam-scanning radar, limited by the flexibilities of electric motors and rotors, can only be rotated in the azimuth plane, enabling this kind of radars to detect, characterize, and revolve objects with respect to their ranges, velocities, and mere azimuthal angles. Although it seems that these parametric characterizations of objects are sufficient in some scenarios such as the space-surveillance at airports, the elevation angle information of objects should be provided to precisely locate objects as well as enrich radar's functionalities. A popular and low-cost solution in the initial stage of radar developments to perform this task is the use of frequency-driven beam-scanning. To be more specific, the beam-scanning in the azimuthal plane is through the mechanical rotation of antennas, while in the

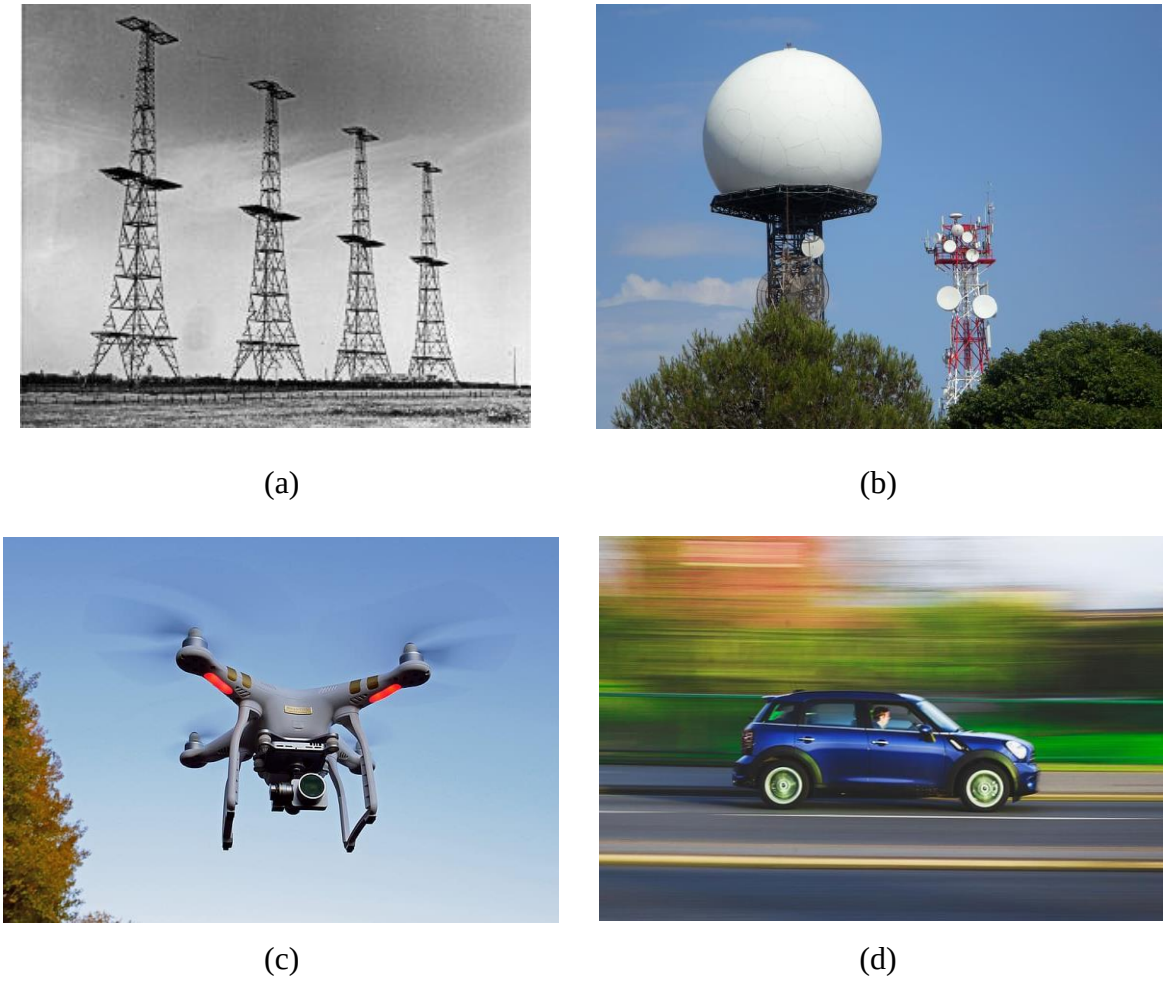

(a) (b)

(c) (d)

Figure 1.1 Selected representative radar applications, from military and civil to commercial scenarios

(a) Chain home radar [3]. (b) Weather radar [4]. (c) Drone [5]. (d) Automotive radar [6]. All of these figures belong to the public domain and/or royalty-free images

elevation plane, the antenna beam is scanned by sweeping the frequency of signal waveform. Figure 1.2(b) shows a possible configuration of the related radar antenna where a travelling-wave "snake" type waveguide section is used to feed an array of standing-wave slotted waveguide antenna. Over the decades when the phased array technique has not entered people's horizon or has not become mature or realistic, the aforementioned hybrid mechanical-frequency beam-scanning solution was proved to be the optimum one to provide four-dimensional (4-D) parametric characterizations of objects, i.e., range, velocity, azimuth angle, and elevation angle.

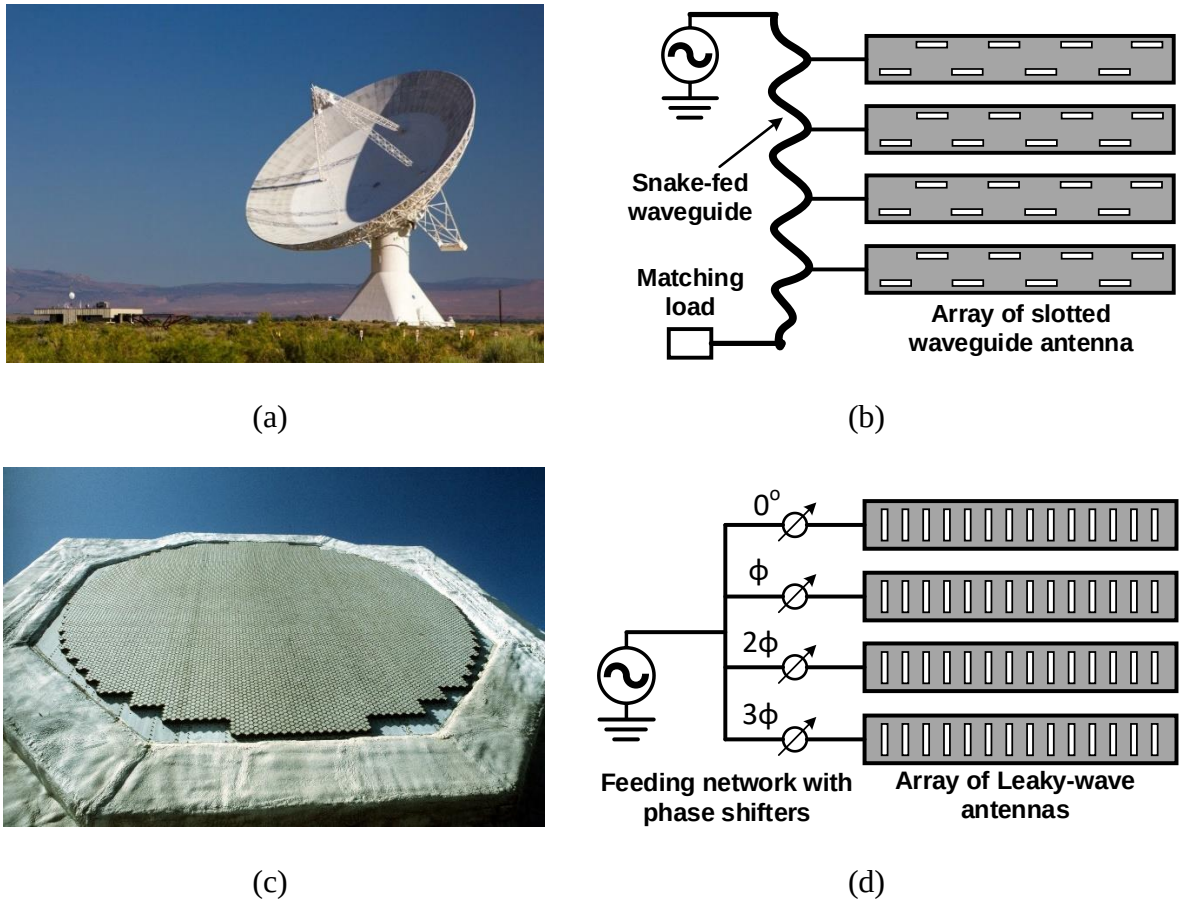

(a) (b)

(c) (d)

Figure 1.2 Typical beam-scanning schemes in the radar world

(a) Mechanical beam-scannning [7] (royalty-free image). (b) Frequency or hybrid mechanical-frequency beam-scanning [1]. (c) Phased beam-scanning [8] (royalty-free image). (d) Hybrid phase-frequency beam-scanning [9]

If there was a competition between various beam-scanning solutions in the radar world and when it comes to the most famous one in terms of electrical performances and system functionalities, the phased array technique should be unquestionably recommended as the first-level candidate, thanks to its fast beam-scanning, beam-shaping flexibility, and system multifunctionalities/robustness, etc [1][2]. Figure 1.2(c) depicts a representative example of the antenna panel of phased array radars. By changing the signal phase input to each antenna element, the radiation beam can be freely scanned and pointed to both the azimuth and elevation planes while without moving/rotating the whole antenna panel and/or sweeping the transmitting frequency. However, no matter the passive

or active phased array techniques are used, it is always true that the desirable beam-scanning indispensably depends on the use of a large number of phase shifters or true time-delay (TTD) devices or T/R modules along with complicated phase-controlling circuits. This undoubtedly imposes a significant consideration to radar designers and/or users about the cost and complexity of system construction and maintenance, which are historically predominant factors that prevent the phased array from being prevailed and popularized, especially in commercial applications. Interestingly, in order to reduce the cost of phased arrays while simultaneously keeping their beam-scanning capabilities for the whole space (i.e., the azimuth and elevation planes), a hybrid phase-frequency beam-scanning, paralleled to the preceding mechanical-frequency counterpart, was proposed as a compromised solution, as illustrated in Figure 1.2(d). In this case, the azimuth plane coverage is enabled by the phase-based scanning mechanism while the elevation plane is by the manner of frequency beam-scanning (e.g., the leaky-wave fashion, as will be described later).

The aforementioned fundamental beam-scanning schemes, namely, the mechanical-, frequency-, and phase-based ones constitute the mainstream beam-scanning solutions for most of radar systems. One or more of them can be deployed in radars, depending on specific design and development considerations such as the designated electrical performances, allocated budgets, and limited space occupations. When making a comparison among these mainstream beam-scanning schemes, it is easy to find that compared to mechanical- and phase-based schemes, the frequency-enabled beam-scanning can provide a set of distinct benefits judging from radar functionalities/performances and system cost/complexity. For example, compared to the mechanical beam-scanning, the frequency beam-scanning is apparently much faster in scanning the space without those bulky inertial devices (i.e., motors and rotators) needed; compared to the phased array techniques, a large number of expensive and lossy phase shifters or TTD devices or T/R modules together with extra controlling circuits can be left out. The crucial significance and critical value of the frequency beam-scanning can be evidently found in the history of radar development as mentioned above, where the hybrid mechanical-frequency or phase-frequency beam-scanning schemes were developed and deployed into practical military and civil uses.

With the rapid development of wireless technologies, it is unavoidable that the working frequency of wireless systems has been continuing to move up to a higher frequency such as millimeter-wave, sub-millimeter-wave, and terahertz (THz) bands. This is because the spectrum resource in the lower

frequency bands is ever-increasingly crowded, while that at high-frequencies such as THz bands is huge and unexplored. This huge spectrum resource can be properly exploited to provide desirable radar performances such as the range resolution, which is impaired and insufficient in conventional low-frequency frequency-scanning radars due to the narrow-band nature of frequency beam-scanning. However, for a high-frequency radar system with the required beam-scanning, commercial phase-shifting devices are either unavailable or extremely expensive in the foreseeable future while the full-digital radar scheme is unrealistic. That is to say, the currently popular phase-based beam-scanning solution may lose its shine in such high-frequency radar domains, while some other beam-scanning solutions may take over from it in the radar world and among which the frequency beam-scanning is a competitive candidate. Comparatively, an interesting approach that may also be potentially useful at such high frequencies is the passive multi-beam or beam-switching technique, which may deploy analog beamforming circuits and components together with a set of switches to discretely scan the antenna beam illuminating a targeted space or object [10]. This method, however, suffers from the need of complicated beamforming circuits/components and costly/lossy switches, and it can only provide a limited number of antenna beams and moderate angle resolution/accuracy. On the other hand, it is interesting to mention that in the currently prevailing 5G communication systems in which massive MIMO antenna techniques are applied, one of their distinct features is that they can digitally produce multiple antenna beams (i.e., digital beamforming) with each narrow beam pointing towards a specific object/user [2][10]. It should be noted that the digital beamforming principle in the 5G communication systems is totally the same as that in the phased array technique. In other words, the 5G massive MIMO antenna system is actually a phased array system in this regard. When considering merely the generation of multiple beams or beam-scanning in 5G communication system, the frequency-enabled beam-scanning solution seems to fit this regime well. However, the 5G communication system needs to provide a narrow directive radiation beam that should be wideband to each user, for which the narrowband-natured frequency beam-scanning solution seems unsuitable in this case. Interestingly, it is expected that in the future communication system (e.g., 6G that uses the sub-millimeter-wave or THz bands) may be well compatible with the frequency-enabled beam-scanning solution, thanks to the huge spectrum resources in this high-frequency band that make the spectrum bandwidth allocated to each spatial angle cell is sufficiently wide for high-

quality communications. Follow this thread, it is anticipated that the joint designs of communication and radar sensing, which may be deployed in the future 6G systems, can be popularized and potentially realized using the frequency-scanning scheme. Therefore, it is confident and reasonable to believe that the frequency beam-scanning solution still has its potential to be exploited in the future, just has it has been continuingly flourishing from the past to present.

1.2 Motivation and Objectives

Just as the role of eyes in our human beings, the antenna component has the similar function and status in wireless applications such as radar and communication systems. For a radar system architecture using the frequency beam-scanning, it is obvious that the radar antenna should be specially designed in the manner that its radiation beam should be scanned with frequency. In addition to this, some other good features or performances should also be embraced by the radar antenna for practical uses. For example, the radar antenna should be capable of providing good electrical performances such as high and stable gain, narrow directive beam, high radiation efficiency, low side-lobe level (SLL), low cross-polarization level, and high frequency beam-scanning rate. What's more, it would be better if the radar antenna can be equipped with other functionalities or benefits such as filtering characteristics and design freedoms/flexibilities/versatilities. Additionally, when considering possible commercial applications such as consumer electronics where the full-planar system-integration and mass production are generally required, the radar antenna should be preferably designed in a planar form and a simple geometry as well as with some other merits such as low cost and low profile. All of these desirable and stringent requirements for the antenna component in a frequency-scanning radar are well compatible with and satisfied by the elegant design of LWAs.

The LWA is a special class of wave-guiding structures in which a travelling-wave propagates while simultaneously leaking energy to the outside free-space for which they are characterized by both wave guidance and wave radiation [9][11]. LWAs have been well known for many decades thanks to their many appealing features such as high gain, narrow directive beam, and simple feeding mechanism, while the most charming feature that makes LWAs distinct from other antenna types and in the spotlight of RF/microwave communities since its inception in 1940s is their natural frequency beam-scanning. Although in the early stages of the antenna community, the class of

travelling-wave series-fed antenna arrays with a frequency-scanning beam have not been recognized as or grouped into the leaky-wave fashion, they are gradually accepted and loosely perceived as LWAs when the leaky-wave theory becomes progressively mature and prevailing. For example, the “snake” type slotted waveguide antenna featuring a frequency-scanned beam in the frequency-scanning radar, as depicted in Figure 1.2(b), can be characterized and analyzed as an LWA where the “snake” waveguide section is deliberately adopted for enhancing its equivalent dispersion characteristic (or slow-wave factor) and thus the beam-scanning rate versus frequency.

Considering the crucial significance of frequency-scanning radars in the radar world and the critical role of LWAs on frequency-scanning radars, we may reasonably remark that the exploration and development of novel leaky-wave concept, theories, and techniques to design LWAs with desirable features including stable radiation, low cross-polarization, low side-lobe, rapid beam-scanning and so on will be significant, practical, and meaningful in the present and future antenna and radar/communication communities. This is one major objective that this thesis is set to achieve. Another objective of this thesis is about how to practically and effectively deploy LWAs into currently prevailing RF/microwave radar and/or communication systems with wideband operations. As mentioned in the last subsection, although the unique frequency beam-scanning embraced by LWAs can provide a relatively low-cost and low-complexity beam-scanning solution compared to mechanical- and phase-based counterparts, it suffers from a deteriorated or reduced available spectrum towards each special angle cell, i.e., narrowband-natured. This drawback unfortunately results in the shrinkage of range resolution in radar applications and reduced transmission rate/capacity in communication systems. That is to say, the frequency beam-scanning scheme is, honestly speaking, a trade-off solution in terms of system cost/complexity and electrical performances for radar or communication system designer. Although this drawback may not be a problem in sub-millimeter-wave and THz frequency bands thanks to the fact that sufficiently wideband spectrum resources can be allocated to each spatial angle in such a high-frequency region as mentioned above so as to provide satisfactory range resolution in radar applications or transmission rate/capacity in communication systems, this is not the case in the RF/microwave and low-millimeter-wave frequency bands. In this context, an LWA array technique relying on the FB (filter-bank) concept is explored and proposed in this thesis, with realizing a stitched frequency-space domain of beam-scanning operation, to solve or suppress the obvious drawback of

narrowband essence of LWAs in system applications. Note that the proposed FB-based LWA array technique is a competitive solution that is paralleled to the prevailing phased array technique.

1.3 Outline of Thesis

This thesis mainly focuses on the exploration and investigation of novel leaky-wave concepts, theories, and techniques for the design and development of various planar functional LWAs with promising circuit and/or radiation characteristics and for the potential radar system applications with improved performances (e.g., range resolution). Thanks to the merits such as low-profile, low-cost, and easy-integration capability, planar transmission technologies such as the SIW and microstrip line are preferably exploited here to implement and demonstrate those original research works. These works regarding various planar functional LWAs characterized by tailored and desirable electrical characteristics can be found from Chapter 3 to Chapter 7, after a literature review described in Chapter 2. In addition, it should be noted that a special contribution of this thesis is devoted to a potential application of LWAs for shifterless radar sensing systems, which is clearly stated in Chapter 8. Chapter 9 and 10 are dedicated to a comprehensive discussion and conclusion of this thesis, together with an outlook of the future works that can be pursued.

A detailed outline of this thesis is listed as follows:

Chapter 1: Introduction

This chapter begins with a comprehensive description of the background information, from a historical perspective, to illuminate the development history of radar techniques of which the role and significance as well as problems of frequency-scanning techniques is particularly highlighted. This lays the foundation and motivation for the research works in the thesis in which a series of leaky-wave concepts, theories, and techniques are proposed, explored, and investigated for frequency-scanning system applications.

Chapter 2: Literature Review

This chapter gives a comprehensive literature review of the development, classifications, and system applications of LWAs.

Chapter 3: Longitudinally Slotted SIW Leaky-Wave Antenna for Low Cross-Polarization Millimeter-Wave Applications

This chapter is devoted to a longitudinally slotted TE_{20} mode-driven SIW LWA with low side-lobe and low cross-polarization that is proposed and presented for millimeter-wave applications. In this work, a pair of long slots are etched symmetrically on the top broadside of an SIW working in TE_{20} mode. With the odd-symmetry of TE_{20} mode field distribution, the even-symmetrically etched long slots paired along the centerline of the SIW have aperture fields of the same direction, thereby resulting in a constructive superposition of radiation. Thanks to these long slots with a meandering shape that is designed according to a specific aperture amplitude illumination (e.g., -35 dB Taylor line-source distribution), and their even-symmetry with respect to the centerline of the SIW, both low side-lobe and low cross-polarization are simultaneously achieved. Two meandering schemes with respect to the centerline of the SIW are adopted and thus two types of the designed LWAs are developed.

Chapter 4: Transversely Slotted SIW Leaky-Wave Antenna Featuring Rapid Beam-Scanning For Millimeter-Wave Applications

In this chapter, loading effects of RDs have been explored to increase the frequency sensitivity of LWAs' phase constant, based on which a quasi-uniform transversely slotted SIW LWA featuring rapid beam-scanning and its hexagonal array have been proposed and investigated for millimeter-wave applications. The design concept is simply based on the use of a short period of unit cells and a long transverse slot with a sharp inductive reactance, and it has been elaborated theoretically and validated effectively by both full-wave and circuit-based simulations. A taper design with -25 dB Taylor amplitude distribution is implemented for the proposed LWA to have a low side-lobe radiation. For practical system applications, a hexagonal array consisting of six proposed LWAs is developed to provide an omnidirectional coverage in the azimuth plane while remaining the rapid frequency-driven beam-scanning in the elevation plane.

Chapter 5: Multifunctional Filtering Leaky-Wave Antenna Exhibiting Simultaneous Rapid Beam-Scanning and Frequency-Selective Characteristics Based on Radiative Bandpass Filter Concept

In this chapter, the concept of RBPF (radiative band-pass filter) is proposed and investigated for developing a class of multifunctional filtering LWAs which exhibit simultaneous rapid frequency-dependent beam-scanning and frequency-selective characteristics. An SIW is periodically loaded

with closed (non-radiative) discontinuities acting as a bandpass filter, where the lower and higher stopbands are respectively stemmed from the SIW's natural cut-off and the Bragg effects' bandgap or bandstop caused by periodic discontinuities. By adequately adjusting the periodicity of filter unit cells and loading effects of closed discontinuities, filtering and dispersion behaviors of the periodic SIW can be flexibly engineered. Open (radiative) discontinuities are then deliberately introduced into the bandpass filter to generate a controllable radiation leakage, thereby accomplishing the design of the RBPF, i.e., the proposed LWA. With this concept, both filtering/dispersion and radiation tasks can be independently managed by different modules for LWAs. For demonstration purposes, two kinds of closed discontinuities, namely non-radiative longitudinal slot-pair (capacitive) and iris (inductive), are separately exploited for periodic SIWs with bandpass and high dispersion characteristics; whereas transverse slot (open discontinuity) is mainly aimed for radiation leakage. Two RBPF-based LWAs are simulated, fabricated and measured.

Chapter 6: Leaky-Wave Antenna Featuring Stable Radiation Based on Multi-Mode Resonator (MMR) Concept

In this chapter, a scheme based on the MMR concept is proposed and demonstrated for the design and development of LWAs to realize stable radiation properties (e.g., stable radiation efficiency and gain). Firstly, two kinds of traditional LWA unit cells possessing typical single-mode resonator and monotonic changing radiation behaviors are theoretically modeled and analyzed. The condition for LWAs featuring stable radiation properties is then derived, based on which the MMR concept is proposed as a solution for radiation stability. For demonstration purposes, two types of MMR-based unit cells and their associated one-dimensional periodic LWAs are studied and developed for millimeter-wave applications. One type is based on the magneto-electric dipole, while the other originates from the aperture-coupled patch antenna. To facilitate the implementation, a detailed design procedure for this class of LWAs is provided in a general manner.

Chapter 7: Multifunctional Leaky-Wave Antenna with Tailored Radiation and Filtering Characteristics Based on Flexible Mode-Control

In this chapter, a class of single-layered multifunctional LWAs with flexibly engineered radiation and filtering characteristics are proposed and demonstrated for microwave and millimeter-wave

applications. RDs exhibiting multiple resonances while particularly possessing flexible model-control capability are exploited to accomplish such design freedoms and multifunctionalities of LWAs. By properly engineering the resonance characteristics of RDs under the mode-control principle, the attenuation constant of relevant LWAs can not only be freely tailored for diverse beamwidth/directivity requirements, but also simultaneously maintain a flat frequency response for radiation stability. Meanwhile, controllable filtering behaviors can be obtained as well by the LWAs thanks to the transmission zeros introduced by resonances. Consequently, both the radiation and filtering performances of LWAs can be adequately tailored by taking advantage of the mode-control capability of RDs. Under this design concept, two types of LWAs based on SIW and microstrip techniques are respectively developed for different system integration platforms. The SIW LWA whose unit cells consist of different longitudinal slots is firstly examined. Additionally, the microstrip LWA, which depends on stub-loaded resonators, is further investigated. The proposed two LWAs are all featured with flexible engineered electrical behaviors, single-layer, low-cost, and easy integration; they may be a potential candidate for various system applications such as 5G communication and Internet of Vehicles (IoVs).

Chapter 8: Filter Bank-Enabled Leaky-Wave Antenna Array Technique for Radar Applications in Stitched Frequency-Space Domain

In this chapter, an array technique of LWAs on the basis of an FB concept is proposed and studied for prospective radar applications characterized in stitched frequency-space domain. With the radar equation, the conditions for the FB-enabled “frequency-space stitching” are analytically derived and equivalently converted into design specifications for an array of LWAs, i.e., engineered or synthesized beam-scanning functions, beam-crossovers, and phase alignments. Moreover, to facilitate a practical implementation of such LWA array technique, a detailed design flow is developed in a generalized manner. An FB-enabled two-channel microstrip combline LWA array is modeled, fabricated, and measured for a direct proof-of-concept. The proposed FB-enabled LWA array technique may be potentially deployed in radars, as a complementary solution to the current phased array counterpart.

Chapter 9: General Discussion

As indicated by the title of this chapter, general discussions of the proposed works in this thesis

will be briefly described.

Chapter 10: Conclusion and Future Works

In this chapter, a comprehensive conclusion will be firstly drawn regarding the original research works and contribution we have made in this thesis to the antenna and radar (or communication) communities. This is followed by an outlook of future works related to the content of this thesis, providing some interesting research topics/directions of LWAs and their potential system applications.

CHAPTER 2 LITERATURE REVIEW

Prior to the formal descriptions and discussions of LWAs, it is interesting to imagine a very common secene in our daily life: in the goldden summer and after dinner, you walk your dog passing through a garden or grassland where you usualy see that the irrigation systems consisting of a set of leaking pipes or hoses are working automatically. Each pipe or hose is distributed with a certain number of small holes by which the water can flow along the pipe while simultaneously spraying out for watering purposes. An LWA is just a special “leaking water-pipe” if one perceives the electromagnetic (EM) energy and waveguide/transmission lines (TLs) in the RF/microwave world as the water and pipe/hose in the irrigation systems shown in Figure 2.1 (Note that although this metaphor is not rigorous, it can be used as a starting point for beginners to figuratively understand LWAs). Certainly, just as the role of those holes which is indispensable to enable a water pipe to spray water out, the RD plays such a equivalent role in LWA—To make the guided mode in a normal waveguide/TL into a leaky mode by which radiation occurs (that is the reason we entitle the “antenna” to such a perturbed waveguide/TL).

Figure 2.1 A vivid example to understand LWAs: leaking pipes/hoses of irrigation systems in a garden or grassland [12] (royalty-free image)

2.1 Brief Introduction to Leaky-Wave Antennas

The last paragraph has provided a vivid example to understand LWAs, and it is believed that this

metaphor or analogy can be easily accepted by beginners who just step into our leaky-wave communities. To be professional, an LWA is basically a wave-guiding structure along which an attenuating travelling-wave propagates, where the attenuation is in the form of radiation leakage if the dissipation loss mechanism (i.e., conductor and dielectric losses) is not considered [9][11]. Also, an LWA can be explained as a series-fed antenna array [recalling Figure 1.2(b)] where the feeding waveguide/TL and antenna elements are seamlessly integrated into a same structure. Note that the antenna elements or more generally, RDs, can be distributed along the wave-guiding structure in either a discrete or a continuous manner. What's more, LWAs can also be interpreted as a class of artificial TLs where the radiation would occur if some conditions can be satisfied, i.e., the structure is opened and the propagating modes or space harmonics have a faster phase velocity than the light speed of free-space.

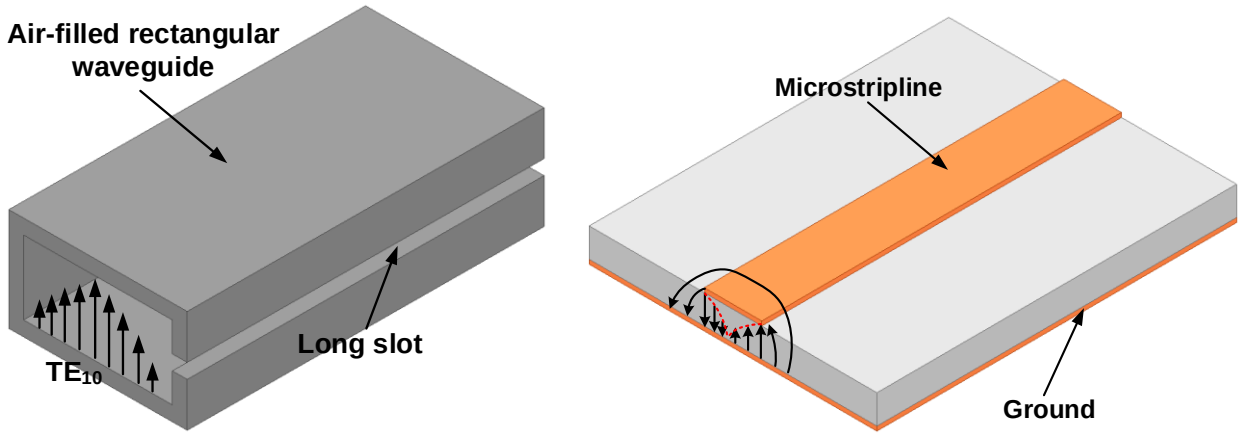

Figure 2.2 Two typical examples of uniform type LWAs [9][11]

(a) Air-filled rectangular waveguide with a continuous long slit cut along its sidewall (the earliest LWA in the LWA community, invented by W. W. Hansen in 1940s). (b) EH_1-mode microstrip LWA

The earliest example of LWAs can date to back 1940s, introduced by W. W. Hansen [13]. It is based on an air-filled rectangular waveguide (RWG) where a continuous long slit is cut along its sidewall, as shown in Figure 2.2(a). The EM energy carried by the RWG is progressively leaked

or escaped away to the outside free-space through the slit when the wave propagates along the waveguide. Since leakage occurs over the length of the slide, the whole slit length constitutes the effective antenna aperture unless the leakage rate is so large that the power has been leaked away effectively before reaching the end of the slit. Because of the slit and energy leakage, the original boundary condition of the waveguide has been broken and its original propagation constants have also been changed. Instead, the complex propagation constants, including a phase constant β and an attenuation constant φ, have been established with the newly formed boundary condition. In this case, the original guided mode inside the waveguide has become a leaky mode that is responsible for the radiation mechanism.

Prior to the design of an LWA, its complex propagation constants are the critical parameters that should be studied and determined comprehensively, thanks to the fact that the two constants (i.e., phase and attenuation constants) are responsible for determining its radiation characteristics such as the main beam direction, beamwidth/directivity, radiation efficiency, and SLL [9][11]. For example, an LWA with a larger leakage constant is prone to produce a shorter antenna aperture and sharp amplitude tapering, thereby resulting in a wider radiation beam and lower directivity. In this case, we may conclude that LWAs are a class of radiating-while-guiding structures whose radiation behaviors as antennas can be tightly linked to their transmission parameters as wave-guiding structures. In other words, if the complex constants can be extracted precisely, the main radiation features of LWAs can be estimated, which is beneficial for the relevant designs.

2.2 Comprehensive Classifications of Leaky-Wave Antennas

Thanks to their many appealing features such as simple feeding mechanism, high directivity, narrow beamwidth, and unique frequency-enabled beam-scanning, LWAs have received much interest since the invention of the first LWA shown in Figure 2.2(a). A large number of LWAs have been proposed as the technology develops, and they can be classified into a variety of types according to different criteria as will be described later.

2.2.1 Uniform, Quasi-Uniform, and Periodic

According to its name, it is obvious to find that the uniform type LWA is the one where the cross-section of the guiding structure is kept the same along the wave propagation direction. The radiation

mechanism of this kind of LWAs is due to the natural leaky mode (the one that satisfies the Maxwell equations and boundary conditions) propagating along the structure. Several typical examples fall into this LWA group, and perhaps the best-known one is the slitted air-filled RWG shown in Figure 2.2(a). In this LWA, the original guided mode of the waveguide is a fast-wave TE_{10} mode without any attenuation if the slit were absent and the conductor losses were not considered. When the slit in introduced, the waveguide structure becomes opened and the original fast-wave mode changes to a leaky mode featuring complex propagation constants (i.e., β and φ), where the attenuation is caused by the radiation leakage. Another representative uniform type LWA is the microstrip LWA as shown in Figure 2.2(b), in which the leaky mode is the high-order mode of a microstrip line such as the EH_1 and EH_2 modes. It is interesting to mention that the half-width microstrip LWA or half-mode SIW LWAs, which are the derivatives of the conventional EH_1-mode microstrip LWA, also belongs to the category of uniform LWAs.

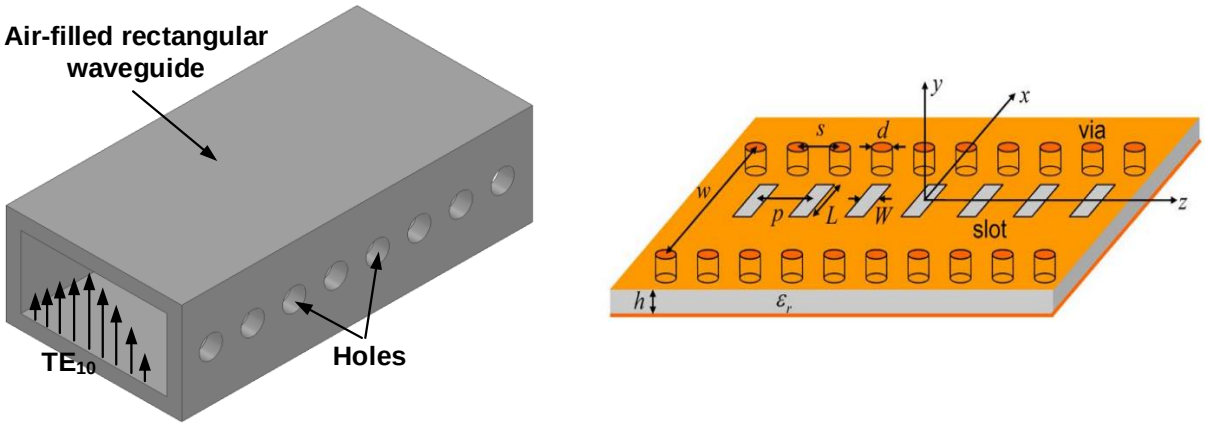

(a) (b)

Figure 2.3 Typical quasi-uniform LWAs

(a) Holey air-filled rectangular waveguide [9]. (b) Transversely slotted SIW LWA [14]. (©2012 IEEE, reproduced with permission)

Quasi-uniform LWAs can be interpreted as a special class of uniform LWAs since most of them have similar radiation mechanism even though the two classes have very different appearances. For the quasi-uniform LWA, it has a periodic appearance that is similar to the periodic type LWA

(this will be described later). Although periodic perturbations in such a structure will introduce an infinite number of space-harmonics, the period length is small enough such that those higher-order space-harmonics are far away from the working frequency band of interest. As a consequence, it is the fundamental "mode" or space-harmonic (also called "Floquet mode") that is responsible for the radiation mechanism. Two representative quasi-uniform LWAs can be found in Figure 2.3. Considering that the phase constant of the fundamental space-harmonic is just a slightly perturbed counterpart of the original host waveguide/TL while the leaky-wave radiation needs the working "leaky mode" to be located in the fast-wave region, the quasi-uniform LWA should has a natural fast-wave guided-mode over the working frequency band of interest, which is similar to the foregoing uniform type LWA. Also note that most of quasi-uniform and uniform LWAs can only provide a forward beam-scanning, from near broadside to near end-fire (or true end-fire) radiation.

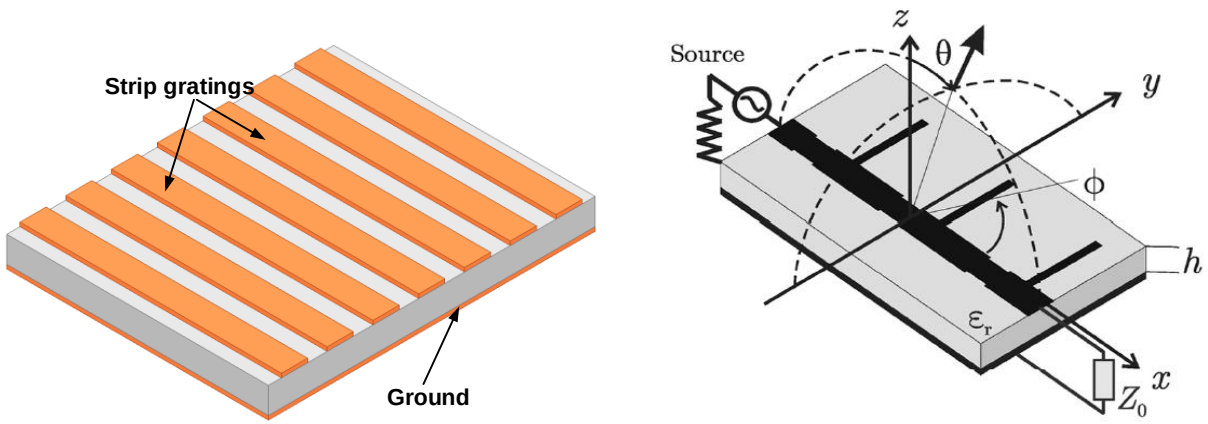

(a) (b)

Figure 2.4 Typical periodic LWAs

(a) Grounded-substrate-based strip-grating LWA [9]. (b) Microstrip combline LWA [15]. (©2013 IEEE, reproduced with permission)

The periodic type LWA has a periodic appearance where the period length of the unit cell is in the order of a guided-wavelength, i.e., one or more guided wavelengths that correspond to the first- or higher-order space-harmonics. For this kind of LWA, the fundamental mode of the host waveguides/TLs is always slow-wave-natured (again, in the working frequency region of interest)

for which there is no radiation occurring as waves propagate along it. Actually, according to the traditional antenna array theory, one can perceive that there is "radiation" occurring in such a slow-wave structure while unfortunately the main radiation beam is moved into the invisible region [16]. However, when a set of opened RDs are periodically loaded along the guiding structure, the propagating wave is in the form of Bloch wave. This Bloch wave can be mathematically expressed as a travelling plane-wave that is modulated by a periodic spatial function. In this context, this propagating Bloch wave can be expanded to an infinite number of space-harmonics, according to the famous Fourier Series that is typical to time-domain periodic signal. Although the fundamental space-harmonic is slow-wave-natured, some high-order space-harmonics, usually the -1st-order, can be designed to be a radiating "leaky mode". Bloch-Floquet theorem [17][18] can be used to analyze this kind of LWA and conveniently extract the complex propagation constants of the leaky space-harmonics. It is interesting to mention that this LWA sometimes can also be interpreted as a travelling-wave series-fed antenna array since they share the same appearances and travelling-wave natures. Two representative periodic type LWAs can be found in Figure 2.4. Compared to the foregoing two types of LWAs (i.e., uniform and quasi-uniform), periodic LWAs have the potential of providing a full-space beam-scanning from backward to forward through broadside direction if some special measures were implemented to overcome the notorious "open-stopband" phenomenon [15].

2.2.2 Waveguide or TL technologies

Since the design of LWA has to depend on the wave-guiding structures (i.e., the construction of LWAs relies on loading RDs, either in a continuous or in a discrete manner, on wave-guiding structures), the design and development of new kinds of LWAs are always accompanied by the invention of new TLs and waveguides. Different transmission technologies can be properly adopted depending on specific considerations such as cost, loss, power-handling capacity, and integration capability. Therefore, LWAs can be classified on the basis of different wave-guiding technologies, such as metallic waveguide [13][19]-[26], microstrip line [27]-[36], co-planar stripline (CPS) [37]-[39], co-planar waveguide (CPW) [40][41], SIW [42]-[66], spoof surface plasmon polaritons (SSPPs) or goubau lines [67]-[77], and gap waveguide [78]-[83]. With the continuous development of RF/microwave technologies, new waveguides/TLs are expected to be

invented to provide suitable solutions. Thus, there are no doubts that new LWAs will be developed accordingly in the future to be adapted into new transmission systems.

2.2.3 Resonance Behaviors of Radiating Discontinuities

Although LWAs, from a macroscopic perspective, are known as a class of non-resonant structures along which travelling-waves propagate and leak out simultaneously, RDs are usually comprised of resonant structures in which localized standing-wave phenomenon is presented, from a microscopic point of view. Note that this remark is especially suitable to those quasi-uniform and periodic LWAs in which the periodicities are used as the true radiation sources. For example, for waveguide-based LWAs, various kinds of slots (e.g., transverse or longitudinal slot) should be cut on the waveguide surfaces (e.g., broadwall or sidewall) to enable the radiation leakage. Those slots are actually resonant structures and the half-wavelength resonance will be presented at a certain frequency point. These slot dimensions are deliberately selected to guarantee that their half-wavelength resonant frequencies are far away from the working frequency band of interest within which the leaky-wave radiation is formed. Depending on the resonance characteristics of RDs, LWAs can be basically classified into two main groups: single-mode-resonator (SMR)- and multimode-resonator (MMR)-based LWAs. The SMR-based LWA is referred to as the one that only uses a single resonance of the RDs, while the MMR-based LWA takes advantage of multiple resonances simultaneously of the RDs. More details can refer to [83][84]. Although the forms of RDs depend on specific waveguide/TL technologies, i.e., slot apertures have to be used in closed waveguide while stubs/gaps can be exploited for microstrip type LWAs, the resonance characteristics of RDs are generally grouped into SMR and MMR. Therefore, it is justified and reasonable to classify LWAs into the related two types.

2.2.4 Electrical Functionality

How to understand the nature of leaky-wave, and efficiently construct and accurately analyze various kinds of LWAs that are based on different wave-guiding structures and RDs are not the destination of research in our LWA communities, although they used to be of great significance in the initial stage of LWA development history. There is also one aspect that is of particular importance with the development of LWAs: how to design additional desirable functionalities or

promising electrical behaviors to LWAs so that they can perform well in the potential system applications? This motivation has inspired a lot of research interests that enable LWAs to be equipped with diversified functionalities and desirable electrical characteristics in addition to the generation and analysis of leaky-wave radiation, including open-stopband suppression [15][30]-[32][36][38][51]-[53][56][59], high radiation efficiency [85][86], circular polarization [87]-[97], end-fire radiation [98]-[104], multi-beam radiation [105]-[114], radiation stability [30][31][83][84], low SLL and/or low cross-polarization [20]-[24][26][30][45][46][48][50][57][61][65][71][115]-[121], multi-band [122]-[135], fast beam-scanning [136]-[154], reconfigurable LWAs [155]-[164], and wideband non-scanning/less-dispersion LWAs [37][78][81][165]-[173], just to name a few. In this section, only several research hotspots that loosely or tightly related to this thesis are properly detailed.

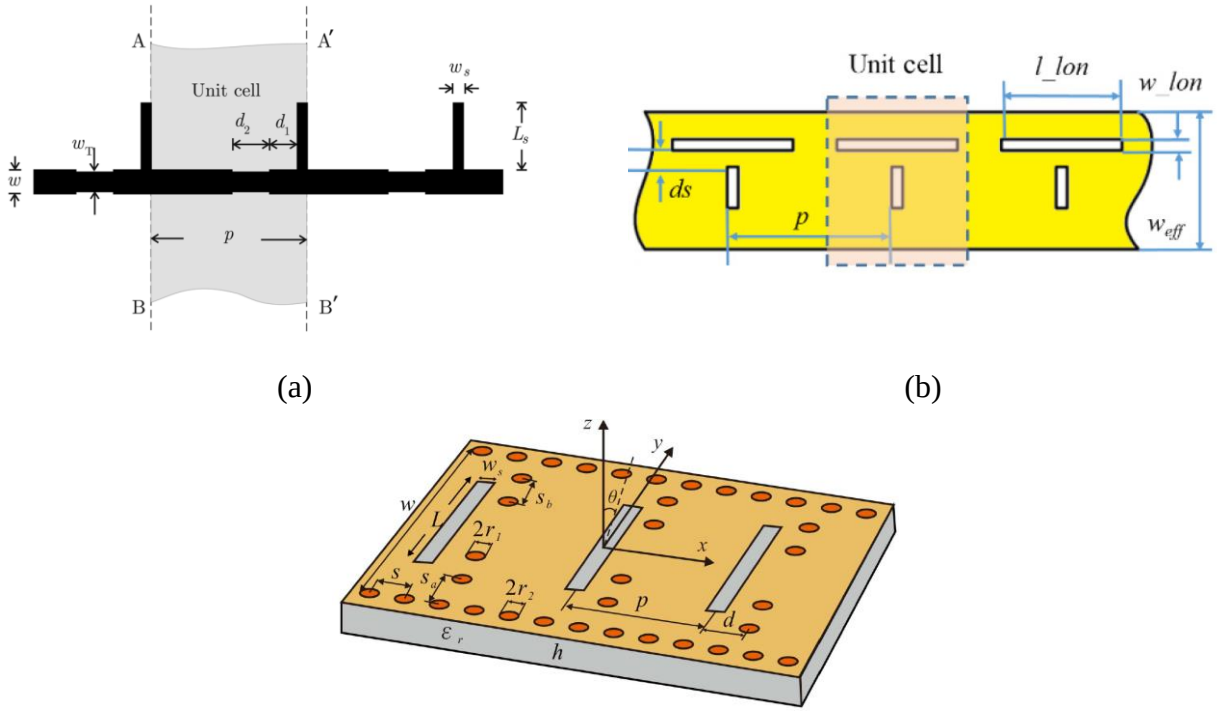

Figure 2.5 Several typical approaches to suppress the open stopband effects with the use of impedance matching mechanism

(a) [32] (©2009 IEEE, reproduced with permission). (b) [51] (©2016 IEEE, reproduced with permission). (c) [56]. (©2018 IEEE, reproduced with permission)

(a) Open-Stopband Suppression or Broadside Radiation

For a periodic structure, the famous phenomenon is the "Bragg effect" which would occur when the spacing between adjacent unit cells is an integer number of half guided-wavelengths at some frequencies [17]. This effect is also called "lattice resonance" since a standing-wave would be formed along the periodic structure at those frequencies. At the frequency point at which the period length corresponds to an integer number of half guided-wavelengths, the waves propagating along the structure are largely reflected back to the source and thus little energy can be injected into the structure. Such a phenomenon of periodic structures can be used to design filters and reflectors in

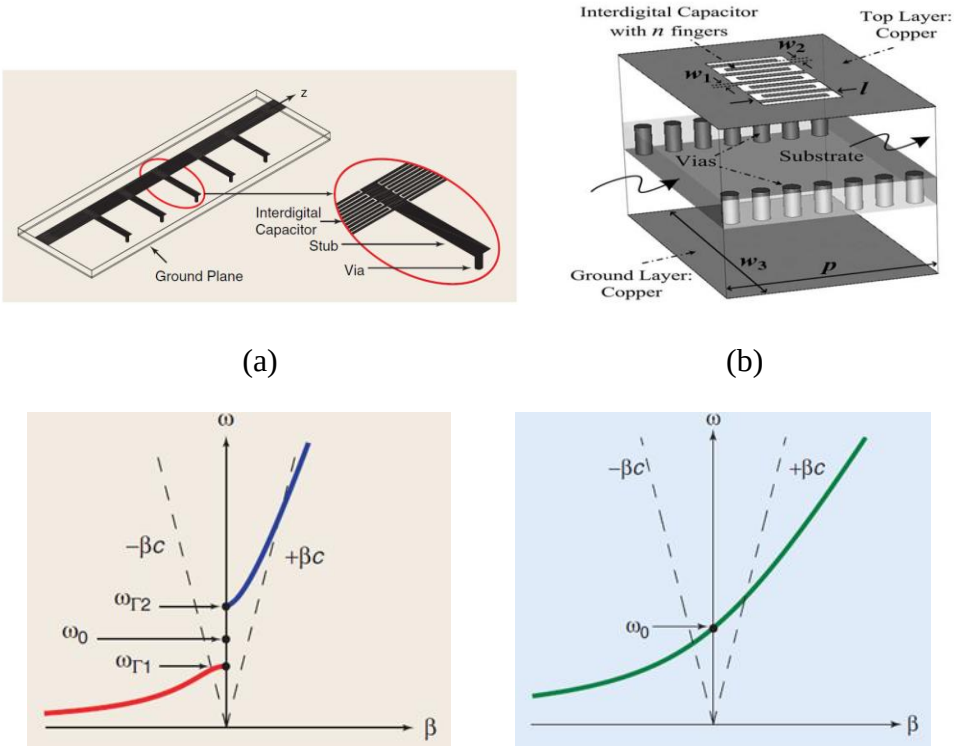

Figure 2.6 Open-stopband elimination/suppression using CRLH-based TLs and principles (a) Microstrip-line-based CRLH LWA [36] (©2004 IEEE, reproduced with permission). (b) SIW-based CRLH LWA [52] (©2011 IEEE, reproduced with permission). (c) Unbalanced (left) and balanced (right) cases [36]. (©2004 IEEE, reproduced with permission)

our RF/microwave region such as the electromagnetic bandgap (EBG) structures [174]. In a periodic type leaky-wave antenna using the -1st space-harmonic, the second Bragg stopband lies within its leaky-wave radiation region. In this case, this stopband is called the "open-stopband" where the word "open" refers to the fact that the periodic structure is a radiative structure that is opened to the outside free-space.

When a periodic LWA is scanned at the broadside direction, the distance between adjacent unit cells is just a guided-wavelength. If no special designs are considered to prevent the open-stopband effects, the periodic LWA will become "blind" or "nearsighted" in the manner that the radiation performances are significantly deteriorated. Fortunately, many methods have been proposed to mitigate this problem. For example, a pair of identical RDs are introduced into a unit cell, where the two elements are spaced by a quarter guided wavelength at the frequency corresponding to the broadside radiation [11]. The identical radiating elements can be stubs, strips, and slots. The principle is that the reflection caused by the first element can be canceled by the reflection resulted from the second element, since a round-trip path will introduce a phase difference of 180 degrees for the reflective waves from the two elements. Further, a remarkable solution based on impedance matching of the unit cell has been proposed in [15][32], in which a delay line and impedance transformer or matching stubs are introduced in a unit cell to do the impedance matching at the broadside frequency point. Based on the concept of "matched unit-cell", several works have been presented, such as the simultaneous cutting of transverse and longitudinal slots [51], and loading of shorting vias [56], and self-matching RDs [38]. Several typical approaches to suppressing the open-stopband effects with the use of impedance matching mechanism are illustrated in Figure 2.5. As a comparison, we can also use another popular method called "composite right/left-handed (CRLH)" principle to construct different kinds of LWAs with a continuous beam-scanning from the backward to forward direction, as long as the "balanced condition" can be satisfied [36][52]. Two typical CRLH-based LWAs based on the microstrip line and SIW are respectively depicted in Figure 2.6 (a) and (b), together with the "unbalanced" and "balanced" conditions illustrated in Figure 2.6 (c).

(b) Low Side-Lobe and Low Cross-Polarization

For an LWA whose RDs are not tapered along the length of the structure, no matter the distribution type of RDs—continuously or discretely, the aperture amplitude of such an antenna is

exponentially-decaying along the length of the structure. Since all practical LWAs have a finite length, the SLL of such antennas will be high and is close to about 13 dB [9][11]. In order to lower the SLL, a tapered aperture distribution can be employed and therefore the RDs should be changed along the length of structure, according to the requirement of SLL. Note that in most cases, when we change the RDs along the structure to modify the value of α, it is likely that the value of β will also be changed since the two constants are coupled with each other. However, the phase constant along the structure should be kept unchanged to keep the radiation from all parts of the aperture points can be directed in the same direction. As shown in Figure 2.7(a), it is a long slot leaky-wave antenna fabricated on an air-filled TE_{10}-based RWG [20]. The long slot is meandered from the centerline to the sidewall and then backed, from the feeding end to the termination end. The shape

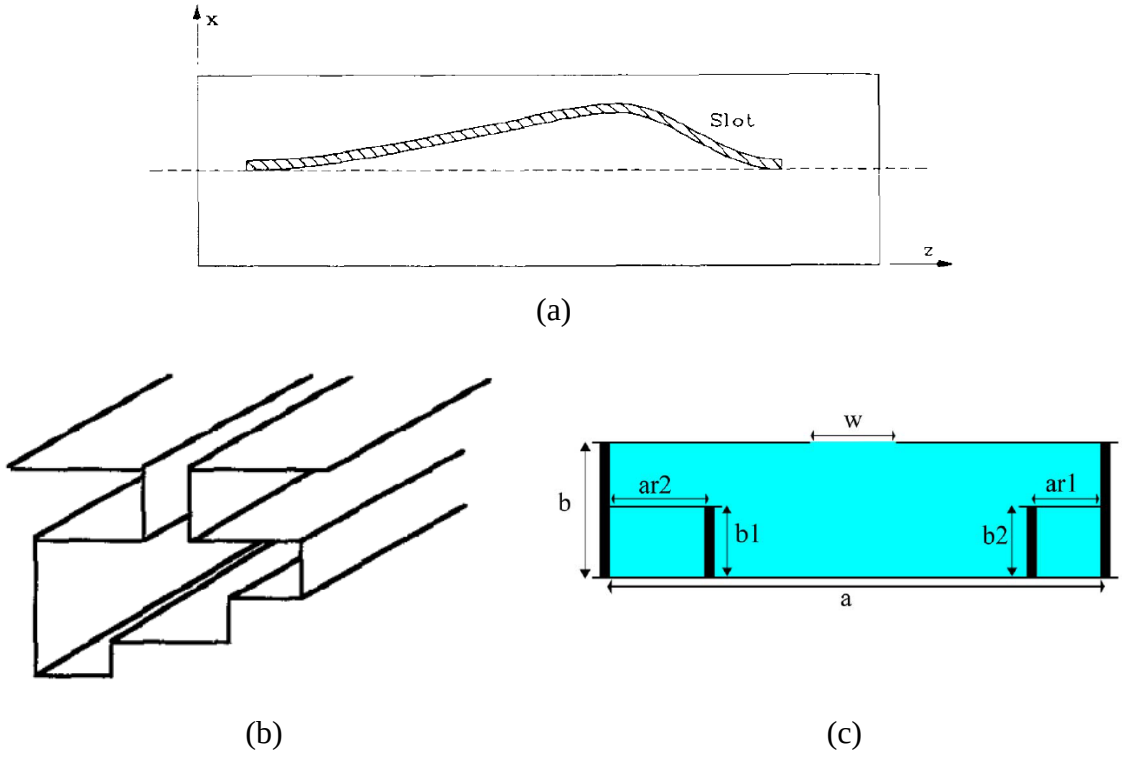

Figure 2.7 Several examples to taper the aperture amplitude distribution of the LWAs

(a) Rectangular waveguide-based long-slot LWA [20] (©1991 IEEE, reproduced with permission). (b) Stepped waveguide-based long-slit LWA [23] (©1997 IEEE, reproduced with permission). (c) Two-layered ridged SIW long-slot LWA [46] (©2014 IEEE, reproduced with permission)

of the long slot is determined by the required SLL and thus the aperture distribution. The same type long slot leaky-wave antenna can be constructed in the SIW technology which owns the advantages of low cost, low profile and easy of fabrication compared to the metallic RWG [45]. However, due to the asymmetry of the meandering long slot, the cross-polar level is high. Also note that when the position of the segment of the long slot changes, both of the attenuation and phase constants are changed. In order to achieve a low side-lobe design together with a low cross-polar level, a stepped metallic waveguide or a two-layer ridged SIW is used together with a straight long slit or slot [20][46], as shown in Figure 2.7(b) and (c), respectively. By changing the dimension of step height or ridge width, the attenuation constant can be altered while the phase constant can be kept constant for related LWAs. Notably, the slot is kept straight and symmetrical for realizing a pure radiation polarization, i.e., radiation with low cross-polarization field components. As a consequence, the proposed LWAs can achieve a low side-lobe and low cross-polar level simultaneously.

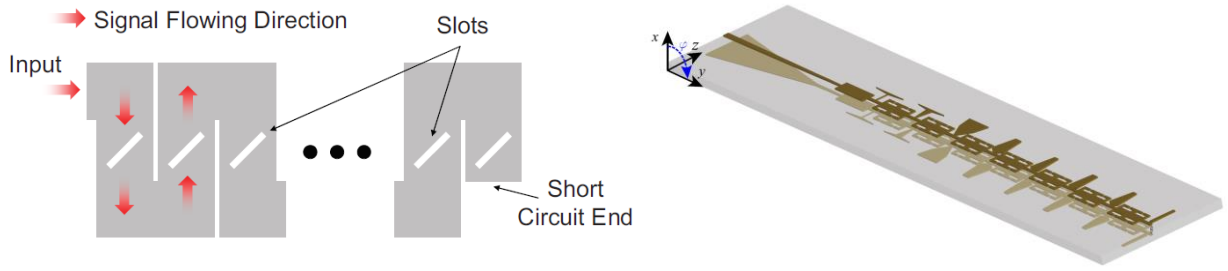

(a) (b)

Figure 2.8 Two examples of LWAs with enhanced beam-scanning rate

(a) Meandering feeding line [136] (©2009 IEEE, reproduced with permission). (b) Phase shifter between adjacent RDs [140] (©2017 IEEE, reproduced with permission)

(c) Fast Beam-Scanning Property

It is well known that the frequency-enabled beam-scanning is a distinct feature of LWAs. For the uniform or quasi-uniform LWAs, the beam-scanning range is normally limited in the forward quadrant. Comparatively, for the periodic LWAs, the beam-scanning range can be extended from the backward to the forward directions. For most of LWAs, a large beam-scanning range usually

needs a large frequency bandwidth. However, for a given beam-scanning range to cover a certain field-of-view (FoV), the narrower required frequency bandwidth has the potential to ease the bandwidth requirement of front-end components and the signal processor, from the viewpoint of a system-level. It means that a fast beam-scanning property within a limited bandwidth is needed for the leaky-wave antenna. A well-known method to increase the beam-scanning rate is to use a TL with high media parameters (i.e., permittivity and permeability). However, this method is too general and some other approaches must be adopted to increase the diversity and possibility of schemes. Besides, a meander TL can be employed between two adjacent RDs in a periodic LWA by which the phase delay (versus frequency) between the adjacent RDs can be sharpened and thus

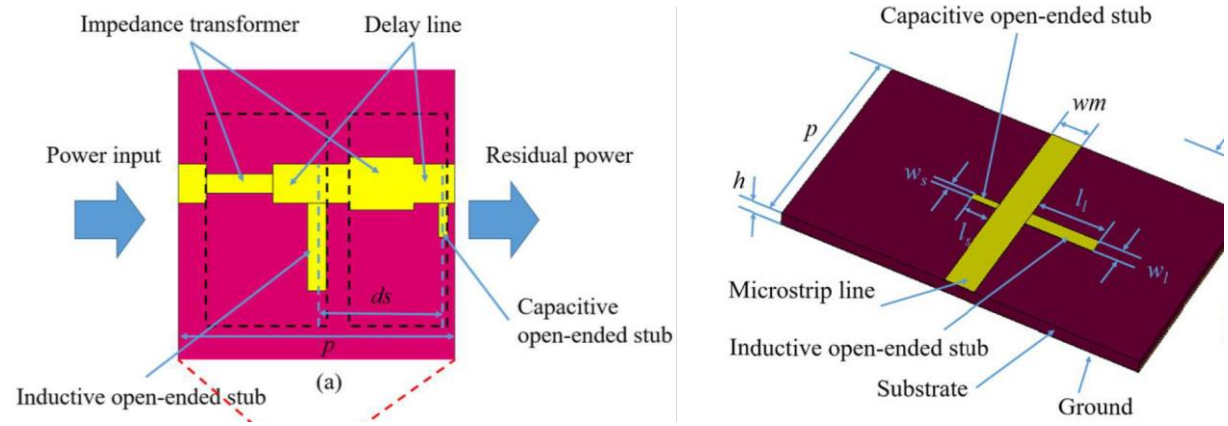

Figure 2.9 Microstrip periodic LWAs loaded with complementary radiating stubs for radiation stability [30][31]

(Both figures are with ©2018 IEEE, reproduced with permission)

the related beam-scanning of LWAs can be more sensitive to frequency. The method can also be found in Figure 1.2(b) as well as the work in [130] as shown in Figure 2.8(a). Similarly, by inserting a specially designed phase-shifter between two adjacent RDs [as shown in Figure 2.8(b)], the phase delay can also be sharpened with frequency to provide a rapid beam-scanning capability for related LWAs. In addition, employing slow-wave structures is another way to implement leaky-wave antennas with fast-beam scanning property, since the phase constant of the slow-wave structure is much more sensitive than those common TLs [135].

(c) Radiation Stability

The complex propagation constants are the key parameters to determine the radiation characteristics of an LWA. The phase constant determines the main beam direction while the attenuation constant is directly related with the aperture length, aperture amplitude distribution and antenna efficiency. In order to realize a stable radiation efficiency with frequency, a stable leakage constant with frequency should be satisfied, and furthermore the stable gain can be approximately obtained. In order to have a stable leakage constant with frequency, there are mainly two methods for design consideration. Firstly, the RDs should have a very small radiating ability (this is especially true for SMR-based RDs). It means that the working frequency band of interest should be far away from the resonance of the RDs. In this case, the resistance or conductance of a RD is small but is relatively flat with frequency, and thus a stable leakage rate can be obtained. However, some drawbacks will appear by using this approach: the length of the leaky-wave antenna should be long enough to make sure that most of the power can be radiated rather than being absorbed by the termination load. Recently, an effective method has been proposed to realize stable gain and efficiency, which is based on the use of a pair of complementary radiating elements in a unit cell of a periodic LWA [30][31], as shown in Figure 2.9. The design concept can be explained briefly by the fact that the complementary radiating elements dominant separately at different sub-frequency band, which is similar to log-periodic dipole array that has different active region with different dipoles [16]. It can also be explained by the MMR design principle proposed in [83]-[84]. This design concept provides a novel perspective to design LWAs with stable gain and efficiency.

2.3 System-Level Applications of Leaky-Wave Antennas

The distinct frequency-driven beam-scanning property embraced by LWAs enables them to fit the frequency-scanning radars well as those mentioned previously in Chapter 1.1. In addition to this application scenario, LWAs can also find other system-level applications such as the direction-of-arrival (DoA) estimation [175]-[182], frequency-scanned monopulse [183], real-time spectrum analyzer [184]-[186], duplexer/diplexer front-end [187][188], frequency-division multiplexing communication [189]-[191], radar and/or imaging [192]-[202], and multi-target concurrent vital sign and location detection [203][204], etc. Figure 2.10 shows several representative examples of system-level application scenarios of LWAs. No matter which kind of system applications, it is the

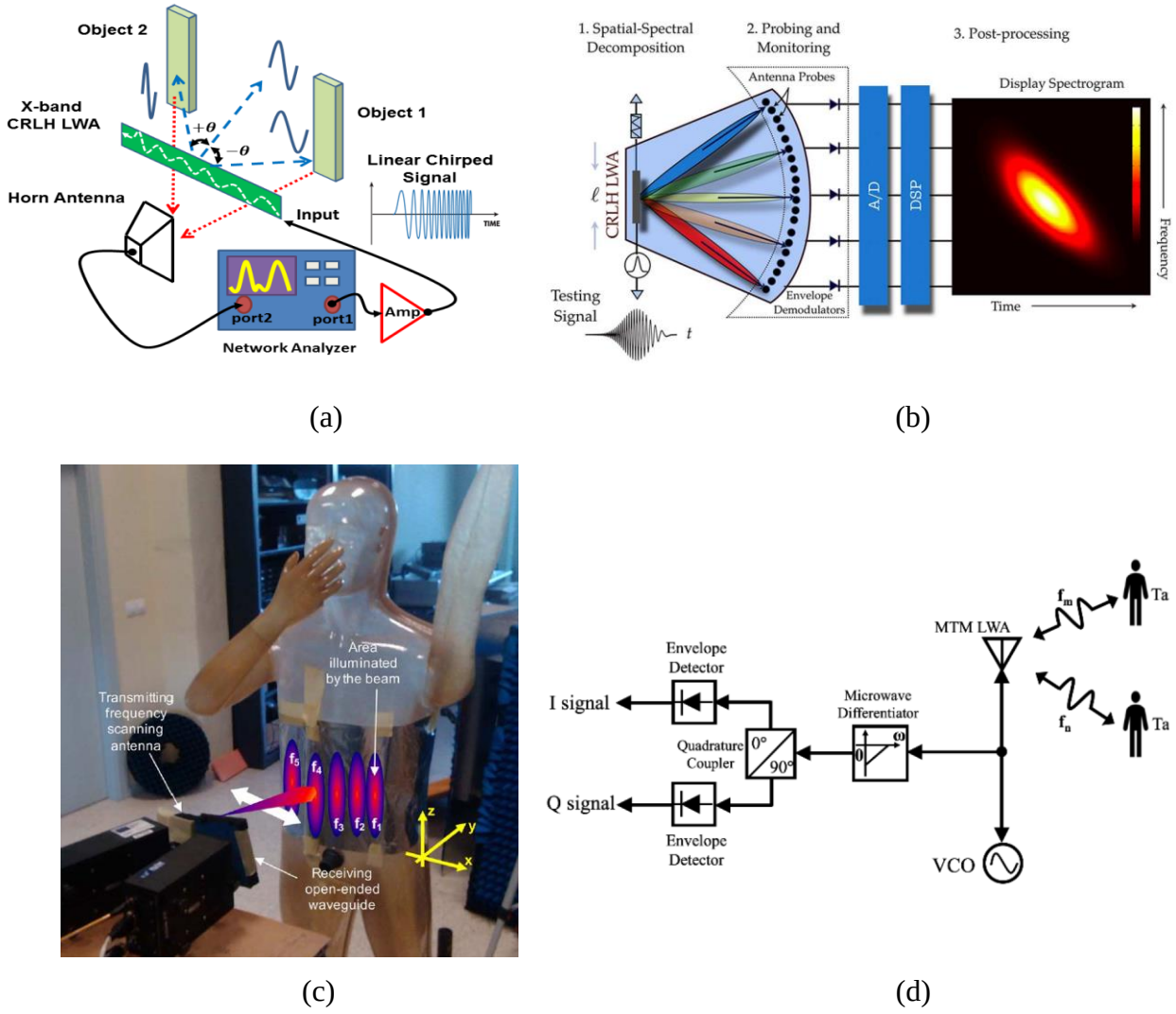

Figure 2.10 Selected typical system-level applications of LWAs

(a) DoA estimation [180] (©2015 IEEE, reproduced with permission). (b) Real-time spectrum analyzer [184] (©2009 IEEE, reproduced with permission). (c) Radar imaging [199] (©2013 IEEE, reproduced with permission). (d) Multi-target vital sign detection and localization [203] (©2019 IEEE, reproduced with permission)

natural frequency-enabled beam-scanning capability of LWAs that plays the dominant role to determine or define system characteristics. Specifically, if a wideband signal waveform is inputted into an LWA, different spectrum components of the signal waveform will be emitted to different spatial locations. This is from the perspective of transmitting (Tx) function of the LWA.

Contrastively, if we evaluate the LWA as a receiving (Rx) antenna, it will output different spectrum components for an incoming waveband signal waveform from different spatial angles. With this feature of LWAs, a simple DoA estimation system as shown in Figure 2.10 (a) can be implemented, and the angle location of the object can be estimated by using the maximum received power spectrum frequency point along with the pre-defined frequency-angle relationship of the LWA. The real-time spectrum analyzer shown in Figure 2.10 (b) also use the spatial-spectral decomposition (or called frequency-space mapping) characteristic of LWAs. Another type of more sophisticated systems such as concurrent vital sign detection and localization [as shown in Figure 2.10 (c)] and radar imaging [as shown in Figure 2.10 (d)] can also be realized using LWAs along with special system setups and digital signal processing (DSP) considerations.

CHAPTER 3 ARTICLE 1: LONGITUDINALLY SLOTTED SIW LEAKY-WAVE ANTENNA FOR LOW CROSS-POLARIZATION MILLIMETER-WAVE APPLICATIONS

Dongze Zheng, Yue-Long Lyu, and Ke Wu

Published in the *IEEE Transactions on Antennas and Propagation*, vol. 68, no. 2, pp. 656-664, Feb. 2020.

A longitudinally slotted TE_{20} mode-driven SIW LWA with low side-lobe and low cross-polarization is proposed and presented for millimeter-wave applications. In this work, a pair of long slots are etched symmetrically on the top broadside of an SIW working in TE_{20} mode. With the odd-symmetry of TE_{20} mode field distribution, the even-symmetrically etched long slots paired along the centerline of the SIW have aperture fields of the same direction, thereby resulting in a constructive superposition of radiation. Thanks to these long slots with a meandering shape that is designed according to a specific aperture amplitude illumination (e.g., -35 dB Taylor line-source distribution), and their even-symmetry with respect to the centerline of the SIW, both low side-lobe and low cross-polarization are simultaneously achieved. Two meandering schemes with respect to the centerline of the SIW are adopted and thus two types of the designed LWAs are developed. For experimental prototypes of the proposed LWAs, a 3-dB directional coupler and 90^{o} phase shifter are combined together to excite the desired TE_{20} mode of the SIW. The proposed two types of LWAs are modeled, simulated and fabricated. Both simulated and measured results are in a good agreement.

3.1 Introduction

LWAs are a class of travelling-wave antennas, in which power-decaying travelling waves propagate along guided-wave structures [9][11]. With this feature, they can be regarded as a special kind of lossy transmission lines where the majority of losses are in the form of radiation. On the other hand, LWAs can also be treated as series-feeding antenna arrays, where antenna building

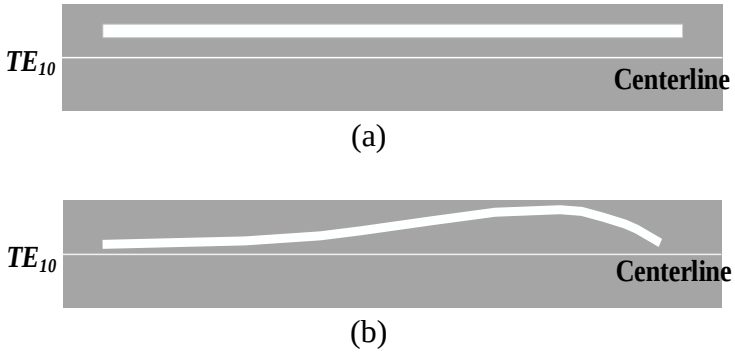

Figure 3.1 Configurations of traditional long slot LWAs [20]

(a) Straight long slot type. (b) Meandering long slot type. The grey area represents the top broad wall of a metallic waveguide while the white area stands for the long slot. The white dotted line is the centerline of a waveguide. (© 2020 IEEE, reproduced with permission)

elements may be distributed continuously or discretely (periodically, for example) along the leaky-wave structures. LWAs have attracted much attention for many years due to their low profile, simple feeding mechanism, high directivity and particularly frequency beam-scanning capability. Consequently, it has a number of possible applications in the areas of wireless communications, sensors and collision-avoidance radars [11].

Many types of LWAs based on different transmission lines have been proposed since the 1940s such as metallic RWG [13][19][20], microstrip line [27]-[36], CPS [37]-[39], CPW [40]-[41], SIW [42]-[65], and SSPPs [66]-[76]. Among different kinds of LWAs, the type based on longitudinally slotted waveguide, referred to as the long slot LWA in this chapter, has been widely used in microwave and millimeter-wave systems due to its simple structure and easy fabrication. However, a traditional straight long slot LWA, as shown in Figure 3.1(a), has an obvious drawback of high side-lobe caused by exponentially decaying aperture amplitude distribution [9][11]. A well-known approach used to tackle this problem is to adopt a meandering long slot with a particular shape, as shown in Figure 3.1(b), to create a desired aperture amplitude distribution and consequently a desired radiation pattern (i.e., low side-lobe) [20]. With the same goal, a hybrid waveguide-planar technique was employed to fabricate a curvilinear slot in RWGs [205][206]. Unfortunately, such meandering or curvilinear long slots are deemed to cause asymmetry in the slot aperture, resulting

in an asymmetric cross-sectional radiation and deterioration of the cross-polarization level in the scanning plane, especially. Therefore, it is difficult to acquire low side-lobe and low cross-polarization simultaneously for long slot LWAs.

Several studies have been conducted to achieve a long slot LWA having low side-lobe and low cross-polarization simultaneously. For example, an LWA in [45] with a straight long slot etched on a meandering SIW was proposed to achieve a symmetrical radiating aperture together with a tapered amplitude distribution. An approach based on effective radiation sections was studied in [117] to control the radiation pattern (e.g., SLL) of a long slot LWA with acceptable performances achieved. In [46], a multi-layer ridged SIW straight long slot LWA was presented. By properly adjusting the widths of two different ridges inside the SIW while remaining the slot shape straight, a tapered aperture amplitude distribution and thus low side-lobe, as well as low cross-polarization, were achieved. The same method was also applied to a ridged metallic waveguide straight long slot LWA [21]. What's more, asymmetric ridged waveguides [22] and stepped waveguides [23] with centered straight long slits were also proposed for the same purpose. Until now, it can be found that almost all these aforementioned approaches used to achieve both low side-lobe and low cross-polarization are based on asymmetrical waveguides or SIWs plus a straight long slot (slit). However, it should be noted that the multi-layer PCB fabrications or bulky metallic waveguides used in [21]-[23][46] to construct LWAs suffer from increased fabrication cost and complexity, which become unsuitable for mass production and planar integration in current millimeter-wave applications.

On the other hand, the use of SIW higher-order modes for antenna system design has been demonstrated to be promising for millimeter-wave applications, since it can not only enhance the stability of performances by relaxing fabrication tolerances, but also simplify the designed structures with reduced fabrication cost and complexity [207][208]. However, very limited works using higher-order modes of SIWs to design LWAs have been reported so far. In [43], a TE_{20} mode-based SIW LWA was realized by enlarging the spacing between plated via holes in a periodic manner so as to make the energy leakage occur. The same approach was also applied to achieve a quasi-uniform counterpart [47]. However, because of their special configurations and radiation mechanisms, both of them suffer from high SLL and large ground size. Also, careful considerations should be paid in the design of this kind of LWAs since potential grating lobes or large side-lobes

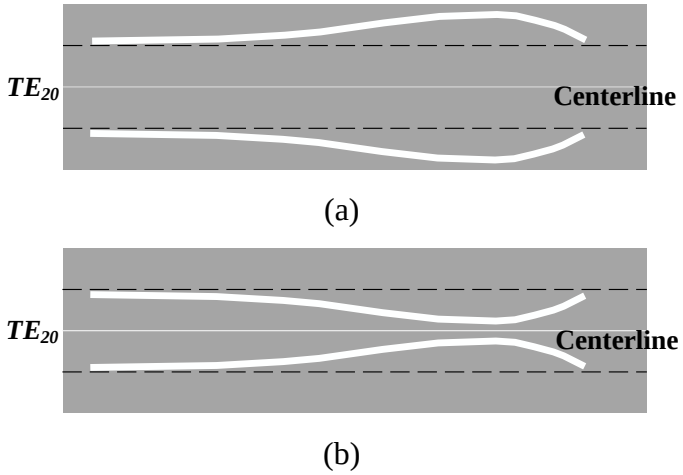

Figure 3.2 Schematics of the proposed two types of TE_{20} mode-based longitudinally slotted LWAs with low cross-polarization and low side-lobe

(a) Type I. (b) Type II. The grey area represents the top broad wall of a metallic waveguide or SIW; the white area stands for the long slots. The white dotted line is the centerline of a TE_{20} mode-based waveguide or SIW while the black dashed line represents the centerline of each half-field distribution of TE_{20} mode. (© 2020 IEEE, reproduced with permission)

may appear in the cross-plane due to a large distance between two equivalent radiating magnetic line-sources.

In this proposed work, TE_{20} mode-driven SIW longitudinally slotted LWAs with low cross-polarization and low side-lobe are proposed for millimeter-wave applications. This design has combined the advantages of SIW higher-order modes and long slot LWA. With the odd-symmetrical E-field distribution inside the TE_{20} mode SIW, a pair of long slots that are etched even-symmetrically along the longitudinal centerline on the top surface of the SIW have the same aperture field distributions, resulting in a constructive superposition in far-field radiation. The pair of long slots are in a meandering shape that is specially designed to achieve a low SLL, and two meandering schemes of the slots can be developed, as shown in Figure 3.2. Due to the specific meandering shape and symmetrical property of the pair of long slots, the radiation with low side-lobe and low cross-polarization can be obtained simultaneously. For experimental prototypes of the designed LWAs, a TE_{20} mode exciter consisting of a 3-dB directional coupler and 90^{o} phase

shifter is designed to drive the proposed antennas. A good agreement is observed between simulated and measured results.

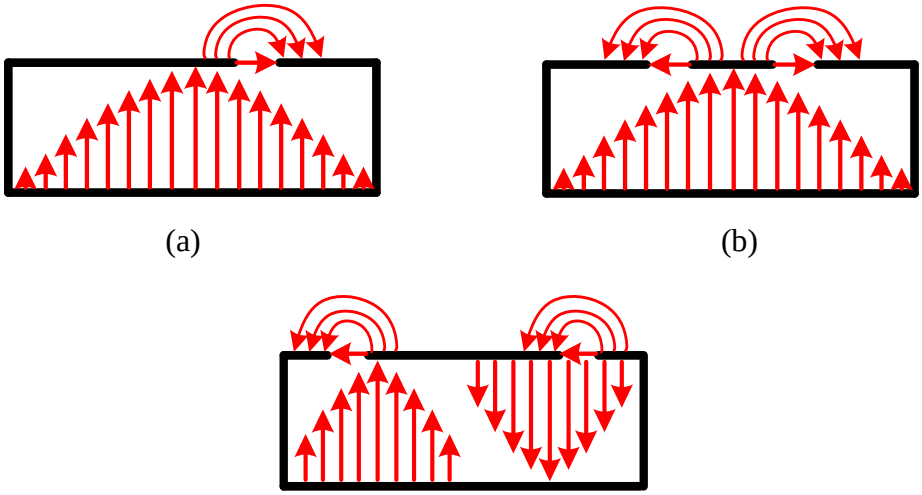

(a) (b)

(c)

Figure 3.3 E-field distributions with respect to different waveguides with longitudinal slots etching on top broad surface

(a) TE_{10} mode-based waveguide with one long slot. (b) TE_{10} mode-based waveguide with two symmetrical long slots. (c) TE_{20} mode-based waveguide with two symmetrical long slots. (© 2020 IEEE, reproduced with permission)

3.2 Working Principle

3.2.1 Radiation Mechanism

The diagram shown in Figure 3.3 depicts the E-field distributions with respect to different waveguides with slots etching on the top broad surfaces. For conventional TE_{10} mode-based metallic waveguide with a longitudinal slot cutting on its top surface, as shown in Figure 3.3 (a), the transverse surface current paths are cut off if the slot is offset from the centerline, and energy inside the waveguide is coupled to the outside free space, thus resulting in radiation. However, if two symmetrical longitudinal slots are etched along the centerline of a TE_{10} mode-based waveguide, as shown in Figure 3.3(b), the two aperture fields existing on the two slots feature opposite directions due to the even-symmetry of the transverse surface currents along the centerline.

Consequently, the radiation introduced by the pair of slots will be cancelled with each other and no net radiation occurs. As a comparison, for the waveguide working in the TE_{20} mode, the E-field distribution is odd-symmetrical along the centerline, as shown in Figure 3.3(c). If two longitudinal slots are cut symmetrically along the centerline, the field distributions in the two slot apertures will have the same direction and thus their radiation will be superposed constructively in the far field, which can be used to operate as an antenna.

It is known that the radiation characteristics of an LWA can be determined by its complex propagation constants of the leaky mode propagating in the leaky structure [9][11]. The complex propagation constants can be expressed as

$$k = \beta - j\alpha \tag{3.1}$$

where β is the phase constant while α is the attenuation constant of the leaky mode. In the proposed antenna, when the pair of long slots are introduced on the top broad wall of the SIW, both TE_{10} and TE_{20} modes will be perturbed to a certain extent and hence leaky modes can be formed. However, according to the previous analysis as shown in Figure 3.3(b), the perturbed TE_{10} mode does not contribute to radiation, thus it can be neglected in the following leaky-mode analysis. Also, it should be noted that the TE_{10} mode can be severely suppressed with a well-designed TE_{20} mode exciter, which will be shown later. Consequently, the phase constant in (3.1) can represent only the perturbed TE_{20} mode of the SIW. For a uniform TE_{20} mode SIW long slots LWA as shown in Figure 3.4, the main beam direction (θ_m, measured from broadside) and 3-dB beamwidth ($\Delta\theta$) can be expressed as

$$\sin\theta_m \cong \beta / k_0 \tag{3.2}$$

$$\Delta\theta \cong \frac{1}{\frac{Ls}{\lambda_0}\cos\theta_m} \tag{3.3}$$

where k_0 and λ_0 represent the free-space wavenumber and wavelength, respectively, while L_s represents length of the slot aperture.

The LWA can be modeled as a travelling-wave line-source current, and most LWAs have a narrow beam in the scanning plane while a wide beam in the cross-plane [9][11]. For the traditional long

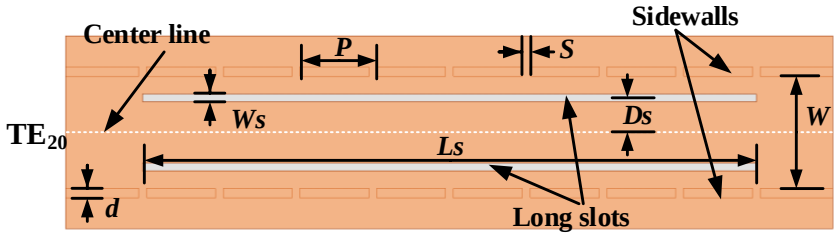

Figure 3.4 Uniform TE_{20} mode-based SIW long slots LWA

Simulated model built in *HFSS* for extracting attenuation and phase constants as a function of slot offset *Ds*. The substrate has a relative permittivity of 2.94 and a thickness of 1.524 mm. The conductor and dielectric are lossless. Copper printed on the substrate has a thickness of 17.5 um. Plated slot-via arrays with parameters of *W*=5.8 mm, *d*=0.6 mm, *S*=0.35 mm, and *P*=1.4 mm are used to form the sidewalls of the SIW. (© 2020 IEEE, reproduced with permission)

slot LWAs proposed in [13][19][20] and [21]-[23][45][46][117], and the half-width microstrip or half-mode SIW LWAs [42][48], their radiating apertures can be modeled as a single magnetic line current. Comparatively, the traditional EH_1 mode-based microstrip LWA [27] and TE_{20} mode SIW LWAs [43][47] can be modeled as two-line-source antennas. It is easy to understand that the two-line-source LWAs, compared to single line-source counterparts, can potentially achieve a narrower beamwidth in the cross plane, thereby realizing a higher directivity according to the traditional antenna theory [16].

The proposed antennas in this work belong to the two-line-source LWAs. As shown in Figure 3.4, half of the distance between the two magnetic line-sources (i.e., long slots) is represented by *Ds*. According to the special properties of the TE_{20} mode SIW, the parameter *Ds* can be varied from almost zero to approximately the full width of the SIW, depending on the required leakage rate (α) and beamwidth ($\Delta\theta$). The radiation pattern (in the scanning plane) of the overall structure can be expressed as a summation of radiations from the two magnetic line-sources [9]. According to the antenna array theory [16], when the distance between two array elements excited with the same amplitude and phase is approaching or over a free-space wavelength, large side-lobes or grating lobes will occur in its array factor pattern. For the traditional EH_1 mode microstrip LWA [27], the distance between the two equivalent magnetic line-sources is approximately half a guided

wavelength; therefore, no potential grating lobes or large lobes occur in its cross plane. However, for the TE_{20} mode SIW LWAs proposed in [43][47], the corresponding distance of the two radiating line-sources is more than a guided wavelength and thus large side-lobes or grating lobes may occur potentially in the upper side of the working frequency region, and therefore careful considerations should be paid when implementing such a design. Contrastingly, the distance of the two line-sources in the proposed scheme shown in Figure 3.4 can be adjusted and hence a flexible beamwidth in the cross plane can be achieved without potential grating lobes or large side-lobes.

3.2.2 Low Cross-Polarization

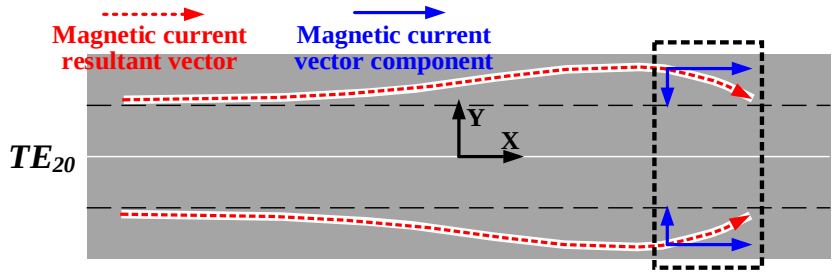

Figure 3.5 Illustration for low cross-polarization property of the proposed LWAs

The proposed *Type I* LWA is depicted here as an example. (© 2020 IEEE, reproduced with permission)

Figure 3.5 illustrates one of the proposed meandering long slots LWAs with its equivalent magnetic current distributions. It can be seen clearly that the two equivalent magnetic currents are strictly even-symmetrical along the centerline of the proposed structure. It should be noted that at any position of the meandering long slot, the corresponding magnetic current vector can be decomposed into two vector components. One vector component (e.g., X-directed component in this demonstrated case) contributes to co-polarization and the other contributes to cross-polarization. This explains why the traditional meandering long slot LWA shown in Figure 3.1(b) has a high cross-polarization level. Fortunately, for the proposed TE_{20} mode-driven meandering long slots LWA, the radiation of magnetic current vector components giving rise to cross-polarization (i.e., Y-directed component in this demonstrated case shown in Figure 3.5) will be totally cancelled, thereby leading to a low cross-polarization property of the proposed antenna. It is interesting to

note that the meandering slot shape can be diversified and solely depends on the required radiation patterns to be achieved (i.e., low SLL) as long as the two meandering slots are kept even-symmetrical so as to maintain a low cross-polarization level.

3.3 Low Side-Lobe Design

In most of practical applications, the radiation pattern with a low side-lobe is often needed, and thus a tapered aperture amplitude distribution should be adopted in the LWA. In the traditional long slot LWA with low side-lobe design [20], the offset of the long slot is changed from the centerline toward the sidewall and then back, along the wave propagation direction. The meandering shape of the long slot depends on the designed aperture amplitude distribution and the specified SLL. However, the drawback of the single meandering long slot is obvious: it causes an asymmetrical aperture and thus deteriorates the cross-polarization level, as explained above. The proposed two types of meandering long slots LWAs have a fully symmetrical structure and thus a low cross-polarization can be achieved, in addition to a low SLL.

Prior to the low side-lobe design of the proposed long slots LWAs, the complex propagation constants (i.e., α and β) as a function of the offset (*Ds*) of the long slots must be extracted. To achieve this goal, a model built in *HFSS*, as shown in Figure 3.4, is used to find the relationship between the complex propagation constants and the slots offset. The substrate chosen here has a relative permittivity of 2.94 and a thickness of 1.524 mm. Note that conductor and dielectric losses are not considered here to make sure that the attenuation of waves is only attributed to leakage radiation. Furthermore, the length of the slot aperture should be long enough to ensure a relatively accurate extraction of the propagation constants of the leaky mode. The slot width is selected as *Ws* = 0.25 mm to have a slight perturbation on the field of the SIW, and it is also beneficial for a judicious realization of low cross-polarization as well as a delicate control of the attenuation constant. The formulas used to calculate the complex propagation constants are

$$\alpha = -\frac{1}{2Ls}\ln\frac{|S_{21}|^2}{1-|S_{11}|^2} \tag{3.4}$$

$$\beta = k_0 \sin\theta_m \tag{3.5}$$

where *Ls* is the slot length in the simulated antenna segment.

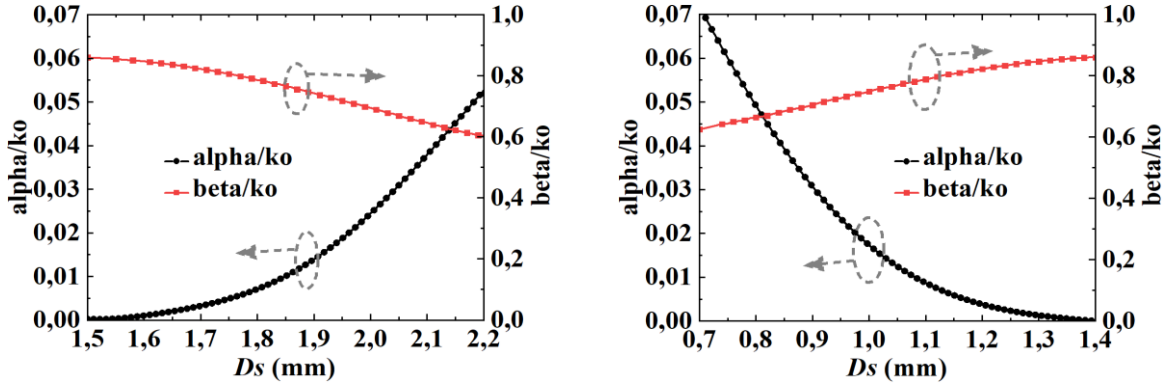

(a) (b)

Figure 3.6 Extracted normalized propagation constants as a function of the offset *Ds* of long slots for (a) *Type I* and (b) *Type II* LWAs

The design frequency is 35 GHz. (© 2020 IEEE, reproduced with permission)

Figure 3.6 gives the plots of extracted normalized complex propagation constants as a function of slots offset *Ds* for *Type I* and *Type II* LWAs, respectively. It can be found that the achievable attenuation constant range is large enough to realize various kinds of low side-lobe LWA design. The Taylor aperture illumination with a SLL of -35 dB is adopted here to implement the taper design. The required attenuation constant distribution can be determined by the following [9]

$$\alpha(x) = \frac{|A(x)|^2 / 2}{\frac{1}{e_r}\int_{-L_a/2}^{L_a/2} |A(\xi)|^2 \, d\xi - \int_{-L_a/2}^{x} |A(\xi)|^2 \, d\xi} \tag{3.6}$$

where $A(x)$ is the normalized amplitude distribution as a function of the location along the leaky structure, er is the radiation efficiency, and *La* is the length of radiating aperture. Here, e_r is chosen as 95% while La is selected as 110 mm, according to the achievable attenuation constant range. As such, the normalized aperture illumination $A(x)$ and the normalized attenuation constant distribution $\alpha(x)/k_0$ can be calculated from (3.6) and are plotted in Figure 3.7.

According to the calculated results from Figure 3.6 and 3.7, we can acquire the offset distribution of slots along the length of leaky-wave structures for *Type I* and *Type II* LWAs, respectively, as shown in Figure 3.8. However, in order to facilitate the modeling and fabrication of proposed

antennas, an equal-spaced sampling with a spacing of 5 mm is used, and thus 23 sampling points are obtained for each type of proposed antennas. It should be noted that along the wave-guiding direction, the phase constant of the leaky aperture is not compensated, which may result in a slightly wider beamwidth and an undesired shoulder of radiation patterns [20][45][50].

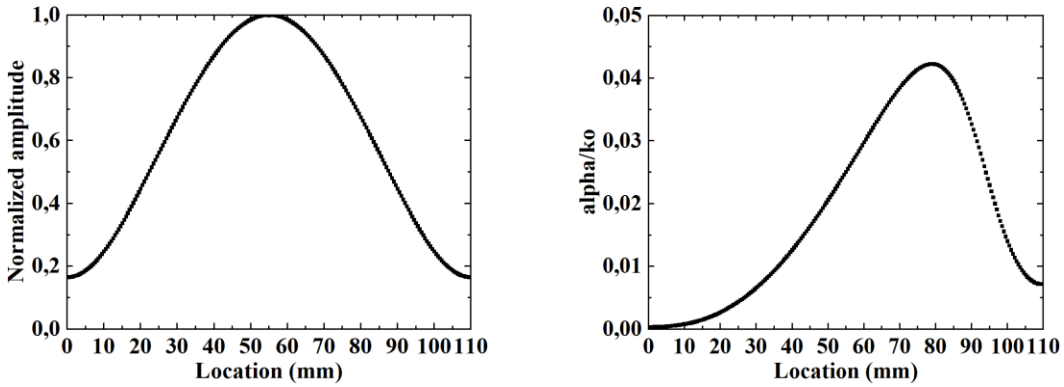

(a) (b)

Figure 3.7 (a) Normalized aperture amplitude distribution with -35 dB SLL of Taylor line-source distribution. (b) Corresponding normalized attenuation constant distribution along the length of the designed LWAs

(© 2020 IEEE, reproduced with permission)

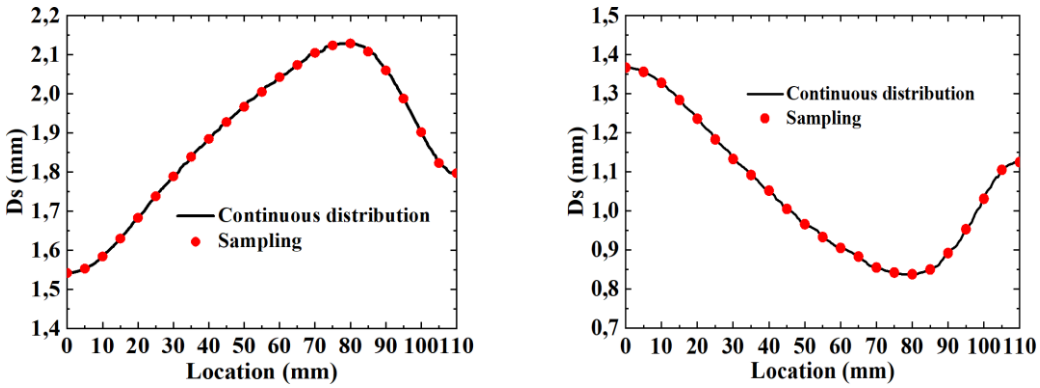

(a) (b)

Figure 3.8 Offset (*Ds*) distribution of long slots along the length of the designed LWAs for (a) *Type I* and (b) *Type II*

Equal-spaced sampling method with a distance of 5 mm is employed to simplify modeling and fabrication procedures. (© 2020 IEEE, reproduced with permission)

3.4 Modeling, Simulation, and Measurement

Based on the data shown in Figure 3.8, two types of meandering long slots LWAs can be modeled. Since the proposed antennas are based on the TE_{20}-mode SIW, it is critical to effectively excite the required TE_{20} mode while highly suppress the harmful TE_{10} mode. The feeding mechanisms proposed in [43][207][208] are not suitable due to large spurious radiation, while the one reported in [36] is essentially narrow-band. Here, a 3-dB directional coupler and a 90° phase shifter are

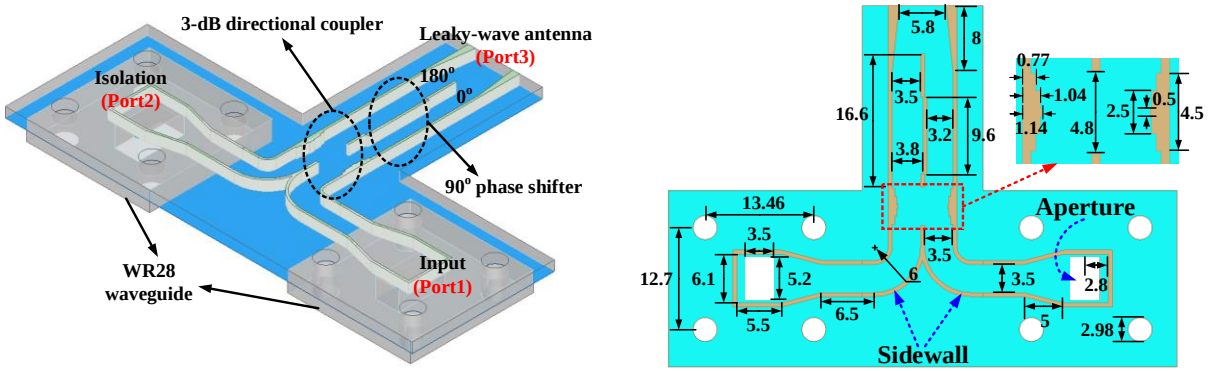

(a) (b)

Figure 3.9 Designed TE_{20}-mode exciter to excite the required TE_{20} mode of an SIW

(a) 3-D view (the top metal layer is hidden). (b) Top view (the top metal layer and substrate are hidden). All the parameter values are in the unit of mm. Continuous metallic sidewalls are employed here to facilitate model construction and simulation. (© 2020 IEEE, reproduced with permission)

combined together to work as a TE_{20}-mode exciter [209], as shown in Figure 3.9. Standard WR28 waveguides are used to work as the feeder and termination to avoid spurious radiation from feed discontinuity that can spoil antenna performances (especially the side-lobe and cross-polarization levels). Simulated *S*-parameters of the proposed TE_{20}-mode exciter are plotted in Figure 3.10, indicating that in a wide frequency band from 32 to 38 GHz, an excellent mode transformation from TE_{10} mode to TE_{20} mode is achieved. Meanwhile, a good mode suppression of the TE_{10} mode of the SIW is also observed. It is important to mention that the TE_{10} mode excited in the proposed antenna only contributes to cross-polarization components, according to the illustration of Figure 3.3 and 3.5. The reflection coefficient of the input port is better than 15 dB and the isolation

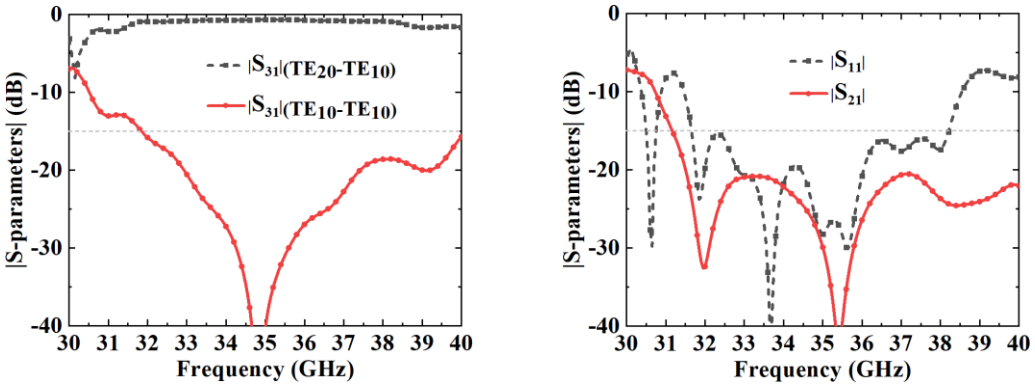

(a) (b)

Figure 3.10 Simulated *S*-parameters of the proposed TE_{20} mode exciter

(a) Transmission coefficients. (b) Reflection coefficient and isolation. Definition of the three ports can be found in Figure 3.9(a). (© 2020 IEEE, reproduced with permission)

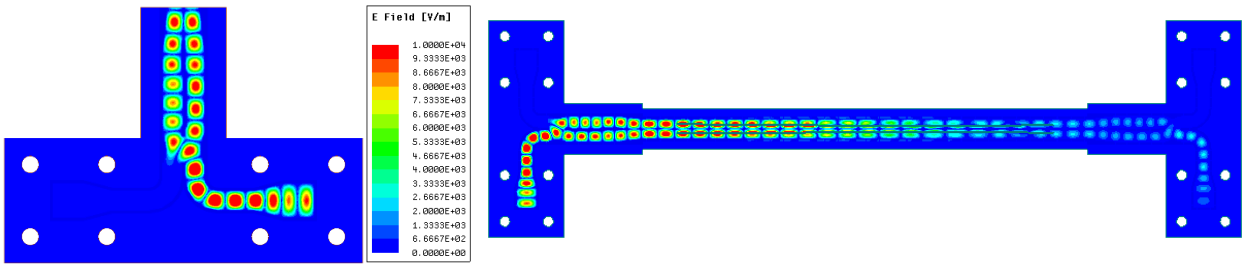

(a) (b)

Figure 3.11 E-field distributions of (a) the proposed TE_{20}-mode exciter and (b) one of the proposed LWAs at the design frequency of 35 GHz

(© 2020 IEEE, reproduced with permission)

between port1 and port2 is larger than 20 dB, from 32 GHz to 38 GHz. The simulated E-field distributions of the proposed TE_{20} mode exciter and one of the proposed antennas at 35 GHz are illustrated in Figure 3.11. It indicates that both a good TE_{20} mode conversion and a good TE_{10} mode suppression are achieved simultaneously, while a perturbed TE_{20} mode (leaky mode) is propagating along the leaky structure.

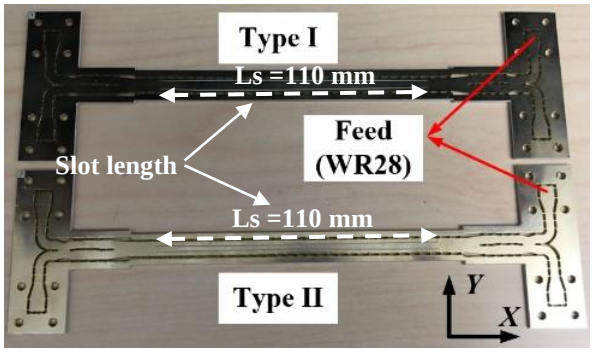

Figure 3.12 Photographs of the fabricated two types of LWAs

The substrate used here is Rogers RT/duroid 6002 with a relative permittivity of 2.94, a dielectric loss tangent of 0.0012 and a thickness of 1.524 mm. (© 2020 IEEE, reproduced with permission)

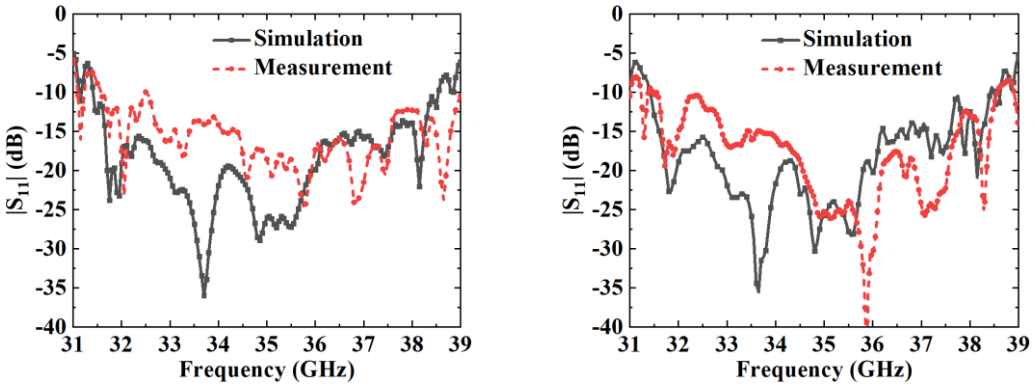

(a) (b)

Figure 3.13 Simulated and measured $|S_{11}|$ of the proposed LWAs

(a) Type I. (b) Type II. (© 2020 IEEE, reproduced with permission)

Two prototypes of the proposed LWAs are fabricated through standard single-layer PCB process, as shown in Figure 3.12, whereas their corresponding simulated and measured $|S_{11}|$ are plotted in Figure 3.13. Each of the proposed antennas has four ports with only one port working as a feeder while the other three terminated with matching loads. Both simulated and measured results indicate that a good impedance matching is achieved from 33 to 37 GHz under the criterion of -10 dB, for both of the two types of prototypes. Simulated and measured H-plane radiation patterns in terms of co-pol and cross-pol at several frequencies (i.e., 33 to 37 GHz with a step of 1 GHz) are plotted

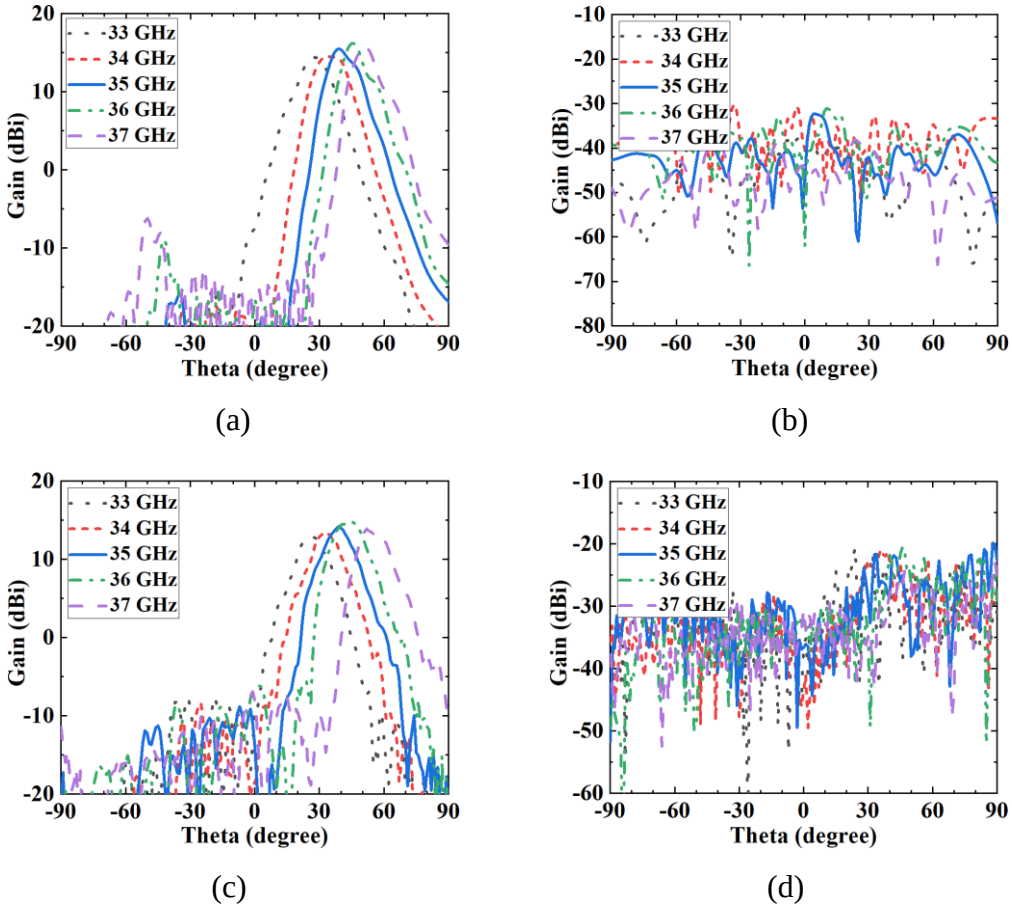

Figure 3.14 Simulated and measured H-plane radiation patterns at several frequencies for *Type I* LWA

(a) Simulated co-polarization. (b) Simulated cross-polarization. (c) Measured co-polarization. (d) Measured cross-polarization. (© 2020 IEEE, reproduced with permission)

in Figure 3.14 and Figure 3.15 for the proposed *Type I* and *Type II* LWAs, respectively. Their specific radiation performances are tabulated separately in Table 3.1 and 3.2. Notably, for the two types of LWAs, cross-polarization levels of almost lower than -50 dB are achieved in the simulations at each main beam direction, while those measured counterparts are lower than -37 dB. The simulated SLLs at the center frequency of 35 GHz are -31.3 dB and -30.6 dB for the *Type I* and *II* antennas, respectively, thereby manifesting the correctness and effectiveness of the performed low side-lobe design procedure. Their measured counterparts are merely -23.1 dB and -22.9 dB, respectively, which may be caused by the fabrication error and measurement issue.

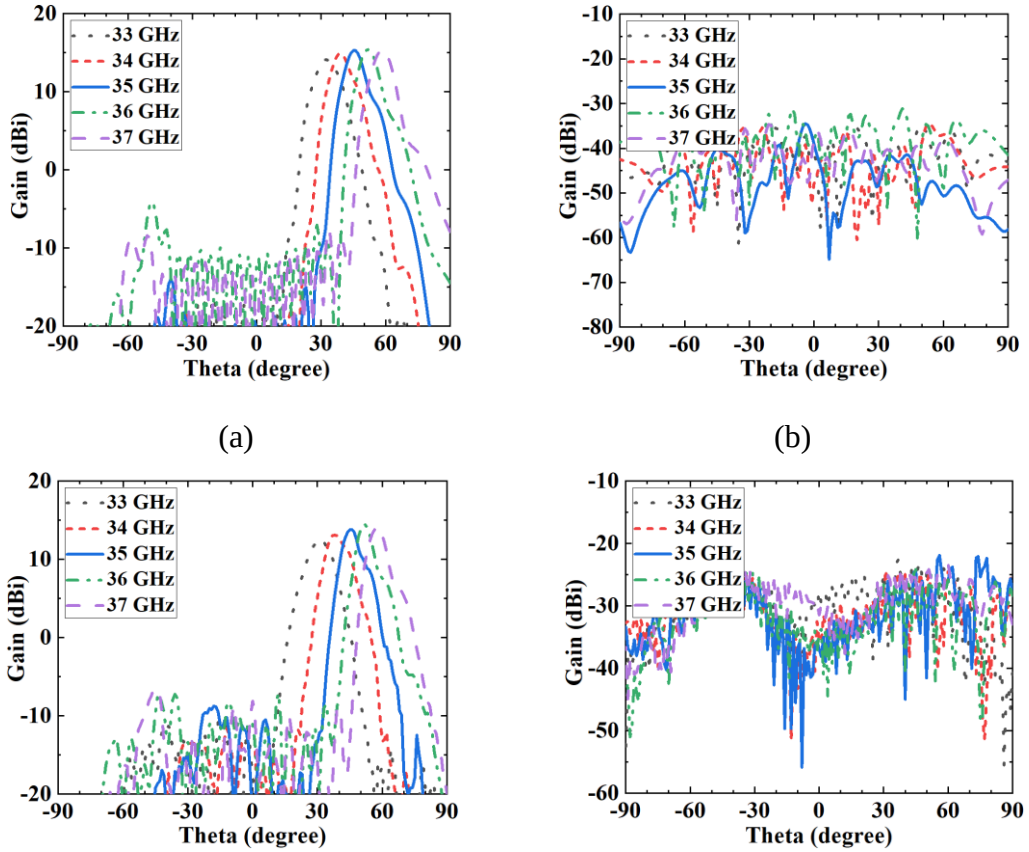

Figure 3.15 Simulated and measured H-plane radiation patterns at several frequencies for *Type II* LWA

(a) Simulated co-polarization. (b) Simulated cross-polarization. (c) Measured co-polarization. (d) Measured cross-polarization. (© 2020 IEEE, reproduced with permission)

Simulated radiation patterns in the E-plane (i.e., the cross-sectional plane along the angle of maximum radiation) at 35 GHz for the proposed LWAs are shown in Figure 3.16. The 3-dB beamwidth for *Type I* and *II* LWAs are 69.2° and 99.1°, respectively, while their cross-polarization levels are all less than -25 dB. It is interesting to find that *Type I* has a narrower beamwidth that *Type II*, and this can be explained by the fact that a wider distance between two radiating line-sources is possessed by *Type I* LWA [16][47]. The measured main beam direction is scanned from 27° to 53° and from 31° to 59° within 33 to 37 GHz for *Type I* and *II* antennas, respectively, showing

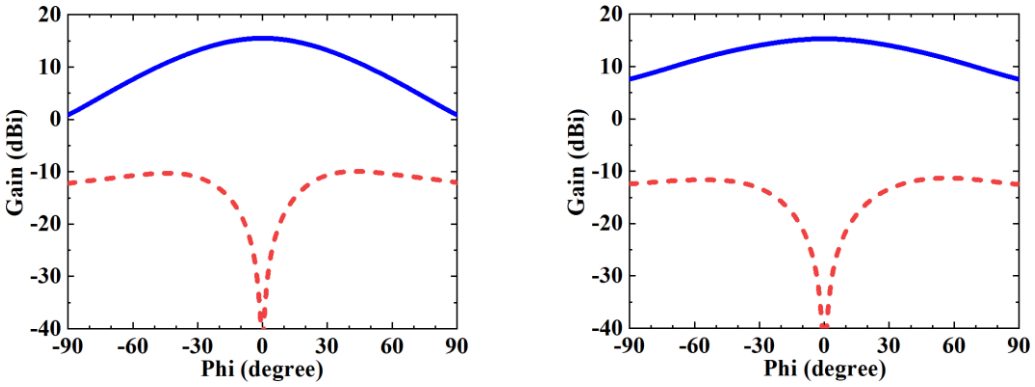

Figure 3.16 Simulated cross-sectional E-plane radiation patterns at 35 GHz with respect to (a) *Type I* and (b) *Type II* LWAs at their corresponding maximum radiation directions

Solid and dashed lines represent co-polar and cross-polar components, respectively. (© 2020 IEEE, reproduced with permission)

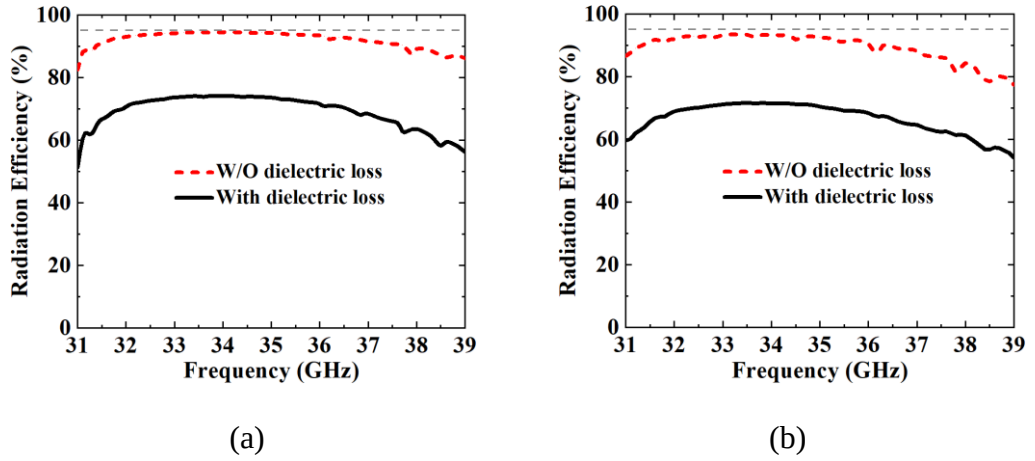

Figure 3.17 Simulated radiation efficiencies of the proposed LWAs with/without dielectric loss

(a) *Type I*. (b) *Type II*. (© 2020 IEEE, reproduced with permission)

a good agreement with simulated counterparts. As for the gain performances, the measured ones exhibit a little but acceptable drop that may be caused by increased dielectric and conductor losses, and the loss from connectors. Since the dielectric loss accounts for majority of losses mechanism in most SIW-based designs (this is especially true for thick SIW as the proposed design employed),

Figure 3.17 depicts simulated radiation efficiencies of the proposed LWAs with/without dielectric loss. It can be seen that for each type LWA, the radiation efficiency is approximately 95% at the design frequency of 35 GHz if the dielectric loss is neglected. It agrees well with the designated one, thereby further manifesting the correctness of low side-lobe design procedure implemented above. Comparatively, the practical radiation efficiency with all losses taken into account only has an average value of about 71% in the working frequency band, which is reasonable and acceptable in millimeter-wave frequency band [45].

3.5 Discussion and Comparison

The proposed work tactfully combines the benefits of a TE_{20} mode SIW and a meandering long slot LWA. First of all, the TE_{20} mode SIW has several advantages compared to its TE_{10} mode counterpart, such as higher performance stability, higher fabrication tolerance, lower fabrication cost, etc. Secondly, the odd-symmetry of E-fields distribution of a TE_{20} mode SIW is artfully used to design an LWA consisting of two even-symmetrical meandering long slots etched on the top surface of the SIW to simultaneously realize both low side-lobe and low cross-polarization. In order to highlight the benefits of the proposed design compared to other similar works, a comparison table has been tabulated in Table 3.3. Compared to the proposed works in [21]-[23][46] that use complex multi-layer ridged SIWs or bulky metallic ridged waveguides to implement the long slot LWAs with low side-lobe and low cross-polarization, the present work just makes use of low-cost single-layer PCB process to achieve comparable performances. Thus, this work possesses the merits of low fabrication cost and complexity, and high fabrication precision, especially suitable for mass production and planar integration in microwave and millimeter-wave systems. Meanwhile, it can be found that the proposed work has improved side-lobe and cross-polarization levels than [42][43][47][48][206]. Also note that this proposed work can be regarded as a two-element line-source array since it has two radiating magnetic line-sources, which can narrow its beamwidth in the E-plane and improve the directivity potentially, compared to those single-line-source LWAs [21]-[23][42][45][46][48][117][205][206]. Furthermore, in contrast to those similar two-line-source LWAs [27][43][47], this work can not only achieve a controllably-low SLL, but also possess a flexible E-plane beamwidth, as well as no potential grating lobes or large side-lobes suffered in the cross-sectional E-plane. However, when making a self-comparison between the

Table 3.1 Simulated and Measured Radiation Properties for *Type I* Long Slots LWA (© 2020 IEEE, reproduced with permission)

Fre. (GHz)	**Mainbeam direction (degree)**		**Gain (dBi)**		**SLL (dB)**		**Cross-Polar Level (dB)**	
	Sim.	Mea.	Sim.	Mea.	Sim.	Mea.	Sim.	Mea.
33	27.9	27	14.4	12.9	-29.5	-20.5	-59.8	-43.6
34	33.6	33	14.5	13.5	-32.8	-21.9	-49.7	-38.1
35	39.1	38	15.5	14.2	-31.3	-23.1	-63.7	-42.2
36	45.5	45	16.2	14.8	-25.2	-20.4	-55.1	-37.4
37	51.1	53	15.8	13.9	-22.3	-20.8	-60.3	-41.5

Table 3.2 Simulated and Measured Radiation Properties for *Type II* Long Slots LWA (© 2020 IEEE, reproduced with permission)

Fre. (GHz)	**Mainbeam Direction (degree)**		**Gain (dBi)**		**SLL (dB)**		**Cross-Polar Level (dB)**	
	Sim.	Mea.	Sim.	Mea.	Sim.	Mea.	Sim.	Mea.
33	32.1	31	14.1	12.6	-30.2	-23.4	-59	-39.4
34	38.9	38	14.9	13.1	-32.7	-24.7	-58.3	-38.7
35	45.2	45	15.3	13.8	-30.6	-22.9	-57.8	-37.1
36	51.5	52	15.4	14.5	-22.4	-21.6	-50.5	-38.5
37	58.2	59	15.3	14.1	-23	-23.4	-54.4	-40.4

proposed two types of LWAs, *Type I* is able to provide a higher directivity and narrower E-plane beamwidth than *Type II*, as illustrated in Figure 3.16 and explained above.

3.6 Conclusion

In this chapter, longitudinally slotted TE_{20}-mode-driven SIW LWAs with low side-lobe and low cross-polarization have been proposed and demonstrated for millimeter-wave applications. Two types of LWAs differed by the meandering direction of the long slots have been developed and

fabricated. Both simulated and measured results are in a good agreement. The proposed antennas can combine the advantages of SIW higher-order modes and long slot LWAs and they may be a good candidate to develop an array in millimeter-wave systems for practical applications, e.g., a planar array with two-dimensional hybrid phase-frequency beam-scanning (pencil beam) for FMCW radars.

Table 3.3 A Comparison between Similar Works and the Proposed Designs (© 2020 IEEE, reproduced with permission)

Ref.	Fractional Bandwidth (%)	Beam-Scanning Range (degree)	Footprint (free-space λ_0 at the center frequency)	Cross-Polar Level (dB)	SLL (dB)	Gain (dBi)	Radiation Efficiency (%)	Line-Source & Operating Mode	Structural Technique
[26]	26.7	56	0.457	N/A	-20	N/A	N/A	Single (TE_{10})	Hybrid waveguide printed circuit
[45]	11.4	18.6	0.447	-38.9	-29.3	12.7	66.1		Single-layered SIW
[117]	N/A	N/A	0.344	-39	-20	18	89.9		
[46]	20	30	0.432	-27	-28	14.6	90.5		Multi-layered SIW
[21]	30.8	32.4	0.624	-41.9	-26.3	16.5	88		Ridged/Stepped RWG
[23]	37.8	20	0.648	-30	-20	N/A	N/A		
[48]	21.5	53	0.515	-7	-11	10.9	90		Single-layered SIW
[42]	5.5	9	0.381	N/A	-10	11.4	N/A	Single ($TE_{0.5, 0}$)	
[43]	19.4	N/A	1.653	-20	-8	9.3	N/A	Dual (TE_{20})	
[47]	3	N/A	0.786	-26	-11	15.1	N/A		
Type I	11.4	26	0.677	-42.2	-23.1	14.2	73.7		
Type II	11.4	28	0.677	-37.1	-22.9	13.8	72.1		

CHAPTER 4 ARTICLE 2: TRANSVERSELY SLOTTED SIW LEAKY-WAVE ANTENNA FEATURING RAPID BEAM-SCANNING FOR MILLIMETER-WAVE APPLICATIONS

Dongze Zheng, Yue-Long Lyu, and Ke Wu

Published in the *IEEE Transactions on Antennas and Propagation*, vol. 68, no. 6, pp. 4172-4185, Jun. 2020.

Loading effects of RDs have been explored to increase the phase constant' frequency sensitivity of LWAs, based on which a quasi-uniform transversely slotted substrate integrated waveguide LWA featuring rapid beam-scanning and its hexagonal array have been proposed and investigated for millimeter-wave applications. The design concept is simply based on the use of a short period of unit cells and a long transverse slot with a sharp inductive reactance, and it has been elaborated theoretically and validated effectively by both full-wave and circuit-based simulations. A taper design with -25 dB Taylor amplitude distribution is implemented for the proposed LWA to have a low side-lobe radiation. For practical system applications, a hexagonal array consisting of six proposed LWAs is developed to provide an omnidirectional coverage in the azimuth plane while remaining the rapid frequency-driven beam-scanning in the elevation plane. Both measured and simulated results are in an acceptable agreement with respect to the LWA block and the associated hexagonal array in terms of circuit and radiation performances. The proposed antenna will be a good candidate to be applied for prospective millimeter-wave systems such as autonomous driving and flying.

4.1 Introduction

As a special class of travelling-wave radiating structures, LWAs have been attractive and inspiring since decades for microwave and millimeter-wave applications such as automotive radar, sensor and wireless communication systems. This is attributed to their numerous appealing features, i.e.,

low profile, simple feeding mechanism, high directivity, narrow beam and frequency beam-scanning capability [9][11][210]. LWAs, in which gradually leaking-out travelling waves are guided along specific wave-guiding structures, can be regarded as a special kind of lossy TLs where majority of losses are in the form of radiation. Interestingly, they can also be interpreted as a series-feeding antenna array where the antenna elements and feeder are seamlessly integrated together. Various TLs have been used to develop different types of LWAs since the 1940s, including the RWG [13][19][20], microstrip line [27]-[36], CPS or CPW [37]-[41], SIW [42]-[65], and SSPPs or goubau lines [66]-[76]. Generally, all the LWAs mentioned above are formed by loading radiating discontinuities or perturbations into original TLs in a continuous or periodic manner, based on which they can be classified into three categories, i.e., uniform, quasi-uniform and periodic LWAs [9][11]. Radiating discontinuities in an LWA should be explicitly analyzed since they are critical for determining the complex propagation constants of the related leaky mode, i.e., they are not only responsible for controlling leakage radiation, but also closely linked to the phase constant of leaky structures.

In practical application scenarios such as traffic-monitoring, automotive collision avoidance, autonomous driving and flying systems, their bandwidth of operation is mainly subject to the antenna components, which are normally constituted of narrowband-natured standing-wave series-fed antenna arrays (e.g., slotted waveguide or series-fed patch antenna arrays) [211]-[214]. Fortunately, in such cases, a desirable wide beam-scanning range aimed for a wide space coverage of target-detection can still be realized with the help of phase shifters or beam-forming networks. Compared to standing-wave series-fed arrays, LWAs are capable of providing a wide beam-coverage as well where the desirable beam-scanning is simply driven by frequency, thereby avoiding the use of expensive phase shifters or complex beam-forming networks. Unfortunately, most LWAs suffer from “slow beam-scanning”, which means that their wide beam-coverage is at the expense of a wide operating frequency bandwidth. As a suitable replacement for standing-wave arrays, promising LWAs should possess a large beam-scanning range within a small fractional frequency bandwidth (i.e., rapid frequency beam-scanning) to relieve the strict bandwidth requirements on front-end system components without sacrificing space-detecting coverage, economize on spectrum resources and also provide a possibility for fast-tracking in radar systems [193][195].

Few works have been reported so far to design LWAs with a rapid beam-scanning property [136]-[154], and they may be classified into three basic types. The first type, as proposed in [136]-[138][153][154], makes use of higher-order (e.g., 2^{nd} or 3^{rd} order) space harmonics of periodic LWAs to perform the beam-scanning. In these cases, higher-order space harmonics are realized by using meandering feedlines between adjacent radiating elements. They are able to provide more phase variations over a given frequency increment (Δf) by enlarging the meandering degree of feedlines, and this will be explained particularly in the next section of this chapter. Note that the works reported in [139]-[140], in which specially designed phase shifters featuring sensitive phase-frequency response were introduced between radiating elements to increase beam-scanning rate, also generally share the similar principle as the aforementioned method. Another approach is based on the use of highly dispersive slow-wave structures to construct periodic LWAs as they have improved effective media parameters (i.e., permittivity and permeability) compared to normal TLs, thereby possessing steeper phase constant versus frequency and enhanced beam-scanning rate [144][146]. The third approach depends on the creation of a stopband close to the cut-off of a leaky mode, due to which the leaky mode's phase constant can be sharpened with exhibiting a strong dispersion and thus the beam-scanning rate is improved. For example, by loading shorting vias to an EH_1 mode-based microstrip LWA, a strong stopband is deliberately created and located near the cut-off of the EH_1 mode [145]. Similarly, a high-impedance-surface (HIS)-loaded hollow waveguide LWA is able to embrace a rapid beam-scanning if the resonance condition introduced by the HIS is placed close to the cut-off of the related leaky mode of the hollow LWA [147].

On the other hand, it is promising and attractive if a radar system is capable of providing a 360^o omnidirectional coverage in the azimuth plane and a beam-scanning capability in the elevation plane, for the purpose of reducing blind spots and achieving a full-space detection. This will be very useful in autonomous driving and flying systems for obstacle avoidance, self-localization and mapping. Also, it has the potential to be used in wireless and satellite communication systems, as well as radar imaging. Although several ground-free LWAs reported in [66][72][73][91] can be used to provide a full-coverage in the azimuth plane and a frequency-scanned beam in the elevation plane, they suffer from slow beam-scanning rate, complex feeding mechanism and difficulty in current system integration. Thus, they are unsuitable for practical millimeter-wave system applications.

In this chapter, impedance/admittance properties (i.e., loading effects) of radiating discontinuities are analyzed in detail and then related to an LWA with respect to its frequency sensitivity of the phase constant. The proposed design is simply based on SIW unit cells characterized by short period length and long transverse slots with sharp inductive reactance. Theoretical analysis based on a simplified equivalent circuit model of the unit cell is performed, and both circuit-based and full-wave simulations are conducted to verify the design concept. In order to have a low SLL radiation, a taper illumination with -25 dB Taylor amplitude distribution is implemented for the proposed SIW LWA. Part of the work described in this chapter can be found in [141], which is merely a preliminary design that was not elaborated in depth and systemically. In addition, a three-dimensional (3-D) hexagonal array consisting of six proposed LWA building blocks is developed to provide an omnidirectional coverage in the azimuth plane while remaining a rapid frequency-driven beam-scanning in the elevation plane for system applications. Both measured and simulated results are in an acceptable agreement with respect to the LWA blocks and the associated hexagonal array in terms of circuit and radiation performances.

4.2 Theory and Principle

4.2.1 Beam-Scanning Properties of LWAs

According to the general LWA theory [9][11], the main beam direction of an LWA can be determined by its effective phase constant, and the related formula is given as follows:

$$\theta_{MB} \approx \sin^{-1}(\beta_{eff} / k_0) \tag{4.1}$$

where θ_{MB} is the main beam direction (as a function of working frequency f) measured from the broadside, k_0 is the free-space wavenumber, and β_{eff} is the effective phase constant of the leaky mode responsible for radiation. It should be noted that the definition of β_{eff} is flexible, depending on the types of LWAs. For example, it can be defined as the phase constant of the fundamental mode (space-harmonic) for uniform or quasi-uniform LWAs; it can also represent the phase constant of a higher-order space harmonic (e.g., -1st order) for periodic LWAs. It is easy to understand that in order to have a larger beam-scanning range over a given frequency band, the derivative of θ_{MB}, expressed as θ'_{MB}, should have a larger value and it is determined by

$$\theta'_{MB} \approx (\beta_{eff}/k_0)' \Big/ \sqrt{1-(\beta_{eff}/k_0)^2} \tag{4.2}$$

Thus, for a given frequency or beam direction, the one with a larger $(\beta_{eff}/k_0)'$ will have a larger θ'_{MB}. Equivalently, if an LWA can have a larger slope of the effective phase constant β_{eff} or normalized effective phase constant β_{eff}/k_0 over frequency, a wider beam-scanning range can be realized in a given frequency range, i.e., the rapid beam-scanning property. Bear this remark in mind as it will run through this chapter.

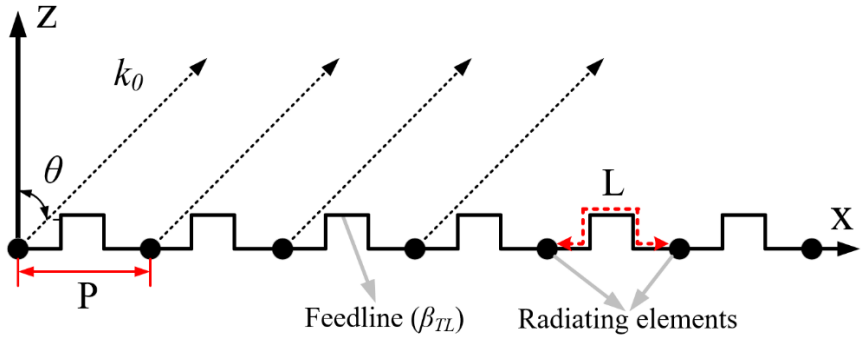

Figure 4.1 Illustration of a generalized periodic LWA

This is applicable to all LWAs that have periodic appearances along wave-guiding structures, including both quasi-uniform and traditional periodic LWAs. (© 2020 IEEE, reproduced with permission)

4.2.2 General Approaches for Rapid Beam-Scanning

Since the beam-scanning rate of an LWA is only concerned with the slope of its effective phase constant β_{eff} or normalized effective phase constant β_{eff}/k_0, general approaches are discussed here to improve such a parameter in this subsection.

Figure 4.1 depicts a generalized periodic LWA. The free-space distance between two adjacent radiating elements (i.e., periodic perturbations or discontinuities) is denoted as P, while the length of the feedline between the two is represented by L. The periodic loading effects of radiating elements on the feedline are ignored here for simplified analysis, and they will be separately considered later. According to traditional antenna array theory [16], the phase difference ψ between two adjacent radiating elements in the far field can be expressed as

$$\psi = -\beta_{TL} L + k_0 P \sin\theta \tag{4.3}$$

where β_{TL} represents the original (unperturbed) phase constant of the feedline. When $\psi = 2n\pi$, n=0, ±1, ±2, …, the array factor can reach its maximum, corresponding to the main beam with a direction of θ_{MB} measured from broadside. Thus, we have

$$\begin{aligned} k_0 \sin\theta_{MB} &= (\beta_{TL} L + 2n\pi)/P \\ &= \beta_{TL} L/P + 2n\pi/P \end{aligned} \tag{4.4}$$

Since the condition of $L \geq P$ is always satisfied and normally β_{TL} is larger than k_0 (i.e., slow wave) for most TLs (e.g., microstrip line, CPS and SIW) in the design of periodic LWAs, the main beam direction θ_{MB} has a real value only if the parameter n in (4.4) is negative. When n = -1, it corresponds to the well-known -1st order space harmonic in periodic LWAs. It is interesting to note that this interpretation of space harmonics of periodic LWAs is simply derived from traditional antenna array theory, and it can be used as a supplementary understanding of the radiation mechanism of periodic LWAs [9][11]. When making a comparison between (4.1) and (4.4), we can express

$$\beta_{eff} = \beta_{TL} L/P + 2n\pi/P \tag{4.5}$$

Therefore, we can formulate the derivative of βeff as

$$\beta'_{eff} = \beta'_{TL} L/P \tag{4.6}$$

It is concluded from (4.5) and (4.6) that (i) all the space harmonics of a periodic LWA have the same slope of the effective phase constant at the same frequency point; (ii) in order to improve β'_{eff}, the original phase constant β_{TL} of a TL should have a large slope, and the length ratio L/P should exhibit a large value, if possible. In principle, β'_{TL} is determined by the chosen substrate material and working frequency region (this is especially for waveguide-based structures having non-TEM propagating modes and cut-off features). For example, for the rectangular waveguide or SIW working in its dominant TE_{10} mode, the slope of its phase constant β'_{TL} can be expressed by

$$\beta'_{TL} = \sqrt{\frac{\varepsilon_r}{c^2\left[1-(f_c/f)^2\right]}} \tag{4.7}$$

where ε_r is the relative permittivity of the filling material, c is the light speed in the free-space, and f_c is the cut-off frequency of the dominant TE_{10} mode. It can be seen from (4.7) that using a substrate with a larger relative permittivity is beneficial for obtaining a larger β'_{TL}. For those TEM or quasi-TEM TLs such as the coaxial cable, microstrip line and CPS, this guideline is applicable as well. It is interesting to mention that slow-wave structures, which usually have a large effective permittivity or permeability that leads to the enhancement of sensitivity of the phase constant, also generally fall into this group. Several works reported in [144][146] are based on this principle to increase the beam-scanning rate of LWAs, as mentioned previously. In addition, it can also be found from (4.7) that choosing the working frequency range closer to the cut-off is able to provide a larger β'_{TL}. On the other hand, when it comes to (4.5) and (4.6) again, it is seen that increasing the length ratio L/P (≥ 1) is also a wise choice for LWAs with beam-scanning rate enhancement. Notably, when the length ratio L/P has a large value, the integer n in (4.5) normally has a large negative value (e.g., $n \leq -2$), corresponding to higher-order space harmonics in periodic LWAs. The related works can be found in [136]-[138][153][154].

4.2.3 Specific Approaches for Rapid Beam-Scanning—Loading Effects of Radiating Discontinuities

Several approaches have been described explicitly in Chapter 4.2.2 to provide a general guideline to improve the beam-scanning rate of LWAs. Note that in (4.4) β_{TL} can also be smaller than k_0 (i.e., fast wave) and this corresponds to quasi-uniform LWA that uses the fundamental space harmonic to radiate [i.e., integer n in (4.4) is set to 0]. For example, the works in [14][50][52] belong to this category. The loading effects introduced by periodic radiating discontinuities, however, have not been considered in the above analysis. In this subsection, a specific approach based on the use of loading effects of radiating discontinuities to increase the slope of the leaky mode's phase constant and associated beam-scanning rate is proposed and demonstrated.

As an implementation of generalized periodic LWAs illustrated in Figure 4.1, two kinds of typical LWA unit cells and their related equivalent circuit models are depicted in Figure 4.2. The first is a transversely slotted SIW LWA unit cell, while the other is a microstrip combline counterpart. It is obvious that the two unit-cells shown here are totally different in terms of TLs (i.e., SIW and microstrip line), RDs (i.e., slot and stub) and equivalent circuit models (i.e., series- and shunt-type).

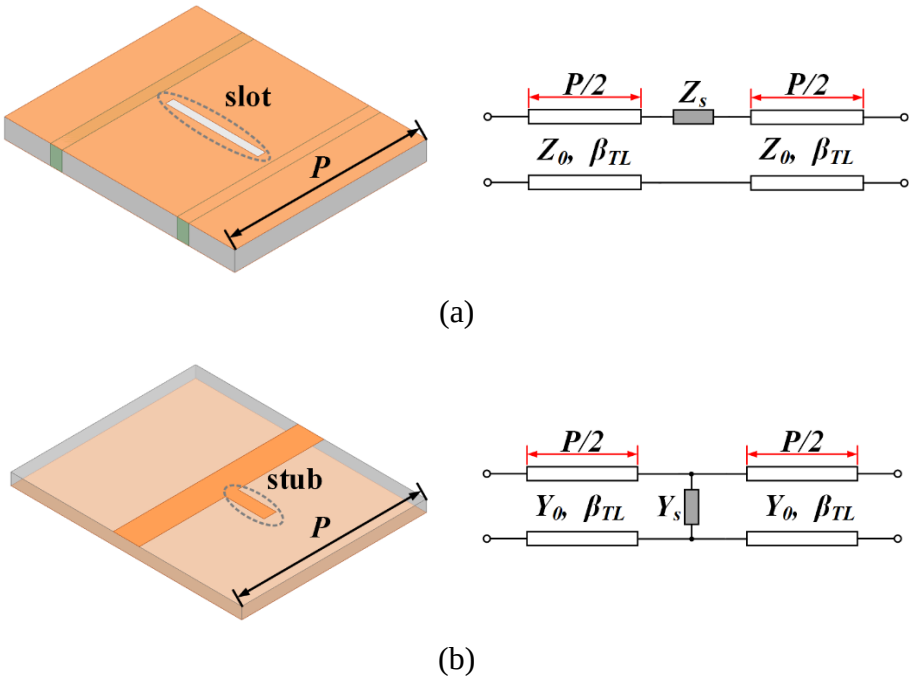

Figure 4.2 Two typical LWA unit cells and their related equivalent circuit models

(a) Transversely slotted SIW LWA unit cell and its series-type circuit model. (b) Microstrip combline LWA unit cell and its shunt-type circuit model. Z_s and Y_s represent loading effects introduced by the slot and stub, respectively. (© 2020 IEEE, reproduced with permission)

More importantly, they can represent most periodic LWAs in the open literature. Note that the two kinds of circuit models are complementary with each other, satisfying the duality theorem [48]. Because of this, they observe the same analysis procedure. Thus, only the series-type circuit model, as shown in Figure 4.2(a), is analyzed in the following for brevity.

Figure 4.3(a) depicts the geometry of a conventional transversely slotted SIW LWA consisting of a number of unit cells like the one in Figure 4.2(a). In order to highlight the loading effects of RDs (i.e., slots), an SIW fabricated in a low relative permittivity substrate is used as the host TL. Specifically, the SIW is designed on a substrate with relative permittivity of ε_r=2.94 and thickness of h = 0.508 mm. Two rows of plated via-slot or trench arrays are employed to form the SIW sidewalls. The distance between adjacent plated via-slots is represented as d and the period of the plated via-slot array is denoted as S. The length and width of the transverse slot are represented as

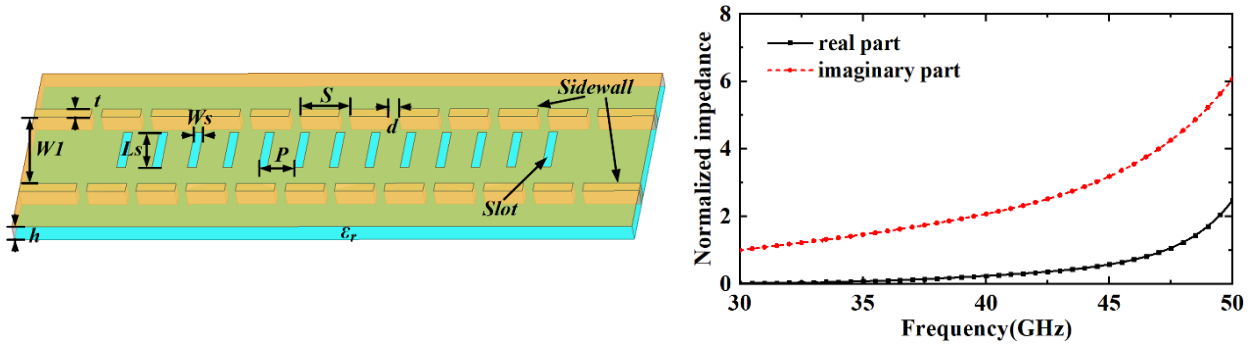

(a) (b)

Figure 4.3 (a) Geometry of a conventional transversely slotted SIW LWA. (b) Normalized impedance of a transverse slot etched on an SIW

Ls and *Ws*, respectively, while the period of these transverse slots is *P*. It can be found that the length ratio "*L*/*P*" defined in the last subsection is unity here and thus it does not contribute to improving the beam-scanning rate. This can further emphasize the role of RDs in shaping the leaky mode's effective phase constant. As shown in Figure 4.2(a), the transverse slot can be modeled as a series impedance (Z_s) consisting of a typical parallel *RLC* resonator (i.e. *Rs*, *Ls* and *Cs*, which are not shown for brevity). S-parameters of the two-port network (the unit cell), according to [18], can be expressed by

$$S_{unit} = \begin{pmatrix} S_{11} & S_{12} \\ S_{21} & S_{22} \end{pmatrix} = \begin{pmatrix} \dfrac{Z_S/Z_0}{2+Z_S/Z_0} e^{-j\beta_{TL}P} & \dfrac{2}{2+Z_S/Z_0} e^{-j\beta_{TL}P} \\ \dfrac{2}{2+Z_S/Z_0} e^{-j\beta_{TL}P} & \dfrac{Z_S/Z_0}{2+Z_S/Z_0} e^{-j\beta_{TL}P} \end{pmatrix} \tag{4.8}$$

where Z_0 and β_{TL} represent the characteristic impedance and phase constant of the host TL, e.g., the original SIW without slot perturbation. Consequently, the phase delay of the whole unit cell can be derived as

$$-\arg(S_{21}) = \beta_{TL}P + \arg(2+Z_S/Z_0)$$

$$= \beta_{TL} P + \varphi_s(f) \tag{4.9}$$

where $\varphi_s(f) = \arg(2 + Z_s / Z_0)$. It is observed from (4.9) that the phase delay of the whole unit cell results from two contributions: the original phase delay of the host TL and the one introduced by the discontinuity, namely, $\varphi_s(f)$. Note that this is generally applicable to all LWAs having periodic appearances. When Z_s is inductive (i.e., $\mathrm{im}(Z_s)>0$), the phase delay of the unit cell is increased compared to that of the host TL; on the contrary, its phase delay is decreased if Z_s is capacitive. The effective phase constant β_{eff} of the unit cell can be approximately derived as

$$\begin{aligned} \beta_{eff} &\approx -\arg(S_{21})/P \\ &= \beta_{TL} + \varphi_s(f)/P \end{aligned} \tag{4.10}$$

The slope of the effective phase constant of an LWA, according to (4.10), can thus be expressed by

$$\beta'_{eff} \approx \beta'_{TL} + \varphi'_s(f)/P \tag{4.11}$$

The general approaches to increasing β'_{TL} have already been described in the last subsection. Here, we only consider the contribution from the radiating discontinuity for improving β'_{eff} of an LWA. From the second item in (4.11) we can conclude that a large β'_{eff} can benefit from (i) decreasing P and/or (ii) increasing $\varphi'_s(f)$. The method regarding decreasing P to increase β'_{eff} is obvious. Here, we consider $\varphi'_s(f)$, which can be expressed as

$$\begin{aligned} \varphi'_s &= \arg'(2 + Z_s / Z_0) \\ &= \arg'\left[2 + r(f) + jx(f)\right] \end{aligned} \tag{4.12}$$

where $r(f)$ and $x(f)$ represent the real and imaginary parts of the normalized impedance introduced by the radiating discontinuity, respectively. Based on the equivalent circuit model of the unit cell and the formula (4.8), the normalized impedance of the slot discontinuity can be easily calculated by simulating a unit cell in a simulator (e.g., *HFSS*) and using the following formula

$$\begin{aligned} Z_s / Z_0 &= r(f) + jx(f) \\ &= \frac{2S_{11}e^{j\beta_{TL}P}}{1 - S_{11}e^{j\beta_{TL}P}} \end{aligned} \tag{4.13}$$

in which a de-embedding to the slot center has already been analytically involved. During the extraction process, reference planes are placed at the two edges of the unit cell. As an alternative approach, however, the de-embedding can be directly conducted in simulators by shifting reference planes to the slot center. Both can yield the same result. Figure 4.3(b) shows the extracted normalized impedance of the slot when some specific values are assigned to the unit cell for simulation, i.e., *W1*=2.62 mm, *Ls*=2 mm, and *Ws*=0.25 mm. It can be found that the slot is more reactive rather than radiative and *r*(*f*) representing the radiation losses is extremely small. Normally, *r*(*f*) should be chosen with a small value to have a slowly attenuated travelling-wave propagating along the guided-wave structure over a frequency band of interest (e.g., 34-36 GHz in this design) [9]11]. Thus, (4.12) can be modified as

$$\begin{aligned} \varphi_s'(f) &\approx \arg'\left[2 + jx(f))\right] \\ &= \arctan'\left[x(f)/2\right] \\ &= \frac{1}{2 + \frac{x^2(f)}{2}} x'(f) \end{aligned} \tag{4.14}$$

From (4.14), it is straightforward to find that a larger $x'(f)$ would result in a larger $\varphi'_s(f)$, generally. Since the slope of the imaginary part of slot impedance is increasing with frequency before resonance as shown in Figure 4.3(b), a longer slot will give rise to a larger $x'(f)$ at a given frequency to some extent, and thus a larger $\varphi'_s(f)$ can be obtained subsequently. As a result, if a longer inductive slot is adopted in a slotted LWA, a larger slope of the effective phase constant of the leaky mode β'_{eff}, associated with a larger beam-scanning range, can be obtained at a given frequency bandwidth.

So far, it can be concluded that for an LWA unit cell having a series-type equivalent circuit model as shown in Figure 4.2(a), two instructive methods can be adopted to increase the beam-scanning rate, in addition to those general approaches that make use of high-permittivity substrates and/or choose the working frequency close to the cut-off as mentioned previously. That is to employ a radiating discontinuity characterized with a sharp inductive reactance versus frequency, together with a short period length of unit cells. On the other hand, for an LWA unit cell having a shunt-type equivalent circuit model like the one shown in Figure 4.2(b), the similar remarks can be easily

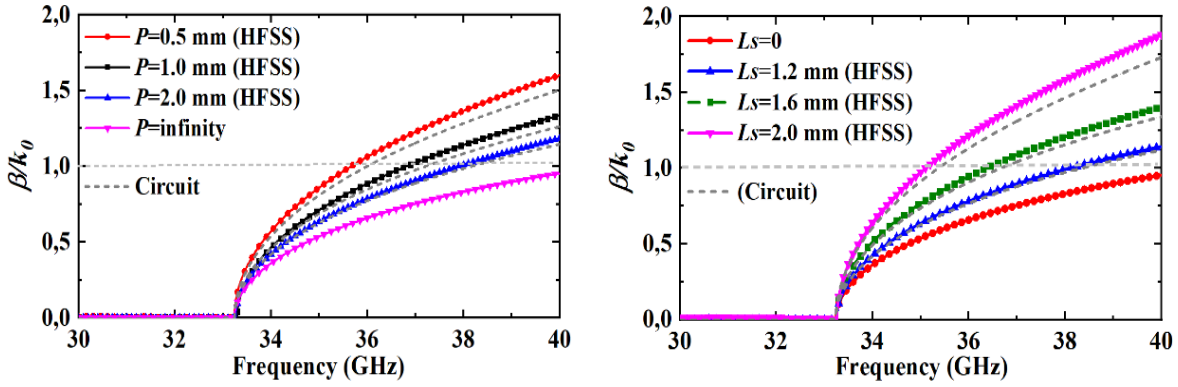

(a) (b)

Figure 4.4 Normalized effective phase constants extracted from full-wave and circuit simulations with respect to different (a) *P* (*Ls*=1.8 mm), and (b) *Ls* (*P*=0.5 mm)

P=infinity and *Ls*=0 represent the cases for the SIW without slot perturbations, i.e., original SIW TL. (© 2020 IEEE, reproduced with permission)

generalized according to the duality theorem: to employ a radiating discontinuity characterized with a sharp capacitive susceptance versus frequency, together with a short period length of unit cells. It is interesting to note that these remarks can be applied to most LWAs having periodic appearance only if they have such kinds of equivalent circuit models.

In order to verify this design concept, a transversely slotted SIW LWA consisting of such unit cells has been implemented, aimed at the target frequency band from 34 to 36 GHz. A unit cell truncated from Figure 4.3(a) is simulated with pre-designated parameters of *W1*=2.62 mm and *Ws*=0.25 mm, together with different slot length *Ls* and period *P*. The effective phase constant can be conveniently extracted from *S*-parameters of the unit cell based on Bloch-Floquet theorem [18], which can be expressed as

$$\beta_{\text{eff}} = \text{Im}\left[\arccosh\left(\frac{1 - S_{11}S_{22} + S_{21}S_{12}}{2S_{21}}\right) \Big/ P \right] \tag{4.15}$$

The normalized effective phase constants extracted from both full-wave and circuit-based simulations are depicted in Figure 4.4. It can be found that when either increasing the slot length *Ls* or decreasing the unit period length *P*, the effective phase constant becomes steeper and the fast-

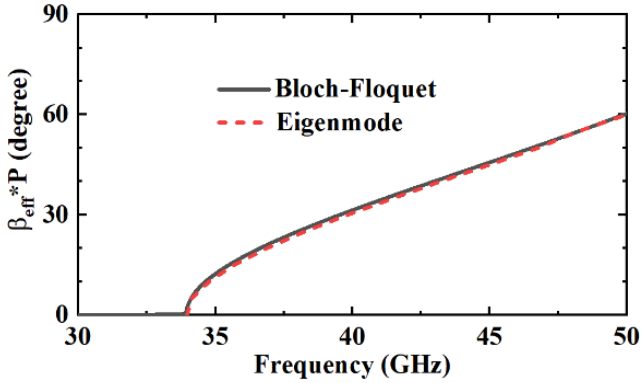

Figure 4.5 Dispersion diagrams of the proposed slotted SIW LWA unit cell, which are separately calculated by Bloch-Floquet theorem and Eigenmode approaches

The unit cell is selected with *P*=0.5 mm, *Ls*=1.6 mm, and *Ws*= 0.25 mm for demonstration. (© 2020 IEEE, reproduced with permission)

wave region is narrower. This is consistent with the theoretical analyses and conclusions drawn above, thereby indicating that a wider beam-scanning coverage and rapid beam-scanning can be realized in the target frequency band with such specific approaches. Since the slot can be modeled as a parallel *RLC* resonator and its impedance can be easily obtained with the aforementioned extraction processes, a circuit simulation package such as Advanced Design System (ADS) is then used to do the circuit simulation, with these values of circuit components (i.e., *Rs*, *Ls* and *Cs*) conveniently acquired by using curve-fitting methods [28][37][40][56][145]. The circuit-based simulations are in a reasonable agreement with the full-wave simulated counterparts, and both can demonstrate the correctness and effectiveness of the proposed design concept in this sense. It is necessary to mention that all the conducted analyses and demonstrated remarks in the above are based on an isolated unit cell; mutual coupling effects among unit cells have not been considered. These simplified actions, generally, can draw only an approximate picture of operating mechanism of the structure, but have the advantage of giving significant insight on how the loading effects of RDs affect the effective phase constant of an LWA. Figure 4.5 depicts the calculated dispersion diagrams of the unit cell by using two different approaches, i.e., Eigenmode and Bloch-Floquet, with mutual coupling effects considered or not. Interestingly, it is illustrated that the two curves coincide well with each other. This indicates that the mutual coupling effects almost have no

influence on the dispersion properties of the unit cell, although the period of the unit cell is very short. The similar phenomenon can also be found in [38][40][52] that only the attenuation constant of an LWA will be influenced by the mutual coupling effects while the phase constant is almost free of that. Consequently, the simplified circuit model together with its relevant theoretical analyses and simulations (full-wave and circuit) in the above is justified and effective for demonstrating the proposed concept.

4.3 Transversely Slotted SIW LWA Featuring Rapid Frequency Beam-Scanning

4.3.1 Low Side-Lobe Design

General and specific approaches for beam-scanning rate enhancement have been described and studied in the last section. Loading effects of radiating discontinuities have been exploited to relate their impedance/admittance properties to the phase constant of the related leaky mode, and a transversely slotted SIW LWA featuring rapid beam-scanning is demonstrated. Since the period length of unit cells is much smaller than the guided-wavelength of the frequency of interest, the proposed LWA belongs to the quasi-uniform type. It is known that for a finite-length LWA having uniformly distributed radiating discontinuities without tapered design, it has an exponentially decaying amplitude illumination and thus a high SLL of approximately -13 dB is usually encountered [9][11]. In most practical applications, the aperture amplitude distribution on an LWA should be tapered to have a low SLL. Here, -25 dB Taylor line-source distribution is implemented on the proposed LWA. The distribution of attenuation constant along the LWA [i.e., $\alpha(x)$], according to [9], can be determined by

$$\alpha(x) = \frac{\left|A(x)\right|^2 / 2}{\frac{1}{e_r}\int_{-L_a/2}^{L_a/2}\left|A(\xi)\right|^2 d\xi - \int_{-L_a/2}^{x}\left|A(\xi)\right|^2 d\xi} \tag{4.16}$$

where $|A(x)|$ is the normalized amplitude distribution, L_a is the aperture length of the LWA, and e_r is the radiation efficiency. $|A(x)|$ can be simply calculated with -25 dB Taylor amplitude distribution. e_r is selected as 90%, which is a general and popular choice. In order to extract the attenuation constant of the LWA with different *Ls*, a large number of unit cells should be cascaded and

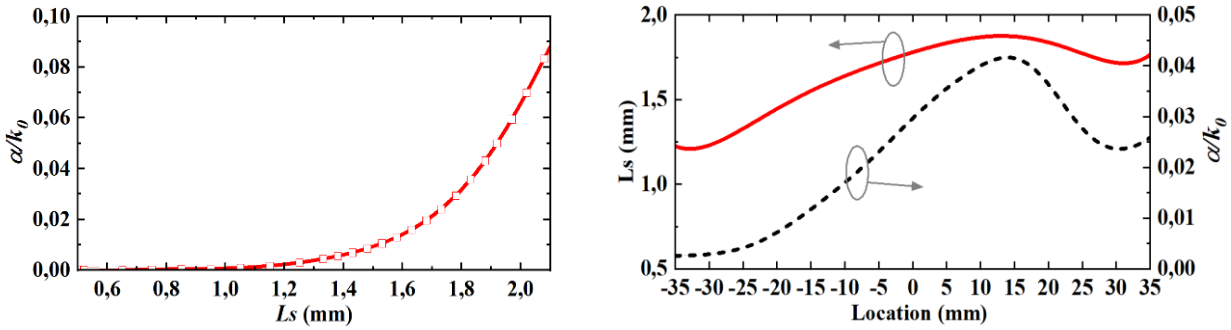

(a) (b)

Figure 4.6 (a) Extracted normalized attenuation constant as a function of slot length *Ls*. (b) Distribution of the normalized attenuation constant and slot length L_s along the LWA with -25 dB Taylor line-source amplitude distribution

The working frequency is 35 GHz. (© 2020 IEEE, reproduced with permission)

simulated in *HFSS*. In this situation, mutual coupling effects among unit cells can be well considered to get a relatively accurate knowledge of the attenuation constant, which is critical for low SLL LWA designs [30][38][45][50]. Since the attenuation constant in formula (4.16) only represents the radiation loss, the conductor and dielectric losses, therefore, are neglected in this extraction process. A segment of the slotted LWA as shown in Figure 4.3 is used to do the extraction. The period length *P* is selected as 0.5 mm; the slot length *Ls* is changed from 0.5 to 2.1 mm with a step of 0.01mm; the other parameters shown in Figure 4.3(a) are *W1*= 2.62 mm, *Ws*=0.25 mm, *S*=1.4 mm, *d*=0.3 mm, *t*=0.3 mm, *h*=0.508mm, and ε_r=2.94. The frequency of operation is 35 GHz. The extracted normalized attenuation constants as a function of slot length *Ls* are depicted in Figure 4.6(a). It shows that a large scope of attenuation constant can be achieved with slot length *Ls* changing from 0.5 mm to 2.1 mm, which is beneficial to acquire different amplitude distributions and low SLLs. However, for a given SLL and radiation efficiency to be designed, a longer length of LWA will result in the requirement of a relatively smaller attenuation constant distributed along the LWA. Although it is favorable to achieve a large directivity and narrow beam if an LWA has a long aperture length, it will be detrimental to have a rapid beam-scanning property in our proposed design. This can be easily understood since for longer LWA to be designed with a designated radiation efficiency, shorter slots should be adopted to slow the

energy attenuation along the LWA, thereby decreasing the slope of effective phase constant and slowing the rate of beam-scanning. After taking into account both directivity and dispersion sensitivity of the LWA, L_a is selected to be 70 mm (about 8 λ_0, where λ_0 is the free-space wavelength at the center frequency of 35 GHz). Thereafter, the normalized attenuation constant distributed along the length of the LWA can be calculated based on (4.16), followed by the slot length Ls distribution; both are shown in Figure 4.6(b).

4.3.2 Modeling, Simulation, and Measurement

When the slot length *Ls* distribution along the structure is determined, the tapered slotted SIW LWA can be modeled. Along the leaky region, 141 slots are distributed discretely with a period of P = 0.5 mm; each slot has a different length according to Figure 4.6(b). The final antenna structure is described in Figure 4.7, together with two impedance matching sections and grounded coplanar waveguide-to-SIW (GCPW-SIW) transitions at its two ends. Note that the working frequency band of the proposed LWA is close to the cut-off of the SIW due to the requirement of fast-wave region. Although it is beneficial to have a phase constant with a large slope as mentioned in Chapter 4.2.2, it will bring the SIW a dramatically changing characteristic impedance versus frequency, causing the trouble of impedance matching and transition design. To solve this problem, a impedance matching sections consisting of a linearly tapered segment with a length of L_{t2}, a delay line with a length of L_{t3} and two matching walls are added to the designed leakage region, as shown in Figure 4.7. Also note that when the matching section is connected to the main leaky region, the length of the SIW line segment between the two parts, i.e., L_{t1}, should be optimized carefully to provide a good impedance matching result. Practically, the two impedance matching sections and the leakage region should be regarded as an entirety. A quarter-wavelength impedance transformer is inserted into the GCPW-SIW transition to have a good return loss. Main parameters of the proposed LWA are tabulated in Table 4.1. An experimental prototype of the proposed LWA was fabricated through a precise laser micromachining process in our group, as shown in Figure 4.8, whereas its simulated and measured *S*-parameters are plotted in Figure 4.9(a). It can be seen that the measured $|S_{11}|$ agrees generally with the simulated one except for a slight frequency shift and impedance matching deterioration, which may be caused by fabrication errors. The measured $|S_{21}|$ is lower than its simulated counterpart, which may be related to the increased dielectric and conductor losses as

well as the connector loss. Simulated and measured realized gains as well as simulated directivity are plotted in Figure 4.9(b). The simulated directivity is more than 15.6 dBi with a variation of less than 3 dBi exhibited in the target frequency band. By contrast, the maximum achievable realized gain for the simulation is about 13.6 dBi while the measured counterpart exhibits a reasonable drop of approximately 1.5 dBi because of the aforementioned losses mechanism. Compared to the stable directivity over the whole frequency band of interest, the realized gain shows a relatively unstable performance (especially at lower frequencies) due to the increasing difference between the

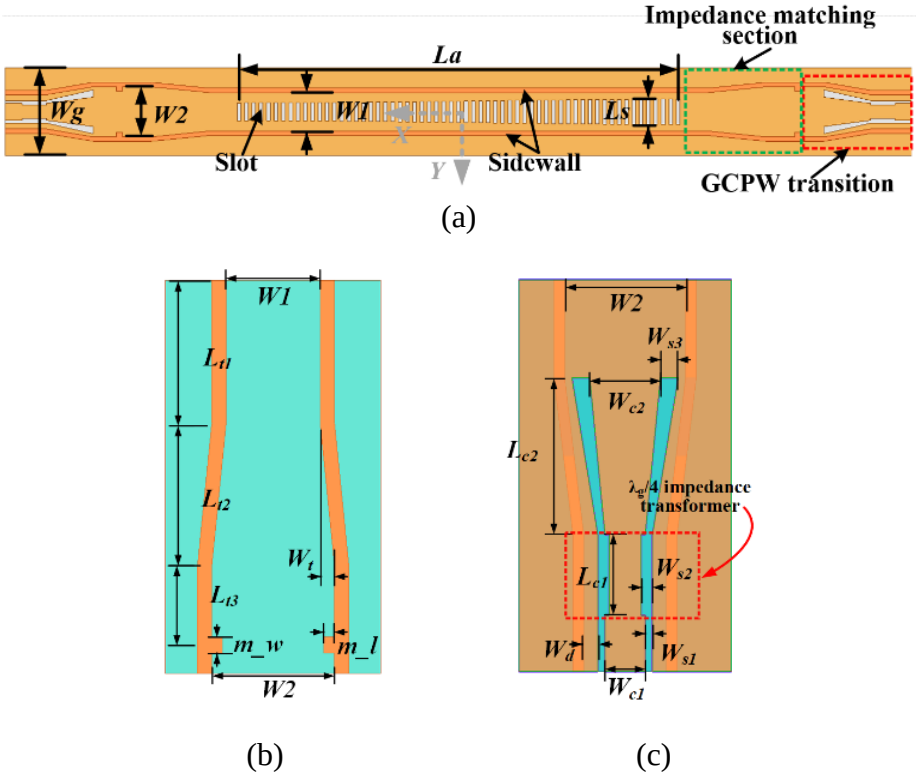

Figure 4.7 Geometry of various structures

(a) Slotted SIW LWA with rapid beam-scanning and low SLL, (b) impedance matching section (top metal layer is hidden), and (c) GCPW-SIW transition inserted with a quarter-wavelength impedance transformer. Continuous sidewalls are used here for modeling and simulation convenience, and they can be easily replaced by plated via-slot/trench arrays in practical fabrication. (© 2020 IEEE, reproduced with permission)

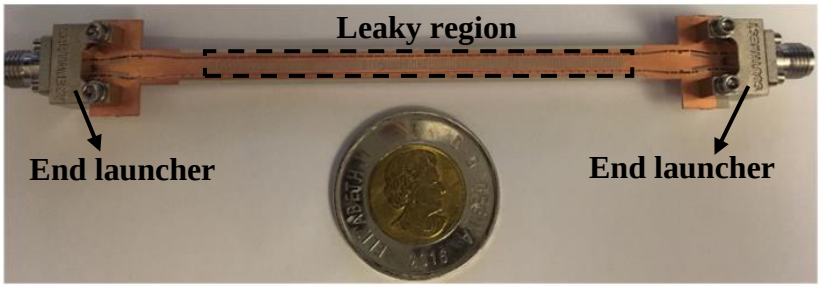

Figure 4.8 Photograph of experimental prototype of the proposed LWA

Rogers 6002 substrate with h=0.508 mm, ε_r=2.94 and $tan\ \xi$=0.0012 is used for PCB fabrication. The copper cladding thickness is 18 um. Plated via-slot arrays with d=0.3 mm, t=0.3 mm and S=1.4 mm (as shown in Figure 4.3) are practically adopted to form the SIW. (© 2020 IEEE, reproduced with permission)

Table 4.1 Main Dimensions of the Proposed Transversely Slotted SIW LWA (Unit: mm) (© 2020 IEEE, reproduced with permission)

Parameter	W_g	L_a	$W1$	$W2$	L_{t1}
Value	6	70	2.62	3.51	4
Parameter	L_{t2}	L_{t3}	W_t	m_w	m_l
Value	4	2.2	0.4	0.45	0.3
Parameter	L_{c1}	L_{c2}	W_{c1}	W_{c2}	W_{s1}
Value	1.65	3.2	1.14	2	0.2
Parameter	W_{s2}	W_{s3}	W_d		
Value	0.32	0.5	0.4		

directivity and realized gain as frequency decreases. This can be explained by the fact that deteriorated losses from materials (dielectrics and conductors) occur with the frequency decreasing and getting close to the cut-off of the SIW. In the frequency region close to the cut-off, the group velocity of signal is small and thus more time should be spent for the signal to travel from one end to the other of the LWA; this will lead to the increased dielectric and conductor losses [14][148]. Both simulated and measured realized gains show a fluctuation of less than 5 dBi over the target

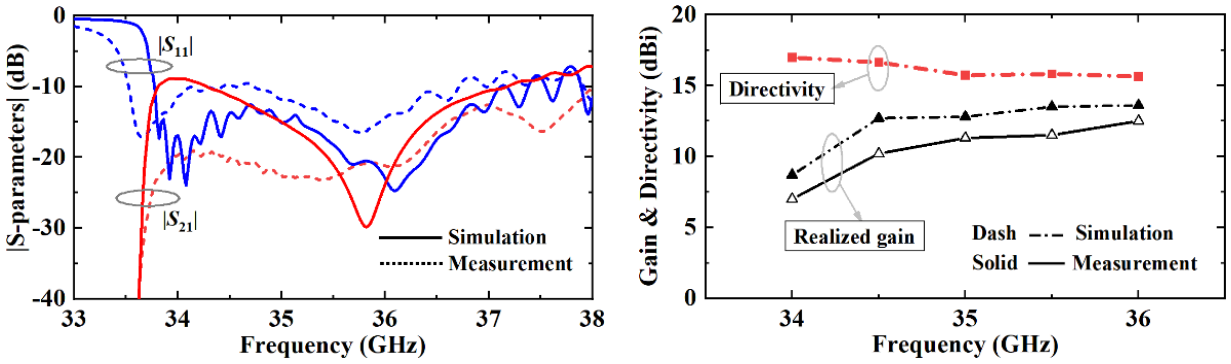

(a) (b)

Figure 4.9 (a) Simulated and measured S-parameters, and (b) simulated and measured realized gain and simulated directivity of the proposed LWA

(© 2020 IEEE, reproduced with permission)

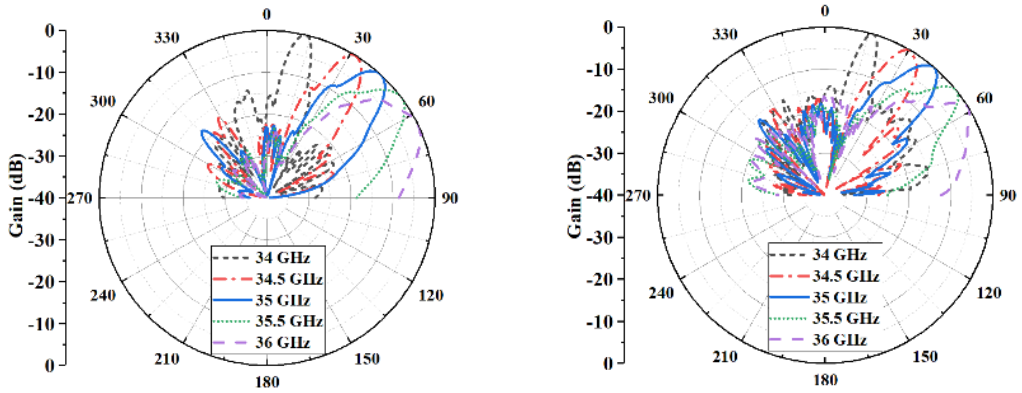

(a) (b)

Figure 4.10 Radiation patterns of the proposed LWA in the *xoz* plane at several frequencies with respect to (a) simulation and (b) measurement

(© 2020 IEEE, reproduced with permission)

frequency band (however, it is less than 3 dBi in the range from 34.5 to 36 GHz). Since the gain fluctuation is related to the aforementioned losses mechanism, some approaches may be potentially adopted to mitigate this issue. For example, low-loss substrate (e.g., Rogers 5880 or Silicon) or air-filled SIW [215] can be employed to reduce the dielectric loss, while thick substrate is beneficial for lowering the conductor loss. Simulated and measured radiation patterns in the *xoz* plane at

different frequencies are plotted in Figure 4.10. It shows that the simulated main beam can be scanned from 13º to 61º from 34 to 36 GHz, in which a beam-scanning range from 17º to 58º was realized experimentally. Also, a good SLL (including the back-lobe level) of about -18 dB at the center frequency of 35 GHz was achieved in simulation. It can be seen that the SLL is mainly constrained by a large back-lobe that is due to reflected waves caused by large slot discontinuities or mismatched termination [20][27]. Note that back-lobes cannot be predicted and calculated by the famous low SLL procedure as implemented above and described in [9]. Although measured SLLs are slightly deteriorated than simulated counterparts that may be due to fabrication errors and measurement issues, they are all in an acceptable level (better than 15 dBi generally) for practical

Table 4.2 A Comparison between the Proposed Work and Several References (© 2020 IEEE, reproduced with permission)

Ref.	**Fractional bandwidth (%)**	**Scanning range (degree)**	**Scanning rate (degree/fractional bandwidth)**	**Approaches**
[145]	7.6	36.5	4.8	Stopband (Vias or HIS)
[147]	37	62	1.7	
[136]	8.3	60	7.2	Meandering feedlines
[138]	17.4	73.5	4.2	
[139]	11.8	30	2.5	Phase shifters
[140]	4	59	14.8	
[144]	3	35	11.7	Slow-wave structures
[146]	9	123	13.7	
[14]	16.2	53	3.3	Conventional Slotted SIW LWAs
[51]	43.5	75	1.7	
[52]	39.3	140	3.6	
This work	5.7	41	7.2	Loading effects

applications. A comparison is conducted between the proposed LWA and several referenced works that use different kinds of approaches to improve the beam-scanning rate as mentioned in the Introduction section, as described in Table 4.2. To have a fair comparison among different LWAs working in different frequency bands, the beam-scanning rate should be defined as the beam-scanning span per fractional bandwidth. It can be seen clearly that the proposed work has a higher beam-scanning rate than most works listed in the table, even though a taper aperture illumination that has an adverse influence on beam-scanning rate was implemented in the proposed design. Furthermore, when making a comparison with those conventional slotted SIW LWAs [14][51][52], the proposed work shares the same merit of simple geometry but exhibits a distinct enhancement of beam-scanning rate. Also, it should be noted that the proposed work is the only one designed in the millimeter-wave range in which most of approaches mentioned in the table will lose their virtues due to their naturally complex structures, high losses and high fabrication difficulties. However, a limitation of this work is that the attenuation and phase constants cannot be independently chosen, since both are related to the loading effects of radiating discontinuities. To be more specific, although the rapid beam-scanning can be achieved by using long slot in the proposed SIW LWA, this will lead to a relatively large attenuation constant and thus highly directive LWA may be hard to be realized. Fortunately, higher-permittivity or lower-thickness substrate can be used to mitigate this issue. In these situations, more guided energy is confined inside the SIW and thus the slot is more reactive rather than radiative, implying that a low radiation attenuation and high directivity may be potentially obtained by the relevant LWA with remaining or even improving the rapid beam-scanning property. Due to such a limitation, the proposed design, in this sense, will be more suitable for short-/middle-range radar or wireless communication application scenarios [1][2][211]-[214]. In sum, the proposed work owns the benefits of simple configuration, easy design and fabrication, low cost, low SLL, and especially the rapid beam-scanning property; thus, it is suitable for mass production and system integration.

4.3.3 Tolerance Analysis

It occurs frequently that measured results deviates from simulated counterparts to some extent, which may be especially obvious with such highly dispersive LWA designed in high frequencies. Tolerance issues from fabrication should be mainly or partially responsible for this. Typically, it is

known that substrate properties such as thickness and relative permittivity have some specific manufacturing tolerances, e.g., the chosen substrate in this proposed design is Rogers 6002 with relative permittivity of 2.94 ± 0.04 and thickness of 20 ± 1 mil. Generally, this kind of tolerances are small enough and thus they are not taken into consideration in most cases. Some other factors contribute to most performance deviation such as the accuracy of position and size of plated via-holes, as well as the width of slot and line in fabrication process. Consequently, it is necessary to perform a tolerance analysis to measure the degrees of performance deviation, which is quite important and practical for mass production.

Since the frequency region close to the cut-off of an SIW is used to implement the proposed quasi-uniform LWA for achieving fast-wave radiation and beam-scanning, there is no doubt that fluctuations of the cut-off frequency of the SIW will give rise to variations of beam-scanning properties, e.g., the range, rate, and starting and ending directions of beam-scanning. Therefore, atolerance analysis of the SIW width (i.e., *W1*, as shown in Figure 4.7) should be analyzed. Figure 4.11(a) describes beam-scanning properties of the proposed design with different fabrication tolerances for *W1*. Although the starting and ending of the beam directions are different for such

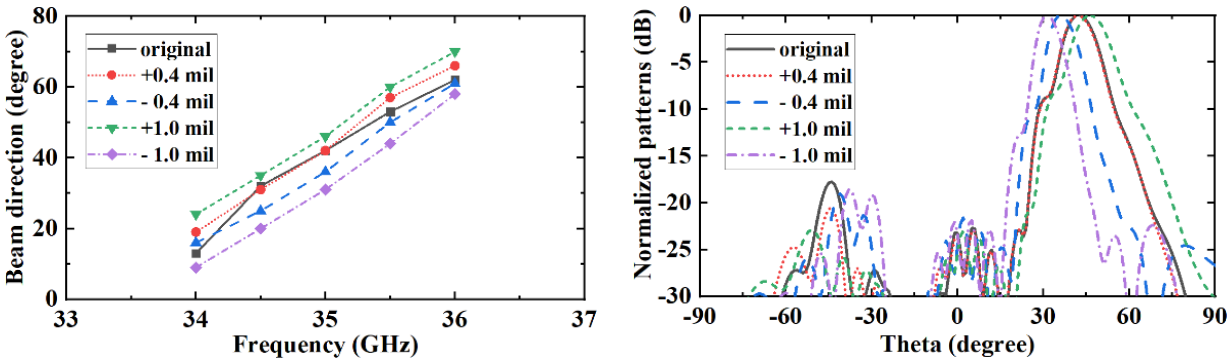

(a) (b)

Figure 4.11 Tolerance analysis of the proposed LWA regarding the width (*W1*) of the SIW

(a) Beam-scanning properties. (b) Radiation patterns at 35 GHz. In the inset of figures, the "original" means the proposed design without any tolerance problem; positive sign "+" represents that the SIW width is enlarged while negative sign "-" denotes opposite situations. (© 2020 IEEE, reproduced with permission)

fives cases as expected, they almost have the same beam-scanning span in the limited frequency band from 34 to 36 GHz, implying that they almost have the same beam-scanning rate. These specific beam-scanning spans are 48^{o}, 47^{o}, 46^{o}, 46^{o}, and 49^{o} for those cases listed in the inset of Figure 4.11(a), respectively. The radiation patterns at the design frequency of 35 GHz for different fabrication tolerances are plotted in Figure 4.11(b), showing that good SLLs are all achieved in such five cases. Notably, all the SLLs are approximately better than 23 dB if back-lobes are not taken into consideration, which are generally consistent with the target performed with low SLL design procedure, i.e., -25 dB.

4.4 Three-Dimensional Hexagonal Array for Omnidirectional Radiation

It is very promising to have an LWA that is able to provide a full-coverage in the azimuth plane and a substantial beam-scanning in the elevation plane, which may find potential applications in autonomous driving and flying, radar imaging, and wireless communication systems. The LWA featuring rapid beam-scanning is a good candidate to be used in such systems as explained previously. However, most LWAs, including the proposed one, only have a fan-shape directional beam scanned with frequency along the direction of wave guidance [9][11]. To satisfy the requirements of both rapid frequency beam-scanning and omnidirectional beam coverage, a 3-D hexagonal array consisting of six proposed LWA elements, six right-angled aperture-coupling transitions and a 6-way radial power divider is developed in this section to provide an omnidirectional coverage in the azimuth plane and a rapid frequency-scanned beam in the elevation plane.

4.4.1 Design of LWA Array Block

The previously proposed SIW LWA should be slightly modified to facilitate array development. The revised LWA array block is depicted in Figure 4.12(a). It is almost the same as the previous one in Figure 4.7(a), excluding the newly designed aperture-coupling transition terminated at the feeding end as depicted in Figure 4.12(b) and (c). In this LWA array block, the slot-coupling aperture is etched on the opposite layer of the slotted radiating layer. The electromagnetic power is fed from the feeding branch belonging to one output of the radial power divider shown in Figure 4.13, passing through the coupling slot aperture, and eventually reaching to the input end of the

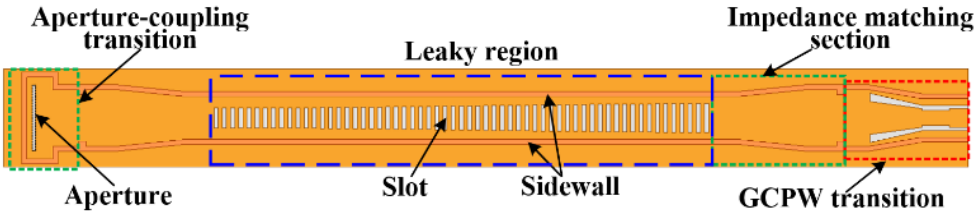

(a)

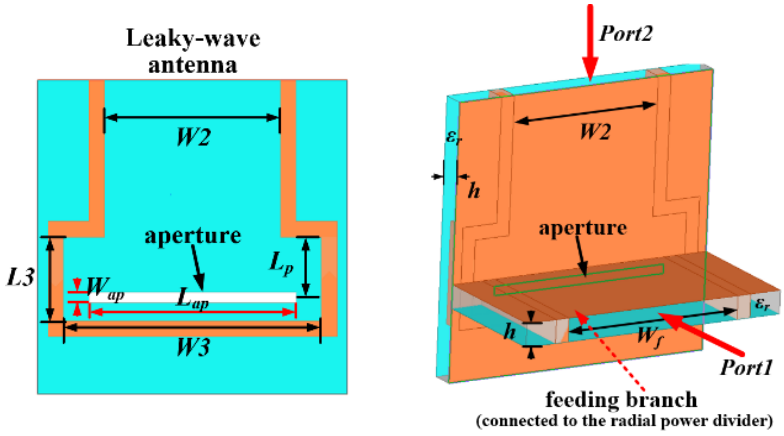

(b) (c)

Figure 4.12 (a) Geometry of the designed LWA block for array implementation. (b) Aperture-coupling transition terminated to the feeding end of the LWA block (top metal layer is hidden). (c) Right-angled transition between the radial power divider and LWA block

In the LWA block, the slot aperture used for energy coupling is located in the opposite metal layer compared to those transverse slots used for radiation. Continuous sidewalls are used here for modeling and simulation convenience, and they can be easily replaced by plated via-slot/trench arrays in practical fabrication. In (c), port2 is connected to the LWA block, while port1 is connected to one branch of the radial power divider. (© 2020 IEEE, reproduced with permission)

LWA. Dimensions of the aperture-coupling transition and radial power divider are tabulated in Table 4.3. Simulated *S*-parameters of the right-angled aperture-coupling transition is shown in Figure 4.14. It is seen that in the target frequency band from 34-36 GHz, the return loss is better than 30 dB while the insertion loss is better than 0.1 dB.

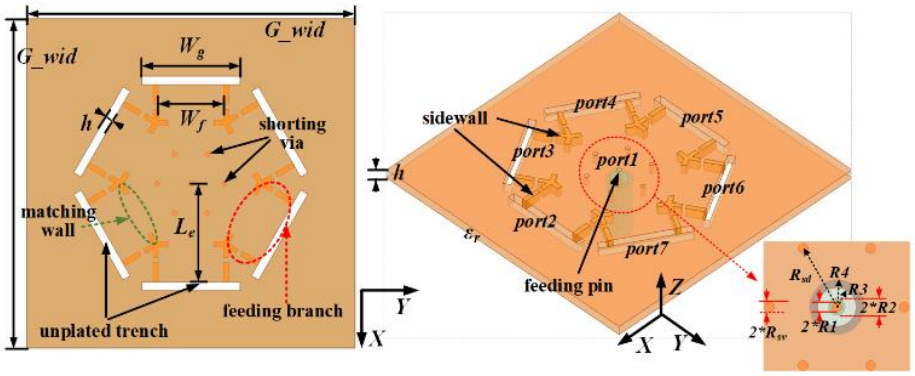

(a) (b)

Figure 4.13 Geometry of the proposed six-way cavity-based SIW radial power divider (a) Top view. (b) 3-D view. The white areas in (a) represent unplated trenches used for installation of LWA blocks. (© 2020 IEEE, reproduced with permission)

4.4.2 Design of Radial Power Divider

Figure 4.13 depicts the geometry of a cavity-based SIW resonant radial power divider, which is inspired by [50]. A set of metallic via-holes are rotational-symmetrically embedded in the cavity to increase the resonant frequency of the TM_{01} mode with only slightly perturbing the TM_{02} mode. By combining the TM_{01} and TM_{02} modes of a circular cavity resonator, a wideband performance can be achieved. In the proposed radial power divider, only six outputs are employed because of the considerations in terms of geometrical limitation of the circular cavity, the compactness of the

Table 4.3 Dimensions of the Proposed Right-angled Transition and Radial Power Divider for Array Implementation (Unit: mm) (© 2020 IEEE, reproduced with permission)

Parameter	*W3*	*L3*	W_{ap}	L_{ap}	L_p
Value	5	1.6	0.2	4	1.15
Parameter	W_f	*h*	R_{sd}	*R4*	*R3*
Value	4	0.508	2.05	0.83	0.584
Parameter	*R2*	*R1*	R_{sv}	*G_wid*	L_e
Value	0.254	0.152	0.152	20	6

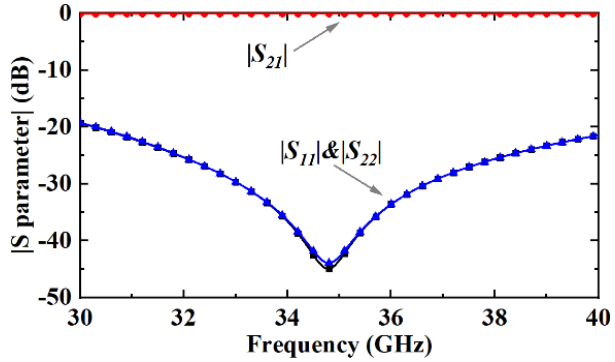

Figure 4.14 Simulated *S*-parameters of the proposed right-angled aperture-coupling transition

Definition of these ports can be found in Figure 4.12(c). (© 2020 IEEE, reproduced with permission)

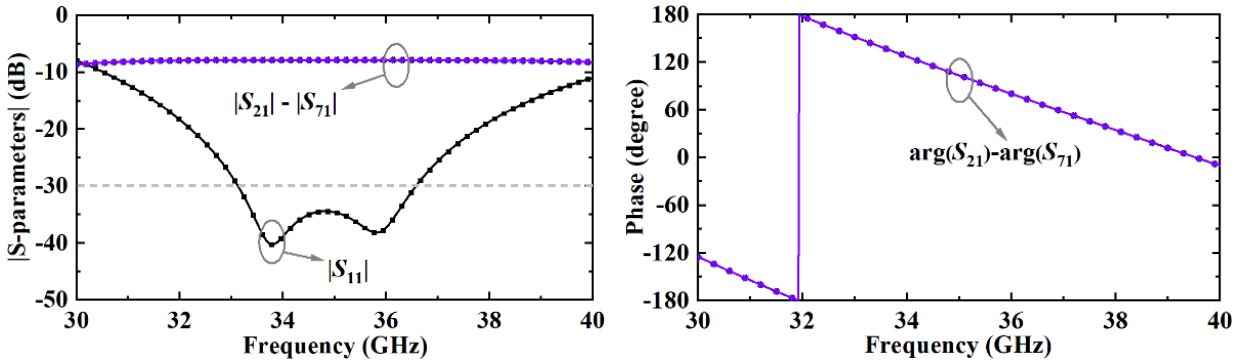

(a) (b)

Figure 4.15 Simulated reflection and transmission coefficients of the proposed six-way radial power divider with respect to (a) amplitudes and (b) phases

Definition of these ports can be found in Figure 4.13(b). (© 2020 IEEE, reproduced with permission)

hexagonal array and the radiation circularity of the array in the azimuth plane. A two-step radial power divider can be alternatively adopted to increase the number of outputs with improving radiation circularity of the array but sacrificing its geometrical compactness [217]. A southwest 2.92 mm (*K*) coaxial connector is used to feed the radial power divider at its center and from its bottom layer. Simulated reflection and transmission coefficients of the radial power divider with

respect to their amplitudes and phases are plotted in Figure 4.15 (a) and (b), respectively. It is seen apparently that a good impedance matching is achieved within 34-36 GHz and all the outputs have the same amplitudes and phases, thus paving the way for achieving good circuit and radiation performances for the hexagonal array.

4.4.3 Modeling, Simulation, and Measurement

After the design of the LWA array block, right-angled aperture-coupling transition and radial power divider, a 3-D hexagonal array can be implemented, as shown in Figure 4.16. All LWA blocks are inserted perpendicularly into those unplated trenches that are located in the radial power divider. To make convenience in fabrication and measurement, all LWA blocks are open-terminated at those unfed ends. It is believed to be reasonable and with a little influence, since there is almost no remaining energy at the matching-end of the LWA element, as can be seen from the measured $|S_{21}|$ in Figure 4.9. Simulated 3-D radiation patterns of the proposed array are plotted in Figure 4.17. It is illustrated that a quasi-omnidirectional radiation beam is realized in the azimuth plane, and circularity of the omnidirectional beam is improved with frequency. Since the array is fed from the bottom of the radial power divider, the energy flows upwardly and thus the beam rises with frequency, from the direction that is perpendicular to the axis (i.e., Z-axis, as shown in Figure 4.16) of the array. The proposed array was simulated, fabricated and measured, with the fabricated prototype shown in Figure 4.16 and measured results described in Figure 4.18 - Figure 4.20.

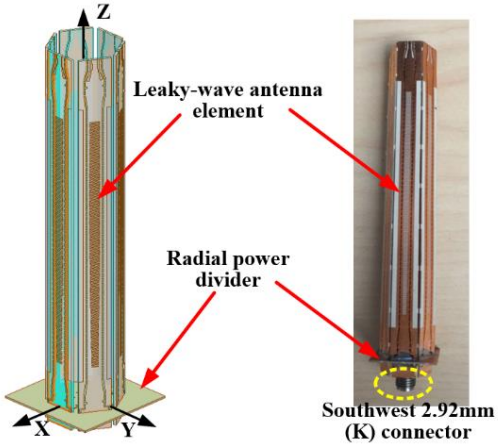

Figure 4.16 Simulated hexagonal array model and its fabricated prototype

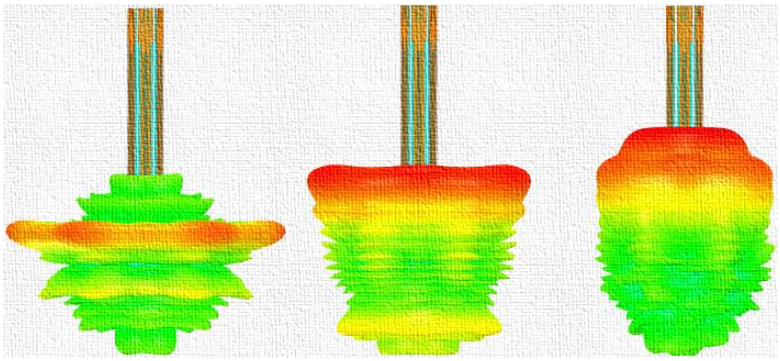

Side view

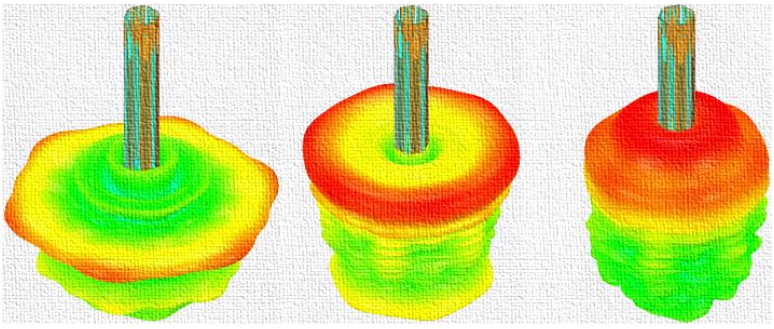

3-D view

(a) (b) (c)

Figure 4.17 3-D radiation patterns of the proposed hexagonal array with respect to different frequencies

(a) 34 GHz; (b) 35 GHz; (c) 36 GHz. (© 2020 IEEE, reproduced with permission)

Simulated and measured $|S_{11}|$ are shown in Figure 4.18; it indicates that both are in a reasonable agreement, with a good impedance matching of better than 10 dB achieved in the target frequency band from 34 to 36 GHz. Figure 4.19 exhibits simulated and measured radiation patterns in the *xoz* plane with respect to difference frequencies. For the simulation results, the beam can be scanned from 14^o to 72^o that are measured from the broadside direction that is perpendicular to the Z-axis of the array, with frequency changing from 34 to 36 GHz. The measured results generally agree with those simulated counterparts, with the beam changing from about 20^o to 69^o in the same frequency range. Simulated and measured gain performances in the azimuth plane with respect to

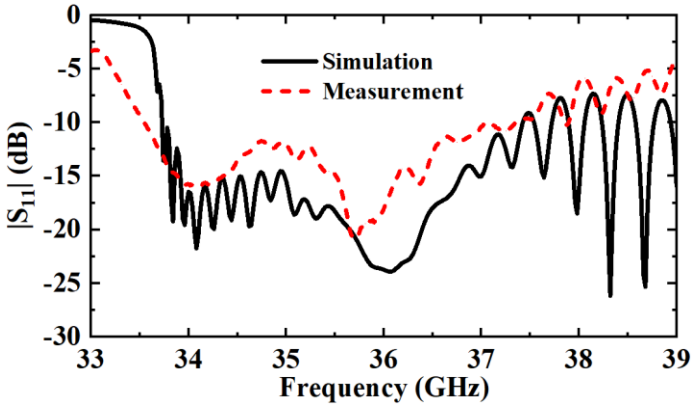

Figure 4.18 Simulated and measured reflection coefficients of the proposed hexagonal array

(© 2020 IEEE, reproduced with permission)

their maximum radiation angles and frequencies are plotted in Figure 4.20. In the measurement, the 3-D radiation sphere was evenly divided into 12 sections along the latitudinal direction, with the starting point being phi=0^{o} (i.e., the *xoz*-plane as shown in Figure 4.16) and adjacent sections separated by 30^{o}. The pattern measurement was conducted repeatedly at each specific azimuth angle. Simulated results show that the maximum gain at each frequency (i.e., 34 GHz, 35 GHz and 36 GHz) are 5.9 dBi, 10.7 dBi, and 12 dBi, respectively, while the measured counterparts are 4.6 dBi, 9.5 dBi, and 10.8 dBi correspondingly. As for gain variations over the azimuthal plane in the simulated cases, 4.6 dBi, 1.9 dBi, and 0.6 dBi are achieved at 34 GHz, 35 GHz and 36 GHz, respectively; their measured counterparts are about 5.1 dBi, 2.2 dBi and 1.1 dBi, correspondingly. It should be noted that the cross-sectional beamwidth of the proposed LWA element shows an increasing trend with frequency (this is not given here for brevity), which is perhaps caused by the increasing attenuation constant and beam solid-angle when the beam is scanned close to the end-fire [9][11][16]. Because of this, the required quantity of LWA building blocks will differ in frequencies if consistent circularity performances over the azimuthal plane are required. This means that more LWA blocks should be used to maintain a relatively stable gain performance in lower frequencies. Consequently, when implementing such a hexagonal array with a certain number of LWA blocks, a relatively higher gain variation over the azimuthal plane of the array is generally existent in lower frequencies compared to that in higher frequencies, and the circularity

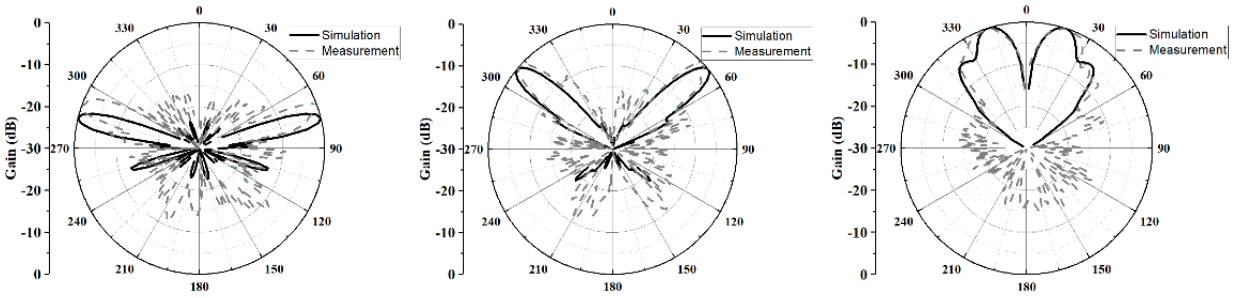

(a) (b) (c)

Figure 4.19 Simulated and measured radiation patterns of the proposed hexagonal array in the xoz plane with respect to different frequencies

(a) 34 GHz; (b) 35 GHz; (c) 36 GHz. (© 2020 IEEE, reproduced with permission)

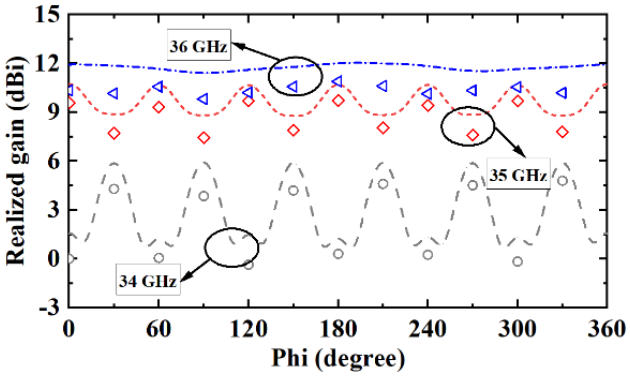

Figure 4.20 Simulated and measured realized gain of the proposed hexagonal array in the azimuth plane with respect to different frequencies

(a) 34 GHz; (b) 35 GHz; (c) 36 GHz. Dashed lines represent simulated results, while scattered symbols represent measured counterparts. Both simulated and measured results refer to the values at corresponding elevation angles and frequencies. (© 2020 IEEE, reproduced with permission)

in the azimuthal plane will be improved with frequency as exhibited in Figure 4.17 and Figure 4.20. For the proposed work, more LWA blocks with a multi-step (e.g., two-step) radial power divider can be used to improve the circularity problem as mentioned before, and this will be considered in our future work. In addition, the gain performance (maximum gain at each elevation angle) of the array also shows an unstable trend with frequency, which is similar to that of the LWA element.

When taking the criterion of 3 dB gain difference over frequency and azimuthal plane simultaneously, the practical bandwidth of the array is approximately limited within 34.5 to 36 GHz. Both simulated and measured results in Figure 4.20 are roughly agreeable due to fabrication errors or measurement issues. The measured gains are smaller than the simulated ones, which may be caused by increased conductor and dielectric losses, as well as connector loss. Slightly increased back-lobes may also be responsible for this.

4.5 Conclusion

In this chapter, a quasi-uniform transversely slotted SIW LWA featuring rapid beam-scanning and its hexagonal array have been proposed and investigated for millimeter-wave systems. General approaches for improving LWA-based frequency beam-scanning rate have been discussed initially, followed by the specific approaches that make use of loading effects of radiating discontinuities to increase the frequency sensitivity of phase constant of LWAs. The proposed SIW LWA is simply based on the use of a long transverse slot with a sharp inductive reactance and a short period of unit cells. For practical system applications, the proposed LWA is tapered to have a low SLL, and a hexagonal array consisting of six proposed LWAs is developed to provide an omnidirectional coverage in the azimuth plane while remaining the rapid frequency-driven beam-scanning in the elevation plane. Both measured and simulated results are in an acceptable agreement. The proposed antenna will be a good candidate to be applied for prospective millimeter-wave systems such as autonomous driving and flying.

CHAPTER 5 ARTICLE 3: MULTIFUNCTIONAL FILTERING LEAKY-WAVE ANTENNA EXHIBITING SIMULTANEOUS RAPID BEAM-SCANNING AND FREQUENCY-SELECTIVE CHARACTERISTICS BASED ON RADIATIVE BANDPASS FILTER CONCEPT

Dongze Zheng and Ke Wu

Published in the *IEEE Transactions on Antennas and Propagation*, vol. 68, no. 8, pp. 5842-5854, Aug. 2020.

In this chapter, the concept of RBPF is proposed and investigated for developing a class of multifunctional filtering LWAs which exhibit simultaneous rapid frequency-dependent beam-scanning and frequency-selective characteristics. An SIW is periodically loaded with closed (non-radiative) discontinuities acting as a bandpass filter, where the lower and higher stopbands are respectively stemmed from the SIW's natural cut-off and the Bragg effects' bandgap or bandstop caused by periodic discontinuities. By adequately adjusting the periodicity of filter unit cells and loading effects of closed discontinuities, filtering and dispersion behaviors of the periodic SIW can be flexibly engineered. Open (radiative) discontinuities are then deliberately introduced into the bandpass filter to generate a controllable radiation leakage, thereby accomplishing the design of the RBPF, i.e., the proposed LWA. With this concept, both filtering/dispersion and radiation tasks can be independently managed by different modules for LWAs. For demonstration purposes, two kinds of closed discontinuities, namely non-radiative longitudinal slot-pair (capacitive) and iris (inductive), are separately exploited for periodic SIWs with bandpass and high dispersion characteristics; whereas transverse slot (open discontinuity) is mainly aimed for radiation leakage. Two RBPF-based LWAs are simulated, fabricated and measured. Simulated and measured results are in a reasonable agreement and both demonstrate the rapid beam-scanning and filtering behaviors, thereby validating the proposed concept.

5.1 Introduction

In the past few decades, there has been an increasing interest in microwave and millimeter-wave periodic structures to develop many devices and components, among which slow-wave structures [218]-[220] and filters [221]-[230] have been in the spotlight of research and receiving much attention. Most of them are 1-D periodic structures and can be developed by loading periodic perturbations (discontinuities) into host TLs, i.e., periodically loaded TLs. The EBG is a specially coined terminology used to describe such periodic structures. Notably, those EBG discontinuities are mostly formed by periodically patterning over a substrate, ground and signal line in different TL technologies such as microstrip line [218][219][221]-[223], CPW [224]-[225], CPS [226] and SIW [220][227]-[230], as shown in Figure 5.1. Accompanied with the periodicity, frequency-selective (filtering) and slow-wave behaviors are normally found along the EBG periodic structures [17]. For example, multiple bandstops or bandgaps are usually encountered due to the Bragg condition, where the period length is approximately equal to multiple half guided-wavelengths that correspond to the center frequencies of those stopbands. Such bandgap/bandstop behaviors embraced by EBG periodic structures are mostly used for the development of various filters as mentioned above.

LWAs are a special type of guided-wave structures along which travelling-wave propagates and leaks simultaneously [9][11]. Generally, LWAs are created by loading open (radiative) elements or discontinuities into various TLs in a continuous or periodic manner, upon which they can be classified into three categories: uniform, quasi-uniform, and periodic LWAs. Most of them physically possess periodic appearances and thus can be treated as periodically loaded TLs, thereby interestingly sharing similar properties as those EBG periodic structures mentioned above, such as filtering properties. Intentionally or unintentionally, a majority of reported EBG periodic structures are also formed with open discontinuities that resemble LWAs, due to which they may suffer from serious and harmful radiation loss (especially in millimeter-wave bands) when working as filters or slow-wave structures [218]-[228]. This not only degrades signal quality and wastes signal power, but also leads to potentially unwanted electromagnetic coupling and interference problems. As a result, closed (non-radiative) discontinuities are preferable to construct periodic EBG structures for such applications, e.g., SIW bandpass filters with periodic shorting vias [229][230].

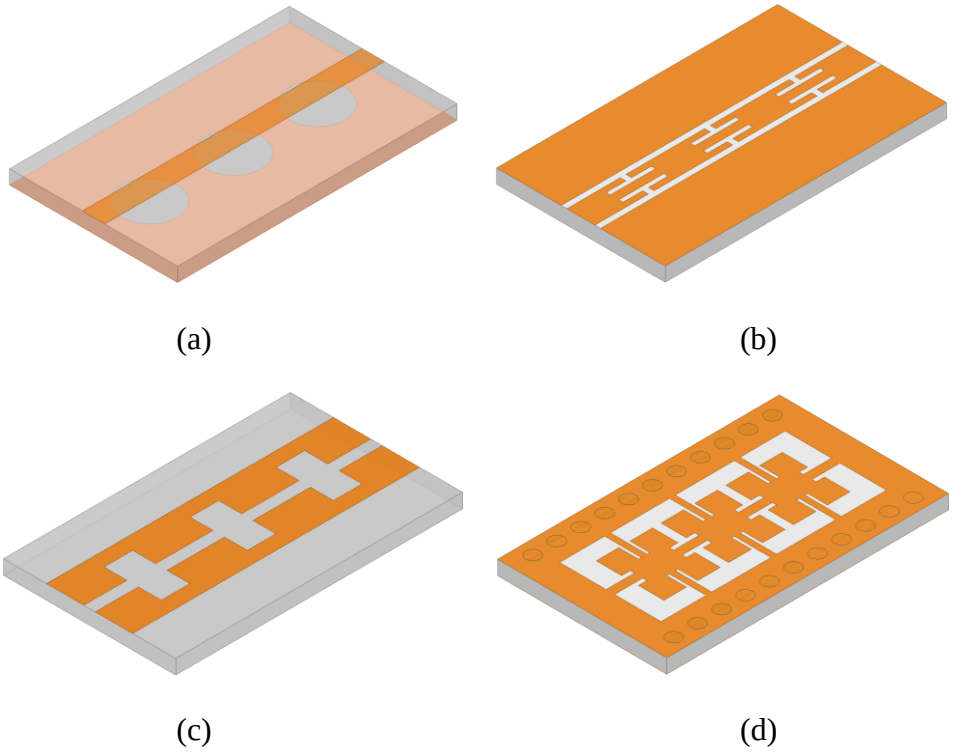

Figure 5.1 Typical 1-D EBG periodic structures based on different TLs for filter applications (a) Microstrip [221]; (b) CPW [225]; (c) CPS [226]; (d) SIW [228]. EBG discontinuities in these structures are open-natured. (© 2020 IEEE, reproduced with permission)

Recently, there has been a growing interest in integrating filters and antennas together as a multifunctional component to reduce circuit area and cost as well as enhance overall system performances [231]-[235]. Broadly, most reported filtering antenna techniques are based on either replacing the filters' final-stage resonators with antennas or directly cascading/integrating filters into antennas. The majority of them, however, have been dedicated to standing-wave (resonant-type) antennas like monopole, slot and patch antennas, while only a few regarding travelling-wave (non-resonant) LWAs equipped with filtering capabilities have been reported so far [236][237]. On the other hand, LWAs with rapid frequency beam-scanning are preferred in the development of radar systems since a wide range of space can be covered within only a relatively narrow frequency bandwidth. Not only can this save the limited spectrum resources, but also relieve the strict bandwidth requirements of front-end components, such as the low-noise amplifier, mixer and A/D

converter. However, limited works have been presented in the open literature to design LWAs with such behavior. Specifically, by using meandering TLs [136]-[138] or specially designed phase shifters [139][140] between adjacent radiative discontinuities, rapid frequency beam-scanning is realized by these related LWAs. Other approaches are devised using slow-wave structures as the host TL [144] or complementary slot-stub as the radiating discontinuity [148] to implement the periodic type LWAs. Besides, resorting to loading a series of shorting pins onto an EH_1-mode microstrip LWA or an HIS onto a hollow waveguide, the phase constant slope of the associated leaky modes can be steepened over frequency, thereby realizing the desirable rapid beam-scanning capability for LWAs [145][147].

As a significant front-end part which may be potentially deployed in automotive radar, sensor, or wireless communication systems, LWAs exhibiting multifunctionalities of both filtering and rapid frequency beam-scanning characteristics are of great interest. In this work, such kind of LWAs reposed on the filter theory, i.e., RBPF concept are proposed and investigated to meet such demands. This scheme simply resorts to introducing open discontinuities to a non-radiative bandpass filter that is formed by periodically loading closed discontinuities onto host TLs (e.g., periodic SIW). First, by combining the high-pass nature of an SIW and the bandstop or bandgap generated by the Bragg effects of periodicity, the bandpass characteristic of the periodic SIW can be obtained. The passband/stopband and dispersion characteristics of the periodic SIW can be flexibly tailored by adjusting the period of filter unit cells and loading effects (impedance/admittance) of closed discontinuities, thus paving the way to realize prospective LWAs with simultaneous frequency-selective and rapid beam-scanning performances. Then, by deliberately adding open discontinuities to the closed bandpass periodic SIW, leaky-wave radiation occurs in its fast-wave passband, thereby forming the LWAs with such desirable features. In this connection, filtering/dispersion and radiation tasks are separately achieved by different modules in this design. Two kinds of susceptance-complementary closed discontinuities, capacitive non-radiative longitudinal slot-pair (NRLSP) and inductive iris, are separately explored to design periodic bandpass SIWs, while transverse slots (TSs) are specially introduced for controllable radiation leakage. Two LWA examples based on this RBPF concept are designed and demonstrated for millimeter-wave applications.

In the rest of this chapter, Chapter 5.2 briefly describes the correlation between typical LWAs and

EBG periodic structures, followed by the introduction of the RBPF concept. Chapter 5.3 depicts the principle of the NRLSP-loaded SIW characterized by both filtering and highly dispersive properties, upon which, in Chapter 5.4, the associated LWA having frequency-selective and rapid beam-scanning characteristics is proposed and demonstrated. As a further proof of the RBPF concept, a traditional iris-based bandpass filter is used to implement an LWA with such behaviors, and this is illuminated in Chapter 5.5. This chapter ends up with a discussion and comparison in Chapter 5.6 as well as a conclusion in Chapter 5.7.

5.2 Background and Principle

5.2.1 Correlation between Typical LWAs and EBG Periodic Structures

Quasi-uniform or periodic LWAs physically have periodic appearances, and thus they are also subject to Bragg effects like typical periodic EBG structures. In this regard, they have a periodic bandgap or bandstop as well, such as the well-known "open-stopband" in periodic LWAs [9][11]. Thus, they may find the feasibility for filter development if some conditions are satisfied. On the other hand, although most open discontinuities-based EBG structures suffer from useless radiation loss when working as filters and slow-wave structures, they have the potential to behave as LWAs when those radiation losses are properly exploited [224]. Such EBG periodic structures can be used for leaky-wave applications if the following three points can be considered.

(i) When the host TLs have a fast-wave region and the EBG period is much less than a half guided-wavelength to roughly satisfy the effectively homogeneous condition and avoid the first Bragg stopband, such EBG periodic structures are related to quasi-uniform LWAs.

(ii) When slow-wave regions of TLs are adopted and the EBG period is approximately in the order of a guided-wavelength, such EBG periodic structures would be converted into periodic LWAs.

(iii) Open EBG discontinuities should have regular shapes to exhibit a predictable and relatively pure polarization of radiation.

Notably, for most reported EBG periodic structures applied as filters or slow-wave structures [218]-[226], the selected host TLs naturally feature a slow-wave, and the frequency band of operation is below the first Bragg bandstop/bandgap. This is beneficial to suppress harmful radiation leakage

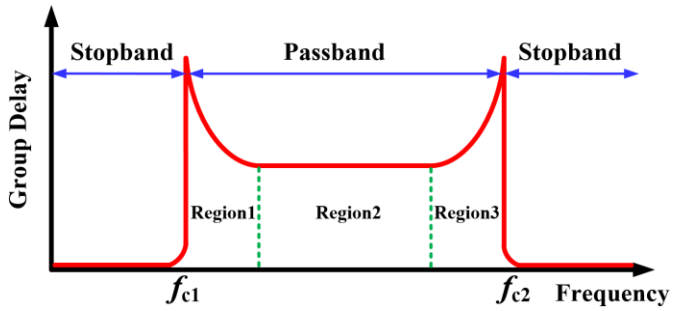

(a)

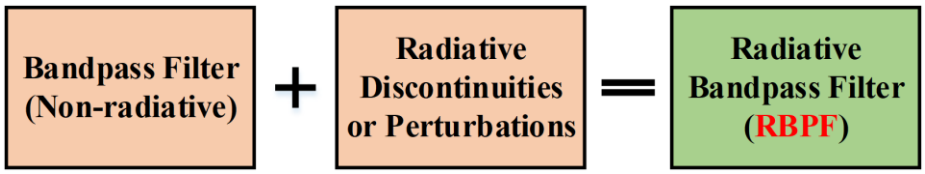

(b)

Figure 5.2 (a) Simplified diagram describing the group delay of a typical bandpass filter. (b) Constitutive principle of the RBPF

f_{c1} and f_{c2} represent the lower and upper cut-off frequencies of the passband. Since a LWA generally has slowly attenuated traveling-waves that result in weak radiation per unit-length along it [9][11], the original bandpass filter should be free from radiation losses (i.e., non-radiative bandpass filter) when constructing the class of RBPF-based LWAs to avoid spoiling useful and controllable radiation created by radiative discontinuities or perturbations. (© 2020 IEEE, reproduced with permission)

losses, though open discontinuities are used. This can be explained by the "close-stopband" of the leaky-wave theory [9][11] since only the guided mode (or bound mode) exists below this stopband, but no leaky mode does. This also explains why LWAs, in a sense, can be potentially employed as filters as stated above. It should be noted that although quasi-uniform or periodic LWAs have both filtering and leaky-wave radiation characteristics, the working frequency bands of these LWAs, unfortunately, are strictly delimited by the natural fast-wave region or the period of open discontinuities. Therefore, the filtering behaviors introduced by the periodicity are usually shelved and cannot be serviceably employed by LWAs in most cases. In other words, both leaky radiation

and filtering characteristics that are introduced by periodic open discontinuities cannot be decoupled from each other and fail to come into play simultaneously for the design of LWAs. As will be shown later, the two functions can be separately achieved and engineered by using different modules in our proposed techniques.

5.2.2 Correlation between Beam-Scanning Properties and Group Delay Dispersion of LWAs

According to the general LWA theory [9][11], the main beam direction of an LWA can be determined by its effective phase constant with the following equation

$$\theta_{MB} \approx \sin^{-1}(\beta_{eff}/k_0) \tag{5.1}$$

where θ_{MB} is the main beam direction (as a function of working frequency f) measured from the broadside; k_0 is the free-space wavenumber; and βeff is the effective phase constant of the leaky mode (or space harmonic) that is responsible for radiation mechanism. Normally, β_{eff}/k_0 is a nonlinear function of frequency and lies in the region from -1 to 1. Depending on the type of LWAs, β_{eff} can be defined as the phase constant of the natural leaky mode or fundamental space harmonic for uniform or quasi-uniform LWAs respectively, or a higher-order space harmonic (e.g., -1st order) for periodic LWAs. It is easy to understand that in order to have a rapid frequency beam-scanning, the frequency derivative of θ_{MB}, expressed as θ'_{MB}, should have a larger value, and it is expressed as

$$\theta'_{MB} = \frac{2\pi}{\sqrt{1-(\beta_{eff}/k_0)^2}} \frac{d(\beta_{eff}/k_0)}{d\omega} \tag{5.2}$$

Thus, for a given frequency or beam direction, the one with a larger $d(\beta_{eff}/k_0)/d\omega$ will have a larger θ'_{MB}. In addition, recalling the definition of phase velocity v_p, there is

$$\theta'_{MB} \propto \frac{d(\beta_{eff}/k_0)}{d\omega} = \frac{d(c/v_p)}{d\omega}$$

$$= \frac{-c}{v_p^2}\frac{dv_p}{d\omega} \propto \frac{dv_p}{d\omega} \tag{5.3}$$

where c is the light velocity in free space and ω represents the angular frequency. It can be found that a larger slope of the phase velocity v_p (i.e., phase velocity dispersion) at a given frequency can also result in a larger θ'_{MB}. To be more specific, if an LWA is highly dispersive with manifesting a larger slope of β_{eff}/k_0 or v_p with frequency, a wider beam-scanning range can be realized in a given frequency range, i.e., the so-called rapid beam-scanning.

On the other hand, since periodic LWAs, EBG structures or SIW TLs can be interpreted as filters due to their filtering or frequency-selective characteristics, the group delay τ_g, as an important figure of merit for filters, can be used and expressed as

$$\tau_g = -\frac{d\varphi}{d\omega} = \frac{d\beta_{eff}}{d\omega} \cdot P = \frac{P}{v_g} \tag{5.4}$$

where φ and P are the phase delay and period length of the unit cell for LWAs or EBG periodic structures, respectively. v_g denotes the group velocity. It is seen that for a fixed period length P, a larger group delay will result in a smaller group velocity, and vice versa. Since the relationship between the phase and group velocities in a medium characterized by a relative permittivity of ε_r can be expressed as

$$v_p \cdot v_g = \left(\frac{c}{\sqrt{\varepsilon_r}}\right)^2 \tag{5.5}$$

Then, equation (5.4) can be rewritten as

$$\tau_g = \frac{\varepsilon_r \cdot P}{c^2} v_p \tag{5.6}$$

Therefore, the group delay dispersion (GDD) can be derived as

$$GDD = \frac{d\tau_g}{d\omega}$$

$$= \frac{\varepsilon_r \cdot P}{c^2} \frac{dv_p}{d\omega} \tag{5.7}$$

Combining (5.7) with (5.3) approximately yields

$$\theta'_{MB} \propto GDD \tag{5.8}$$

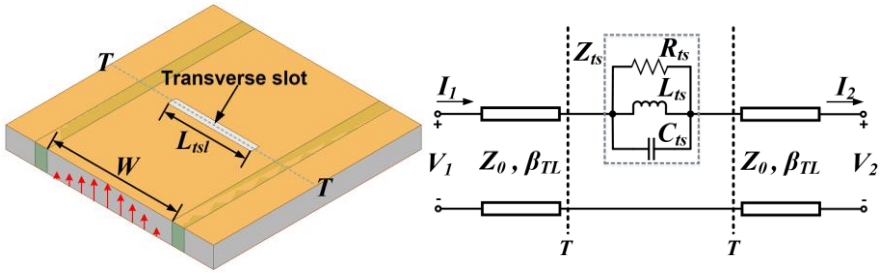

(a)

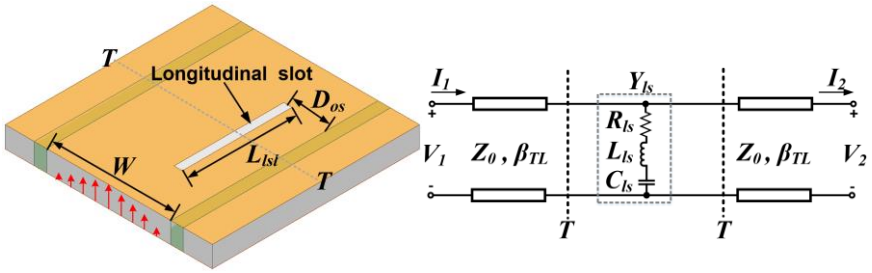

(b)

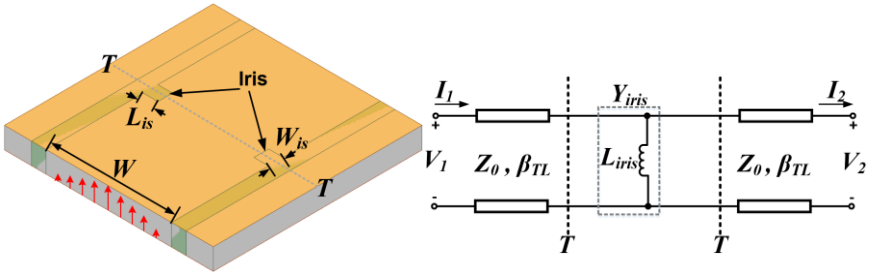

(c)

Figure 5.3 Three kinds of basic discontinuities in SIW or waveguide and their two-port equivalent circuit models [239]

(a) Transverse slot. (b) Longitudinal slot. (c) Iris. Both (a) and (b) are radiative, while (c) is purely closed. (© 2020 IEEE, reproduced with permission)

It is concluded from (5.8) that if an LWA unit cell can have a large GDD, it has the potential to realize the rapid frequency beam-scanning properties, i.e., a large value of θ'_{MB}. Contrastively, the LWA unit cell with constant group delay (i.e., *GDD*=0) may achieve a fixed beam with frequency. Figure 5.2(a) illustrates a simplified diagram describing the group delay of a typical bandpass filter.

Within the passband and close to the cut-off frequencies (i.e., f_{c1} and f_{c2}), there are two highly dispersive regions (i.e., "Region 1" and "Region 3") with large values of GDD exhibited. In filter applications, such highly dispersive regions should be avoided since they will cause serious signal distortion [238]. Interestingly, they can be suitably explored for LWAs featuring a rapid beam-scanning (the filtering behavior is also preserved) based on the above analysis. Follow this thread, since the GD is relatively constant in the center region of the passband (i.e., "Region 2", which is always the choice for practical filter applications), fixed-beam LWAs may be potentially achieved by properly using this behavior. Note that in addition to bandpass filters, similar conclusions are also applicable to lowpass or highpass filters, which are not illuminated here for brevity. Figure 5.2(b) describes the constitutive principle regarding how to use bandpass filters to design LWAs. By deliberately introducing controllable radiative discontinuities to a bandpass filter that has no harmful radiation losses, an LWA based on the RBPF concept can be constructed. Depending on the GDD properties of bandpass filters, the associated LWAs may be capable of exhibiting flexible beam-scanning properties, i.e., either rapid beam-scanning or fixed-beam when sweeping frequency, in addition to the filtering behaviors.

5.3 Non-Radiative Periodically Loaded SIW—Design of an SIW Bandpass Filter

In this section, three kinds of conventional discontinuities that can be easily implemented in SIW technology by using standard PCB process, as shown in Figure 5.3, are briefly introduced to provide a background; they will work as elemental building blocks to accomplish the proposed designs, as will be discussed later. Transmission parameters in terms of the propagation constants, Bloch impedance and group delay are investigated to illustrate guided-wave characteristics (e.g., dispersion and filtering) of the periodic SIWs.

5.3.1 Modeling of Basic Discontinuities in SIW

These discontinuities, namely transverse slot, longitudinal slot, and iris or shorting wall, together with their corresponding equivalent circuit models, are respectively illustrated in Figure 5.3(a), (b) and (c). According to [239], the transverse slot is modeled as a parallel *RLC* resonator that is series-connected with two host SIW segments, while the longitudinal slot can be modeled as a series *RLC*

resonator that is parallel-connected. As for the iris, it behaves as a paralleled inductor. Note that both the transverse and longitudinal slots are conventional open discontinuities or elements that mostly act as radiators (antennas), while the iris is purely closed (non-radiative) and can be used for filter and matching circuit designs. To extract the impedance or admittance of these SIW discontinuities, reference plans can be shifted to the midpoint of each unit cell that is represented as a symmetrical two-port network, and then *S*-parameters or *ABCD* matrix can be used to calculate the impedance or admittance of these discontinuities [18]. A commercial package such as ANSYS HFSS can be used to conduct the full-wave simulation and extraction processes.

5.3.2 SIW Periodically Loaded with Non-Radiative Longitudinal Slot-Pair (NRLSP)

Generally, non-TEM waveguides (e.g., waveguide or SIW) that usually have cut-off properties are demonstrated to be promising in high frequency bands, such as microwave and millimeter-wave frequencies. However, if their fast-wave regions—close to the cut-off—are employed to design RF/microwave EBG periodic structures like [220][227][228], non-radiative discontinuities will be a better choice to avoid detrimental radiation losses accompanied by electromagnetic mutual coupling and crosstalk, which will be more severe over such high frequency bands.

5.3.2.1 Radiation and Circuit Behaviors of the NRLSP

A segment of an SIW symmetrically etched with a pair of longitudinal slots along its centerline is shown in Figure 5.4(a), with its equivalent circuit model described in Figure 5.4(b). Under the dominant TE_{10} mode of the SIW, the E-field distributions in its cross-sectional plane are simply depicted in Figure 5.4(c). Due to the even-symmetrical E-fields distributions of the TE_{10} mode, the aperture field distributions over the two slots will cancel out each other and thus no net radiation would occur. It is interesting to mention that such field behaviors of the NRLSP are strongly localized and resemble that of a typical quasi-TEM microstrip line and CPW. Consequently, the pair of slots will hereon be referred to as “non-radiative longitudinal slot-pair” (NRLSP). Similar to the equivalent circuit model of a single longitudinal slot as shown in Figure 5.3(b), the NRLSP can be ideally modelled as a lossless series *LC* resonator. However, when considering modeling accuracy and practical situations of unavoidably exhibiting little radiation loss, the resistance

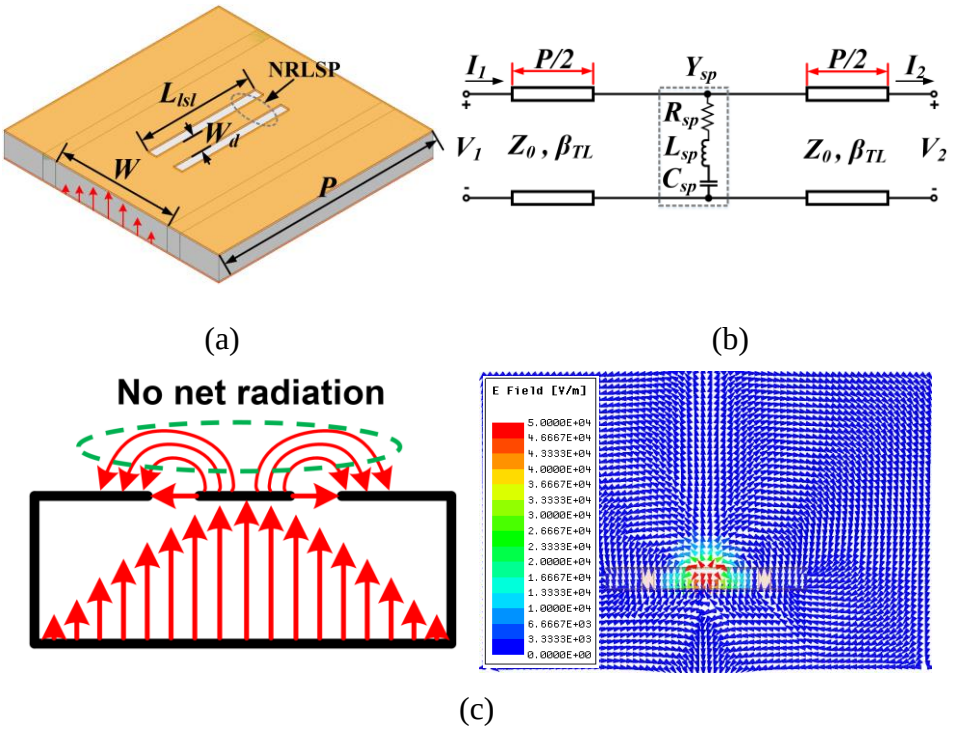

Figure 5.4 NRLSP-based SIW filter unit cell with respect to its (a) geometry, (b) equivalent circuit model, and (c) simplified and simulated *E*-fields distributions

(© 2020 IEEE, reproduced with permission)

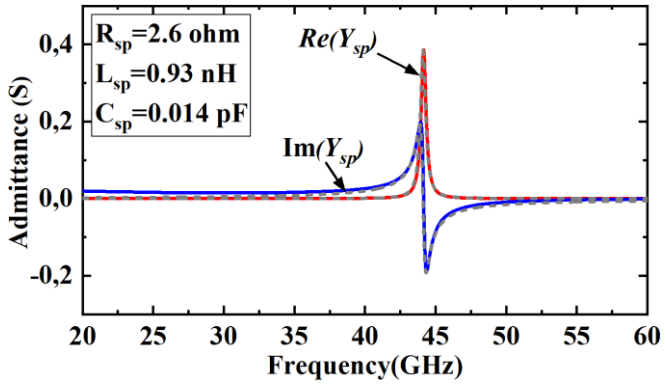

Figure 5.5 Admittance frequency responses of the proposed NRLSP with respect to full-wave and circuit simulations

Solid line and dash lines represent full-wave and circuit results, respectively. Dimensions of the NRLSP-based SIW filter unit cell are P=4.5 mm, W=2.7 mm, L_{lsl}= 2.6mm, and W_d= 0.4 mm. All the slots are with a width of 0.2 mm. (© 2020 IEEE, reproduced with permission)

component representing such radiation loss is also included in the circuit, as shown in Figure 5.4(b). Figure 5.5 shows the admittance frequency responses of the NRLSP with respect to both full-wave and circuit simulations. A relatively good agreement between the two results can be observed in the vicinity of the resonance, while the slight difference in the lower frequencies is perhaps caused by the modeling accuracy. The display of strong resonance with sharp curves indicates the low-loss and high-Q nature of the series resonator (i.e., NRLSP). Values of these circuit components (i.e., R_{sp}, L_{sp}, and C_{sp}) are extracted by using a curve-fitting approach with the help of Advanced Design System (ADS) software. It can be easily observed that radiation resistance R_{sp} introduced by the NRLSP is extremely small and can be neglected (comparatively, the single longitudinal slot with the same dimensions has a resistance component of about 64.5 ohm). To avoid heavily perturbing surface currents of the SIW and thus suffering from potential radiation loss, the NRLSP is suggested to be operated in the capacitive frequency region (before the resonance). As a consequence, the capacitive NRLSP is a good candidate to be used for the development of SIW EBG periodic structures with merits of low radiation loss, low cost and easy fabrication.

5.3.2.2 Guided-wave Characteristics of NRLSP-loaded Periodic SIW

The original and NRLSP-loaded SIWs in terms of their group delays are shown in Figure 5.6(a). Compared to the original SIW which behaves as a highpass filter exhibiting non-zero group delay and larger GDD close to the cut-off frequency, the NRLSP-loaded SIW has typical bandpass behaviors like in Figure 5.2(a) but without the so-called “region 2” presented. The non-zero group delay with large GDD occurs across the whole frequency region that is sandwiched between the two peaks corresponding to the lower and upper cut-off frequencies of the passband. Since filters are a kind of transmission-type components that can be interpreted as equivalent filtering TLs [47], their guided-wave characteristics can be described through transmission parameters, i.e., complex propagation constants $\gamma = \alpha_{eff} + j\beta_{eff}$ and Bloch impedance $Z_B = \mathrm{Re}(Z_B) + j\mathrm{Im}(Z_B)$, in addition to the group delay as mentioned above. In order to explore the behaviors of the NRLSP-loaded SIW, such two parameters can be extracted by simulating a unit cell with the *S*-parameters as follows:

$$e^{\gamma P} = \frac{1 - S_{11}^2 + S_{21}^2 + \sqrt{(1 + S_{11}^2 - S_{21}^2)^2 - 4S_{11}^2}}{2S_{21}} \tag{5.9}$$

$$Z_B = Z_0 \sqrt{\frac{(1+S_{11})^2 - S_{21}^2}{(1-S_{11})^2 - S_{21}^2}} \tag{5.10}$$

where Z_0 represents the characteristic impedance of the host TL, i.e., SIW. Normalized complex propagation constants and Bloch impedance of the periodic SIW, together with the corresponding counterparts of the original SIW, are plotted in Figure 5.6 (b) and (c), respectively. As expected, the original SIW possesses a lower stopband below the cut-off frequency (e.g., 30 GHz), below which the normalized propagation constant is real-valued while the characteristic impedance is purely imaginative (reactive). When the NRLSP is added to the SIW, a bandgap or bandstop occurs at a higher frequency. Within this newly presented stopband, the normalized attenuation constant α_{eff}/k_0 presents a large bump and the normalized phase constant β_{eff}/k_0 shows a linear descending trend with frequency, while the Bloch impedance has only a non-zero imaginative part [225]. By making the two stopbands, lower and higher, closer to each other, the middle fast-wave passband is squeezed. Thus, the normalized phase constant can be significantly sharpened, thereby displaying a high dispersion in accordance with (5.3). This is consistent with a large GDD in the passband according to (5.7), as shown in Figure 5.6(a). It is straightforward that if the periodic SIW with such fast-wave passband characterized by non-zero group delay and larger GDD could be employed to develop LWAs, both filtering and rapid beam-scanning performances could be realized simultaneously.

According to the Bragg effects, the center frequency of the first bandgap or bandstop is related to the periodicity that corresponds to half a guided-wavelength, while the stop-bandwidth is influenced by the scale of loading effects of the discontinuities (e.g., admittance of the NRLSP in the proposed design) [17][18]. To have a comprehensive insight regarding how the parameters of the NRLSP-based unit cell influence its filtering and dispersion performances, a parametric study is conducted in the following. Only the normalized propagation constants $\gamma/k_0 = \alpha_{eff}/k_0 + j\beta_{eff}/k_0$ are shown here for brevity since they can provide similar information as the group delay in accordance with (5.2), (5.3), (5.7) and (5.8). When one parameter of the unit cell is changed, the others are kept constant except for the SIW width which is slightly adjusted to fix the lower cut-off frequency and the lower stopband. As can be seen in Figure 5.7(a), γ/k_0 curves are plotted for different unit cell period length P varying from 3.5 mm to 5.5 mm. The proposed unit cell is related to P=4.5

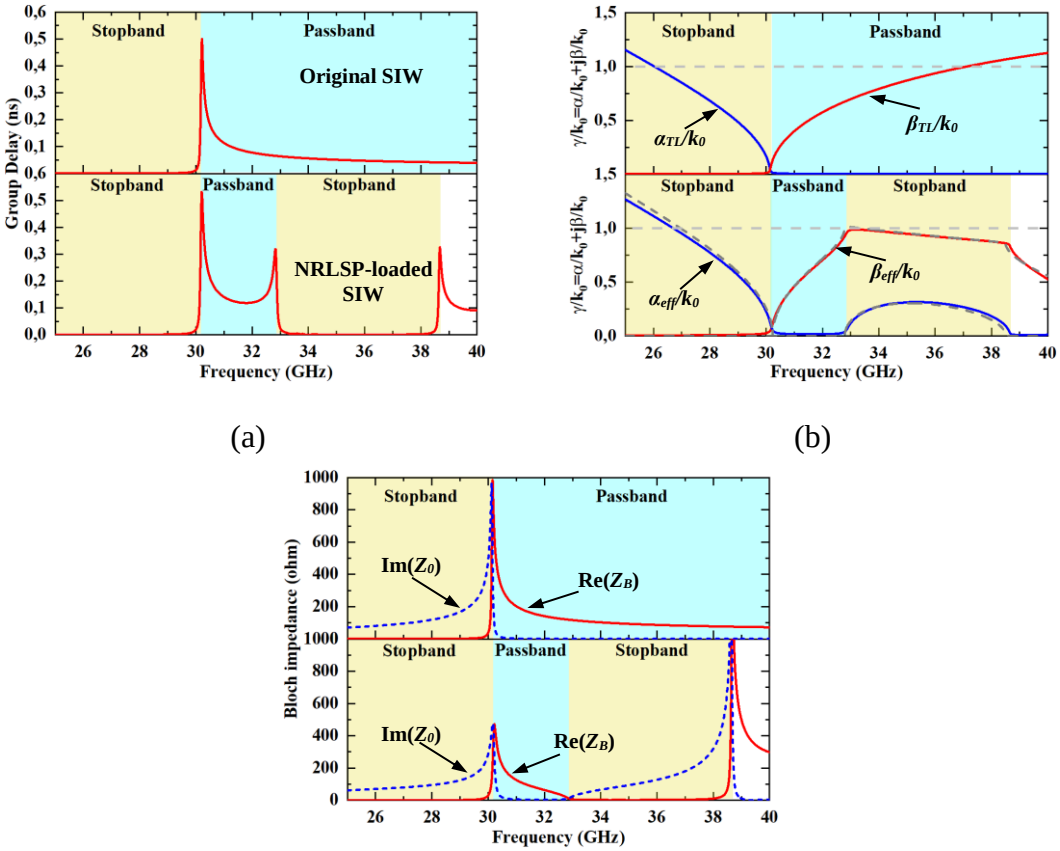

Figure 5.6 Guided-wave characteristics of the proposed non-radiative NRLSP-based SIW filter unit cell

(a) Group delay. (b) Normalized complex propagation constants. (c) Bloch impedance. The lower cut-off frequency is fixed at 30 GHz. Such parameters of the original SIW are also plotted in the top-half of each subfigure for comparison. (© 2020 IEEE, reproduced with permission)

mm and the corresponding results have already been shown in Figure 5.6(b). As P increases, the higher stopband is shifted to a lower frequency, thereby narrowing the middle passband and thus the fast-wave region. Consequently, the β_{eff}/k_0 curves are sharpened and the dispersion is enhanced. Effects of the spacing between two slots of the NRLSP (i.e., W_d) on γ/k_0 are exhibited in Figure 5.7(b). As W_d increases, the center frequency of the higher stopband is kept almost unchanged, which can be explained by the fixed period length P of the unit cell. However, the higher stop-

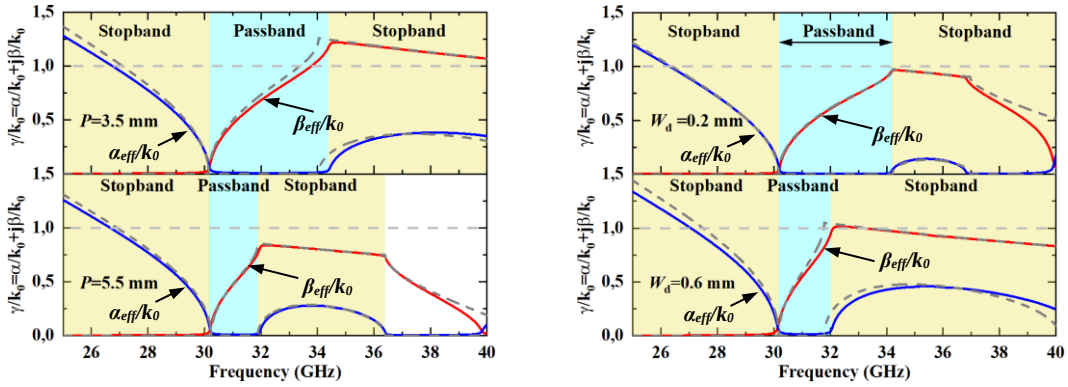

Figure 5.7 Normalized complex propagation constants of the proposed non-radiative NRLSP-based SIW filter unit cell with respect to different (a) period P and (b) slot offset W_d

The proposed unit cell is with P=4.5 mm and W_d=0.4 mm, with these behaviors already plotted in Figure 5.6(b). Solid line and dash lines represent full-wave and circuit simulations, respectively. The effects of P and W_d on the group delay and Bloch impedance can be inferred from Figure 5.6 and Figure 5.7, and thus are not given here for brevity. (© 2020 IEEE, reproduced with permission)

bandwidth is significantly widened, since more transverse currents on the surface of the SIW are cut and thus the admittance of the NRLSP is increased. This implies that the perturbations or loading effects of the NRLSP on the SIW are enhanced. It should be mentioned that properly increasing slot length L_{lsl} also shares the same mechanism, thereby resulting in a similar phenomenon that is not described here for brevity. Both full-wave and circuit simulations are in a reasonable agreement with a slight difference perhaps caused by parasitic effects of the slots that are not considered in circuit modeling.

Up to now, the non-radiative properties of the NRLSP has been demonstrated with its field and circuit behaviors. The related NRLSP-based filter unit cell regarding the filtering and dispersion characteristics have been studied and investigated with resort to the group delay, normalized propagation constants and Bloch impedance. A series of NRLSP-loaded unit cells can be cascaded to develop a filtering and highly dispersive TL or bandpass filter that is also almost free of harmful radiation losses. Its lower cut-off frequency is mainly determined by the width of the SIW, while

the higher cut-off frequency can be tailored by those parameters that have just been studied: P, W_d and L_{lsl}. Therefore, the passband can be flexibly controlled. More importantly, the fast-wave region within the passband can be narrowed to provide an enhanced dispersion, laying the foundation for LWAs with a rapid beam-scanning, as will be demonstrated later.

5.4 NRLSP-based SIW Leaky-wave Antenna—Verification of the RBPF Concept

5.4.1 Modeling and Analysis of NRLSP-based LWA Unit Cell

After the design of the non-radiative NRLSP-based bandpass filter unit cell, radiative discontinuities, such as the TSs shown in Figure 5.3(a), can be loaded to the filter unit cell to introduce controllable radiation leakage. As shown in Figure 5.8, the NRLSP is etched on the bottom layer of an SIW while several identical TSs are uniformly distributed on the top layer. Those fundamental building blocks in Figure 5.3 are used to construct the NRLSP-based LWA unit cell, whose equivalent circuit models are different depending on the position of TSs relative to that of the NRLSP. Specifically, Figure 5.8(a) and (b) describe the cases with odd and even TSs, while their corresponding simplified circuit models are given in Figure 5.8(c) and (d), respectively. For the sake of brevity, only the case with odd TSs is analyzed here and note that the case with even TSs also abide by the same principles. Figure 5.9 shows the effects of the number of TSs on the normalized propagation constant of the unit cell. As N increases, the upper stopband slightly moves to a lower frequency with an almost fixed stop-bandwidth, while the lower stopband remains unchanged. Therefore, the passband and fast-wave region is further squeezed, thus exhibiting a steeper curve of the normalized phase constant than that of the filter unit cell without TSs. The detailed principle explaining this phenomenon can be found in our previous work [142]. When comparing NRLSP and TS with respect to their influence on filtering and dispersion behaviors of the periodic SIW, the TS merely has a relatively minor effect. Consequently, for the proposed LWA, the NRLSP is the predominant mechanism for the characteristics of filtering and high dispersion while the TS is mainly for radiation leakage. Namely, the NRLSP and TS play different roles in determining the behaviors of the proposed LWA: the NRLSP is mainly for filtering and dispersion engineering while the TS is primarily responsible for radiation. Besides, Figure 5.9(b) shows that

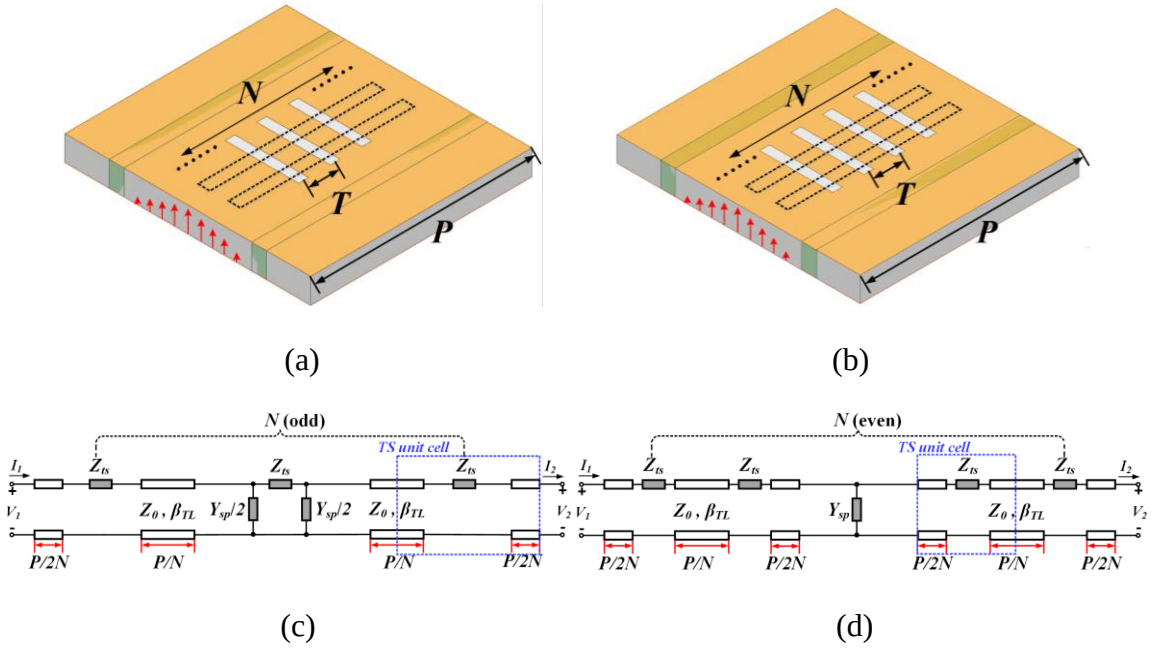

Figure 5.8 NRLSP-based LWA unit cell with *N* uniformly distributed TSs etched on the top layer of the SIW

(a) *N* is odd. (b) *N* is even. (c) Simplified equivalent circuit model corresponding to (a). (d) Simplified equivalent circuit model corresponding to (b). The dashed rectangles in (a) and (b) represent the NRLSP that is etched on the bottom layer of the SIW. These equivalent circuit models are simply constructed by integrating those building blocks shown in Figure 5.3 and 5.4. Dimensions of the NRLSP-based LWA unit cell are P=4.5 mm, W=2.7 mm, T=0.9 mm, L_{tsl}=1.5 mm, L_{lsl}= 2.6mm, and W_d= 0.4 mm. Some definitions of these parameters can be found in Figure 5.3 and 5.4. All the slots are with a width of 0.2 mm. (© 2020 IEEE, reproduced with permission)

the more TSs etched on a filter unit cell, the more radiation occurs in the passband to a certain extent, which is quite understandable. This means that by adjusting the number of TSs within a unit cell, the attenuation constant of the proposed LWA can be flexibly controlled, not to mention the conventional approach of adjusting the length of TSs to elegantly control the radiation leakage [21][49][50]. The phase constant can also be easily manipulated or compensated to realize a designated value by adjusting the parameters of the NRLSP such as W_d and L_{lsl} but without just resorting to the width of SIW like [116] does. Consequently, the proposed LWA can provide

independently controllable attenuation and phase constants, which is advantageous for the design of diverse beamwidth and low side-lobe designs [9][11], in addition to the filtering and rapid beam-scanning performances as particularly discussed above.

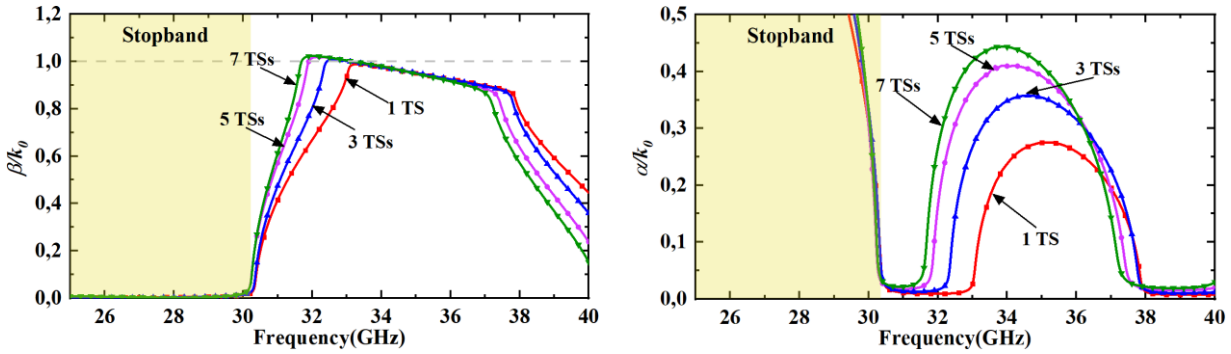

(a) (b)

Figure 5.9 Normalized (a) phase constant and (b) attenuation constant of the NRLSP-based LWA unit cell with *N* transverse slots (*N*=1, 3, 5, and 7, respectively) etched on its top layer

(© 2020 IEEE, reproduced with permission)

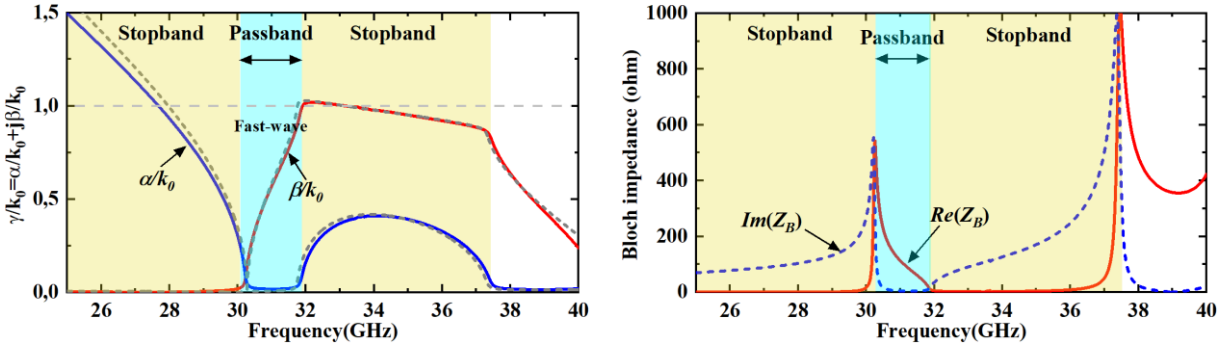

(a) (b)

Figure 5.10 Proposed NRLSP-based LWA unit cell with 5 TSs, with respect to its (a) normalized complex propagation constants and (b) Bloch impedance

(© 2020 IEEE, reproduced with permission)

5.4.2 Simulation and Measurement of NRLSP-based LWA

Since the NRLSP-based LWA unit cell described above has both fast-wave bandpass and highly dispersive characteristics, a set of such unit cells can be cascaded to form a quasi-uniform type

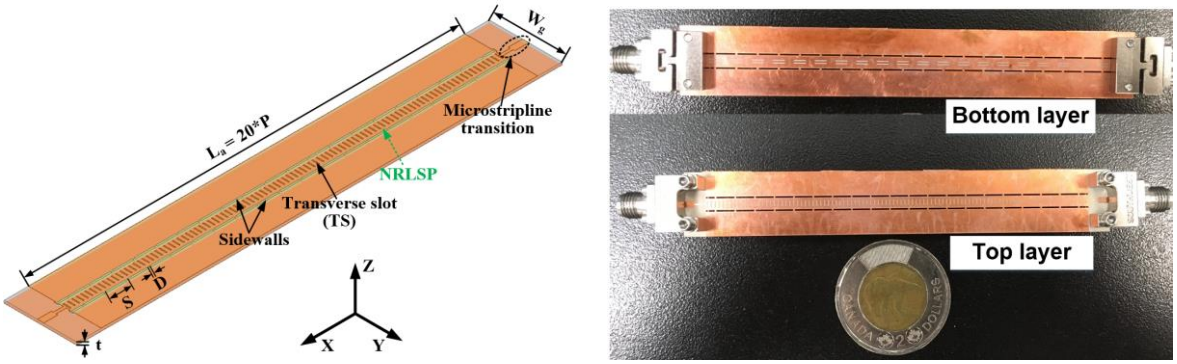

(a) (b)

Figure 5.11 (a) Configuration of the proposed NRLSP-based LWA. (b) Photograph of the fabricated prototype

The substrate used here is RT/duroid 6002 with a relative permittivity of 2.94, a dielectric loss tangent of 0.0012 and a thickness of 0.508 mm. The copper cladding on the substrate has a thickness of 17.5 um. Plated slot-via arrays with parameters of *S*=4.5 mm and *D*=0.35 mm are used to form the sidewalls of the SIW. (© 2020 IEEE, reproduced with permission)

LWA featuring both filtering and rapid beam-scanning properties. Here, the LWA unit cell with 5 TSs is selected to provide fairly rapid beam-scanning and moderate radiation leakage per unit-length, for demonstration purposes. Its normalized propagation constant and Bloch impedance are plotted in Figure 5.10(a) and (b), respectively. In this case, 20 unit cells are cascaded to ensure that 90% of the power can be consumed while the remaining is absorbed by a matching load. Figure 5.11 depicts the proposed LWA model and the photograph of its prototype fabricated through the standard PCB process. A quarter-wavelength impedance transformer is designed to transform the Bloch impedance of the LWA to a 50-ohm microstrip line for good impedance matching and measurement convenience. Simulated and measured *S*-parameters are plotted in Figure 5.12. It is seen that a good impedance matching with $|S_{11}|$ less than -10 dB is realized experimentally from 30.6 to 32.3 GHz. Meanwhile, the measured $|S_{21}|$ is approximately lower than -20 dB in this frequency range, implying that more than 90% of the power is consumed. A small frequency shifting of about 0.3 GHz—less than 1% of the center frequency—is observed between the simulated and measured results, which may be caused by the fabrication error of slot-via holes in

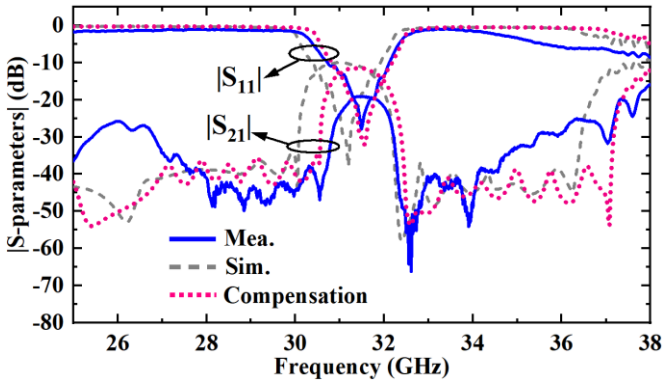

Figure 5.12 Simulated and measured *S*-parameters of the proposed NRLSP-based LWA

The curves marked as "Compensation" represent the corresponding simulated results when considering fabrication tolerances of the slot-via. (© 2020 IEEE, reproduced with permission)

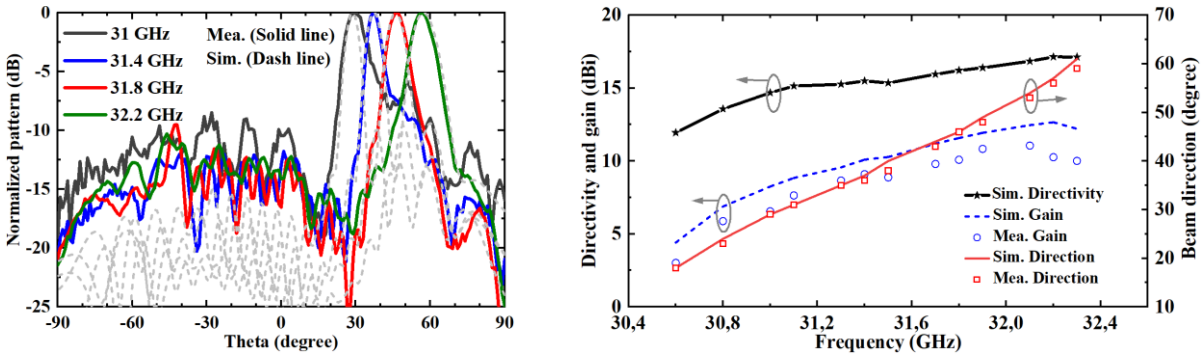

(a) (b)

Figure 5.13 (a) Simulated and measured radiation patterns on the *xoz* plane with respect to several frequencies. (b) Simulated and measured gains and simulated directivity

With frequency shifting considered, the simulated results described in the two figures are the ones with 0.3 GHz lower than the nominal frequencies. (© 2020 IEEE, reproduced with permission)

our Poly-Grames Research Center. Because of the enlarged slot-via holes, the practical width of the SIW is reduced, implying that the lower cut-off frequency of the periodic SIW will increase (the upper one is just slightly influenced as explained above). By suitably decreasing the width of

the SIW in the simulated model, compensated (parametrically corrected) results are described in Figure 5.12 for comparison. It can be seen that the measured results coincide well with the compensated counterparts, except for the increased insertion loss that may be caused by increased dielectric and conductor losses as well as the loss from connectors. Most importantly, obvious filtering behaviors are illustrated with more than 20 dB out-of-band suppression in both simulated and measured $|S_{21}|$. Simulated and measured radiation performances on the scanning plane (i.e., *xoz* plane) are depicted in Figure 5.13. It should be noted that the presented simulated results are the ones with 0.3 GHz lower than the nominal frequencies. As indicated in Figure 5.13(a), a reasonable agreement is observed between simulated and measured radiation patterns. Figure 5.13(b) shows simulated and measured realized gains as well as simulated directivity. In the simulated cases, the maximum directivity and gain of about 17.1 dBi and 12.7 dBi are respectively achieved in the frequency band from 30.6 to 32.3 GHz, in which the main-beam scans from 18^{o} to 61^{o} with a rapid beam-scanning rate. The measured results agree generally with their simulated counterparts, except for a reasonable gain drop of approximately 1.7 dBi that may be caused by measurement issues, increased dielectric and conductor losses, and/or connector loss [14][52] [85][116][127][142]. In practical situations, since the bottom metal layer of the NRLSP-based LWA is actually a semi-closed structure that may make the proposed antenna potentially suffer from detrimental interferences from other components and circuits, a grounded substrate layer, with the use of low-cost multi-layered PCB techniques, can be placed underneath it to act as a shielding layer and also improve the structural strength of the whole antenna structure.

5.5 IRIS-based SIW Leaky-wave Antenna—A Further Demonstration of the RBPF Concept

In addition to the NRLSP, the iris or shorting wall [as shown in Figure 5.3(c)] can also be used as a kind of closed discontinuities for developing periodic TLs or filters [229][230], which can be easily implemented in SIW technology. It is necessary to mention that the NRLSP and iris have complementary susceptance behaviors: the NRLSP generally features capacitive behaviors (it is intentionally designed before the resonance to avoid potential radiation losses), while the iris is purely inductive. Figure 5.14(a) depicts the proposed iris-based SIW LWA unit cell with five identical TSs uniformly etched on its top layer. Figure 5.14(b) and (c) show the normalized

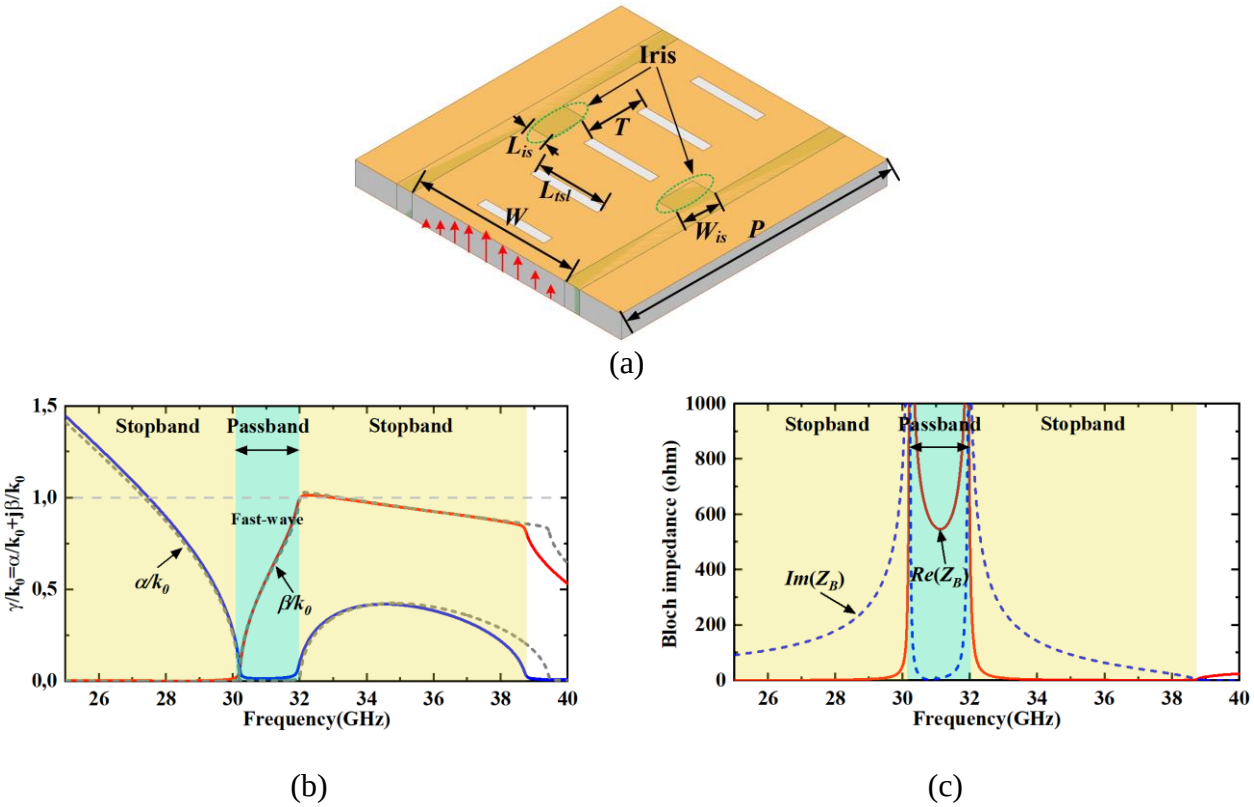

Figure 5.14 Iris-based LWA unit cell with respect to its (a) configuration, (b) normalized complex propagation constants, and (c) Bloch impedance

Dimensions of the iris-based unit cell are P=4.5 mm, W=3.45 mm, T=0.9 mm, L_{tsl}=1.5 mm, L_{is}= 0.62 mm, W_{is}= 0.4 mm. All the slots have a width of 0.2 mm. (© 2020 IEEE, reproduced with permission)

propagation constants and Bloch impedance of the LWA unit cell, respectively. It can be seen that a very narrow fast-wave passband is sandwiched between two stopbands, which is similar to that of the NRLSP-based counterpart. However, the Bloch impedance has a very high value in its passband, which may suffer from an impedance matching problem. To this end, a tapered segment inspired from [14][66][144][223] is specially designed, as shown in Figure 5.15(a), to transform the high Bloch impedance of the periodic SIW to the port impedance of the host SIW. In addition, it plays a role in converting the guided mode inside the host SIW to the leaky Bloch mode of the LWA. This transformer mainly consists of four period-varying unit cells embedded with linearly

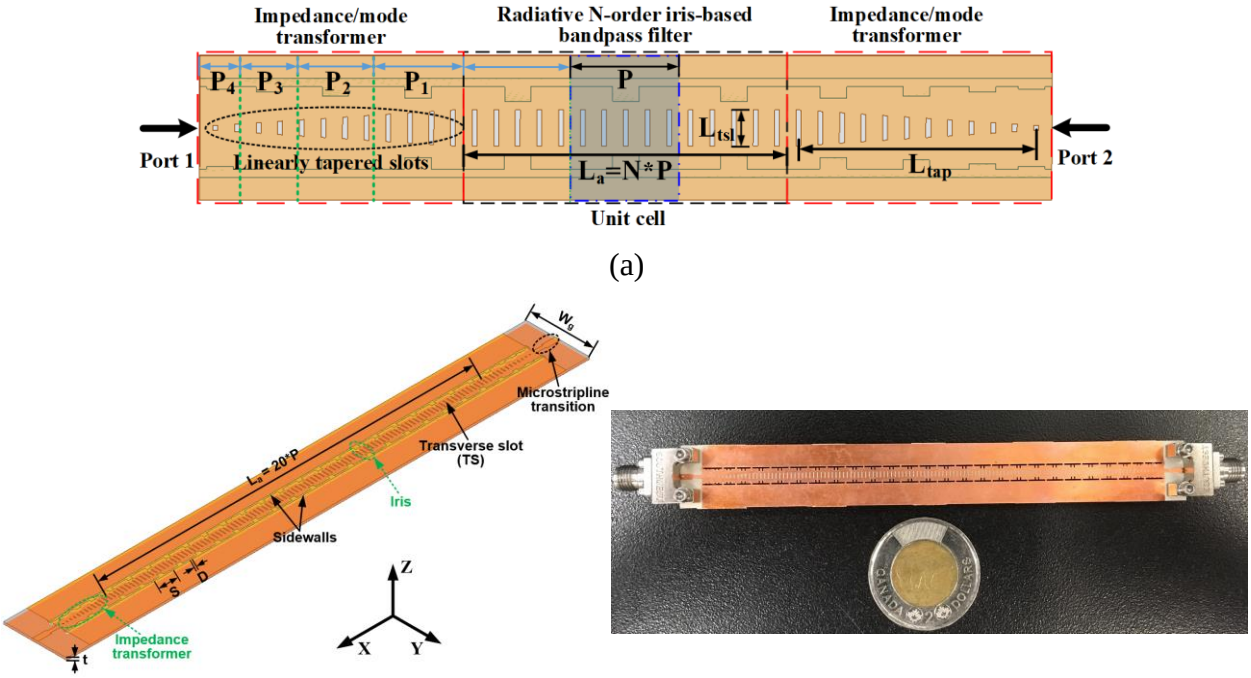

Figure 5.15 (a) Geometry of the proposed impedance/mode transformer. (b) Configuration of the proposed iris-based LWA. (c) Photograph of the fabricated prototype

For the impedance/mode transformer, tapered parameters include the length of the period length, iris and slot. Specifically, the period length of each unit cell follows P_n=P-0.7*n, while the slots is linearly tapered from L_{tsl} to zero with the quantity of approximately $\sum P_n / T$. The length of the iris (i.e., L_{is}) in each unit cell complies with a reduction factor of 0.2 along the direction to the termination. The width of the iris and slot, as well as the spacing between tapered slots are fixed and kept the same as those of the LWA unit cell. The substrate used here is the same as the one in the NRLSP-based design. (© 2020 IEEE, reproduced with permission)

tapered slots and irises. Figure 5.15(b) and (c) respectively depict the final simulated model and fabricated prototype of the proposed iris-based LWA with two microstrip transitions terminated at the two ends to facilitate measurement. Again, 20 unit-cells are cascaded to make 90% of the injected power can be consumed, and a matching load is used to absorb the remaining power. Similar to the NRLSP-based LWA, a small frequency shift of about 0.25 GHz is also observed in this iris-based LWA by comparing its simulated and measured S-parameters, as shown in Figure

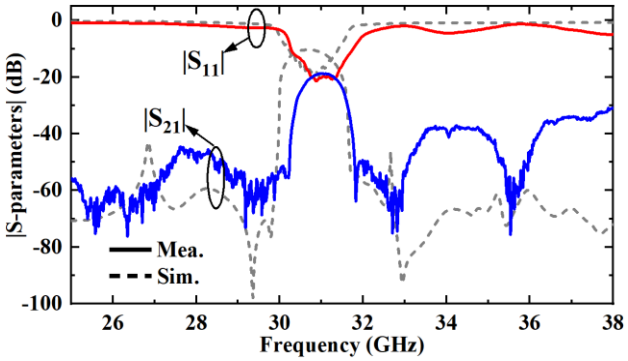

Figure 5.16 Simulated and measured *S*-parameters of the proposed iris-based LWA

(© 2020 IEEE, reproduced with permission)

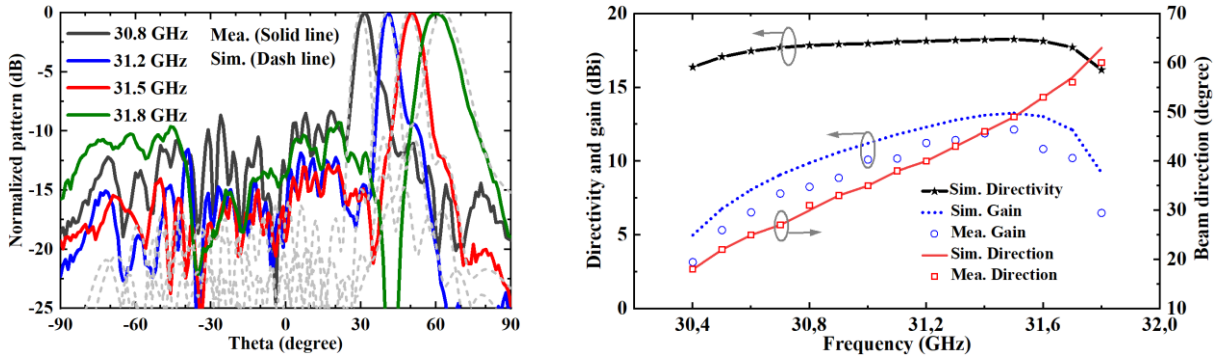

(a) (b)

Figure 5.17 (a) Simulated and measured radiation patterns on the *xoz* plane with respect to several frequencies. (b) Simulated and measured gains and simulated directivity

With frequency shifting considered, the simulated results described in the two figures have 0.25 GHz lower than the nominal frequencies. (© 2020 IEEE, reproduced with permission)

5.16. This may be attributed to the fabrication tolerance of the slot-vias as explained before. Measured results indicate that from 30.4 to 31.8 GHz the reflection coefficient is lower than -10 dB while the insertion loss is greater than 19 dB. Filtering performances of more than 40 dB out-of-band suppression are observed in both simulated and measured $|S_{21}|$. Figure 5.17 describes the simulated and measured radiation performances on the scanning plane (i.e., xoz plane), with the simulated ones compensated by 0.25 GHz. A relatively good agreement is observed between simulations and measurements in terms of radiation patterns and beam directions. Notably, the beam can be scanned from 18^o to 63^o within a narrow frequency range from 30.4 to 31.8 GHz. As

for the gain performances shown in Figure 5.17(b), a small but reasonable drop is found in the measured results compared to the simulated counterparts, with the maximum of about 12.1 dBi achieved experimentally. The large difference between simulated directivity and gain indicates serious losses from the conductor and dielectric close to the lower cut-off region. This phenomenon can also be found in [20][21][49][51] which make use of natural fast-wave regions of an SIW to design LWAs.

5.6 Discussion and Comparison

So far, the NRLSP- and iris-based 1-D LWAs have been proposed and studied elaborately to demonstrate the RBPF concept in the development of multifunctional LWAs possessing both filtering and rapid frequency beam-scanning characteristics. In order to highlight the benefits of this design, the proposed iris-based LWA is selected on behalf of the class of RBPF-based LWAs and compared with conventional transversely slotted SIW LWAs which are similar to [14][52] [85][116][127][142]. For a fair comparison, the two LWAs are kept almost the same except for the SIW's width which is slightly adjusted to maintain similar cut-off frequencies. Figure 5.18 depicts the comparison between the two LWAs with respect to their $|S_{21}|$ and beam-direction performances. Compared to the traditional one, the proposed scheme has an apparent filtering capability with exhibiting a good out-of-band suppression or frequency-selectivity as well as a rapid frequency beam-scanning property. When marking a comparison with the reported filtering LWAs [236][237], it is noted that the proposed concept relies on adding extra radiative discontinuities to specially pre-designed filters by which both of the two highlighted characteristics can be simultaneously realized for LWAs. However, the works in [236][237], contrastively, are just dependent on conventional filtering antenna techniques similar to [231]-[235] and ride on introducing extra filtering elements into the feeding ends or unit cells of LWAs to realize filtering capability. Also note that both of the aforementioned two works are short of rapid beam-scanning characteristics and are also potentially subject to harmful radiation brought by the filtering elements. Another comparison conducted between the proposed and other reported works is tabulated in Table 5.1 to further highlight the merits of the propose designs. Firstly, apart from the controllable filtering capability possessed by the proposed designs, the dispersion and radiation behaviors can be independently engineered by separate modules (e.g., NRLSP and TS, accordingly). In other words,

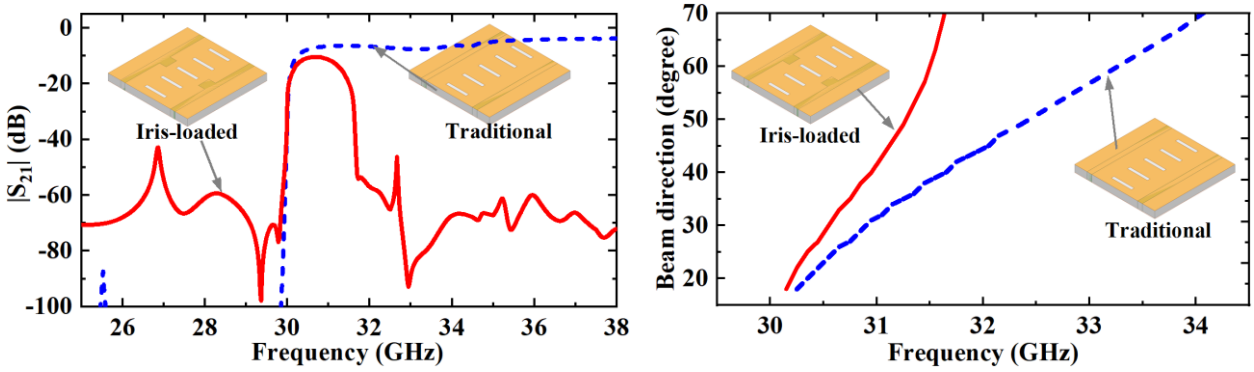

(a) (b)

Figure 5.18 Comparison of (a) $|S_{21}|$ and (b) beam-direction with respect to the proposed iris-based LWA and its traditional counterpart without the iris

The two LWAs are kept almost same except for the SIW' width that is adjusted to maintain the similar lower cut-off frequencies. (© 2020 IEEE, reproduced with permission)

the phase and attenuation constants can be independently controlled, which is beneficial for diverse beamwidth and low side-lobes LWA designs but is not merely limited to the rapid beam-scanning as demonstrated in this chapter. Most other reported works in the table, however, fail to embrace these features, and so do the works in [236][237]. Additionally, with the proposed RBPF concept, the filter theory aimed for constant group delay, e.g., Bessel-Thomson filters [238], can be potentially exploited to construct prospective LWAs that are capable of fixed-beams with frequency. This will be explored in our future work. Finally, when making a quantitative comparison in the table, it is seen that the proposed designs are superior to most works in terms of the beam-scanning rate. Also note that the proposed work is the only one designed in the millimeter-wave range with additional virtues of simple structure, easy fabrication and low cost, which may find potential applications in millimeter-wave systems.

5.7 Conclusion

In this chapter, a class of quasi-uniform 1-D multifunctional LWAs simultaneously possessing both rapid beam-scanning and frequency-selective characteristics based on the RBPF concept have been proposed, studied and demonstrated. Two kinds of susceptance-complementary non-radiative discontinuities, namely the NRLSP and iris that can be easily realized in SIW technology, are

respectively exploited to construct EBG periodic structures exhibiting flexible bandpass and dispersion behaviors, upon which RDs (i.e., TSs) are deliberately introduced for implementing LWAs with controllable radiation leakage. Guided-wave characteristics in terms of dispersion and frequency-selectivity behaviors of the proposed periodic SIW bandpass filters have been investigated by resorting to group delay, complex propagation constants and Bloch impedance. Besides, the relationship between the GDD and beam-scanning properties of an LWA is established, by which the filter theory can be borrowed for designing LWAs with flexible beam-scanning behaviors. For demonstration purposes, two RBPF-based LWAs are developed with both filtering and rapid beam-scanning characteristics confirmed by both simulated and measured results, thereby validating the correctness and effectiveness of the RBPF concept in the design of such a class of multifunctional LWAs. As a complementary implementation, the RBPF concept with constant group delay may be potentially explored for LWAs possessing fixed beam with frequency.

Table 5.1 A Comparison between the Proposed Work and Several References (© 2020 IEEE, reproduced with permission)

Ref.	Operating Bandwidth	Scanning Range	Beam-Scanning Rate (º / %)	Maximum Gain (dBi)	Filtering Capability	Structural Technique & LWA Type
[14]	10.2-12 GHz (16.2%)	15º – 72º (57º)	3.5	8.9	No	SIW, Quasi-Uniform
[52]	8.6-12.8 GHz (39.3%)	-70º – 60º (130º)	3.3	10.8		
[139]	24-27 GHz (11.8%)	-17º – 13º (30º)	2.5	12.5		
[51]	9-14 GHz (43.5%)	-40º – 35º (75º)	1.7	12		SIW, Periodic
[144]	13.5-13.9 GHz (3%)	2º – 37º (35º)	11.7	13.3		
[147]	11-16 GHz (37%)	5º – 67º (62º)	1.7	12.2		Hollow waveguide, Quasi-uniform
[33]	6.9-8.75 GHz (23.6%)	38º – 75º (37º)	1.6	12.7		Microstrip, Uniform
[145]	3.43-3.7 GHz (7.6%)	40º – 76.5º (36.5º)	4.8	15.5		
[138]	8.9-10.6 GHz (17.4%)	-27.5º – 46º (73.5º)	4.2	15.5		Microstrip, Periodic
[148]	2.4-2.6 GHz (8%)	8º – 35º (27º)	3.4	7		
[237]	22-28 GHz (24%)	-44º – 40º (84º)	3.5	12.5	Yes	SIW, Quasi-Uniform
NRLSP-based	30.6-32.3 GHz (5.4%)	18º – 59º (41º)	7.6	12.7		
Iris-based	30.4-31.8 GHz (4.5%)	18º – 60º (42º)	9.3	12.1		

CHAPTER 6 ARTICLE 4: LEAKY-WAVE ANTENNA FEATURING STABLE RADIATION BASED ON MULTIMODE RESONATOR (MMR) CONCEPT

Dongze Zheng and Ke Wu

Published in the *IEEE Transactions on Antennas and Propagation*, vol. 68, no. 3, pp. 2016-2030, Mar. 2020.

In this chapter, a scheme based on the MMR concept is proposed and demonstrated for the design and development of LWAs to realize stable radiation properties (e.g., stable radiation efficiency and gain). Firstly, two kinds of traditional LWA unit cells possessing typical SMR and monotonic changing radiation behaviors are theoretically modeled and analyzed. The condition for LWAs featuring stable radiation properties is then derived, based on which the MMR concept is proposed as a solution for radiation stability. For demonstration purposes, two types of MMR-based unit cells and their associated one-dimensional periodic LWAs are studied and developed for millimeter-wave applications. One type is based on the MED, while the other originates from the ACPA. To facilitate the implementation, a detailed design procedure for this class of LWAs is provided in a general manner. The proposed two MMR-based periodic LWAs are modeled, fabricated and measured. Simulated and measured results are in a reasonable agreement and both illustrate the stability of radiation efficiency and gain performances, thereby demonstrating the correctness and effectiveness of the proposed MMR design concept.

6.1 Introduction

As a significant member of the family of travelling-wave antennas, the LWA has attracted much attention for many decades due to its many appealing features, such as low profile, narrow beam, high directivity, simple feeding and particular frequency beam-scanning capability, which may find many potential applications in broadband wireless communications, sensors and FMCW radar systems [9][11]. A large variety of LWAs based on various transmission line technologies have

been proposed and studied since the 1940s, such as metallic RWG [13][19][20], microstrip line [27]-[36], CPS [37]-[39], CPW [40]-[41], SIW [42]-[65], and SSPPs [66]-[76], etc. Among these LWAs, some belong to the uniform or quasi-uniform type LWAs that make use of the fundamental mode or space harmonic to radiate. The others, contrastively, are classified into the periodic group, where the fundamental space harmonic is normally a slow wave (bound wave) that does not radiate while a higher-order one (e.g., the -1st space harmonic) is used to work as the main radiation mechanism. However, no matter the categories of LWAs that differ in appearances (i.e., uniform, quasi-uniform or periodic) or in radiating space harmonics (i.e., fundamental or higher-order), all the LWAs must be formed by creating RDs that are distributed discretely or continuously along host transmission lines. These RDs are generally developed by slots [14][19]-[21][40][45][50]-[52][56][57], stubs [15][30]-[32], gaps [37][41][43], coupled-patches [66][67], etc. They operate to break up the original boundary conditions and field distributions of the host transmission lines. Then, equivalent lossy transmission lines are established where the losses are mainly in the form of radiation.

The impedance/admittance properties of RDs should be extracted and analyzed prior to the design of an LWA. This is because they are not only responsible for the LWA's total circuit performances, but also closely linked to its overall radiation characteristics that are mainly determined by complex propagation constants of the leaky mode. For example, general formulas for two-dimensional LWAs based on partially reflective surface (PRS) were derived to relate the PRS's shunt admittance to the far-field patterns of LWAs [240]-[242]. However, the relationship between the impedance/admittance properties of RDs and radiation behaviors of LWAs has not been fully developed, as in the radiation stability in 1-D periodic LWAs for instance. Although several works reported in [30]-[31][243]-[245] make use of composite unit cells or double-layered PRSs exhibiting both inductive and capacitive behaviors as well as accompanied radiation stability, most of RDs in LWAs have only singular reactance/susceptance properties practically. This implies that they are either inductive [14][15][38][50][51][56][57] or capacitive [32][37][40][41][52] in the frequency band of leaky-wave operation. Due to such characteristics of RDs, radiation performances of these LWAs suffer from monotonic changing trend with frequency. This phenomenon will be particularly explored in this chapter.

On the other hand, the MMR concept has been used for many years in the design of wide/multi-

band antennas [246]-[251] and filters [252]-[255]. They all share the similar working principle in that by controlling and collocating several resonant modes in a certain manner, a wideband or multi-band performance can be formed. However, these aforementioned works are merely related to either resonant-type radiator (antenna) or non-radiator (filter). Although the LWA design based on typical magneto-electric dipole unit cells has already been considered in [58], to the authors' knowledge, a generalized MMR design concept for LWAs has not been reported so far and thus the underlying features remain unexplored. In this work, the impedance/admittance properties of RDs are analyzed in detail, and the design concept based on the MMR is proposed for the first time in the design of LWAs for realizing stable radiation properties (i.e., radiation efficiency and gain). Prior to the introduction of the MMR, two kinds of conventional unit cells for periodic LWAs featuring monotonic changing radiation characteristics are analyzed, and their typical single-mode resonator (SMR) behaviors over the working frequency range are demonstrated. Subsequently, the condition to achieve stable radiation for LWAs is derived, upon which the MMR concept is naturally proposed as a solution for radiation stability. For demonstration purposes, two popular MMR-based radiators, i.e., the magneto-electric dipole (MED) and aperture-coupled patch antenna (ACPA), are employed, and their associated 1-D periodic LWAs are studied and developed for millimeter-wave applications. Impedance matching techniques are adopted in these unit cells to effectively suppress the open-stopband issue for a continuous beam-scanning through broadside. For easy implementation, a detailed design procedure is provided in a general manner to design such a class of MMR-based LWAs. The proposed two types of LWAs are simulated, fabricated and measured. Both simulated and measured results are in a reasonable agreement, showing that stable radiation properties such as efficiency and gain are achieved. Therefore, the correctness and effectiveness of the MMR concept in the design of LWAs is successfully demonstrated.

The rest of this chapter is organized as follows. In Chapter 6.2, the radiation stability of LWAs are theoretically analyzed and related to the impedance/admittance of RDs, followed by the introduction of the MMR design concept. In Chapter 6.3, the MED is selected as an MMR to design a 1-D periodic LWA, and a specific design guideline is provided in a general way for this class of MMR-based LWAs. Another typical MMR-based radiator, the ACPA, is employed to construct a second LWA for further verification of the design concept, and this is described in Chapter 6.4. Finally, this chapter ends up with a discussion and comparison in Chapter 6.5 and a conclusion in

Chapter 6.6.

6.2 Theory and Principle

6.2.1 Analysis of Two Representative Unit Cells

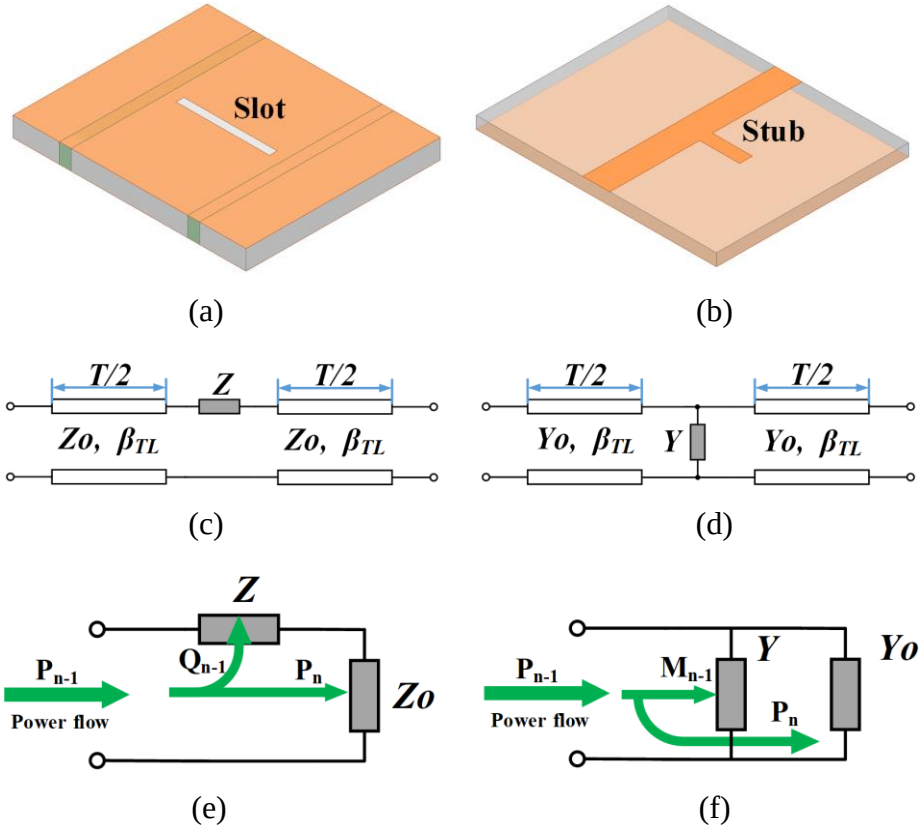

Figure 6.1 Two typical LWA unit cells and their relevant equivalent circuit models and power-flow diagrams

(a) Transversely slotted SIW LWA unit cell. (b) Microstrip combline LWA unit cell. (c) Series-loading type circuit model corresponding to (a). (d) Shunt-loading type circuit model corresponding to (b). (e) Power-flow diagram corresponding to (c). (f) Power-flow diagram corresponding to (d). These power-flow diagrams are under the assumption that perturbation caused by RDs is very small, i.e., $Z \ll Z_0$ and $Y \ll Y_0$, and thus pure travelling waves propagate inside unit cells. The Bloch impedance of the perturbed transmission line is approximate to the characteristic impedance of the original one. (© 2020 IEEE, reproduced with permission)

Figure 6.1 depicts two kinds of typical LWA unit cells. The first one, as shown in Figure 6.1(a), is a transversely slotted SIW LWA unit cell, and its equivalent circuit model is described in Figure 6.1(c). The second shown in Figure 6.1(b) refers to a microstrip combline counterpart with its equivalent circuit model plotted in Figure 6.1(d). It is necessary to mention that these unit cells analyzed here are made of totally different types of transmission line technologies, RDs and equivalent circuit models. More importantly, they can represent most periodic LWAs in the open literature. As shown in Figure 6.1(c) and (d), Z_0 and Y_0 represent the characteristic impedance and admittance of the host transmission lines, respectively. β_{TL} is the phase constant of the host transmission lines while T denotes the period length of unit cells. Z and Y represent the impedance and admittance properties (i.e., loading effects) of RDs, respectively. The normalized impedance Z/Z_0 or admittance Y/Y_0 of the RDs can be calculated with the help of *ABCD* matrix or *S*-parameter of the unit cell [17]. They can be expressed as

$$Z = Z/Z_0 = \frac{2S_{11}e^{j\theta_{TL}}}{1-S_{11}e^{j\theta_{TL}}} \tag{6.1}$$

$$Y = Y/Y_0 = -\frac{2S_{11}e^{j\theta_{TL}}}{1+S_{11}e^{j\theta_{TL}}} \tag{6.2}$$

where θ_{TL} is the electrical length of the unit cell and can be expressed as $\theta_{TL} = \beta_{TL}T$.

In order to find frequency responses of the normalized impedance/admittance of RDs (i.e., slot and stub), a single unit cell as shown in Figure 6.1(a) or (b) is simulated, and the formula (6.1) or (6.2) can be used to conduct the extraction. Full-wave simulation package ANSYS HFSS is used here to facilitate this process. It is found that both RDs share a similar frequency response in terms of their normalized impedance/admittance. Thus, a generalized form of that is simply plotted in Figure 6.2 for illustration. It can be seen that for both RDs, there is only one resonance over a wide frequency bandwidth of two octaves, demonstrating their typical SMR behaviors. Both real and imaginary parts show a monotonic increasing trend before the resonance and a descending trend after, with respect to frequency. Since LWAs are a class of non-resonant antennas and the RDs should avoid operating in the vicinity of the resonant region to have a slowly attenuated travelling wave, the alternative working frequency region should be in the inductive or capacitive region (i.e., before or after the resonance accordingly) and far away from the resonance as in most periodic

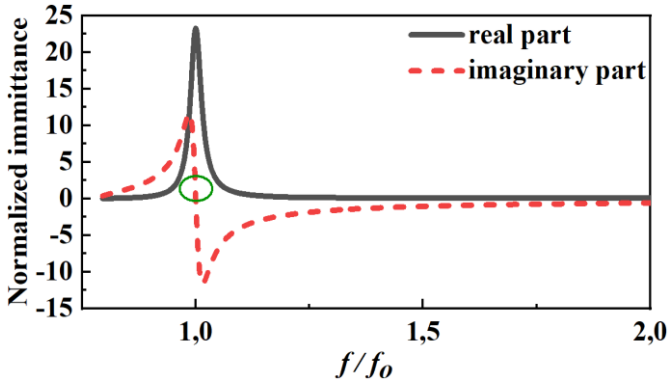

Figure 6.2 Normalized impedance/admittance behaviors of RDs in a general manner corresponding to different kinds of unit cells shown in Figure 6.1

f_0 is the resonant frequency (e.g., 25 GHz) of the related RDs. (© 2020 IEEE, reproduced with permission)

LWAs. As a result, RDs will exhibit monotonic changing resistance/conductance in the leaky frequency region, and this will give rise to LWAs suffering from monotonic changing radiation characteristics as explained later.

6.2.2 Condition for Stable Radiation Efficiency

To find the relationship between the normalized impedance/admittance performances of RDs and the radiation behaviors (e.g., radiation efficiency) of LWAs, the power-flow diagrams of series-type and shunt-type circuit models are depicted in Figure 6.1(e) and (f), respectively. Here, it is assumed that pure traveling waves propagate inside the unit cells with no reflections encountered in their input ports. This is reasonable for most periodic LWAs since perturbations caused by RDs are generally very small (i.e., $Z \ll Z_0$ and $Y \ll Y_0$) and therefore the Bloch impedance of the perturbed transmission line is close to the characteristic impedance of the original one [9][11]. Also it should be noted that other losses from conductors and dielectrics are not considered in these cases; only the radiation loss is included. This allows us to clearly identify the radiation properties of LWAs since the conductor- and dielectric-related losses contributions can be linearly superposed in the end. Consequently, for the series-type circuit model shown in Figure 6.1(e), there is

$$P_{n-1} = Q_{n-1} + P_n \tag{6.3}$$

where P_{n-1} is the injected power to the nth unit cell, Q_{n-1} is the radiated power manifested through the real part of the impedance/admittance of RDs, and P_n represents the remaining power of the unit cell (i.e., the power flowing to the rest of the LWA). The radiated power, therefore, can be expressed as

$$\begin{aligned} Q_{n-1} &= P_{n-1} \cdot re\left[Z/(Z+Z_0)\right] \\ &\approx P_{n-1} \cdot re(Z/Z_0) \\ &= P_{n-1} \cdot re(Z) \end{aligned} \tag{6.4}$$

The approximation within (6.4) is reasonable without losing generality, since the perturbation of RDs is normally small and thus it can be neglected compared to the characteristic impedance of the host transmission line, as discussed above. Based on this condition, the radiation efficiency of a unit cell $e_{r(unit)}$ can be defined and expressed as

$$\begin{aligned} e_{r(unit)} &= Q_{n-1}/P_{n-1} \\ &\approx re(Z) \end{aligned} \tag{6.5}$$

Thus, according to [9], the attenuation constant α of the unit cell can be approximately derived as

$$\alpha \approx -\ln\left[1-re(Z)\right]/2T \tag{6.6}$$

Consequently, the total radiation efficiency e_r of an LWA consisting of N unit cells can be expressed as

$$\begin{aligned} e_r &= 1-e^{-2\alpha L} \\ &= 1-e^{-2\alpha NT} \\ &\approx 1-\left[1-re(Z)\right]^N \end{aligned} \tag{6.7}$$

where $L = NT$ is the overall length of an LWA.

As for the shunt-type circuit model, the corresponding radiation efficiency of an LWA can be expressed as $e_r \approx 1\text{-}[1\text{-re}(\tilde{Y})]^N$, sharing a similar expression as (6.7). From the above analysis, it is concluded that the radiation efficiency of a periodic LWA is only concerned with the real part of normalized impedance/admittance of RDs. In other words, if the real part of normalized impedance/admittance of RDs can be kept stable with frequency, the radiation efficiency of the related LWA can remain constant accordingly. Now, bearing this remark in mind and paying attention to Figure 6.1 and Figure 6.2, it is understandable that why most periodic LWAs having typical SMR behaviors cannot achieve a stable radiation efficiency and gain.

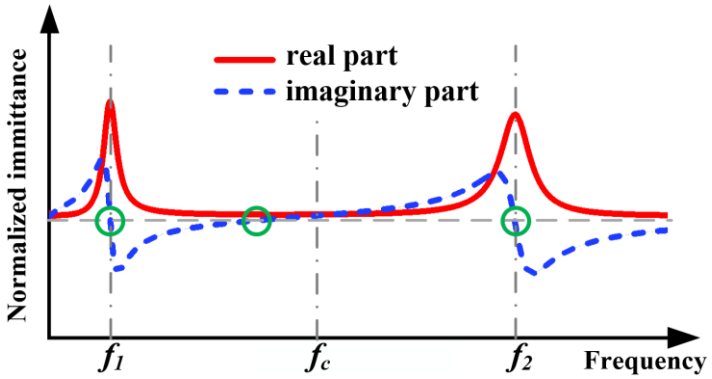

Figure 6.3 Impedance/admittance behaviors of a typical MMR

The three resonances can be observed with green circles in the illustrated resonator. Specifically, the three resonances consist of two shunt- and one series-resonances for the impedance case, or two series- and one shunt-resonances for the admittance counterpart. (© 2020 IEEE, reproduced with permission)

6.2.3 Resonance Behavior of Multi-Mode Resonator (MMR)

The MMR concept has been successfully used to design wide/multi-band antennas and filters by flexibly changing the spacing and location of several resonant modes as previously described. Since the antenna is a radiative component, the use of the MMR concept for wide/multi-band resonant-type antennas should be carefully considered to make sure that those resonant modes have similar radiation behaviors (e.g., radiation patterns and polarizations) rather than different states, for the sake of achieving relatively stable and coherent radiation performances in the working frequency band of interest. Interestingly, the same requirement of the MMR should also apply to the design

of non-resonant LWAs. As shown in Figure 6.3, it is the impedance/admittance behaviors of a classic triple-mode resonator. f_1 and f_2 are the two typical resonant frequencies that can represent either shunt-resonances for the impedance case or series-resonances for the admittance counterpart, whereas $f_c = (f_1 + f_2)/2$ denotes the center frequency. All the resonances of the MMR are assumed to have similar radiation behaviors when the resonator is a radiator. It can be seen that in the frequency range between f_1 and f_2, the real part of the impedance/admittance decreases with frequency and then shows an increasing trend, featuring a relatively stable curve close to the center frequency of f_c. It should be noted that for an antenna, its radiated power in the far field is manifested by and proportional to its real part of the input impedance [16], implying that a stable antenna resistance will give rise to a stable radiated power. As a consequence, if RDs are designed with such a triple-mode resonance behavior, and the working frequency region is centered at f_c and sandwiched between f_1 and f_2, the LWAs consisting of such unit cells will have a stable radiation efficiency according to (6.7) and its gain performance can also be relatively constant in principle.

6.3 Magneto-Electric Dipole-Based LWA—Verification of the MMR Concept

It is interesting to observe that the required MMR behaviors for LWAs with stable radiation is quite similar to that of dual-band resonant components (i.e., antennas and filters). However, the employed frequency regions between the two cases are totally different. From this section, two types of LWA unit cells based on the MMR concept, simply borrowed from resonant antenna regions, are proposed and studied for verification purpose. The first is the MED-based unit cell and the other is based on the ACPA. Different from their popular applications for wide/multi-band purposes [256]-[258], they should be designed deliberately to avoid resonant operations for radiation stability of leaky-wave applications. Hence, a specific design guideline will be provided for this class of MMR-based LWAs.

6.3.1 Geometry of Unit Cell

The geometry of the proposed MED-based unit cell is depicted in Figure 6.4. Basically, the unit cell is comprised of two substrates and three metal layers. Both substrates have the same attributes (i.e., RT/duroid 6006 with a relative permittivity of 6.15 and loss tangent of 0.0027) aside from thickness. In the bottom substrate, a conventional SIW is formed. Continuous metal walls are used

here for modeling and simulation convenience, and in practice they can be conveniently replaced by plated slot-via/trench arrays. In the top metal layer of the bottom substrate, a folded slot is etched transversely, and hence a magnetic dipole (M-dipole) is formed. A planar strip dipole is printed on the top of the upper substrate. Two shorting vias are used to connect the strip dipole to the top

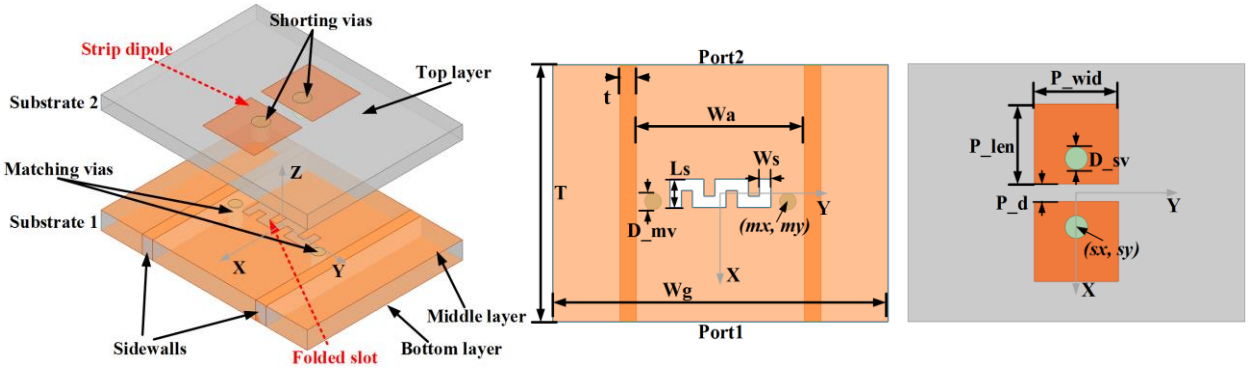

(a) (b) (c)

Figure 6.4 Geometry of the proposed MED-based LWA unit cell

(a) Exploded view. (b) Top view of substrate1 (bottom substrate). (c) Top view of substrate2 (upper substrate). Continuous sidewalls are used here to form the SIW for convenience in modeling and simulation, and they can be easily replaced by plated slot-via/trench arrays in practical fabrication. Some key parameters are tabulated in Table 6.1. (© 2020 IEEE, reproduced with permission)

Table 6.1 Optimized Dimensions of the MED-Based LWA Unit Cell (© 2020 IEEE, reproduced with permission)

Parameter	***T***	***Wg***	***Wa***	***t***	***Ls***
Value (mm)	4.56	6	3	0.4	0.5
Parameter	***Ws***	***D_mv***	***mx***	***my***	***P_wid***
Value (mm)	0.2	0.3	0.132	1.17	1.5
Parameter	***P_len***	***P_d***	***D_sv***	***sx***	***sy***
Value (mm)	1.4	0.3	0.4	0.6	0

metal layer of the bottom substrate, thus establishing the electric dipole (E-dipole). In order to suppress the open-stopband effects, a matched unit cell is usually needed, and thus a pair of matching vias are specially embedded into the SIW to complete this impedance matching process [15][32]. The operating principle and design considerations of the proposed unit cell, as well as the matching vias for suppressing the open-stopband effects will be explained later.

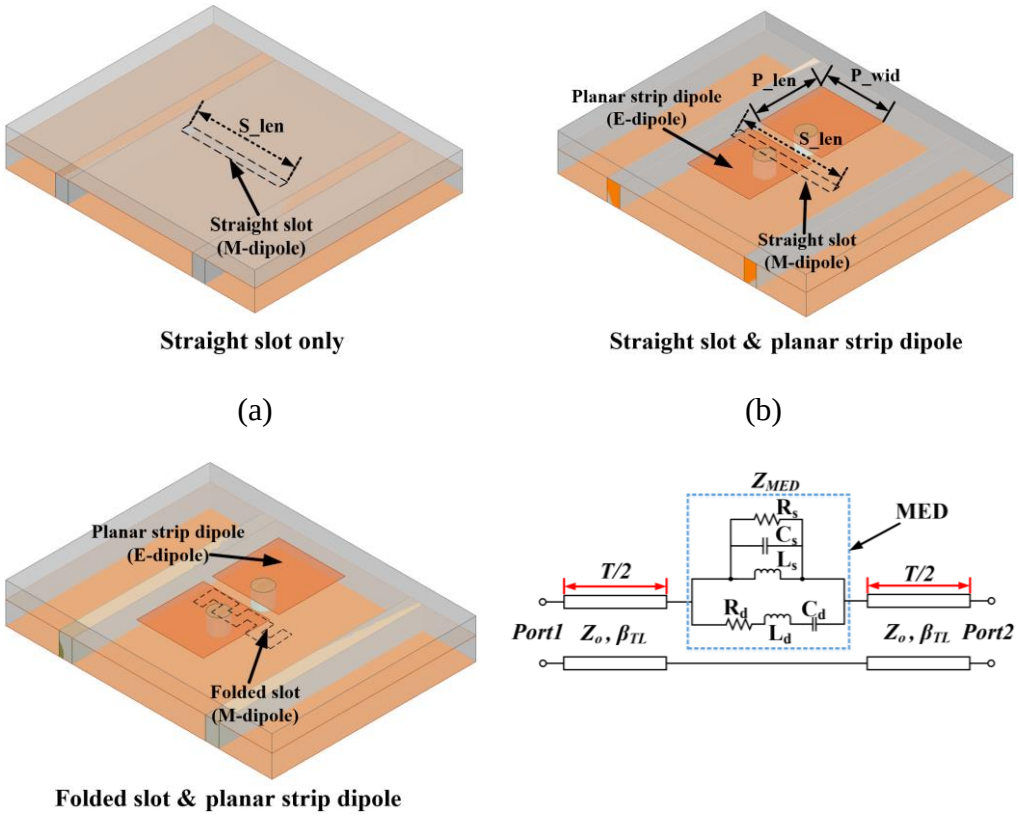

Figure 6.5 Evolution of the proposed MED-based LWA unit cell

(a) Straight slot only (unit I). (b) Straight slot plus planar strip dipole (unit II). (c) Folded slot plus planar strip dipole (unit III). (d) Simplified equivalent circuit model of the MED-based unit cell. The unit III depicted in (c) is the proposed (final) MED-based unit cell neglecting matching vias in the bottom substrate (Substrate1), which are used to suppress the open-stopband. The slot is modeled as a parallel *RLC* resonator (R_s, L_s and C_s), while the dipole is modeled as a series *RLC* resonator (R_d, L_d and C_d); both of them are parallel-connected to establish a hybrid-resonator circuit representing the MED [48]. (© 2020 IEEE, reproduced with permission)

6.3.2 Working Mechanism of Unit Cell

Figure 6.5 shows the evolution of the proposed MED-based unit cell and its simplified equivalent circuit model [257], while the corresponding normalized impedance performances of various RDs are displayed in Figure 6.6. To extract the impedance properties of the MED, a "black-box" can represent its entire loading effects on the host SIW line. Its normalized impedance denoted as $\tilde{Z}_{MED}$ can be conveniently extracted by using the theory described in Chapter 6.2. A. It is worth noting that both the transverse slot and MED, as shown in Figure 6.5(a) and (b) respectively, share the same type of loading or perturbation effects to the host SIW line. They play the same role in determining the complex propagation constants of the perturbed SIW structure (i.e., leaky structure) based on the Bloch-Floquet theorem [18], since the propagating waves inside the SIW can only "see" or "feel" the loading-type and scale of discontinuities but are incapable of detecting what the discontinuities are (i.e., "black-box"). As observed in Figure 6.6(a), when only a straight slot (unit I) is introduced, which is the general case of a transversely slotted SIW LWA [14][50][52][56][57], only one resonance is found from 20 to 60 GHz, exhibiting typical SMR behaviors as illustrated before. When a strip dipole is attached symmetrically above the transverse straight slot [i.e., unit II, as shown in Figure 6.5(b))], additional series- and shunt-resonances are created at a higher frequency with just a little influence on the former one as illustrated in Figure 6.6(b). Hence, the

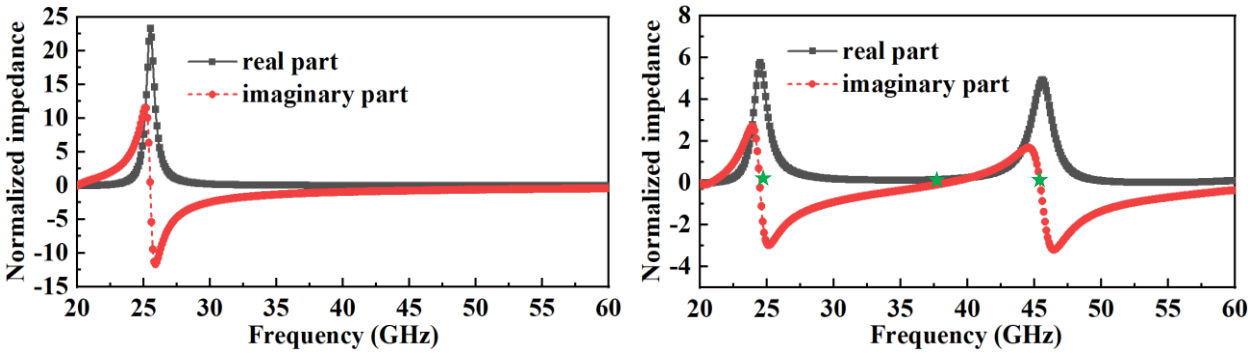

(a) (b)

Figure 6.6 Normalized impedance behaviors corresponding to different kinds of unit cells shown in Figure 6.5

(a) Unit I. (b) Unit II. Such impedance behaviors of the unit III are similar as that of the unit II and thus are not provided here for brevity. (© 2020 IEEE, reproduced with permission)

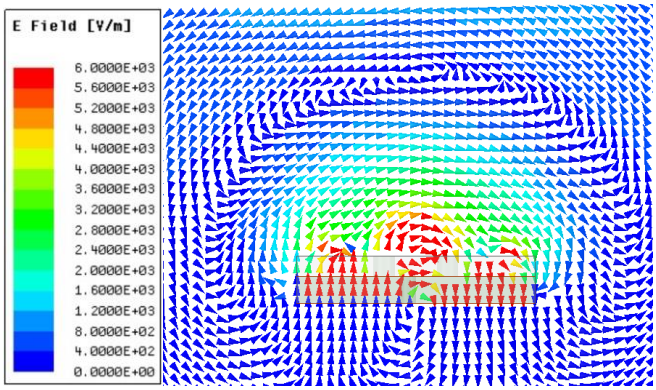

Figure 6.7 Simulated E-field distribution in E-plane (*xoz*-plane) at 35 GHz of the proposed MED-based unit cell

MED-based unit cell is established with MMR behaviors displayed, which can be explained by its equivalent circuit model. As shown in Figure 6.5(d), the circuit has two branches in parallel, where one of them is a parallel *RLC* resonator that models the slot (M-dipole) while the other is a series one that represents the strip dipole (E-dipole). If the parallel resonator is at resonance itself, the overall circuit is close to resonance because the series resonator represents only a small perturbation in this frequency (its own resonance frequency is higher and relatively far in this case). Then it is reasonable to conclude that the first shunt-resonance in Figure 6.6(b) is mainly related to the slot; this remark can also be drawn by comparing Figure 6.6(b) with Figure 6.6(a). Similarly, the series-resonance of the MED is primarily concerned with the series resonator branch (strip dipole). Comparatively, the second shunt-resonance is caused by the cancellation between the capacitive susceptance of the parallel resonator and the inductive one of the series resonator. In other words, this resonance is a combination of the effects of both resonator branches and it will be influenced when either changing the parallel or series resonator as shown later. Interestingly, all the resonances have coherent radiation performances that are similar to the well-known structures reported in [256][257]. Figure 6.7 depicts the simulated E-field distribution at 35 GHz in the E-plane (*xoz*-plane) of the proposed MED-based unit cell. Both E-fields created by the slot and dipole have the same directions, indicating that the total radiation is constructively contributed by the two kinds of radiators (i.e., M- and E-dipoles) just like the radiation mechanism of those popular resonant-type

MED antennas. However, it is necessary to highlight their difference that the MED operating in a leaky-wave manner should not be resonant and does not exhibit strong radiation. Therefore, the height of the strip dipole in the proposed MED is not limited to a quarter wavelength, which is the customary choice for those resonant-type counterparts. Also note that the proposed one is a two-port component, while those in [256][257] are single-port.

6.3.3 Design Procedure

6.3.3.1 Determination of SIW Dimensions

The center frequency of this design is chosen at f_c = 35 GHz and the targeted working frequency band is ranged from f_L= 30 GHz to f_U = 40 GHz. The substrate selected here is RT/duroid 6006, and the thickness of the bottom and upper substrates are 0.508 mm and 0.381 mm, respectively. Note that a substrate with a low relative permittivity is not recommended here since in such a case the beam scanning range is very limited in the forward quadrant due to the appearance of grating lobes in the backward region [9]. The cut-off frequency of the SIW is set to about 20 GHz to make sure that the target frequency band lies in a region controlled only by the dominant TE_{10} mode. Based on the above-discussed specifications, the width of the SIW, denoted as W_a as shown in Figure 6.4, can be calculated.

6.3.3.2 Determination of Dimensions Regarding Slot and Dipole

The radiation stability of unit cells over the working frequency band is the prerequisite for related periodic LWAs to achieve such performances. Because of this, the real part of RDs' normalized impedance/admittance properties of should be kept stable as analyzed in Chapter 6.2. As shown in Figure 6.6(b), the normalized resistance of the MED characterizes a relatively stable behavior in the central frequency region between the two shunt-resonances that are determined by the slot and dipole. Consequently, this part of the frequency band is preferred to implement LWAs with potentially stable radiation. In order to provide a design criterion to choose dimensions of the slot aperture and strip dipole, the two shunt-resonances, f_1 and f_2, are considered to be centered at the design frequency of $f_c = (f_1 + f_2)/2 = (f_L + f_U)/2$. Meanwhile, $f_1 < f_L$ and $f_2 > f_U$ should be strictly satisfied to avoid resonance occurring in the frequency band of the leaky-wave operation. In this case, a relatively symmetrical frequency response regarding the normalized resistance can be

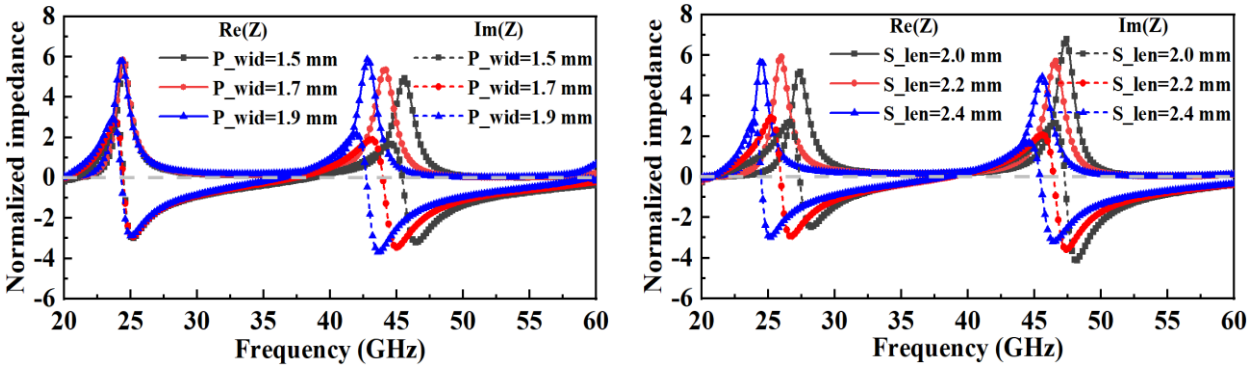

(a) (b)

Figure 6.8 Dimensional effects of the strip dipole and straight slot on the normalized impedance of the MED

(a) *P_wid*; (b) *S_len*. The two studied parameters are the width of the strip dipole and length of the straight slot, respectively. The studied model is the one shown in Figure 6.5(b). (© 2020 IEEE, reproduced with permission)

potentially obtained. According to the characteristics of an MMR, it can be understood that if the two shunt-resonances are moving far away from the center frequency at the same pace, the real part of the impedance will decrease, and therefore the radiation ability of the unit cell is reduced according to (6.5) and (6.6). The reverse situation is also applicable in that evenly decreasing the spacing between the two shunt-resonances will result in enhanced radiation of the unit cell. It is noted that during these processes stable radiation behaviors can still be maintained. Therefore, by selecting the two shunt-resonances properly, the radiation ability of the unit cell can be designed flexibly, which is beneficial for achieving diverse beamwidth and directivity, as well as a low side-lobe design for LWAs [9][11].

To have a clear understanding of how the MED dimensions affect the resonance behaviors, a parametric study is performed. The unit cell studied here is the one shown in Figure 6.5(b). When one parameter is changed, the others are kept constant. Figure 6.8(a) depicts the effects of *P_wid*, the width of the strip dipole, on the normalized impedance of the MED. Notably, the first shunt-resonance is not influenced while the series- and second shunt-resonances shift to a lower frequency as *P_wid* increases. This can be explained through the equivalent circuit model shown

in Figure 6.5(d) that the variation of *P_wid* will result in the change of the series resonator, and thus both the series- and second shunt-resonances will be influenced simultaneously. The same phenomenon can be also observed by altering *P_len*, the length of the strip dipole, which is not given here for brevity. Figure 6.8(b) describes how both shunt-resonances are influenced simultaneously while the series counterpart remains fixed when changing the slot length *S_len*. The equivalent circuit model can also explain this since both shunt-resonances can be adjusted by the parallel resonator (i.e., slot), sharing the complementary principle with that in Figure 6.8(a). Although these shunt-resonances cannot be controlled independently by altering the dimensions of the slot and dipole due to the hybrid-resonator circuit model of the MED, a simple strategy can be used to adjust the two shunt-resonances flexibly. First, only the slot is introduced and adjusted to locate the first shunt-resonance, such as approximately 25 GHz as shown in Figure 6.6(a). Next, the strip dipole is attached. By adjusting the slot length *S_len*, the first shunt-resonance can be easily moved back to the original place. Finally, the width and length of the strip dipole, *P_wid* and *P_len* respectively, are tailored to independently locate the second shunt-resonance without influencing the first one, ensuring that the two shunt-resonances can be centered at the design frequency [e.g., 35 GHz as shown in Figure 6.6(b)]. In the proposed design, the two shunt-resonances are initially located at about f_1 = 25 GHz and f_2 = 45 GHz respectively, and they can be chosen flexibly by using this simple strategy according to the radiation ability to be achieved by the unit cell.

6.3.3.3 Determination of Size and Position of Matching Vias for Open-Stopband Suppression

If no special considerations are taken into account in the design of a periodic LWA, there will be an open-stopband when the beam is scanned through the broadside in which the period of unit cells corresponds to a guided-wavelength at the working frequency [9][11]. Here, a pair of matching vias are adopted symmetrically to the unit cell and a matched unit is thus completed, indicating that the open-stopband can be suppressed effectively. In order to leave enough space to install the matching vias in the bottom substrate, a folded slot is employed instead of a straight one, as shown in Figure 6.5(c). The corresponding normalized impedance of the new MED is kept similar to the one in Figure 6.6(b). The final matched MED-based unit cell (the proposed one) has already been

depicted in Figure 6.4.

Figure 6.9 depicts a simplified transmission line model of the proposed MED-based unit cell for open-stopband suppression. The working principle is similar to the approach described in [15][32] but is for SIW applications. It should be noted that Z_{in2} or Y_{in2} shown in Figure 6.9 should have a capacitive imaginary part since the matching vias can only introduce inductance. This is the limitation compared to that in [15][32] that makes use of microstrip open-stub as the matching

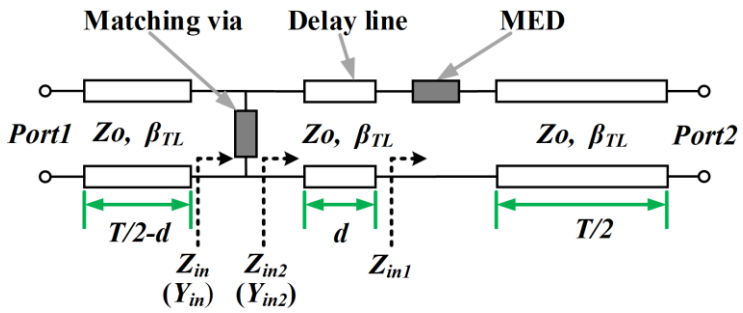

Figure 6.9 Simplified TL model for open-stopband suppression of the proposed MED-based unit cell

mechanism. Fortunately, the proposed matching vias own the benefit of no spurious radiation that may deteriorate cross-polarization and SLL of total radiation, especially in the millimeter-wave frequency range. Therefore, the length of the delay line, denoted as d (corresponding to mx in Figure 6.4), should be selected carefully and conditionally. Since the design frequency is selected at the center of the normalized resistance curve of the MMR, as shown in Figure 6.3 or 6.6(b), Z_{MED} only has a small value and thus the perturbation introduced by the MED to the host SIW is very small. This is consistent with the assumptions made for power-flow diagrams in Figure 6.1(e) and (f). Consequently, Z_{in1} is very close to Z_o and only a short delay line is required to transform re(Z_{in1}) to re(Z_{in2}) = Z_o or re(Y_{in2}) = Y_o, after which matching vias are employed to eliminate im(Y_{in2}) and eventually force $Y_{in} = Y_o$. Figure 6.10 gives the plot about the normalized phase and attenuation constants of the unit cell with and without matching vias, both of which can be extracted by simulating a single unit cell and using the Bloch-Floquet theorem [18]. The phase and attenuation

constants of the unit cell can be expressed as

$$\begin{cases} \beta = \mathrm{Im}\left[\cosh^{-1}((A_u + D_u)/2)\right]/T \\ \alpha = \mathrm{Re}\left[\cosh^{-1}((A_u + D_u)/2)\right]/T \end{cases} \tag{6.8}$$

where A_u and D_u are the two components of the *ABCD* matrix of the whole unit cell. It is worth noting that the attenuation constant extracted here will be the same as the one in (6.6) only if loading effects of RDs are infinitesimal and pure travelling waves propagate inside the unit cell without

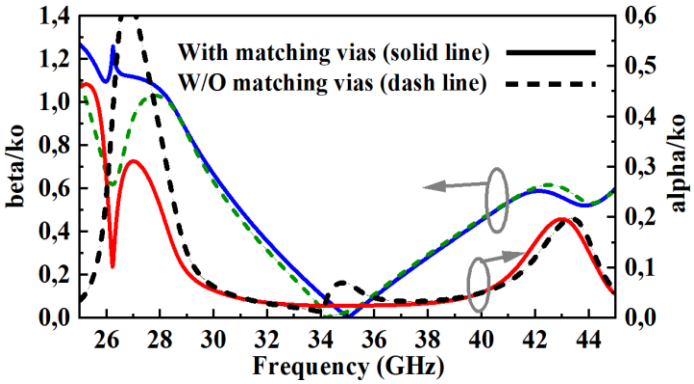

Figure 6.10 Normalized phase and attenuation constants of the proposed MED-based unit cell with and without matching vias

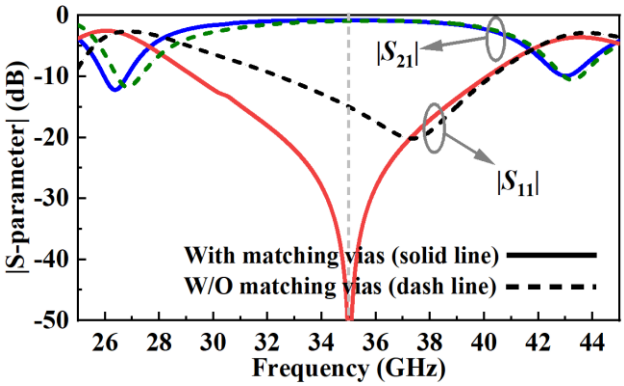

Figure 6.11 Simulated *S*-parameters of the proposed MED-based unit cell with and without matching vias

reflections at its two ends. The period length of the unit cell *T* corresponds to a guided-wavelength at the design frequency of 35 GHz, i.e., the frequency for broadside radiation of the LWA, which can be approximately calculated by using the original phase constant of the unperturbed SIW, i.e., β_{TL}. This is reasonable due to the small perturbation caused by the MED on the host SIW, as discussed before. As seen from Figure 6.10, when matching vias are absent, there is a large bump appearing at approximately 35 GHz for the normalized attenuation constant, whereas the normalized phase constant shows a distinct nonlinearity as it gets close to zero. By contrast, when matching vias are added, both normalized phase and attenuation constants change smoothly at the center frequency of 35 GHz, implying that the open-stopband is effectively suppressed [9][11]. Simulated *S*-parameters of the unit cell with and without matching vias are plotted in Figure 6.11 to provide further evidence, indicating that an excellent matching is obtained at exactly 35 GHz with matching vias introduced. Contrastingly, when there are no matching vias, impedance matching of the unit cell is merely modest with small reflection encountered. However, attention should be paid to the unit cell at the design frequency (i.e., open-stopband or broadside frequency) where reflections of unit cells will be superposed in phase; even a minor reflection will be magnified by the factor *N* in response to the overall LWA consisting of *N* unit cells [38]. Consequently, it is critical to have a well-matched unit cell at this frequency point. Meanwhile, stable curve patterns are also observed in Figure 6.10 and Figure 6.11 in terms of the normalized attenuation constant and $|S_{21}|$ versus frequency, respectively. It can be concluded that (i) the open-stopband effects are successfully suppressed, and (ii) the radiation ability of the proposed unit cell is kept relatively stable within a wide frequency band. This paves the way for relevant periodic LWAs to realize continuous beam-scanning (through broadside) with stable radiation characteristics.

6.3.3.4 Determination of Quantity of Unit Cells

Until now, the design of the MED-based unit cell has been completed. To ensure that the LWA consisting of such unit cells is able to provide a specific radiation efficiency in the frequency band of interest, a certain number of unit cells should be cascaded. To this end, the quantity of unit cells should be determined, depending on the radiation efficiency to be achieved.

According to the power-flow diagrams shown in Figure 6.1(e) or (f), there is

$$P_n / P_{n-1} \approx e^{-2\alpha T} \tag{6.9}$$

$|S_{21}|_{dB}$ of the unit cell, therefore, can be expressed as

$$\begin{aligned} \left|S_{21}\right|_{dB} &= 10\log(P_n / P_{n-1}) \\ &\approx 10\log(e^{-2\alpha T}) \end{aligned} \tag{6.10}$$

For a periodic LWA consisting of N unit cells with a total length of $L = NT$, its radiation efficiency e_r can be found in (6.7). Therefore, there is

$$\begin{aligned} e^{-2\alpha NT} &= 1 - e_r \\ N \cdot 10\log(e^{-2\alpha T}) &= 10\log(1 - e_r) \end{aligned} \tag{6.11}$$

Substituting (6.10) into (6.11) gives

$$N \approx 10\log(1 - e_r) / \left|S_{21}\right|_{dB} \tag{6.12}$$

Meanwhile, since $|S_{21}|_{dB}$ of the unit cell is also approximately related to the real part of normalized impedance of RDs according to (6.6) and (6.10), (6.12) can also be expressed as

$$N \approx \log(1 - e_r) / \log(1 - re(Z)) \tag{6.13}$$

Generally, 90% radiation efficiency is selected as the target to be realized at the design frequency. Thus, setting (6.12) or (6.13) with e_r = 90% gives

$$\begin{aligned} N &\approx -\frac{1}{10\log(1 - re(Z))} \\ \text{or} \quad & -10 / \left|S_{21}\right|_{dB} \end{aligned} \tag{6.14}$$

As observed from (6.14), if $|S_{21}|$dB of the unit cell or normalized impedance of RDs is obtained, the quantity of unit cells to realize the 90% radiation efficiency can be determined straightforwardly. However, attention should be paid since the mutual coupling among unit cells is not considered. The obtained $|S_{21}|$dB or $\tilde{Z}$ may be inaccurate, and thus the calculated N should be just considered as an initial value. It can be found from Figure 6.11 that at 35 GHz the $|S_{21}|_{dB}$ of the proposed MED-based unit cell is about 0.65 dB, while the MED's normalized resistance is approximately 0.14. Thus, the number of unit cells can be calculated with an approximate value of $N \approx 16$.

6.3.3.5 Modeling, Fine-tuning, and Optimization

Up to now, the proposed MED-based unit cell featuring stable radiation ability and open-stopband suppression has been designed, and the quantity of unit cells has been determined according to the criterion of 90% efficiency. In the final step, a certain number of unit cells should be cascaded to model the LWA, and a full-wave analysis should be carried out to fine-tune the overall structure to accomplish the design.

There are several parameters that should be slightly adjusted and optimized for the proposed LWA as only an isolated unit cell is considered in the above design steps, without taking into consideration any mutual coupling that mainly results from radiation among those unit cells. First of all, the period length *T* may be adjusted delicately to ensure that the beam direction is pointed exactly to the broadside direction at the center frequency of 35 GHz. The size and position of matching via-holes may be the next parameters to be fine-tuned for a complete open-stopband suppression of the overall structure [9][11], followed by the quantity of unit cells *N* for adequate power consumption. Since initial values of these parameters have already been obtained in the preceding steps, this fine-tuning/optimization step can be easily conducted with the help of built-in modules in *ANSYS HFSS*, and eventually optimal results can be acquired. For example, the positions of matching vias (i.e., *mx* and *my*, as shown in Figure 6.4) can be optimized and determined by setting a goal with the reflection coefficient less than -40 dB at the center frequency of 35 GHz to effectively suppress the open-stopband effects. It is worth mentioning that optimized parameters will not remarkably deviate from, or even remain the same as, those initial values because the spacing between adjacent unit cells is in an order of one guided- wavelength and the mutual coupling is very small.

6.3.4 Simulation and Measurement Results

A specific and systematic design procedure regarding the proposed 1-D periodic MMR-based LWA has been provided in Chapter 6.3.3. Almost all 1-D periodic LWAs can follow this guideline without loss of generality. The final dimensions of the proposed MED-based unit cell are tabulated in Table 6.1. Figure 6.12(a) depicts the configuration of the proposed MED-based LWA that consists of 16 unit-cells, with two conventional GCPW-SIW transitions terminated at its two ends. The photograph of the fabricated prototype is shown in Figure 6.12(b). Simulated and measured *S*-

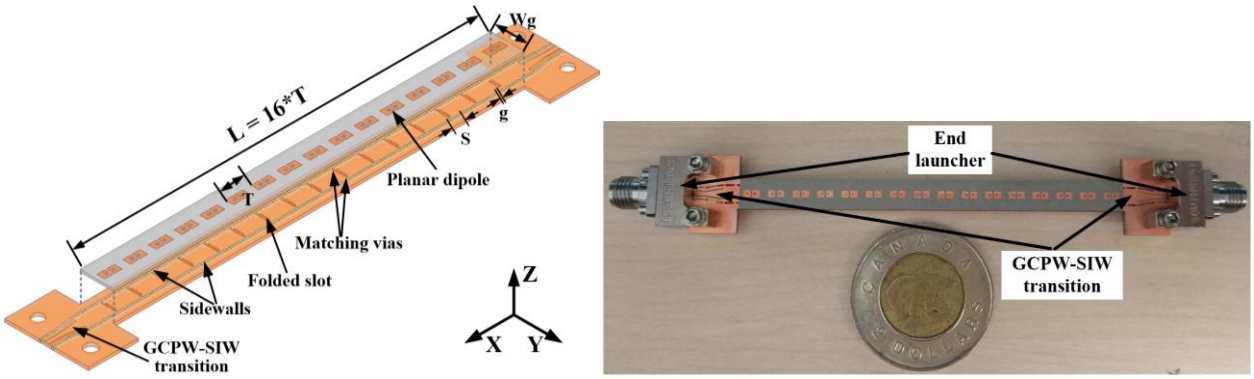

(a) (b)

Figure 6.12 (a) Configuration of the proposed MED-based LWA. (b) Photograph of the fabricated prototype

Plated slot-via/trench arrays with S = 2.3 mm and g = 0.36 mm are used to construct sidewalls of the SIW. (© 2020 IEEE, reproduced with permission)

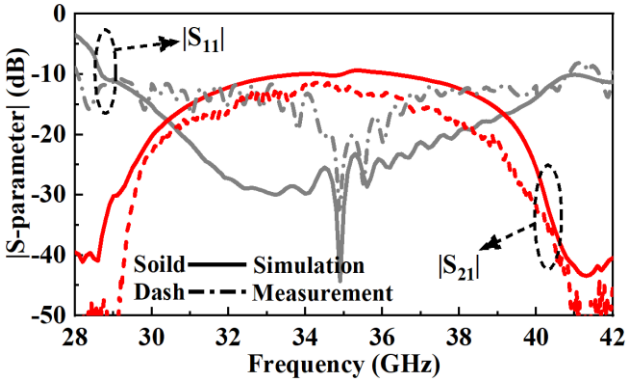

Figure 6.13 Simulated and measured *S*-parameters of the proposed MED-based LWA

(© 2020 IEEE, reproduced with permission)

parameters are plotted in Figure 6.13, and an acceptable agreement is observed. In the target band from 30 to 40 GHz, both results illustrate that the reflection coefficient is below -10 dB, implying that a good impedance matching without open-stopband effects is achieved. Meanwhile, $|S_{21}|$ is lower than -10 dB, indicating that more than 90% power is consumed. This also manifests the relative accuracy of the quantity of unit cells calculated above and thus the effectiveness of the unit cell analysis. Besides, it should be noted that $|S_{21}|$ increases initially and then decreases with

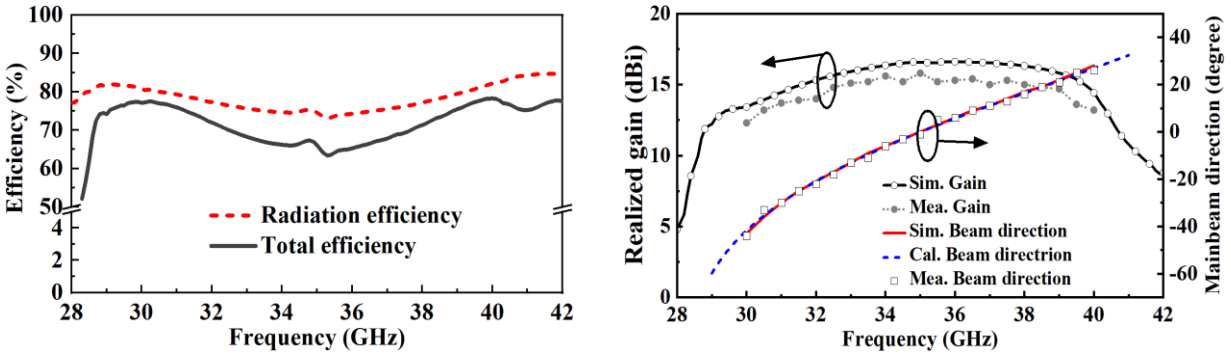

(a) (b)

Figure 6.14 Radiation properties of the proposed MED-based LWA with respect to (a) radiation efficiency and total efficiency, and (b) realized gain and main beam direction

The calculated main beam direction based on the extracted normalized phase constant shown in Figure 6.10 is also plotted as a comparison. (© 2020 IEEE, reproduced with permission)

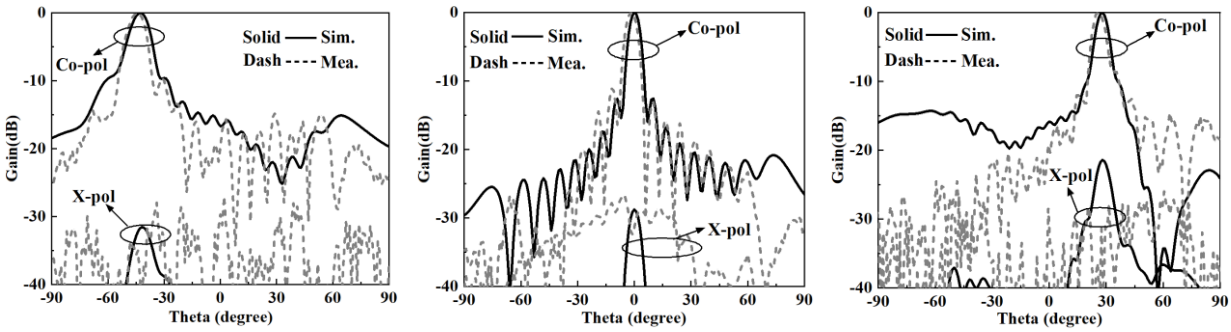

(a) (b) (c)

Figure 6.15 Radiation patterns of the proposed MED-based LWA at several frequencies

(a) 30 GHz; (b) 35 GHz; (b) 40 GHz. (© 2020 IEEE, reproduced with permission)

frequency, exhibiting a symmetrical curve pattern with its peak located at the center frequency of 35 GHz. This is consistent with the normalized resistance of the MED and *S*-parameters of the unit cell analyzed above. Interestingly, such a curve pattern will result in a relatively stable radiation efficiency η_r, which is defined as the ratio between radiated power and accepted power of an LWA, as shown in Figure 6.14(a). A good radiation efficiency of about 77.7% with a variation of ±4.5%

is achieved in simulation. Contrastingly, the total efficiency that is calculated as $\eta_t = (1-|S_{11}|^2-|S_{21}|^2)\eta_r$ exhibits a smaller value of 70.9 ± 7.4% due to the considered return loss and matching-load loss. Both efficiencies can be obtained conveniently with commercial simulation software such as *ANSYS HFSS*. Figure 6.14(b) depicts simulated and measured results with respect to the realized gain and main beam direction versus frequency. In the simulated cases, a maximum gain of 16.6 dBi with a variation of less than 3 dBi has been achieved within the targeted band from 30 to 40 GHz, in which the main beam direction scans from -43^o (backward) to 28^o (forward) continuously with a broadside radiation at the design frequency of 35 GHz. In addition, the calculated main beam direction based on the normalized phase constant β/k_0 described in Figure 6.10 is plotted as a comparison. It shows a good agreement with the simulated counterpart of the whole LWA structure. Therefore, the validity of the above dispersion analysis based on a single unit cell is further demonstrated. The measured results agree generally with their simulated counterparts except for a little gain drop that may be related to the connector loss, deteriorated return loss and increased conductor and dielectric losses, having a stable gain of averagely 14.1 dBi achieved. The radiation patterns in terms of co- and cross-polarization components at several frequencies are given in Figure 6.15. An acceptable agreement is observed between simulated and measured results, with a slight deviation that may be caused by fabrication errors or measurement issues. For example, spurious radiation introduced by feeding discontinuities of end launchers (they are not considered in simulation), distorted aperture illumination caused by increased conductor and dielectric losses, and non-ideal matching termination in practical prototype might be the difference contributors [14][27][33][45].

6.4 Aperture-Coupled Patch Antenna-based LWA—A Further Proof of the MMR Concept

The MMR concept has been proposed to instruct the design of 1-D periodic LWAs with stable radiation properties, upon which the MED-based LWA has been successfully developed and demonstrated above. In this section, as a further demonstration, the ACPA that also operates as a conventional MMR is applied to the design of a periodic LWA for the same purposes.

The geometry of the ACPA-based unit cell is plotted in Figure 6.16, which shares the similar configuration as its MED-based counterpart. RT/duroid 6006 material with thickness of 0.635 mm

is used as the bottom substrate, whereas the upper one is constructed by RT/duroid 6002 material with relative permittivity of 2.94, loss tangent of 0.0012 and thickness of 0.381 mm. A bow-tie slot is etched on the top metal layer of the bottom substrate, whereas a patch antenna is printed on the top of the upper substrate. A pair of matching vias are embedded in the unit cell to suppress the open-stopband effects. Compared to the configuration of the MED-based unit cell, the ACPA-based one does not need the shorting vias in the upper substrate, thus simplifying the fabrication. The normalized impedance of the ACPA is described in Figure 6.17, illustrating an MMR behavior that is similar to that of the MED. The first shunt-resonance is mainly introduced by the bow-tie slot, while the second one can be adjusted by the patch. All the resonances have similar radiation patterns. Figure 6.18 depicts the simulated E-field distribution in the E-plane (*xoz*-plane) of the unit cell at the center frequency of 35 GHz. It can be seen clearly that its radiation is from the two edges of the patch, exhibiting the same radiation mechanism as its traditional resonant-type counterpart [50] and also showing a distinct difference compared to that of the MED-based unit cell, as shown in Figure 6.7. Both Figure 6.7 and Figure 6.18 can provide further evidence that the proposed two MMR-based radiators have smooth radiation states just as their usual features for

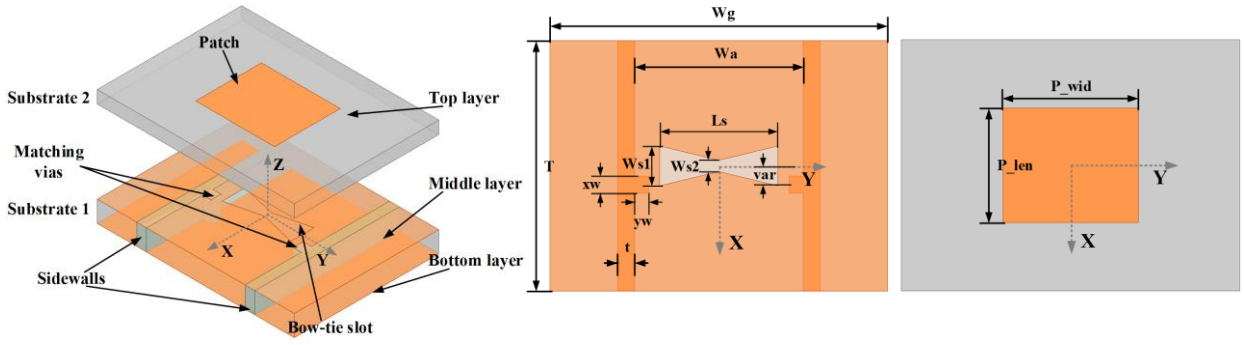

(a) (b) (c)

Figure 6.16 Geometry of the proposed ACPA-based LWA unit cell

(a) Exploded view. (b) Top view of substrate1 (bottom substrate). (c) Top view of substrate2 (upper substrate). Continuous sidewalls are used here to from the SIW for convenience in simulation, and they can be easily replaced by plated slot-via/trench arrays in practical fabrication. Some key parameters are tabulated in Table 6.2. (© 2020 IEEE, reproduced with permission)

Table 6.2 Optimized Dimensions of the ACPA-Based LWA Unit Cell (© 2020 IEEE, reproduced with permission)

Parameter	***T***	***Wg***	***Wa***	***Ls***	***Ws1***
Value (mm)	4.38	6	3	2.1	0.2
Parameter	***Ws2***	***var***	***xw***	***yw***	***P_wid***
Value (mm)	0.6	0.32	0.26	0.25	2.4
Parameter	***P_len***	***t***			
Value (mm)	2.0	0.4			

conventional wideband applications. This is consistent with the assumption made in Chapter 6.2.3. The design procedure proposed in Chapter 6.3.3 can be employed directly here to design the ACPA-based LWA with stable radiation properties and continuous beam-scanning through broadside.

In order to further demonstrate the effectiveness of the MMR concept, the proposed ACPA-based LWA consisting of 16 unit-cells is simulated, fabricated and measured. The simulated model and fabricated prototype are shown in Figure 6.19. The dimensions of the ACPA-based unit cell are tabulated in Table 6.2. Figure 6.20 shows simulated and measured *S*-parameters, both illustrating that a good impedance matching is achieved in the targeted frequency band from 30 to 40 GHz and also demonstrating that the open-stopband is effectively suppressed. Similar to the relevant results of the MED-based LWA, the $|S_{21}|$ here also shows an increasing trend before the center frequency of 35 GHz and after shows a decrease with frequency, thus exhibiting a smooth and symmetrical curve pattern. Both simulation and measurement are in an acceptable agreement. Figure 6.21 depicts the radiation efficiency and total efficiency of the proposed ACPA-based LWA, with 79.3 ± 1.1% and 72.7 ± 3.4% achieved respectively. A small bump presented at the center frequency is due to the remaining open-stopband effects. However, a good impedance matching as shown in Figure 6.20, together with the smooth gain and radiation patterns that will be shown later, illustrates that the open-stopband has been effectively suppressed without spoiling total performances of the

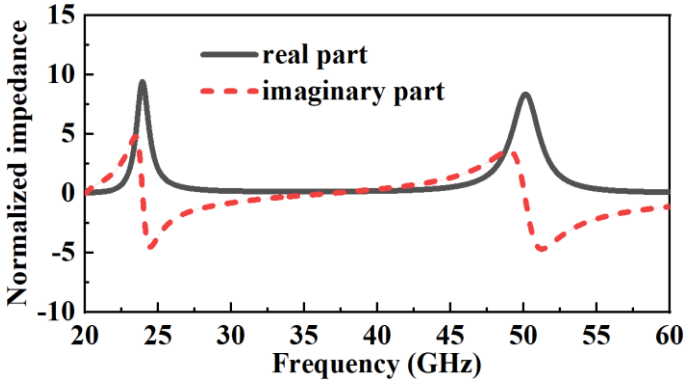

Figure 6.17 Normalized impedance behaviors corresponding to the ACPA

(© 2020 IEEE, reproduced with permission)

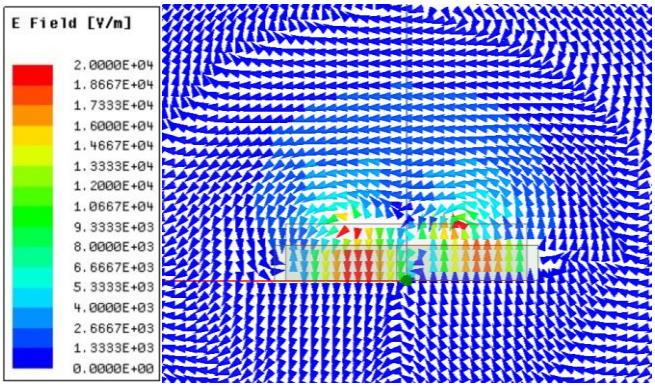

Figure 6.18 Simulated E-field distribution in E-plane (*xoz*-plane) at 35 GHz of the proposed ACPA-based unit cell

(© 2020 IEEE, reproduced with permission)

proposed periodic LWA. It is interesting to note that those curves including the normalized resistance shown in Figure 6.17, the simulated $|S_{21}|$ plotted in Figure 6.20 and the radiation efficiency displayed in Figure 6.21(a) are all consistent with each other. This demonstrates that relatively stable radiation properties have been achieved successfully. The simulated gain and main-beam direction are depicted in Figure 6.21, which shows that an average gain of about 15.7 dBi with less than 3 dBi variation and main beam direction from -39^o to 27^o are achieved in the target frequency band, respectively. The measured gain shows a reasonable drop but still remains

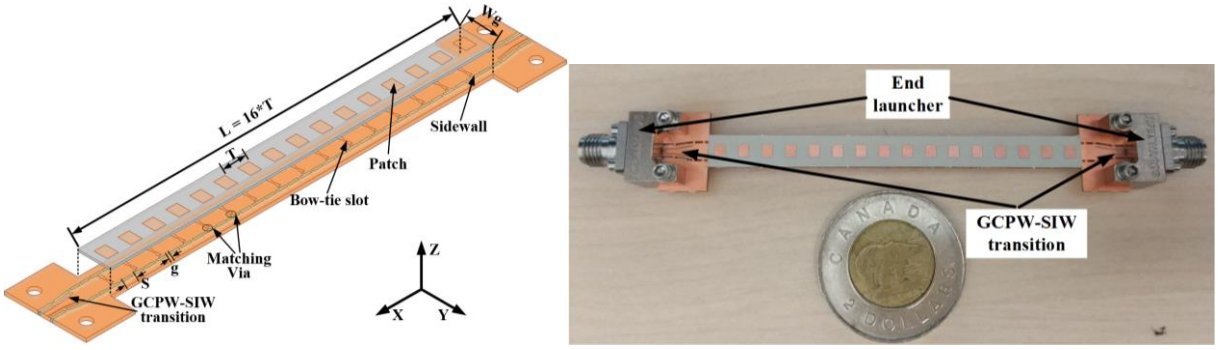

(a) (b)

Figure 6.19 (a) Configuration of the proposed ACPA-based LWA. (b) Photograph of the fabricated prototype

Plated slot-via/trench arrays with S=2.19 mm and g=0.36 mm are used to construct sidewalls of the SIW. (© 2020 IEEE, reproduced with permission)

stable (about 14.9 dBi). Simulated and measured radiation patterns at several frequencies are shown in Figure 6.22, illustrating a reasonable agreement between the two cases, with a slight difference that may be caused by fabrication errors and measurement issues as explained above. Note that the simulated cross-polar patterns are too small to be visible.

6.5 Discussion and Comparison

MED- and ACPA-based 1-D periodic LWAs have been proposed and studied elaborately in the above to demonstrate that the MMR concept can be used to design periodic LWAs featuring stable radiation properties. In order to highlight the benefits of the design concept, the proposed ACPA-based LWA, on behalf of the class of MMR-based LWAs, is selected and compared to two conventional transversely slotted SIW LWAs that are similar to [14][50][52][56][57] and characterized by typical SMR behaviors. For a fair comparison, both kinds of SMR-based LWAs, referred to as SMR#1 and SMR#2, are also designed with 16 unit-cells and the same broadside frequency of 35 GHz. Meanwhile, RDs (i.e., transverse slots) of SMR#1 and SMR#2 have the resonant frequencies corresponding to lower and higher shunt-resonance counterparts of the selected MMR, respectively. A comparison of the three kinds of LWAs in terms of normalized attenuation constant and radiation efficiency is illustrated in Figure 6.23. It can be clearly seen that

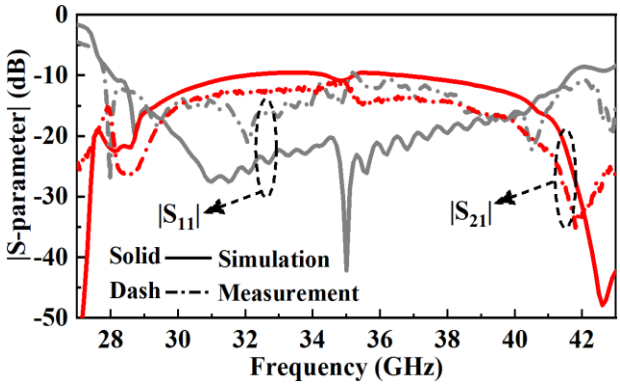

Figure 6.20 Simulated and measured *S*-parameters of the proposed ACPA-based LWA

(© 2020 IEEE, reproduced with permission)

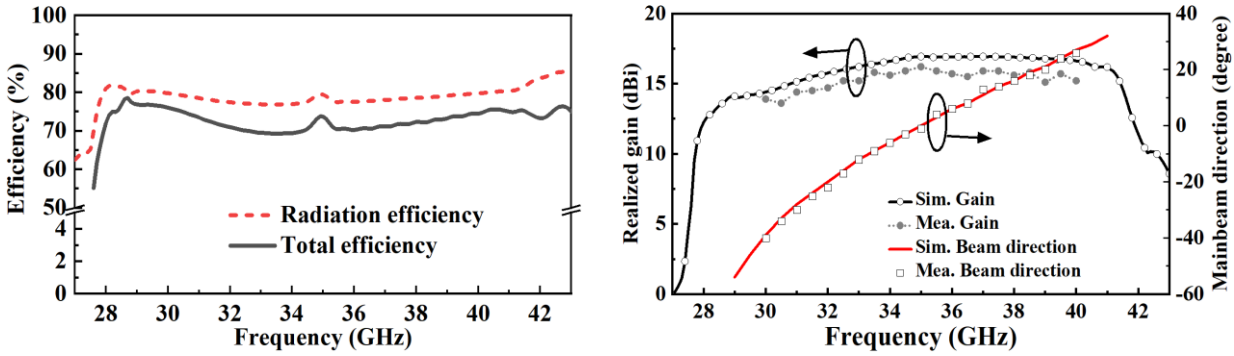

(a) (b)

Figure 6.21 Radiation properties of the proposed ACPA-based LWA with respect to (a) radiation efficiency and total efficiency, and (b) realized gain and main beam direction

(© 2020 IEEE, reproduced with permission)

the MMR-based LWA characterizes a stable attenuation constant, whereas those SMR-based ones feature monotonic changing counterparts. Meanwhile, in the target frequency band from 30 to 40 GHz, the MMR-based LWA exhibits a more stable radiation efficiency (with only ± 1.1% variation) than that of SMR-based ones, as expected. Specifically, the radiation efficiency of SMR#1 illustrates a monotonic decreasing trend with a variation of 38.2%, while that of SMR#2 increases progressively and the corresponding variation is about 60%. Both curve patterns of the attenuation constant and radiation efficiency coincide with each other and the theoretical analysis in Chapter 6.2. Another comparison between the proposed MMR-based LWAs and other similar published

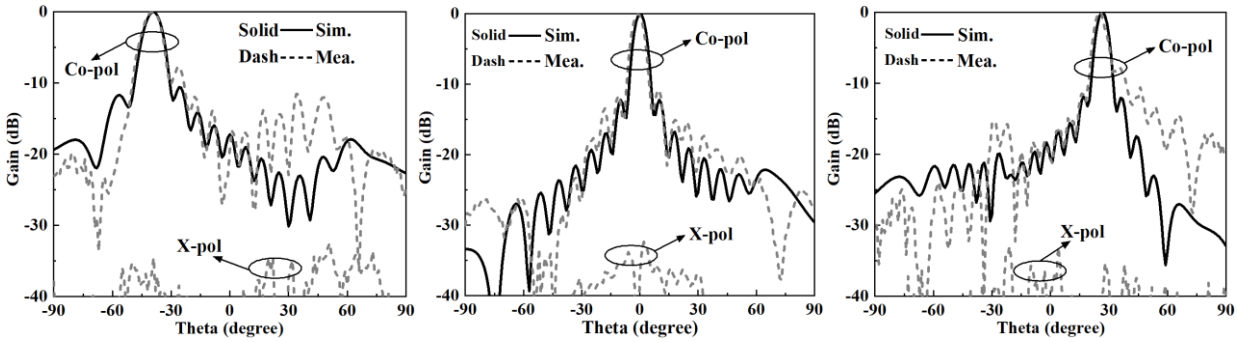

(a) (b) (c)

Figure 6.22 Radiation patterns of the proposed ACPA-based LWA at several frequencies

(a) 30 GHz; (b) 35 GHz; (b) 40 GHz. (© 2020 IEEE, reproduced with permission)

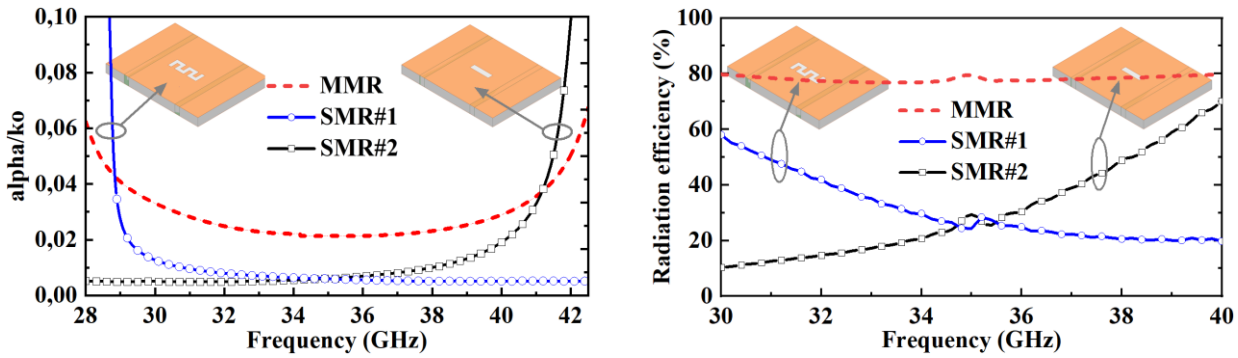

(a) (b)

Figure 6.23 Comparison of (a) normalized attenuation constant and (b) radiation efficiency with respect to three kinds of LWAs that are based on MMR/SMR concepts

The resonant frequency of SMR#1 and SMR#2 approximate the lower and higher resonance counterparts of the selected MMR, respectively. (© 2020 IEEE, reproduced with permission)

works has been tabulated in Table 6.3 for further highlighting the merits of the proposed work. It can be observed that dramatically changing radiation performances are possessed by [14][51][52[56], and the similar phenomenon can be speculated as well in those LWAs [15][32][37][38][40][41][50][57] because all of them share the typical SMR behaviors like the two in Figure 6.23. Although the composite unit cell consisting of diverse open-circuited stubs was employed for implementing periodic LWAs with stable radiation [30][31], it is based on microstrip

line technology and thus suffers from the limitation to be applied in high frequency bands (e.g., millimeter-wave bands) because of the high-loss nature. Compared to the work in [58], our proposed work is capable of providing a continuous beam-scanning through broadside and the potential for realizing near-endfire radiation [9][14][56], as well as no risks of encountering second-order beams or large side-/grating-lobes in the cross-sectional plane [16]. However, it can be found that the proposed two MMR-based LWAs have limited forward beam-scanning range, which can be easily enlarged by employing a substrate with a higher permittivity [9][11][56]. Besides, the employed MMR-based radiators in this work suffer from multi-layered structures like [58], and this can be improved by using single-layered MMR with other forms of transmission lines. For example, multi-mode pin-loaded patch [248] or U-slot patch [249] with the microstrip line technology will be a good candidate for the further development of single-layered MMR-based LWAs featuring radiation stability.

6.6 Conclusion

In this chapter, a class of 1-D periodic LWAs based on the MMR concept have been proposed, studied and demonstrated. Compared with traditional periodic LWAs characterized by SMR behaviors and suffered from monotonic changing radiation, the proposed LWAs are comprised of MMR-based unit cells and feature stable radiation properties over the entire frequency band of operation. A distinct difference regarding applications of the MMR concept is observed from resonant antennas/filters with wide/multi-band performances to non-resonant LWAs with radiation stability. Two kinds of typical MMR-based radiator, MED and ACPA, are exploited to construct unit cells for demonstration purposes. A detailed design procedure has been provided for this class of LWAs to facilitate their practical implementation. Both simulated and measured results of the proposed LWAs show that stable radiation properties such as efficiency and gain have been achieved successfully, thereby demonstrating the correctness and effectiveness of the MMR concept for radiation stability in the design of LWAs. It is interesting to mention that the proposed design concept is simple and straightforward. Based on this, a large variety of wide/multi-band resonant antennas can be borrowed and implemented directly on various transmission line technologies (e.g., microstrip line, CPS, and CPW) for the design and development of periodic LWAs with stable radiation.

Table 6.3 Comparison of the Proposed 1-D MMR-Based LWAs and Other Similar Works (© 2020 IEEE, reproduced with permission)

Ref.	Operating bandwidth	Beam-scanning range	Maximum gain with variation (dBi)	Maximum radiation efficiency with variation (%)	Structural technique	Radiating discontinuity	Unit cell characteristic
[14]	16.2% (10.2-12 GHz)	15^o - 72^o	14 (8)	N/A	SIW	Transverse slot	SMR-based unit cell
[51]	43.5% (9-14 GHz)	-40^o - 35^o	12 (9)	N/A	SIW	Longitudinal slot	
[52]	34.2% (8.5-12 GHz)	-70^o - 60^o	13.5 (5)	N/A	SIW	Transverse slot	
[56]	16.1% (13.2-15.6 GHz)	-61^o - 42^o	14.1 (3)	60 (30)	SIW	Transverse slot	
[30]	39.8% (13-19.45 GHz)	-48^o - 35^o	14 (3)	N/A	Microstrip	Open-circuited stub	Composite unit cell
[31]	52.9% (12.5-21.5 GHz)	-56^o - 75^o	15 (3)	N/A	Microstrip	Open-circuited stub	
MED-based LWA	28.6% (30-40 GHz)	-43^o - 28^o	15.1 (2.6)	82.2 (9)	SIW	MED	MMR-based unit cell
ACPA-based LWA	28.6% (30-40 GHz)	-39^o - 27^o	15.5 (2)	80.4 (2.2)	SIW	ACPA	

CHAPTER 7 ARTICLE 5: MULTIFUNCTIONAL LEAKY-WAVE ANTENNA WITH TAILORED RADIATION AND FILTERING CHARACTERISTICS BASED ON FLEXIBLE MODE-CONTROL PRINCIPLE

Dongze Zheng and Ke Wu

Published in the *IEEE Open Journal of Antennas and Propagation*, vol. 2, pp. 858-869, Jul. 2021.

In this chapter, a class of single-layered multifunctional LWAs with flexibly engineered radiation and filtering characteristics are proposed and demonstrated for microwave and millimeter-wave applications. RDs exhibiting multiple resonances while particularly possessing flexible model-control capability are exploited to accomplish such design freedoms and multifunctionalities of LWAs. By properly engineering the resonance characteristics of RDs under the mode-control principle, the attenuation constant of relevant LWAs can not only be freely tailored for diverse beamwidth/directivity requirements, but also simultaneously maintain a flat frequency response for radiation stability. Meanwhile, controllable filtering behaviors can be obtained as well by the LWAs thanks to the transmission zeros introduced by resonances. Consequently, both the radiation and filtering performances of LWAs can be adequately tailored by taking advantage of the mode-control capability of RDs. Under this design concept, two types of LWAs based on substrate-integrated waveguide and microstrip techniques are respectively developed for different system integration platforms. The SIW LWA whose unit cells consist of different longitudinal slots is firstly examined. Additionally, the microstrip LWA, which depends on stub-loaded resonators, is further investigated. The proposed two LWAs are all with flexible engineered electrical behaviors, single-layer, low-cost, and easy integration; they may be a potential candidate for various system applications such as 5G communication and IoVs.

7.1 Introduction

LWAs have been well-known for the unique frequency-driven beam-scanning capability, thanks to which they may find potential in system applications such as wireless communications, real-

time spectrogram analyzers, and automotive radar sensors [9][11]. Most LWAs physically manifest periodic appearances and are normally realized by periodically loading RDs along the host guides or TLs. Among these LWAs, some using the fundamental space-harmonic for radiation are referred to as quasi-uniform LWAs, while others employing the higher-order (e.g., -1st-order) counterparts are termed periodic LWAs. Different from the above-mentioned classifications that are conventionally based on the radiating harmonics or geometry, LWAs, however, can also be classified into two basic groups from the perspective of resonance behaviors of RDs, i.e., SMR and MMR [83]. This is because various kinds of resonant structures are commonly used as RDs to construct LWAs, such as slots [14]40][50][52][57][116][142][144][164], stubs [15][31[32], dipoles [74][91][138], patches [66][75][260], and composite structures [58][83][148], etc. Notably, those RDs are not just limited to enable host TLs radiative; their resonance characteristics certainly have a significant influence on the complex propagation constants of the leaky modes or space-harmonics. Thus, they critically impact the electrical performances of LWAs, such as the realization of high directivity [15], stable radiation [30][31][58][83], and rapid beam-scanning [142][144][148], etc.

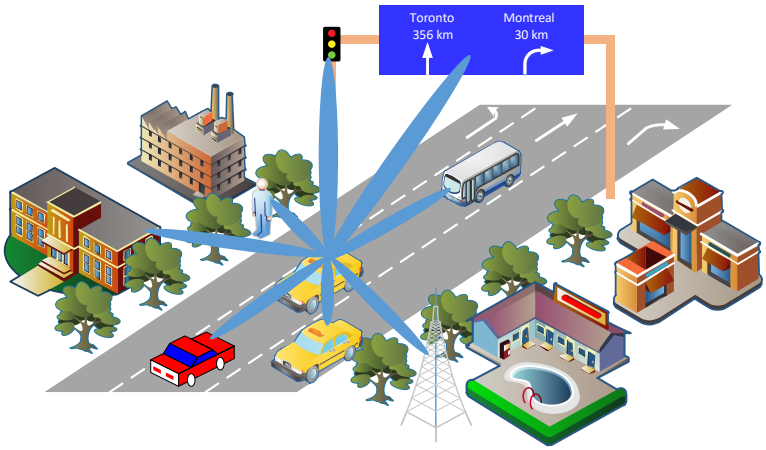

Figure 7.1 A simplified illustration of 5G-enabled IoV

As one of the most significant application scenarios of Internet of Things (IoTs), IoV has recently experienced an unprecedented development thanks to the emergence of 5G technologies [261]-[263]. 5G-enabled IoV (5G-IoV) makes vehicle-to-everything (V2X) realizable with significant benefits of latency, data speed, reliability, and security, thanks to which autonomous driving developments will become practicable in the short future. As a critical RF frond-end component in

such 5G applications (i.e., IoV), antennas implemented on the host vehicles should be capable of providing a specific narrow and directive beam to each "user" (e.g., other guest vehicles, pedestrians or infrastructures), as shown in Figure 7.1. Such required multiple beams (or beam-scanning) are usually realized by complicated beam-forming networks, costly phase shifters, or computationally intensive back-end digital signal processing techniques. Comparatively, beam-scanning simply driven by frequency is a relatively cost-effective and straightforward solution. Due to the features of simple feeding, narrow directive beam, and unique frequency-driven beam-scanning property, LWAs present a promising candidate, which have already been developed for automotive radar sensors [193][194] and may be deployed for prospective 5G-IoV applications. Nevertheless, a well-designed LWA for potentially practical use should simultaneously have some desirable merits and functionalities, e.g., adequate design freedoms and flexibilities of electrical characteristics (radiation and circuit performances), low-cost, easy fabrication and integration, etc. To be specific, it is of great significance and necessity for an LWA that can be customized in terms of its beamwidth/directivity to meet different practical specifications. Simultaneously, the LWA should also maintain stable beam-scanning performances so as to provide uniform effective isotropically radiated power (EIRP) in the FoV of V2X communication. Moreover, it would be better if this LWA can also be equipped with filtering capability to reduce total circuit size and improve overall front-end system performances (e.g., insertion loss, noise figure and dynamic range). Although a singular functionality of LWAs such as radiation stability [30][31][58][83] or filtering characteristics [143][236][237] can be found in the open literature, no reported works, to the best of the authors' knowledge, have been specially dedicated to combining multifold functionalities such as radiation stability and filtering behavior as well as flexible engineering capability into a single LWA. More critically, practical industrial significance of LWAs such as low-cost and easy fabrication/integration properties should also be simultaneously taken into account aimed for mass-production.

In this work, such kind of LWAs, taking advantage of the flexible mode-control principle of RDs and simple single-layer PCB processing, are developed for microwave and millimeter-wave system applications. The main contribution of this work is reflected on the artful use of MMR-based RDs featuring flexibly controlled modes for LWAs with good design freedoms and multifunctional electrical performances such as manageable beamwidth, controllable bandwidth/filtering

characteristics, and stable radiation. Different TL technologies such as SIW and microstrip are respectively exploited as the host TLs, aimed for diverse system integration platforms. An SIW LWA, whose unit cell consists of different longitudinal slots exhibiting multiple independently controllable resonances, is first to be investigated. Comparatively, an open-circuited stub-loaded resonator (OCSLR) with the similar flexible model-control behavior is subsequently proposed and implemented for a microstrip combline LWA. It is demonstrated that by properly controlling the RD's several resonant modes simultaneously (i.e., the so-called flexible mode-control), the attenuation constant of related LWAs can be freely adjusted during which a stable frequency response of it can always be maintained. This is not only useful for LWAs to realize radiation stability, but also beneficial to accomplish diverse beamwidth specifications as well as wideband behaviors of low side-lobe radiation. On the other hand, strong resonances of the RD will cut off the whole transmission link of relevant LWAs and thus introduce transmission zeros, exhibiting desirable filtering characteristics in the frequency band of LWAs. Due to the multifold benefits such as flexibly engineered radiation and filtering characteristics, single-layer, low-cost, and easy fabrication/integration, the proposed LWAs may find potentials in practical applications such as the 5G communication and IoV.

7.2 Problem Analysis and Design Principle

For an LWA that is not tapered along its wave-propagation direction, its radiation characteristics can be easily predicted by its complex propagation constants, namely the attenuation constant α and phase constant β. For a periodic LWA using the -1st order space-harmonic to radiate, its main-beam direction θ_m and 3-dB beamwidth $\Delta\theta$ can be expressed by the following equations [9]

$$\theta_m \simeq \sin^{-1}\left(\frac{\beta}{k_0}\right), \qquad \Delta\theta \simeq 5\frac{\alpha/k_0}{\cos(\theta_m)} \tag{7.1}$$

where k_0 and λ_0 are the free-space wavenumber and wavelength, respectively. The 3-dB beamwidth $\Delta\theta$ in (7.1) assumes 90% efficiency provided that there are no material losses, and the remaining 10% of the injected power is absorbed by a matching-load at the end (i.e., matching-load loss). It can be seen from (7.1) that to realize various beamwidths of an LWA customized for different application scenarios, its attenuation constant should be altered accordingly. It has already been demonstrated in [83] that there is an approximate one-to-one mapping relation between the RD's

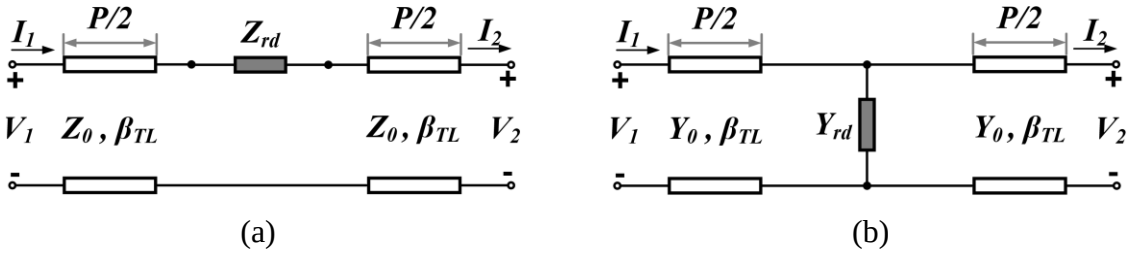

Figure 7.2 Generalized equivalent circuit models of a periodic LWA

(a) Series loading type. (b) Shunt-loading type. The radiating discontinuities (i.e., Z_{rd} and Y_{rd}) can represent an SMR or MMR

normalized resistance/conductance and the attenuation constant of the related LWA, which can be expressed as

$$\alpha \simeq -\ln\left[1-re\left(\frac{Z_{\mathrm{rd}}}{Z_0}\right)\right]\Big/2P \text{ or } -\ln\left[1-re\left(\frac{Y_{\mathrm{rd}}}{Y_0}\right)\right]\Big/2P \tag{7.2}$$

corresponding to the series-loading and shunt-loading circuit models as shown in Figure 7.2(a) and (b), respectively. Z_{rd} and Y_{rd} represent the impedance and admittance of the loaded RDs, while Z_0 and Y_0 denote the characteristic impedance and admittance of the host TLs, respectively. P is the period length of unit cells. According to (7.1) and (7.2), two effective approaches can be used to control the attenuation constant or beamwidth of an LWA: change either the absolute resistance/conductance of the RD, or the characteristic impedance/admittance of the host TLs. In general, the realization of various attenuation constants for an LWA is usually realized by resizing the RD and shifting its resonance close to or away from the design frequencies so as to manage its absolute resistance/conductance value. For example, by changing the length of the slot/stub/dipole, the related resonance frequency and thus the attenuation constant can be adjusted to facilitate a low side-lobe design of the LWAs [30][50][116][140][142]. However, it should be noted that although the attenuation constant can be altered by shifting the resonance frequency of the RD, it is hard for these relevant LWAs to simultaneously hold a flat frequency response of the attenuation constant over the frequency band of interest. Thus, the design freedoms and flexibilities as well as the electrical performances of LWAs have to be compromised to some extent. This is especially true for SMR-related LWAs [83]. To make matters worse, a further deterioration of radiation fluctuation would be encountered when requiring a larger attenuation constant in these LWAs. The

reason for this is easily understood since such a situation usually needs to shift the RD's resonance closer to the design frequency band. Thus, a more dramatic variation would occur for the resistance/conductance properties of such an RD as well as for the radiation behaviors of associated LWAs over frequencies.

Recall that in our RF/microwave communities resonance behaviors are always crystallized in a periodic manner over the frequency domain thanks to the periodic essence of time-harmonic electromagnetics and specific boundary conditions [17]. Because of this, a simple resonant structure such as a dipole, slot, stub, and patch naturally possesses several resonant modes over frequency as simply illustrated in Figure 7.3, and these multiple resonances may be simultaneously used for operations such as the design of multiband or wideband antennas [16]. Nevertheless, in most cases, only one of these modes (usually the fundamental one) is used for operations because it is easier to manipulate only one mode at a time compared to the simultaneous control of multiple modes. This partially explains why most of resonant structures are usually under the treatment of an SMR in some typical applications like those LWAs with a low side-lobe design [30][50][116][140][142]. Interestingly, multiple simple structures with each donating only one of its modes can also be combined to constitute a composite structure presenting MMR behaviors like Figure 7.3, such as the well-known magneto-electric dipole and aperture-coupled patch [58][83][264]. Notably, even though MMR-based RDs can be adopted to construct LWAs for radiation stability like the works in [58] and [83], the design freedoms and flexibilities of diversified beamwidths while maintaining the radiation stability are still difficult to be simultaneously realized, since this requires that several resonances of the RD could be flexibly controlled to stabilize the normalized resistant/conductance curve over the frequency band of interest as revealed in Figure 7.3. Obviously, to realize a changeable resistance/conductance value while simultaneously keeping its flat frequency response, the two relevant strong resonances (i.e., curve peaks in Figure 7.3) of the MMR-based RD should be engineered on the beat. In other words, the flexible-mode control capability should be equipped for the RD. Since the resistance/conductance value is normally related to the frequency locations of the two strong resonances, they can be controlled to be far away from the center frequency to lower the resistance/conductance value of the RD and thus the attenuation constant according to (7.2). Contrastively, improved radiation leakage can be achieved by shorting the frequency distance of

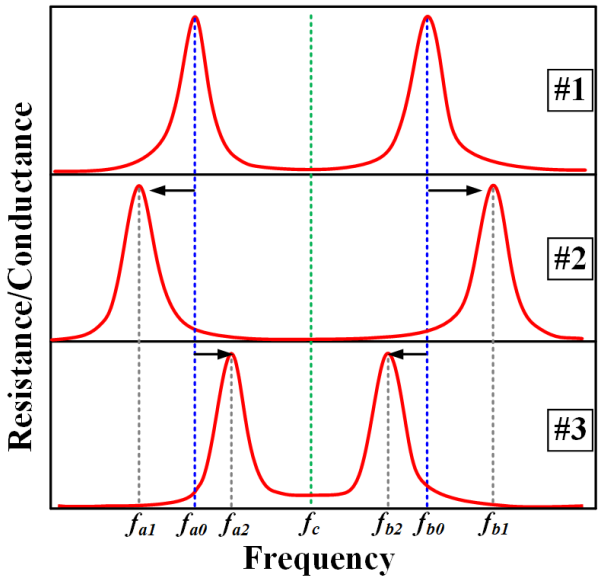

Figure 7.3 Mode-control principle for the design flexibilities and multifunctionalities of LWAs

Curve peaks can represent either series- or shunt-resonances, corresponding to the conductance or resistance case accordingly. While the #1 is referred to as the reference, the #2 is with an increased frequency distance of resonances and the #3 has the reverse situation

such two modes. In both cases, stable frequency response can always be held if frequency locations of the two modes are kept symmetrical about the center frequency. It is interesting to mention that another significant benefit of the flexible mode-control principle illustrated in Figure 7.3 can be found in LWAs' low side-lobe design over a wide bandwidth. This is because in this case the attenuation constant distribution along the leaky structure according to a specific aperture illumination would be frequency-independent, which cannot be meet by most of current low-side lobe designs [30][50][116][140][142]. On the other hand, when relating the resonance behaviors illustrated in Figure 7.3 to the LWAs' equivalent circuits shown in Figure 7.2 (a) or (b), it can be found that the two strong resonances, which represent shunt-resonances in the impedance case or series-resonances in the admittance one, would respectively behave as "open" in Figure 7.2(a) or "short" in Figure 7.2(b). Thus, such two strong resonances can turn off the energy transmission and produce two relatively symmetrical transmission zeros or stopbands in LWAs [17]. These stopbands can be potentially used to control operating bandwidth of the periodic LWAs. Namely,

the operating bandwidth of the periodic LWAs can be flexibly adjusted by resorting to the MMR-based RDs featuring flexible mode-control capability. In conclusion, the resonance behaviors of an RD should have the merit of flexible mode-control capability for prospective LWAs to simultaneously realize stable radiation, manageable beamwidth, and controllable bandwidth/filtering behaviors. This kind of LWAs featuring such design flexibilities and benefits will be investigated and developed in the following sections.

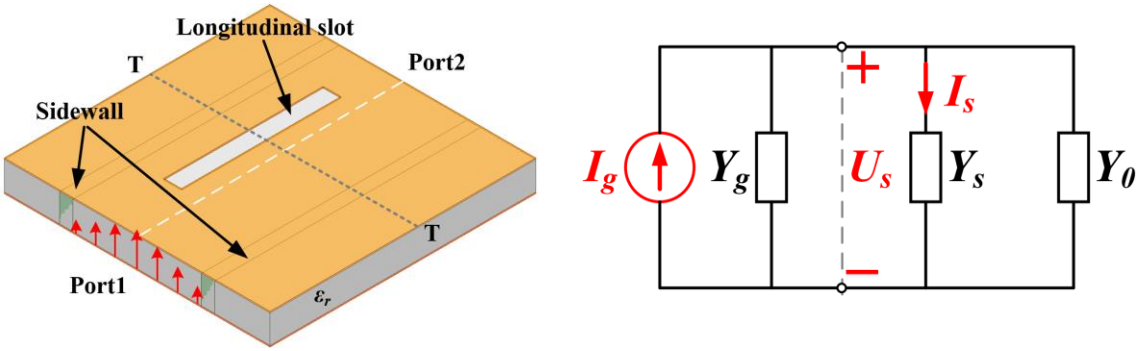

(a) (b)

Figure 7.4 Traditional longitudinally slotted SIW LWA unit cell with a single slot [239]

(a) Geometry. (b) Norton equivalent circuit model. The longitudinal slot is simply modeled as a series *RLC* resonator that is parallel-connected into the SIW, similar to Figure 7.2(b). In (b), I_g denotes the current source, and it also represents the transverse currents flowing on the broad wall of the SIW. Y_g is the source admittance, which is equal to the characteristic admittance of the SIW, i.e., Y_0. The slot's admittance is represented as Y_s

7.3 Asymmetrically Longitudinally Shunt-Slot-Pair (ALSSP)-Based SIW LWA

7.3.1 Development of the ALSSP-based RD

Figure 7.4(a) depicts the geometry of a traditional longitudinally slotted SIW LWA unit cell [36]. Only a single longitudinal slot is etched on the top broad wall of the SIW along which the dominant TE_{10} mode is assumed to be excited and guided. Radiation occurs when the longitudinal slot is

offset from the longitudinal centerline, since transverse currents on the SIW's broad wall would be cut off by the slot. Simplified excitation mechanism of the slot can be explained by the Norton equivalent circuit model, as shown in Figure 7.4(b), where the transverse currents behave as a current source and excite the slot resonating at a half-wavelength mode. Notably, the admittance property of the slot is usually characterized as an SMR without exhibiting higher-order modes which are hardly excited under such a slot-excitation-mechanism. Thus, the slot is simply modeled as a series *RLC* resonator that is parallel connected to the host SIW lines, similar as Figure 7.2(b). In order to create multiple resonances behaviors in the slot, extra structures must be incorporated with it. For example, planar electric dipole or patch can be additionally attached over the longitudinal slot to form multi-layered composite structures, presenting multiple resonances [58][83][264]. However, strong electromagnetic coupling is used as the feeding mechanism in these structures, for which those relevant resonant modes are mutually coupled and cannot be flexibly controlled for operations to some extent, not to mention that such multilayer geometries would bring the cost and fabrication issues in practical applications. Inspired from the excitation mechanism of the longitudinal slot [239] and the works in [250][265], multiple longitudinal slots with different dimensions and resonant frequencies can be etched on the SIW. Typically, two slots are taken into account, and thus two arrangements, namely unilateral and bilateral cases, can be deployed as shown in Figure 7.5, in which the simplified aperture field and transverse current distributions are also illustrated. For the unilateral case, the two slots will feature oppositely directed aperture field distributions, which can be conveniently expounded by the Norton

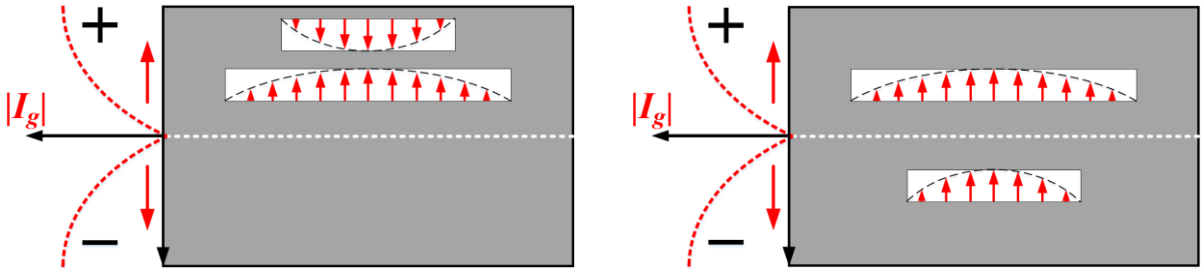

(a) (b)

Figure 7.5 Longitudinally slotted SIW LWA unit cell with two different slots

(a) Unilateral and (b) bilateral (proposed) arrangements with respect to the longitudinal centerline. Both slots resonate at a half-wavelength mode

equivalent circuit shown in Figure 7.4(b). Specifically, in the target frequency band (i.e., the band between the two resonances respectively introduced by the two slots), the two slots behave with opposite susceptance behaviors. One is inductive (after its own resonance) while the other is capacitive (before its own resonance) over such a frequency range. They will possess reversely directed electrical potential differences (voltages) and so do their aperture fields since their driven currents share the same direction, as illustrated in Figure 7.5(a). Obviously, it is difficult for this unit cell to radiate since most of radiation originated from the two slots cancel each other out. As a comparison, thanks to the reversely directed transverse currents on the two halves of the SIW, the two oppositely signed (susceptance-complementary) slots will embrace the same-directed aperture fields, and this corresponds to the bilateral arrangement as shown in Figure 7.5(b). In this case, the two slots can work together as an effective radiator characterized by multiple resonances, as will be exhibited later. Although a similar dual-slot geometry can also be found in [265], more physical insights and extensive characterizations are explored and clarified in this chapter in terms of the circuit modeling and radiation mechanism of the structure, as described above and also will be illustrated later. Also note that the research purposes between the two are totally different. Due to the fact that the two slots are different in size and distributed on the two halves of the SIW along the longitudinal centerline and all share the same type of shunt-loading effects on the SIW, the two slots are thus referred to as "asymmetrically longitudinal shunt-slot-pair" (ALSSP).

7.3.2 Multiple Resonances Behavior and Flexible Mode-Control of the ALSSP

The geometry, cross-sectional E-field distribution, and transmission-line equivalent circuit model of the proposed ALSSP-based SIW LWA unit cell can be found in Figure 7.6. Note that a pair of matching vias are embedded into the unit cell for an open-stopband suppression [83]. The simulated cross- sectional E-field distribution of the unit cell is consistent with Figure 7.5(b), illustrating that radiated fields emanated from the two slots are constructively superposed to form effective radiation that interestingly resembles a rectangular patch antenna's radiation mechanisms, i.e., equivalent two-element slot array [16]. In Figure 7.6(d), each longitudinal slot of the ALSSP is simply modeled as a series *RLC* resonator, and the full-wave and circuit simulation results in terms of the ALSSP's admittance are illustrated in Figure 7.7. The circuit simulation results are in a reasonably good agreement with their full-wave counterparts, and both exhibit multiple resonances

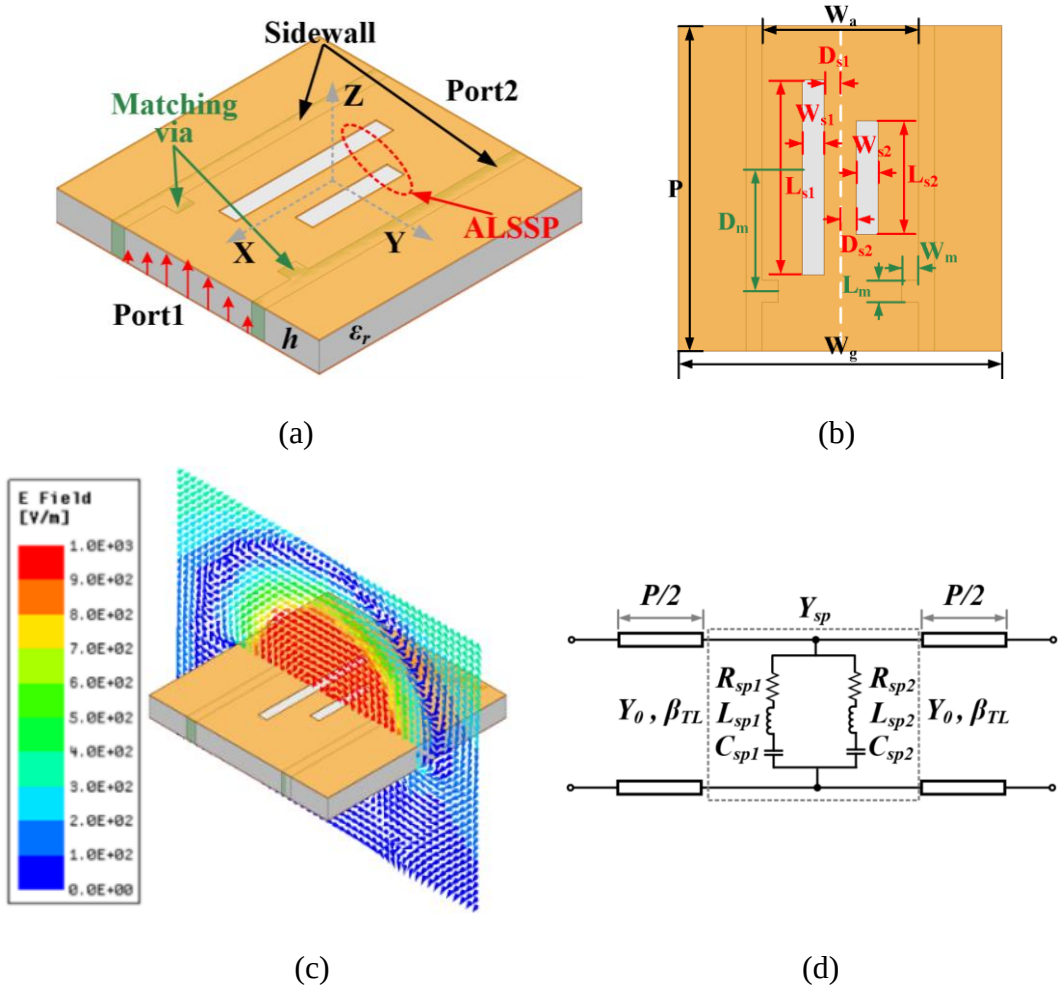

Figure 7.6 ALSSP-based SIW LWA unit cell

(a) 3-D view (not to scale); (b) top view (not to scale); (c) cross-sectional E-filed distribution (35 GHz); (d) equivalent circuit model neglecting the matching vias. The substrate is RT/duroid 6006 with a thickness of 0.635 mm, relative permittivity of 6.45, and loss tangent of 0.0027. Specific dimensions are P=4.15, W_g=2.9, W_a=6, L_{s1}=3.4, W_{s1}=0.3, D_{s1}=0.2, L_{s2}=2.1, W_{s2}=0.6, D_{s2}=0.3, D_m=1.96, L_m=0.356, W_m=0.266, h=0.635, t=0.4 (unit: mm)

behavior. Values of those circuit components (R_{sp1}, L_{sp1}, C_{sp1} for the long slot, while R_{sp2}, L_{sp2}, and C_{sp2} for the short slot) are obtained by a curve-fitting approach with the help of Advanced Design System (ADS) software. Notably, apart from the two series-resonances that are individually introduced by the two slots, there is an additional shunt-resonance between the two. The reason for its occurrence can be explained using the ALSSP's equivalent circuit model shown in Figure 7.6(d).

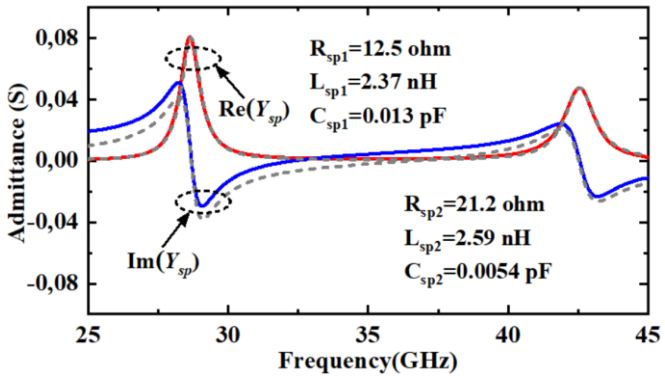

Figure 7.7 Admittance frequency responses of the proposed ALSSP-based RD with respect to full-wave (solid line) and circuit (dash line) simulations

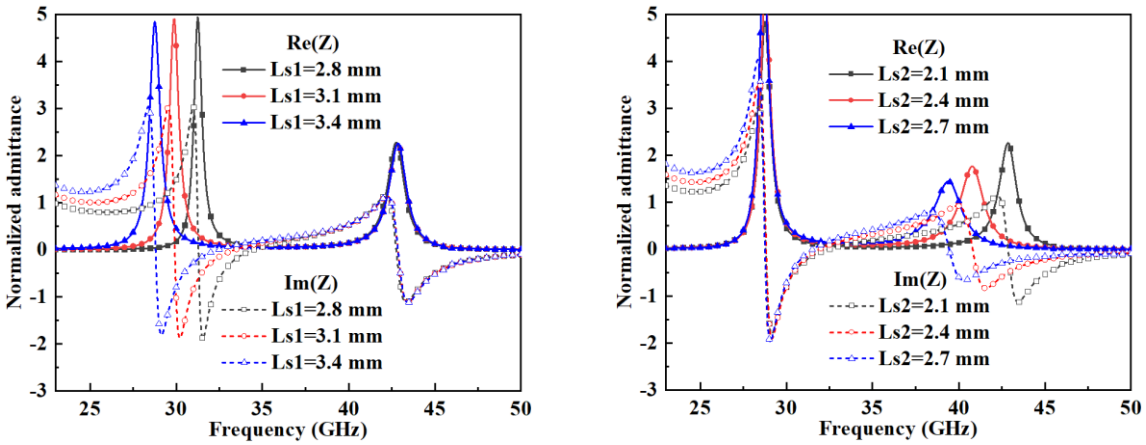

(a) (b)

Figure 7.8 Dimensional effects of the ALSSP on its normalized admittance behaviors (a) L_{s1}. (a) L_{s2}. The two studied parameters are the length of the longer and shorter slots, respectively

Since the two slot-resonator-branches have complementary susceptance properties in the target frequency range as mentioned previously, the inductive slot (long slot) will compensate the capacitive slot (short slot) in terms of their susceptance at one specific frequency point, at which the whole resonator circuit tank (i.e., ALSSP) will satisfy the shunt-resonance condition. Figure 7.8 depicts the dimensional effects of the ALSSP on its normalized admittance performances. The two studied parameters L_{s1} and L_{s2} represent the length of the long and short slots, respectively. It

is clearly seen that the two series-resonances can be controlled independently, i.e., flexible mode-control capability. Specifically, by increasing L_{s1}, the first series-resonance will be shifted to a lower frequency without influencing the second series-resonance, as shown in Figure 7.8(a). A similar phenomenon can also be found with changing L_{s2}, as plotted in Figure 7.8(b). The width of the slot is not studied here for brevity since it just shows a little influence on the resonance frequency, beyond our main considerations regarding the flexible mode-control principle [16][239].

7.3.3 Customized Characteristics of the ALSSP-based SIW LWA under Flexible Mode-Control

In order to verify the claimed benefits of the flexible model-control capability, i.e., design flexibilities of manageable beamwidth and controllable bandwidth/filtering behaviors as well as the radiation stability, resonance behaviors of the ALSSP in terms of its two series-resonances are engineered by changing length of the two slots, i.e., L_{s1} and L_{s2}. Specifically, three groups of (L_{s1}, L_{s2}) are assigned to the ALSSP in such a way that the two series-resonances are with different frequency distances but approximately centered at the design frequency of 35 GHz, as shown in Figure 7.9(a) which depicts the normalized conductance of each type of ALSSPs. It can be seen clearly that a shorter frequency distance of the two series-resonances will lead to an increased normalized conductance at the center frequency. This is similar to Figure 7.3 and thus will give rise to a wider beamwidth for the relevant LWAs according to (7.1) and (7.2), as shown in Figure 7.9(b). Herein, each type of the ALSSPs, namely #1, #2, and #3, is periodically loaded onto a lossless SIW line to establish an LWA that has a certain quantity of unit cells for 90% radiation efficiency. Notably, the introduction of matching vias for the open-stopband suppression would not significantly influence the previously configured behaviors of the ALSSP. This is due to the fact high-order waveguide modes excited by the matching vias are in a cut-off status and thus are highly attenuated and localized; they hardly reach the slot RD in general [17]. Figure 7.9(c) exhibits the $|S_{21}|$ performances of these relevant LWAs, in which stable and symmetrical curve patterns over the middle passband are displayed, thus implying that stable radiation efficiencies can be realized. In this sense, LWAs with diverse beamwidths while simultaneously having stable radiation performances can be realized by taking advantage of the flexible mode-control capability of the ALSSP. Note that a controllable operating passband is also observed in Figure 7.9(c), which

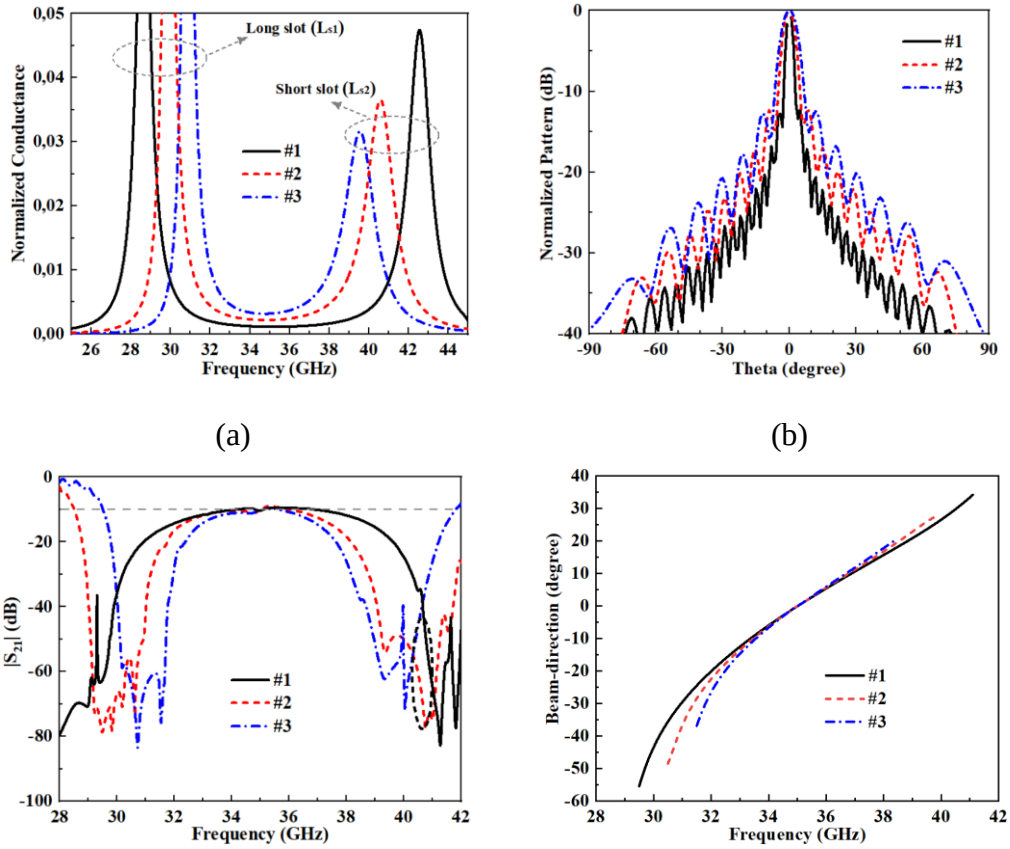

Figure 7.9 Illustration of design flexibilities of the ALSSP-based LWA under mode-control principle

(a) Normalized conductance of ALSSPs. (b) Normalized radiation pattern, (c) $|S_{21}|$ and (d) beam-scanning behaviors of ALSSP-based LWAs. #1, #2 and #3 correspond to different assignments of the slot-length (L_{s1}, L_{s2}), with specific values of (3.4 mm, 2.1mm), (3 mm, 2.4 mm), and (2.8 mm, 2.6 mm), respectively. Also, #1-, #2-, and #3-related LWAs are respectively designed with 36, 19, and 14 unit cells for 90% radiation efficiency

is sandwiched by two stopbands that are formed by the transmission zeros introduced by the two series-resonances of the ALSSP, as explained previously. Beam-scanning behaviors of these LWAs can be found in Figure 7.9(d); it also manifest apparent bandpass characteristics only within which the beam is scanned with frequency. As a result, with the flexible mode-control of the ALSSP, the proposed LWA can provide good design freedoms and flexibilities as well as those

multifunctionalities as mentioned previously. Also note that the proposed LWA is only single-layered and can be fabricated using low-cost and simple PCB processing, which is suitable for mass-production in practical use.

7.4 Evolutionary Microstrip Combline LWA Based on Open-Circuited Stub-Loaded Resonator (OCSLR)

7.4.1 Evolutionary Design of Microstrip Combline LWA using Multiple Resonances

The microstrip open-circuited stub can be interpreted as a microstrip dipole with its one end shorted to the main microstrip line while the other being a radiating edge. Due to its simple geometry and easy fabrication, it is usually used to develop a series of standing-wave antenna arrays [259] and LWAs [15][30][31]. This kind of antennas are often referred to as microstrip "combline" antennas, as shown in Figure 7.10(a) and (b) illustrating the two conventional schemes [259]. It is worth noting that the open-circuited stub resonator adopted in these schemes usually has a uniform width or characteristic impedance, and herein it is entitled open-circuited uniform impedance resonator (OCUIR). A unit cell of the conventional microstrip combline LWA [15] and its several modal

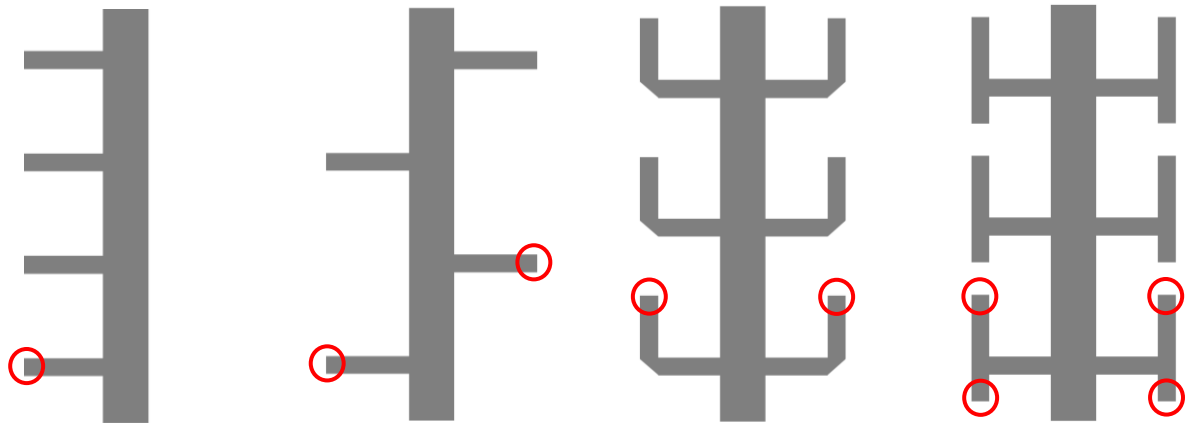

Figure 7.10 Evolution of microstrip combline antennas

Conventional (a) unilateral and (b) bilateral cases. Proposed (c) case #1 and (d) case #2. Red circles represent radiating edges within a unit cell

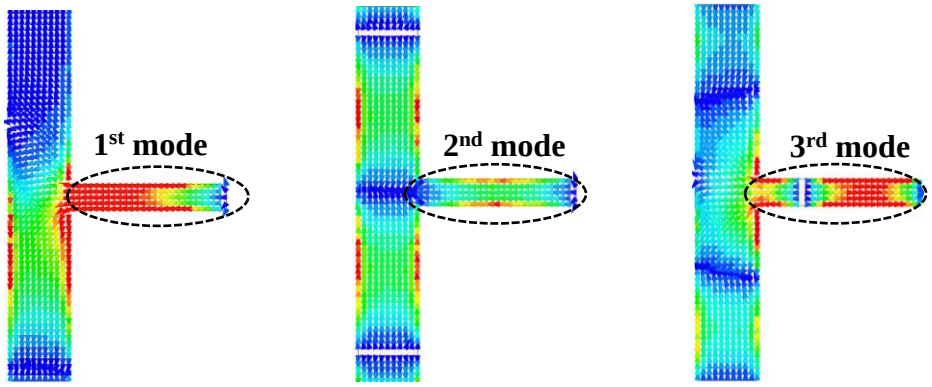

Figure 7.11 Conventional microstrip combline LWA unit cell with respect to its modal current distributions

The first three resonances are exhibited. The 1st and 3rd modes are series-resonances, while the 2nd mode is shunt-resonance. The related equivalent circuit model is the same as Figure 7.2(b)

currents can be seen in Figure 7.11. The first three resonant modes respectively correspond to the series-, shunt- and series-resonances, where the electrical length of the stub is approximately equal to one, two, and three quarter-wavelengths accordingly. The equivalent circuit model of the unit cell is the totally same as the one in Figure 7.2(b). Due to the natural MMR behaviors of the OCUIR, these resonant modes may be used simultaneously (as mentioned previously) to design microstrip combline LWAs with stable radiation according to the MMR design rules in [24]. Note that this fact has not been recognized and explored in reported similar microstrip stub-based designs [15][30][31]. However, the two conventional schemes shown in Figure 7.10(a) and (b) are not symmetrical along the longitudinal direction, which may possibly lead to a high cross-polarization level or asymmetrical cross-sectional radiation pattern [16][259]. They are also subject to the scanning blind in end-fire directions due to the radiation null of element pattern from such radiating edges of the OCUIR [5]. What is worse, for the conventional bilateral case shown in Figure 7.10(b), it would largely suffer from large side-lobes or even grating-lobes in the cross-sectional plane when the working frequency becomes high, since in this case the physical distance between the two bilateral radiating edges would be electrical large that may close to or more than a free-space wavelength. Also note that the common issue of the second-order radiation beams is easily encountered in such an alternatively bilateral arrangement [239][259]. Consequently, to tackle all

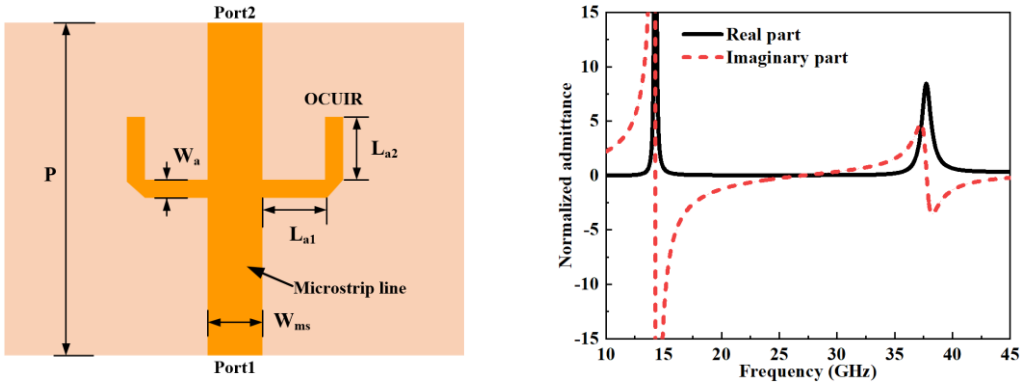

(a) (b)

Figure 7.12 (a) Unit cell of the proposed microstrip combline LWA using stub's natural multiple resonances. (b) Normalized admittance of the folded OCUIR

Dimensions of the unit cell are P=7.15 mm, W_{ms}=1.12 mm, L_{a1}=1.6 mm, L_{a2}=1.6 mm, and W_a=0.4 mm. The substrate is RO3035 with a thickness of 0.508 mm, relative permittivity of 3.6, and loss tangent of 0.0015

the possible issues aforementioned that can also be potentially suffered in [15][30][31], and simultaneously to make use of multiple resonances for stable radiation [83], an evolutionary microstrip combline LWA whose unit cell consists of a pair of symmetrical folded OCUIRs is established as shown in Figure 7.10(c). Its specific unit cell geometry can be found in Figure 7.12(a) having a trident-like shape. The folded or bend point is located at the center of each OCUIR, where a right-angled corner is delicately cut to reduce the bend discontinuity [259]. Notably, the two radiating edges of the pair of OCUIRs possess identical fringing field distributions and form a two-element array [266]. The distance between them would never exceed 0.75 free-space wavelength over the whole target frequency band under the MMR design rules even if the employed substrate has a relative permittivity of unity. Thus, the associated LWA will be totally free from side-or grating-lobes in its cross-sectional plane, which cannot be meet by the schemes in Figure 7.10(b) and [30]. Also note that in this case, the radiating edge's element pattern is null at the end-fire directions of the cross-sectional plane, which will also play a role in further preventing possible appearances of side- or grating-lobes in this plane. Figure 7.12(b) shows the normalized admittance of the pair of OCUIRs. Three resonant modes (two series-resonances and one shunt-resonance) can

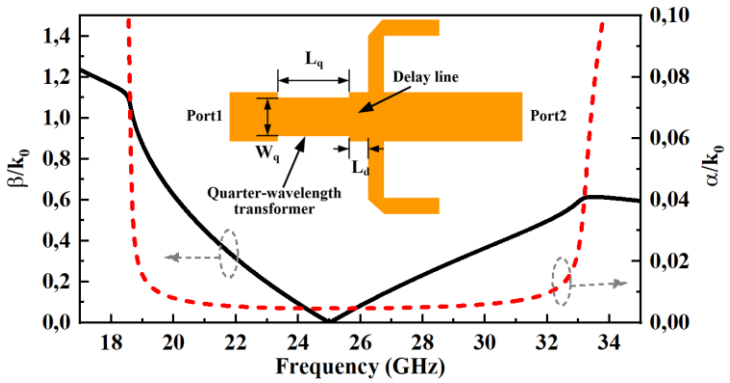

Figure 7.13 Normalized phase and attenuation constants of the proposed LWA

Open-stopband issue is effectively suppressed by using a delay line and quarter-wavelength impedance transformer [10], as shown in the inset. Dimensions of them are L_d=0.55 mm, L_q=1.75 mm, and W_q= 0.89 mm

be clearly observed with a fixed frequency ratio. The overall stub length can be changed to shift frequency locations of the two series-resonances so as to deploy the MMR design rules for the LWAs with stable radiation. For example, we choose 25 GHz as the center/design frequency, and the stub length is altered so that its two series-resonances are approximately centered at this frequency. As for the width of the stub, it can be suitably used to adjust the stub's radiation ability while without significantly influencing its resonance frequencies [17][259]. For the open-stopband suppression and continuous beam-scanning of the relevant LWA, impedance matching techniques such as a delay line plus a quarter-wavelength transformer can be used [15]. This is shown in Figure 7.13 which depicts the normalized complex propagation constants of the LWA together with an inset of the final unit cell. It also shows that a stable attenuation constant is achieved for the unit cell over the target frequency band from 21 to 29 GHz. This stems from the stable frequency response of the normalized conductance of the OCUIR and will lead to the relevant LWA to be equipped with a stable $|S_{21}|$ and radiation efficiency as will be shown later. For demonstration convenience, only 20 unit-cells are cascaded to form the proposed OCUIR-based LWA with the fabricated prototype depicted in Figure 7.14(a). Good impedance matching exhibited in Figure 7.14 (b) indicates that the open-stopband issue has been effectively suppressed, while both stable $|S_{21}|$ of -4.6 ± 0.8 dB and stable radiation efficiency of 59.5 ± 4.2% [as shown in Figure 7.14(c)] verify

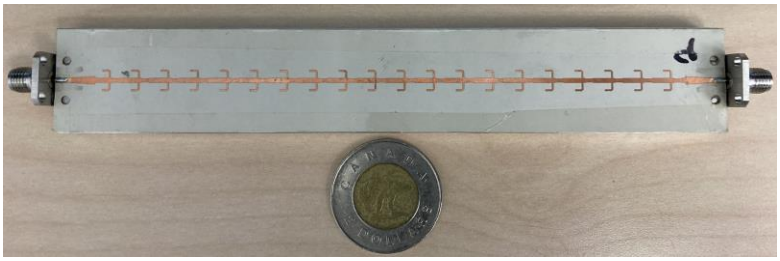

(a)

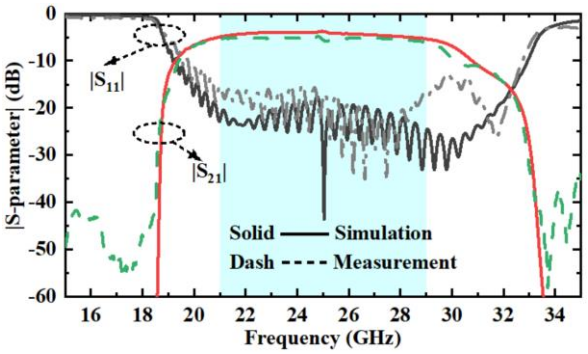

(b)

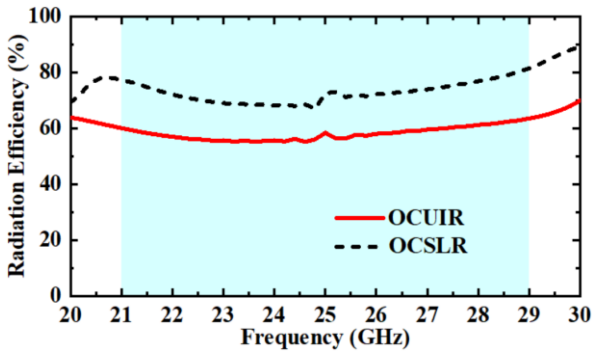

(c)

Figure 7.14 (a) Fabricated prototype of the proposed OCUIR-based microstrip combline LWA. (b) Simulated and measured *S*-parameters. (c) Simulated radiation efficiency

Radiation efficiency of the OCSLR-based counterpart (this design can be found in Chapter 7.2.2) is also plotted in (c) for a comparison

the effectiveness of the evolutionary microstrip combline LWA using the natural multiple resonances of the OCUIR for radiation stability.

7.4.2 Microstrip Combline LWA Based on Stub-Loaded Resonator—An RD with Flexible Mode-Control Capability

As we have demonstrated previously, an MMR-based RD with flexible mode-control capability is beneficial for LWAs to realize good design freedoms and flexibilities like governable beamwidth and filtering behaviors while simultaneously holding the stable radiation. Although the microstrip combline LWA has been evolved by using multiple resonances of the OCUIR for stable radiation, it is inconvenient for this LWA to be versatilely tailored for different application requirements due

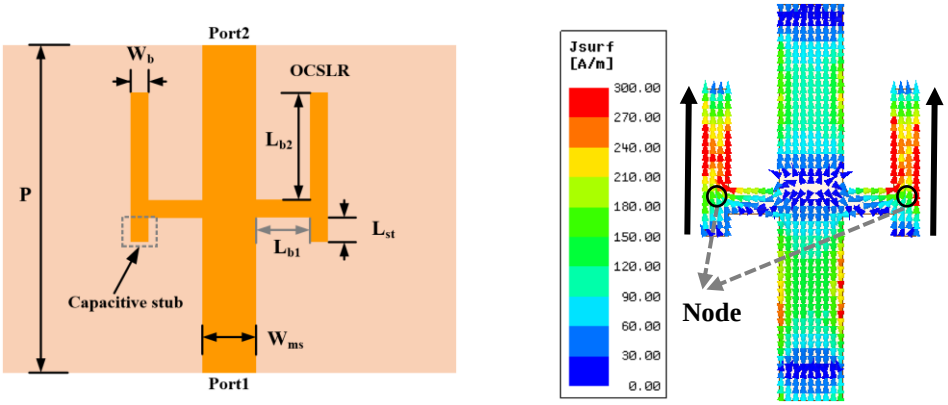

(a) (b)

Figure 7.15 Unit cell of the proposed OCSLR-based microstrip combline LWA

(a) Geometry. (b) Current distributions at the center frequency. The proposed OCSLR consists of a folded OCUIR loaded with a short capacitive stub. Dimensions of the unit cell are P=7.25 mm, W_{ms}=1.12 mm, L_{b1}=0.9 mm, L_{b2}=1.8 mm, L_{st}=0.45 mm, W_b=0.4 mm. The substrate is RO3035 with a thickness of 0.508 mm, relative permittivity of 3.6, and loss tangent of 0.0015

to the fixed frequency ratio of these resonant modes. Illuminated by [248][267][268] where loaded stubs or pins can be used to perform the flexible mode-control, a short piece of capacitive open-circuited stub is loaded to the folded OCUIR. Thus, an OCSLR-based LWA is established, as shown in Figure 7.10(d) and Figure 7.15(a). It is necessary to mention that there are two aspects that should be carefully considered when constructing the folded OCSLR. The first is concerned with the selection of the loading point of the short stub for realizing the flexible mode-control. According to the modal current distributions shown in Figure 7.11 and the works in [248][267][268], the middle current null point of the 3rd resonance can be loaded with the short capacitive stub for the purpose of realizing an independent control of this mode. Besides, differing from the folded OCUIR described in the last subsection in which the bend point is centrally located and the bend discontinuity is removed, the microstrip bend discontinuity can be artfully used here when folding a straight stub at the middle current null point of 3rd resonance. In this case, the bend discontinuity can cooperate with the loaded capacitive stub to adjust this mode independently, as can be seen in Figure 7.16. When the loaded capacitive stub is absent (i.e. L_{st}=0), the folded OCUIR

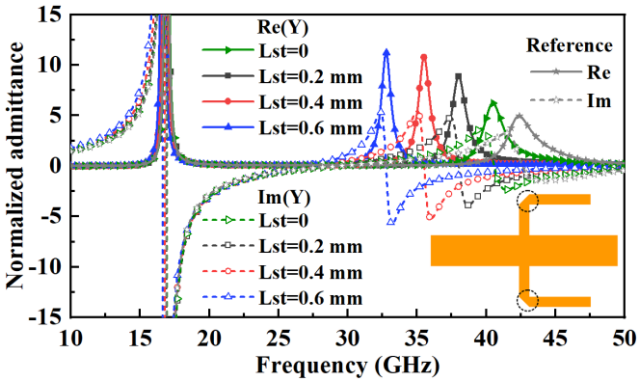

Figure 7.16 Dimensional effects of the short capacitive stub on the normalized admittance of the OCSLR

The curves marked as "Reference" represent the special case removing both the bend discontinuity and short capacitive stub, i.e., the one similar to the proposed OCUIR with a corner cut (as shown in the inset)

whose bend discontinuity is located at the current null point of the 3rd mode has an obvious lower modal frequency compared to its counterpart that has no bend discontinuity, regarding this resonance. Meanwhile, this resonance can be progressively shifted toward a lower frequency by increasing the length of the loaded capacitive stub. The reason for this mode-shifting phenomenon can be simply explained by the fact that both the bend discontinuity and the loaded short stub behave like a shunt-capacitor [17]. They will increase the effective capacitance of the *RLC* series resonator circuit representing the 3rd mode (series-resonance), and thus lower the related resonance frequency. It is necessary to mention that the loaded capacitive stub will also introduce a radiating edge involved into the total radiation mechanism; this is the second aspect that should be noticed for the proposed design. Thus, for the sake of radiation purity, this loaded short capacitive stub should be placed collinearly with the longer segment (i.e., the part that is parallel to the host line). In this case, the fringing fields of the loaded short stub's radiating edge will interestingly share the same direction with that of the folded OCUIR. This is because at the bend point (the "node"), the loaded short stub is capacitive while the longer segment of the folded OCUIR normally behaves inductively. At such "node" they will share the same electrical potential and hence their current directions will be totally reversed with respect to the "node". Namely one flows inward while the

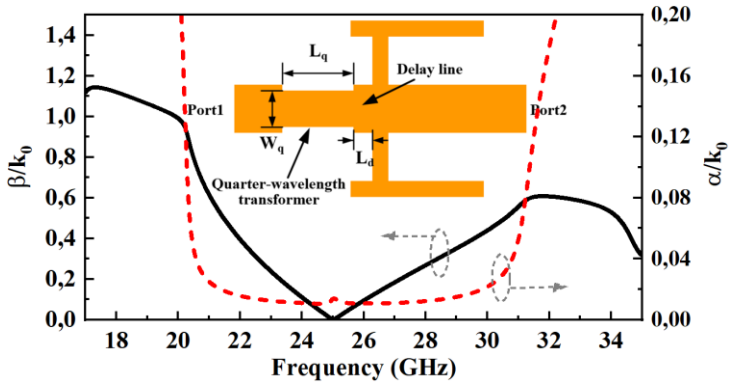

Figure 7.17 Normalized phase and attenuation constants of the proposed OCSLR-based microstrip combline LWA

Open-stopband issue is effectively suppressed by using a delay line and quarter-wavelength impedance transformer [10], as shown in the inset. Dimensions of them are L_d=0.58 mm, L_q=1.74 mm, and W_q= 0.65 mm

other flows outward of the "node", as displayed in Figure 7.15(b) which illustrates the typical current distributions of the OCSLR. Consequently, it is concluded that the loaded short capacitive stub is able to play a significant role in the flexible mode-control of the proposed folded OCSLR yet without contaminating the overall radiation performances. In this context, the proposed OCSLR-based LWA is also capable of providing such good design freedoms and multifunctional electrical performances analogous to the above demonstrated ALSSP-based LWA. These would not be repeated here just for brevity. Figure 7.17 depicts the normalized complex propagation constants of the proposed OCSLR-based LWA, where similar matching techniques as those in the OCUIR-based counterpart are also employed to suppress the open-stopband issue. The attenuation constant is not only kept relatively stable across the frequency band from 21 to 29 GHz, but also exhibits an obvious value improvement compared to the OCUIR counterpart shown in Figure 7.13. For verification purposes, 20 OCSLR-related unit cells are cascaded to form a microstrip combline LWA, and the fabricated prototype is shown in Figure 7.18(a). Figure 7.18(b) shows its simulated and measured *S*-parameters, illustrating that a good impedance matching is achieved without presenting an open-stopband issue. We are more interested in the $|S_{21}|$ performance, which shows a stable curve pattern in the target frequency band from 21 to 29 GHz. Meanwhile, a larger insertion

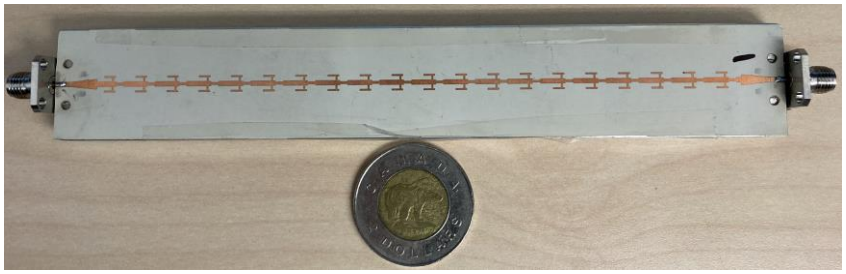

(a)

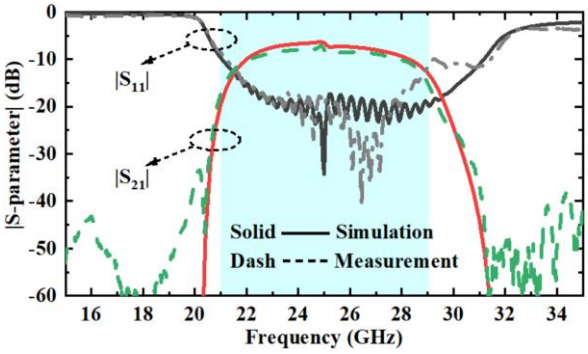

(b)

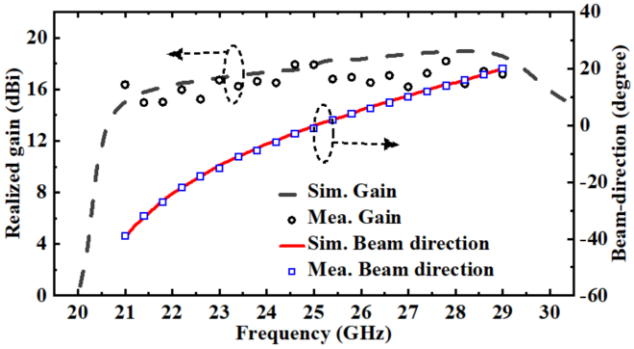

(c)

Figure 7.18 (a) Fabricated prototype of the proposed OCSLR-based microstrip combline LWA. (b) Simulated and measured *S*-parameters. (c) Simulated and measured realized gain and beam-direction

loss (i.e., improved radiation capability) can be found compared to Figure 7.14(b), thanks to the flexible mode-control induced by the loaded capacitive stub and the shortened frequency-distance between the two series-resonances as indicated in Figure 7.3. More importantly, an obvious filtering behavior with good out-of-band rejection is obtained. The radiation efficiency of the proposed OCSLR-based LWA is already depicted in Figure 7.14(c). Not only is the stable efficiency realized (i.e., 74.3 ± 7.2 %) that is consistent with such a $|S_{21}|$ curve pattern, but an apparent efficiency enhancement of about 15% than that of the OCUIR-based LWA is observed. The simulated and measured realized gain and beam-direction are displayed in Figure 7.18(c). The simulated results suggest that an average gain of about 16.8 dBi with variation of ± 1.8 dBi is realized in the frequency range from 21 to 29 GHz, where the beam-scanning span is from -40^o (backward) to 20^o (forward). The measured gain reasonably agrees with its simulated counterpart except for a little drop that may be due to an increased material losses and measurement tolerances,

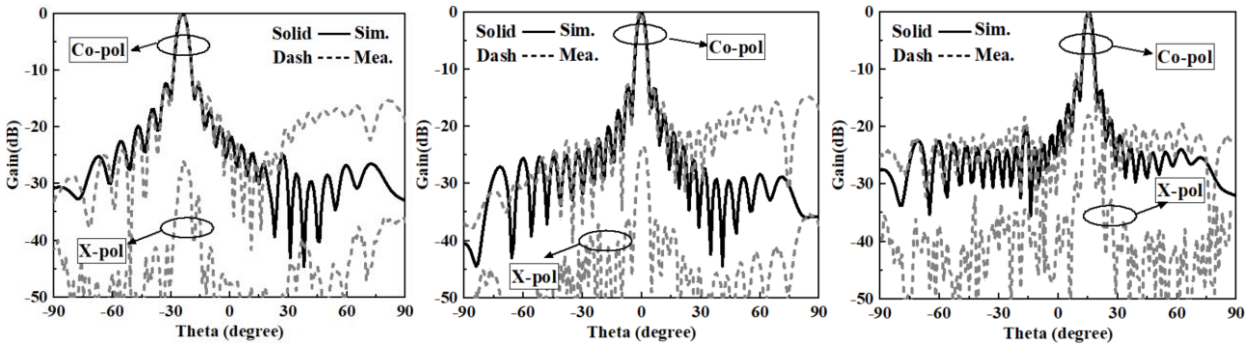

Figure 7.19 Normalized radiation patterns of the proposed OCSLR-based microstrip combline LWA

(a) 22 GHz; (b) 25 GHz; (c) 28 GHz

with a stable trend still remained (i.e., 16.5 ± 1.5 dBi). Simulated and measured radiation patterns at several frequencies are shown in Figure 7.19, indicating that a reasonable agreement is realized between the two cases with a slight difference that may be caused by fabrication errors or measurement issues. Notably, the simulated cross-polar components are too small to be visible.

7.5 Discussion and Comparison

So far, two types of 1-D periodic LWAs based on different transmission line technologies and RDs, i.e., ALSSP-based SIW LWA and SLR-based microstrip LWA have been elaborately studied. Thanks to the flexible mode-control capability owned by their RDs, good design freedoms and multifunctionalities in terms of circuit and radiation performances including controllable bandwidth/filtering characteristics, manageable beamwidth, and radiation stability have been achieved. However, there is a limitation behind this design concept when it comes to the achievable bandwidth and beamwidth of the related LWA: a larger beamwidth is always accompanied by a narrower bandwidth (or beam-scanning range), as revealed in Figure 7.9. This is because increasing the attenuation constant and thus the beamwidth of the LWA simply relies on shorting the frequency distance between the two strong resonances of the relevant RD so as to enhance the absolute resistance/conductance value of the RD. Fortunately, the characteristic impedance/admittance of the host TLs, according to equation (7.2), can also be exploited as an

additional parameter to control the attenuation constant and thus beamwidth of the LWA. Besides, the width of the slot/stub in our proposed LWAs can be used as well to adjust the absolute resistance/conductance value of the RD without significantly influencing its resonance frequencies as mentioned before. In this sense, a fixed bandwidth can be realized by controlling the locations of the RD's two strong resonances, while the beamwidth can be conveniently tailored by suitably selecting the characteristic impedance/admittance of host TLs and/or the width of the slot/stub RD. Consequently, the proposed LWAs can be of more freedoms and versatilities when customizing their electrical performances in terms of beamwidth and bandwidth.

In order to highlight the benefits of our proposed LWAs using the flexible mode-control principle, a comparison has been conducted and tabulated as displayed in Table 7.1. Here, the proposed SLR-based microstrip LWA is selected as a representative of our works; then, it is used to compare with other references. It can be observed that compared to those SMR-related works [14][52], the proposed SLR-based LWA is capable of simultaneously providing both the radiation stability and controllable filtering characteristics thanks to the MMR design rule together with the flexible mode-control principle. The advantages of such two functionalities in the proposed SLR-based LWA are still sustained when compared with those works aimed for either radiation stability [30][31][58][83] or controllable filtering capability [143][237]. In addition to these, it also should be noted that a systematic or strategic approach to design an LWA with rich freedoms and versatilities in terms of circuit and radiation characteristics has been uniquely investigated in our work compared to others in the table. Thanks to these benefits, the proposed antennas, especially the OCSLR-based microstrip LWA, may potentially be a competent candidate or standard scheme to substitute those traditional counterparts as shown in Figure 7.10(a) and (b) in practical system applications that, for example, need different bandwidths and beamwidths.

7.6 Conclusion

In this chapter, a class of single-layered multifunctional LWAs exhibiting flexibly engineered radiation and filtering characteristics, with the aid of mode-control principle, have been systematically explored and developed for microwave and millimeter-wave applications. It is demonstrated that by properly controlling the modal behaviors of the RD, the related LWAs can be freely tailored with respect to its attenuation constant while simultaneously maintaining

radiation stability and possessing filtering behaviors. Aimed for different system-integration platforms, both microstrip and SIW transmission-line technologies are separately employed to implement LWAs whose RDs possess flexible mode-control capabilities. In addition to those desirable electrical performances as mentioned above, the proposed LWAs also have some merits from the perspective of industrial practicability, e.g., good design flexibilities and versatilities, single-layer, low-cost, easy fabrication/integration. Therefore, they may be a good candidate for practical system applications such as 5G communication and the IoV.

Table 7.1 A Comparison between the Proposed Work and Several References

Ref.	Operating Bandwidth	Beam-Scanning Range	Maximum Gain & Variation (dBi)	Radiating Discontinuity	Unit Cell Characteristic	Flexible Mode-Control Capability	Controllable Filtering Capability
[14]	16.2% (10.2-12 GHz)	15^o – 72^o	14 (8)	Slot (SIW)	SMR-based unit cell	No	No
[52]	34.2% (8.5-12 GHz)	-70^o – 60^o	13.5 (5)				
[30]	39.8% (13-19.5 GHz)	-48^o – 35^o	14 (3)	Stub (Microstrip)	Composite unit cell		
[31]	52.9% (12.5-21.5 GHz)	-56^o – 75^o	15 (3)				
[58]	16.9% (27-32 GHz)	4^o – 20^o	16.6 (3)	ME dipole (SIW)	MMR-based unit cell		
[83]	28.6% (30-40 GHz)	-43^o – 28^o	15.1 (2.6)				
[237]	24% (22-28 GHz)	-44^o – 40^o	12.5 (2.8)	Patch (Microstrip)	SMR-based unit cell		Yes
[143]	4.5% (30.4-31.8 GHz)	18^o – 60^o	12.1 (9)	Slot (SIW)			
OCSLR-based LWA	32% (21-29 GHz)	-40^o – 20^o	18 (3)	Stub (Microstrip)	MMR-based unit cell	Yes	

CHAPTER 8 FILTER BANK-ENABLED LEAKY-WAVE ANTENNA ARRAY TECHNIQUE FOR RADAR APPLICATIONS IN STITCHED FREQUENCY-SPACE DOMAIN

In this chapter, an array technique of LWAs on the basis of a FB concept is proposed and studied for prospective radar applications characterized in stitched frequency-space domain. First of all, the frequency-modulated continuous-wave system architecture is selected as a representative to exemplify the characteristics of an LWA-enabled radar with emphasis on the unsolved coupling dilemma between range and angle resolutions, upon which an unprecedented solution called "frequency-space stitching" using an array of FB-enabled LWA channels is introduced for refining the range resolution while maintaining a predefined angle resolution. With the radar equation, the conditions for the FB-enabled "frequency-space stitching" are analytically derived and equivalently converted into design specifications for an array of LWAs, i.e., engineered or synthesized beam-scanning functions, beam-crossovers, and phase alignments. Moreover, to facilitate a practical implementation of such LWA array technique, a detailed design flow is developed in a generalized manner. Finally, for a simple proof-of-concept, a FB-enabled two-channel microstrip combline LWA array is modeled, fabricated, and measured. Simulated and measured results are in a reasonable agreement and both demonstrate the stitched spectral and spatial behaviors, i.e., enhanced spectrum bandwidth and widened radiation beamwidth. The proposed FB-enabled LWA array technique may be potentially deployed in radars, as a complementary solution to the current phased array counterpart.

8.1 Introduction

Fundamental requirements for a high-performance modern radar system are its capabilities to detect multiple targets over a large FoV and estimate their range, angle, and other parametric information with good resolution and accuracy. This requires the radar system operates with wideband modulated signal waveforms such as linear frequency-modulated pulse (LFM) or FMCW, and simultaneously its antenna front-end should provide a wideband and narrow/directive beam (i.e., this narrow/directive beam is kept fixed over the wideband spectrum of the signal waveform) that can be scanned to sample the whole targeted space, i.e., wideband spatial

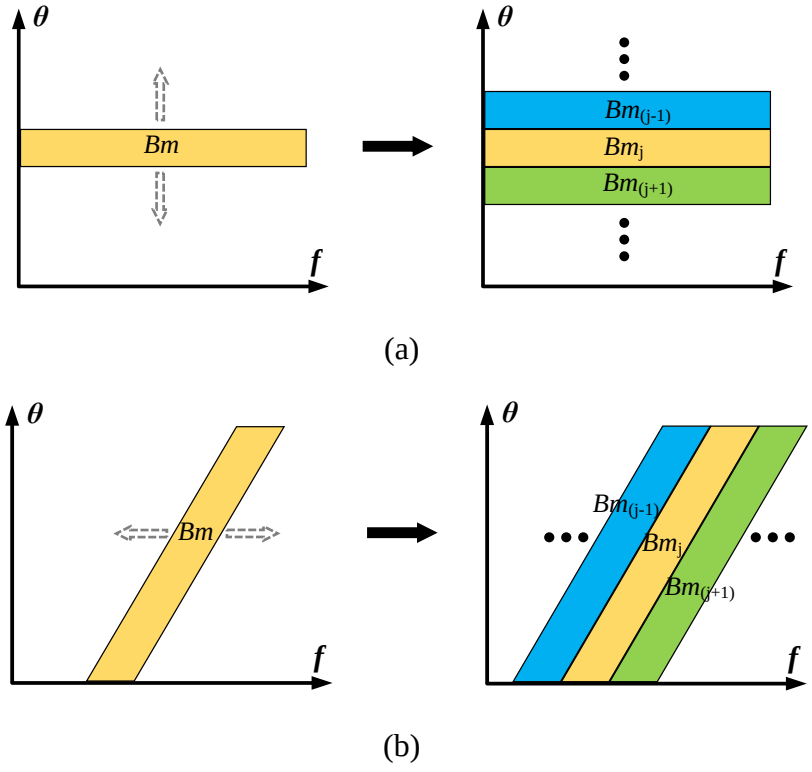

Figure 8.1 Simplified characterization of radar operations with respect to different coverage plans in frequency-space domain [1][2][269]

(a) Traditional mechanical or electrical beam-scanning using wideband fixed-beams. (b) LWA-enabled beam-scanning using frequency-scanning features. The left of (a) corresponds to the frequency-space domain coverage of a single beam (or "Bm" in abbreviation) towards a specific spatial angle, while the left of (b) represents the counterpart of a single LWA channel

sampling [1][2][269]. This process can simply be described using a frequency-space domain coverage of radar operations, as conceptually illustrated in Figure 8.1(a). Generally speaking, there are essentially three mainstream solutions that are used to conduct such required wideband spatial sampling (or beam-scanning), and perhaps the most representative one is the mechanical beam-scanning where a wideband fixed-beam antenna (e.g., parabolic reflector antenna) is exploited to produce a narrow beam that is mechanically scanned with the aid of electro-motors and rotors [1]. Another popular method is the multi-beam scheme (or called "beam-switching"), where a group of wideband directive beams pointing toward different predetermined angles may be realized by reflector-/lens-based antennas with a cluster of feeders [270]-[273], or by an array of antennas

together with beamforming circuits [274]-[276]. Comparatively, the phased array technique using a set of phase shifters or more often true-time-delay devices proves to be the most flexible approach to produce a wideband scanned narrow beam among the three schemes [277].

While those wideband, directive and fixed-beam antennas required by modern radar systems normally work in a standing-wave mechanism, e.g., slotted waveguides/SIWs [213][278][279] and series-fed microstrip patches/stubs [212][214][280], the LWA is a shining member of the class of travelling-wave antennas, and it has been well-known for its numerous appealing features such as the directive and narrow beam and particularly the natural frequency-enabled beam-scanning property [9][11]. Thanks to such properties, LWAs may provide a low-cost, low-complexity, and simple beam-scanning solution along with a good angle resolution [as shown in the left of Figure 8.1(b)], and several other benefits compared to those preceding mainstream schemes [1][2]. For example, compared to the mechanical beam-scanning, the frequency-enabled beam-scanning is apparently much faster in scanning the space and without inertial devices needed; compared to the multi-beam solution, it no longer suffers from cumbersome arrangement of illumination sources or complicated beamforming circuits; compared to the phased array techniques, expensive and lossy phase shifters/time delay devices together with extra controlling circuits can be left out. However, these benefits as just mentioned are only related to the keyword of "beam-scanning", and we should bear in mind that the "wideband" property should also be simultaneously considered when the beam is scanned for the sake of detecting multiple targets with a good range resolution over a certain FoV [1][2]. Although it is the unique frequency-enabled beam-scanning that brings such desirable benefits to LWA-based radars, it would undesirably degrade certain radar performances such as the reduced available spectrum bandwidth along with deteriorated range resolution in each spatial angle cell (strictly speaking, it brings a coupling-related dilemma between the range and angle resolutions, and more details will be particularly revealed later). Unfortunately, this dilemma, to the best of the authors' knowledge, remains to be considered and tackled in the technical community. This fact may partly explain the phenomenon why there are just a few works regarding LWA-based radar demonstrations [192]-195] that have been reported so far in our RF/microwave communities, even though a large variety of LWAs based on multifarious TLs, radiating discontinuities, and radiation mechanisms have been invented and studied since the 1940s [9][11].

On the other hand, the inherent frequency-based beam-scanning owned by LWAs may be more useful and present greater potentials in the terahertz (THz) band [199]-[202] compared to the

microwave/millimeter-wave band [192]-[195]. One of reasons for this is that there are tremendous spectrum resources available in the THz band, and thus the absolute spectrum bandwidth allocated for each spatial angle cell in an LWA-enabled radar is abundant enough to realize an adequate range resolution for most real-world scenarios. By comparison, this issue would be more intractable and serious in a lower frequency band, as a result of which it is of more stringency and practical significance to solve it for possible applications in current microwave/millimeter-wave developments. To this end, an array scheme of LWAs based on a FB concept [282] is proposed in this chapter as a potential solution for LWA-enabled radar systems with improved range resolution while maintaining a good predefined angle resolution. This resorts to properly stitching the frequency-space domain of an array of LWA channels as conceptually illustrated in Figure 8.1(b). To obtain an extended and gapless frequency-space domain coverage for radar operations, those front-end FB-based LWA channels have to observe several design specifications or called "stitching conditions" with respect to their beam-scanning functions (BSFs), beam-crossovers, and phase alignments. These stitching conditions are analytically derived with the aid of the radar equation [1][2] and numerically verified from the Rx and Tx perspectives of an antenna. Furthermore, a generalized design flow is specially developed to facilitate the design of a practical FB-enabled LWA array. This is followed by an implementation example of a two-channel FB-based microstrip combline LWA array for demonstration purposes. Notably, such two LWA channels are combined in the RF analog domain in this work just for a simple and convenient proof-of-concept about such stitched frequency-space domain phenomenon, while they would be connected to separate Rx channels for a practical use. As can be deduced from Figure 8.1, the uniqueness and contribution of the proposed FB-enabled LWA array technique are manifested by the fact that its relevant radars would put the angle resolution rather other the range resolution into the first priority for consideration. In this regard, this feature is artfully contrary to the prevailing phased array scheme [277], and thus may be applied to some scenarios that need a good angle resolution while moderate range resolution.

8.2 Background Review, Problem Analysis, and Proposed Solution

Considering the simplicity and popularity of CW radars compared to pulse radars in civil/commercial applications [1][283], the dilemma regarding the coupling between the range and angle resolutions suffered by an LWA-enabled radar will be explicitly analyzed in this chapter

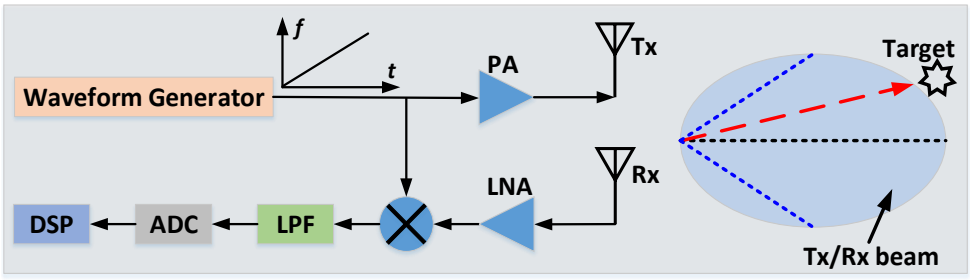

(a)

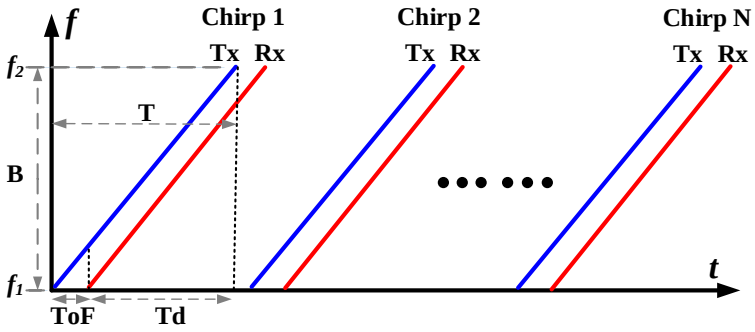

(b)

Figure 8.2 (a) Simplified block diagram of an FMCW radar with only a single Tx-Rx chain presented [283]. (b) Frequency-time diagram of a typical fast chirp-sequence waveform with *N* chirps involved in a single frame (or CPI)

using an FMCW radar system architecture as an example, before which we will first briefly review the principle of operation of a typical FMCW radar using wideband fixed-beam Tx and Rx antennas. This is then followed by the proposed solution, i.e., FB-enabled LWA array technique.

8.2.1 Principle of Operation of Typical FMCW Radar

Figure 8.2(a) shows the simplified block diagram of a typical FMCW radar system. Although in practice, such as automotive radars [284], multiple Tx-Rx chains are normally deployed to provide good angle estimation/resolution capabilities together with improved detection performances [1], only a single Tx-Rx chain is presented here for illustration convenience. Figure 8.2(b) depicts a popular FMCW waveform—fast chirp sequence, with respect to its frequency-time diagram of the transmitted and received signals within a coherent processing interval (CPI) [1]. When the FMCW radar is under operation, a frame of wideband chirp signals generated by the waveform generator are emitted into the free space by the Tx antenna, and then are reflected back from targets and

captured by the Rx antenna. The received signal, which is considered as a time-delayed and attenuated duplicate of the transmitted signal, will mix with a fraction of the transmitted signal to produce an intermediate frequency (IF) signal. After passing a low-pass filter and analog-to-digital converter, the IF signal will be processed in the DSP module, usually using the 2-D Fast Fourier Transform (FFT) algorithm (also called Range-Doppler FFT), to estimate and resolve the range and velocity parameters of multiple targets [1]. In general, consider that both the Tx and Rx antennas operate with a fixed-beam over the whole spectrum bandwidth of the chirp signal as mentioned previously. This means that toward any spatial directions within their beam-coverages, all the frequency components of the chirp signal would be radiated out and then captured by the radar as shown in Figure 8.2(b), without serious magnitude/phase distortion in principle. The relevant frequency-space coverage of the radar with such a single Tx-Rx chain is illustrated in the left of Figure 8.1(a). The range resolution of the radar, according to [1][283], can be expressed as

$$\Delta R = \frac{c}{2B}\frac{T}{T_d} \simeq \frac{c}{2B} \tag{8.1}$$

where c represents the light speed in the free space while B is the nominal spectrum bandwidth of the chirp signal. T denotes the sweeping time of the chirp, while Td stands for the measurable time-duration of the IF signal. The approximation in (8.1) is always made considering that the round-trip time-of-flight (ToF) of the signal, in general, is extremely smaller than the sweeping time T of the chirp signal. In this sense, nearly the whole spectrum bandwidth of the chirp signal can be dedicated to the range resolution. Namely, it is the signal's spectrum bandwidth that determines the range resolution of the radar. On the other hand, multiple Rx antennas each equipped with a channel are normally deployed to estimate and resolve the angle information of targets. The angle resolution $\Delta\theta$ is defined as and equal to the 3-dB beamwidth $\Delta\theta_{3dB}$ of the whole Rx antenna array. As for the velocity resolution, it is mainly determined by the CPI and the carrier frequency f_c of the chirp signal waveform. It is irrelevant to both the available spectrum bandwidth of the received signal and the number of Rx channels, and thus will not be involved in the following sections.

8.2.2 Characteristics of LWA-Enabled FMCW Radar

Although the range resolution of a conventional FMCW radar can easily be refined by simply increasing the spectrum bandwidth of the signal waveform according to (8.1), the radar has to be equipped with multiple Rx antenna elements or channels for achieving a good angle resolution.

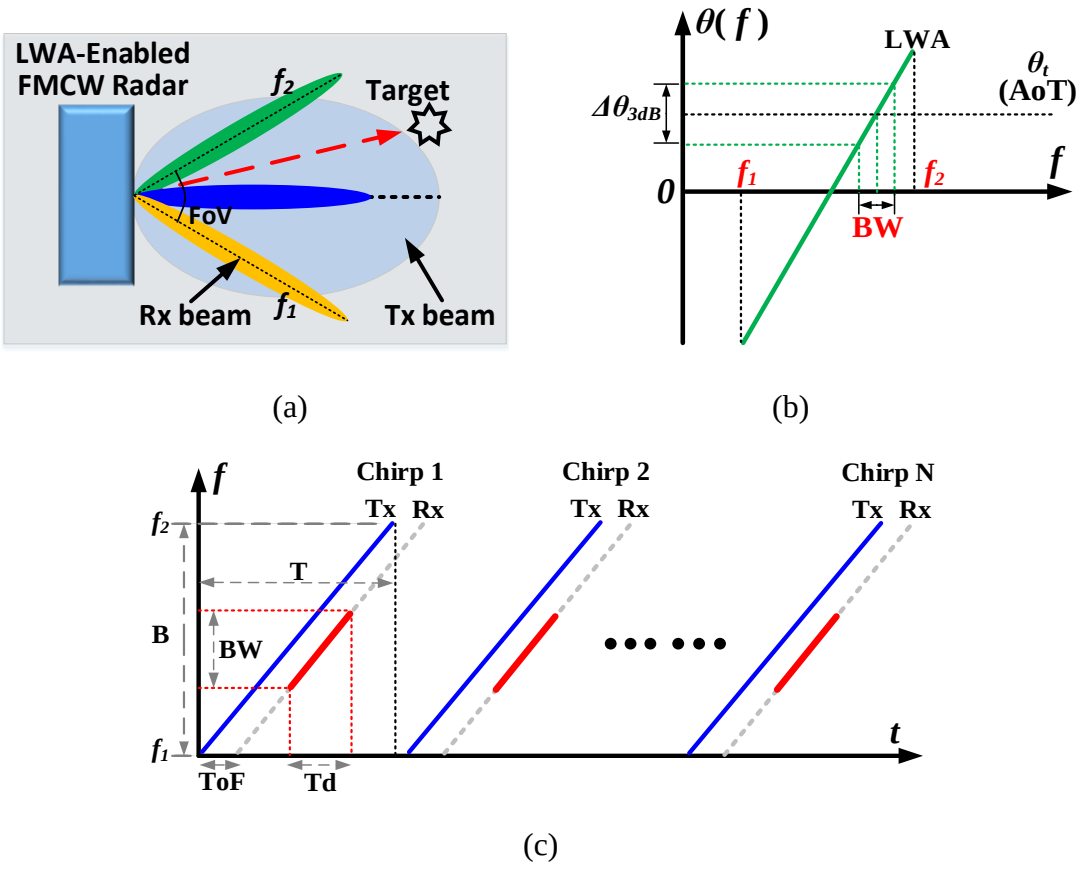

Figure 8.3 (a) Simplified beam-coverage illustration of an LWA-enabled FMCW radar using an LWA as its Rx antenna. (b) BSF of the Rx LWA. (c) Frequency-time diagram of the transmitted and received chirp signals

The better the angle resolution is needed, the more Rx channels should be configured for the radar. This is especially the case when the "point cloud" data are needed for high-quality imaging in automotive radars aimed for autonomous driving [285]. It is apparent that this would bring several main concerns such as high cost, large system layout, heavy data volume/computation burden, complicated DSP algorithm, cumbersome channel calibration and maintenance, and severe power consumption. Consequently, only a few Rx channels are deployed for most practical uses, e.g., 3Tx-4Rx with 12 virtual Rx channels in Texas Instrument (TI) product series of automotive radar sensors such as AWR1243, AWR1443, and AWR1843 [284], where a good range resolution relying the wideband FMCW signal waveform is given the first priority to guarantee reasonable radar performances while the angle resolution only plays a secondary role.

LWAs can also be exploited for radar applications [192]-[195][199]-[202]. Evolved from Figure 8.2(a), Figure 8.3(a) illustrates the beam-coverage scenario of a revised FMCW radar in which the Rx antenna is replaced by an LWA, i.e., LWA-enabled FMCW radar. Within the working frequency band ranged from f_1 to f_2 (i.e., the bandwidth of the chirp waveform $B = f_2 - f_1$), the Tx beam is presumptively kept fixed, while the Rx beam is scanned from backward to forward as displayed in Figure 8.3(b). In this sense, the Rx LWA only can receive signals when the target is "seen" by the Rx beam or when the Rx beam dwells on the target. Therefore, the frequency contents of the received signals are dependent on the spatial angles of targets, which enable LWA to present a spatially dependent band-pass behavior [179]. Here, we assume that the Rx LWA has a linear BSF with a slope of S_m, i.e., $\theta_m(f) = S_m \cdot f + b_m$, and a constant 3-dB beamwidth $\Delta\theta_{3dB}$ that does not change with frequency. For a certain direction where the target is located, i.e., angle-of-target (AoT), the spectrum bandwidth of the received chirp signal, BW, is

$$BW = \frac{\Delta\theta_{3dB}}{S_m} \tag{8.2}$$

which is obviously narrower than the spectrum bandwidth of the transmitted chirp signal since most of its frequency contents cannot be captured by the Rx LWA, as illustrated in Figure 8.3(c) exhibiting the frequency-time diagram of the transmitted and received signals. Consequently, the time-duration (*Td*) of the IF signal is seriously shortened and thus the frequency resolution after performing the Range-FFT is deteriorated [1]. The original range resolution formulated in (8.1), therefore, should be modified as

$$\Delta R = \frac{c}{2BW} \tag{8.3}$$

which is significantly deteriorated. Considering that the angle resolution $\Delta\theta$ of the related radar is equal to the 3-dB beamwidth $\Delta\theta_{3dB}$ of the LWA, we can get

$$\Delta R \cdot \Delta\theta = \frac{c}{2} S_m \tag{8.4}$$

after substituting (8.2) into (8.3). Obviously, from equation (8.4) we can find that for an LWA-enabled FMCW radar, its range and angle resolutions are coupled and contradictory for a given beam-scanning rate of LWAs. This is easily understandable since both the two resolution-metrics are set to rely on the 3-dB beamwidth of the Rx LWA but have reverse trends.

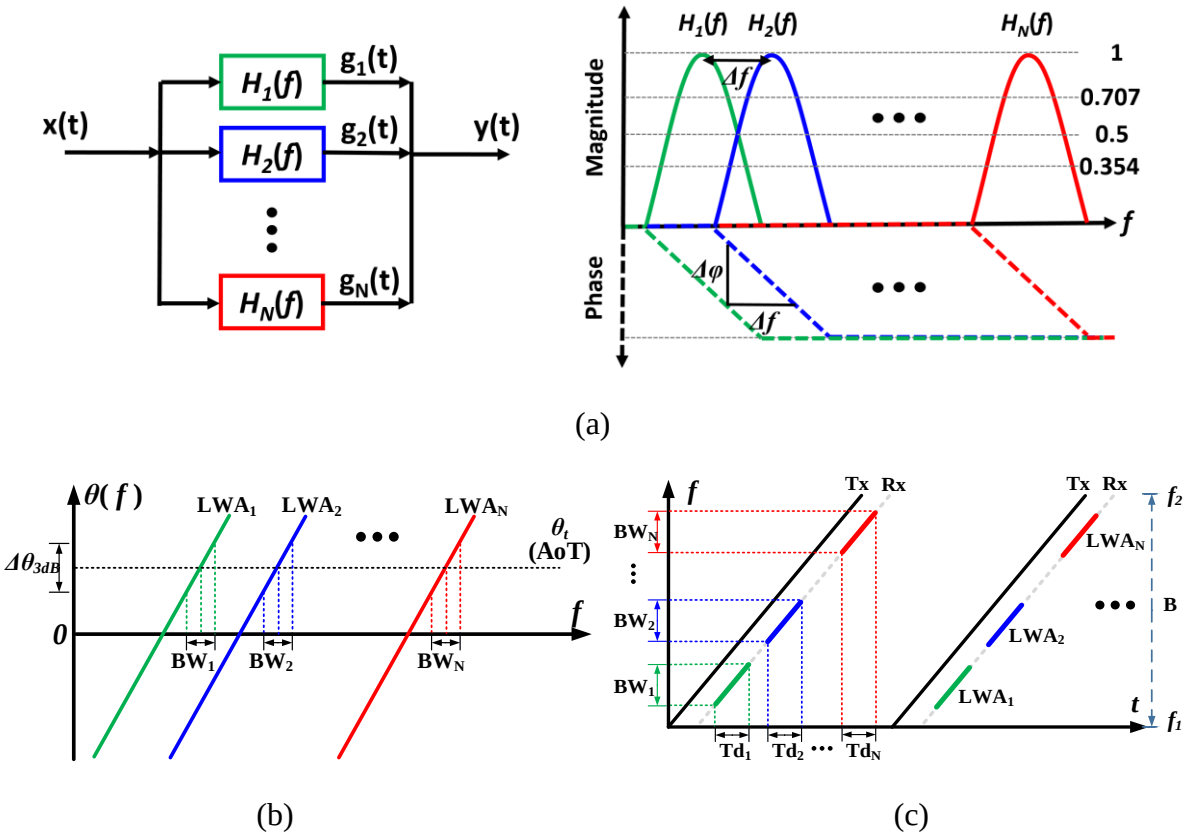

Figure 8.4 Simplified illustration of an FB [37] and its associated LWA array technique for radar operations

(a) An FB with respect to its typical sub-band decomposition-summation process (left), and the ideal transfer function of each band-pass filter (right). (b) An array of FB-based LWAs with interleaved BSFs. (c) Frequency-time diagram of the transmitted and received chirp signals using an array of FB-based LWA channels

8.2.3 Frequency-Space Domain Stitching Using Filter Bank Concept—A Potential Solution

Although the LWA-enabled FMCW radar can be exploited to provide a low-cost and low-complexity beam-scanning solution with only a single Tx-Rx chain needed in principle [192]-[195][199]-[202], the price it has to pay is the suffered range resolution due to the fact that the nominal spectrum of the signal waveform (e.g., chirp signal) has to be shared by both the beam-scanning and range resolution. This issue would be further deteriorated when a better angle resolution is needed according to (8.4). Therefore, performance trade-off between the attainable

range and angle resolutions normally needs to be considered for practical uses [192]-[195][199]-[202]. Recall that an LWA behaves as a spatially dependent band-pass filter that has different spectrum passbands toward different AoTs as mentioned previously. Thus, for a given AoT, if two or more Rx LWA channels with elegantly interleaved filtering responses could be used simultaneously and their individual received spectrums could be coherently stitched in the backend module, a wider spectrum bandwidth than that a single LWA can capture may be received for signal processing. For the related radar with such a multi-channel LWA array scheme, its frequency-space domain coverage is illustrated in Figure 8.1(b). In this regard, the range resolution could be significantly improved according to (8.3), while the angle resolution would remain the same as the situation of a single LWA channel. Specifically, all of these LWA channels would corporately contribute to the range resolution, while each of them may be used for the angle resolution similar to [192]-[195][199]-[202]. The better the range resolution is needed by the system, the more LWA channels should be configured. The angle resolution, herein, is given a higher priority to be realized than the range resolution. Interestingly, this is complementary to the traditional phased array-related FMCW radar shown in Figure 8.2 (a) where each Rx channel provides the range resolution while all those channels work together for the angle resolution [1][2][283]. The proposed design scheme originates from the FB concept [282] as illustrated in Figure 8.4(a), where its typical sub-band decomposition-summation process and the transfer function of each band-pass filter are presented. Here, a bank of frequency-interleaved band-pass filters can be practically realized by an array of LWAs with different BSFs, as simply illustrated in Figure 8.4(b). In a practical scenario, the wideband spectrum of a reflected chirp signal is first decomposed into several sub-bands by those LWA channels. Subsequently, these sub-band signals are summed for the range resolution, while each is used for the angle resolution as mentioned. The relevant frequency-time diagram of the transmitted and received signals is conceptually plotted in Figure 8.4(c). To obtain a gapless and stitched frequency-space coverage for the related radar as illustrated in Figure 8.1(b), the transfer function of each band-pass filter or LWA channel should be deliberately organized to make sure that the summed transfer function would present a widened and relatively flat frequency response toward any spatial angles within the FoV. This requirement can be translated to several stitching conditions or design specifications for an array of LWAs, i.e., engineered BSFs, beam-crossovers, and phase alignments, as will be elaborately derived later.

8.3 Technicality of FB-Enabled LWA Array for Frequency-Space Stitching

For a single Tx-Rx chain of the FMCW radar that uses an LWA as the Rx antenna while a fixed-beam antenna as the Tx antenna, the received power spectrum, according to the radar equation [1], can be expressed as

$$P_r(\theta, f) \simeq \frac{P_t(\theta, f)G_t(\theta, f)G_r(\theta, f)\sigma\lambda_c^{\,2}}{(4\pi)^3 R^4} \tag{8.5}$$

where P_r is the received power from the Rx antenna while P_t is the transmitted power to the Tx antenna. G_t and G_r are the power gains of the Tx and Rx antennas, respectively. All of these parameters are a function of both frequency f and spatial angle θ (only one plane is considered here, corresponding to the scanning plane of the Rx LWA or the azimuth plane of the radar). R refers to the distance between the target and the radar, σ represents the radar cross section (RCS) of the target, while λ_c denotes the free-space wavelength of the chirp signal's carrier frequency f_c. For the convenience of analysis yet without loss of generality, the transmitted power P_t is assumed to be a constant over frequencies, e.g., 1 watt. This is reasonable since the chirp waveform has a nearly uniform power spectrum [1]. Considering that the Tx antenna is assumed with a fixed-beam over the frequency band of operation, the power gain G_t is set to be unity for simplicity (it may be different for other directions but still remain a constant over frequencies). As for the Rx LWA that has a fixed 3-dB beamwidth of $\Delta\theta_{3dB}$ and linear BSF of $\theta_m(f) = S_m \cdot f + b_m$ as assumed above, its absolute power gain radiation pattern is modeled by a normalized Gaussian function [1], i.e., Gaussian LWA, which is expressed as

$$G_r(\theta, f) = \mathrm{e}^{\left\{\frac{-2\ln 4[\theta-\theta_m(f)]^2}{\Delta\theta^2_{3dB}}\right\}} \tag{8.6}$$

Obviously, it can be deduced from (8.6) that for a certain spatial angle, the power gain frequency response of the Rx LWA is also related to a Gaussian profile. In this connection, the received power spectrum of the radar towards this angle is approximately with a Gaussian profile as well thanks to its linear relationship with the power gain of the Rx LWA when the above-mentioned assumptions are all considered. Recall that the physical significance of an antenna's transfer function is actually manifested by or equivalent to its voltage gain/field pattern [16][269]. Thus, we may simply consider

$$\left|H_r(\theta, f)\right| = \sqrt{G_r(\theta, f)} \tag{8.7}$$

where $H_r(\theta, f)$ represents the transfer function of the Rx LWA. The received voltage magnitude spectrum can be then expressed as

$$\begin{aligned}\left|U_r(\theta, f)\right| &= \sqrt{2\,\mathrm{Re}(Z_o)P_r(\theta, f)} \\ &= g \cdot \left|H_r(\theta, f)\right|\end{aligned} \tag{8.8}$$

where Z_o is the load impedance of the Rx antenna while $g = \sqrt{2\,\mathrm{Re}(Z_o)\sigma\lambda_c^2 / \left[(4\pi)^3 R^4\right]}$ is a constant.

When considering the FB concept illustrated in Figure 8.4(a) and employing an array of N LWA channels to receive signals simultaneously, the total magnitude spectrum of the resultant voltage signal from these Rx LWA channels can be derived as

$$\begin{aligned}\left|U_{rt}(\theta, f)\right| &= \left|\sum_{j=1}^{N} U_{rj}(\theta, f)\right| \\ &= \sum_{j=1}^{N} \left|U_{rj}(\theta, f)\right| \\ &= g \cdot \sum_{j=1}^{N} \left|H_{rj}(\theta, f)\right|\end{aligned} \tag{8.9}$$

where $U_{rt}(\theta, f)$ represents the spectrum of the combined voltage signal; $U_{rj}(\theta, f)$ and $H_{rj}(\theta, f)$ denote the output voltage spectrum and transfer function of the j^{th} LWA, respectively. Note that all of these LWAs (or band-pass filters) here are assumed to have the same group delay (or slope of linear phase frequency responses of transfer functions) in their passbands, which is normally the case for a FB [282]. In this context, the individual output spectrums of these LWA channels could be added coherently as already involved in (8.9) if the phase difference $\Delta\varphi$ between adjacent LWAs in the overlap frequency region [as shown in the right of Figure 8.4(a)] has been compensated (if not specified, it is always assumed that this phase alignment or compensation process has been automatically conducted before combining the output spectrums of those LWAs, and this will be specially discussed later). As a consequence, we may conclude that according to (8.9) and Figure 8.4(a), one key point to obtain an enhanced spectrum bandwidth of the total received signal at a

certain AoT is to make the individual transfer function of each LWA overlap at a proper frequency point. This can be translated to special design specifications of these LWAs, considering the fact the transfer function of an LWA at a certain angle is determined by its BSF according to (8.6) and (8.7). In order to derive such design specifications of LWAs, we consider an array of two adjacent LWA channels having interleaved BSFs expressed as $\theta_{mj}(f) = S_m \cdot f + b_{mj}$ and $\theta_{m(j+1)}(f) = S_m \cdot f + b_{m(j+1)}$, respectively. As deduced from (8.6) and (8.7), the transfer function of a Gaussian LWA, at a given angle, is also with a Gaussian profile that only pertains to frequency, with the 3-, 6-, and 9-dB spectrum bandwidth of $\Delta\theta_{3dB}/S_m$, $\Delta\theta_{6dB}/S_m$, and $\Delta\theta_{9dB}/S_m$, where $\Delta\theta_{6dB}$ and $\Delta\theta_{9dB}$ refer to the 6- and 9-dB radiation beamwidth of the LWA, respectively. To obtain a relatively flat-while-wide summed transfer function, their individual counterparts should approximately overlap at the frequency point at which a half of the maximum absolute value is reached as illustrated in Figure 8.4(a). This corresponds to the 6-dB frequency point of each transfer function, indicating that the required frequency offset or distance Δf between the two LWAs' transfer functions is $\Delta\theta_{6dB}/S_m$. This can be translated to a limiting condition of their BSFs, expressed as

$$\begin{aligned} \theta_{mj}(f) - \theta_{m(j+1)}(f) &= b_{mj} - b_{m(j+1)} \\ &= \Delta\theta_{6dB} \\ &= \sqrt{2}\Delta\theta_{3dB} \end{aligned} \tag{8.10.1}$$

where a scaling factor of $\sqrt{2}$ between $\Delta\theta_{3dB}$ and $\Delta\theta_{6dB}$ of the Gaussian LWA is applied (similarly, the scaling factor between $\Delta\theta_{3dB}$ and $\Delta\theta_{9dB}$ is $\sqrt{3}$). From (8.10.1), we can find that at a certain frequency f, the two adjacent LWAs should be separated by an angular spacing of $\Delta\theta_{6dB}$ with respect to their BSFs. This also means that their radiation power gain beams, at a certain frequency, should be overlapped at the 6-dB angular point, i.e., 6-dB beam-crossover. Equation (8.10.1) can thus be called "*magnitude stitching condition*". On the other hand, recall that these design specifications related to (8.10.1) such as BSFs and beam-crossovers are subject to the condition that all the received spectrums from those LWA channels could be phase-aligned and thus coherently combined. However, this is not case since there is a fixed phase difference $\Delta\varphi$ in the overlapped spectrum between the two adjacent LWAs, which can be expressed as

$$\Delta\varphi \approx 2\pi \cdot \Delta f \cdot GD$$

$$= 2\pi \cdot \frac{\Delta\theta_{6dB}}{S_m} \cdot GD \tag{8.10.2}$$

according to the linear phase frequency responses of an FB as illustrated in the right of Figure 8.4(a). Here, *GD* refers to the shared group delay of each band-pass filter in the FB, while Δf is selected as $\Delta\theta_{6dB}/S_m$ in accordance with the 6-dB overlap criterion adopted in (8.10.1). Equation (8.10.2) can be called "*phase stitching condition*", which should be simultaneously satisfied along with the magnitude stitching condition (8.10.1). If so, the frequency-space domain of each channel would be seamlessly stitched, and the individual received spectrum bandwidth from the two Rx LWAs towards a certain angle could be coherently added and expressed as

$$BW_{FB-2} = \frac{\Delta\theta_{3dB} + \Delta\theta_{6dB}}{S_m} \tag{8.11}$$

Analogously, if an array of *N* LWA channels is used simultaneously based on the two stitching conditions in (8.10), the total received spectrum bandwidth can be deduced as

$$\begin{aligned} BW_{FB-N} &= \frac{\Delta\theta_{3dB} + (N-1)\Delta\theta_{6dB}}{S_m} \\ &\simeq N\frac{\Delta\theta_{6dB}}{S_m} \\ &= \sqrt{2}N\frac{\Delta\theta_{3dB}}{S_m}\text{ , N>1} \end{aligned} \tag{8.12}$$

As a result, the relation of the range and angle resolutions formulated in equation (8.4) should be revised as

$$\Delta R \cdot \Delta\theta = \frac{c}{2\sqrt{2}N} S_m \tag{8.13}$$

Clearly, for an FMCW radar configured with an array of *N* Rx LWA channels sharing a certain 3-dB beamwidth (angle resolution) and beam-scanning rate, the attainable spectrum bandwidth and range resolution could be improved by a factor of $\sqrt{2}N$ if the FB-related stitching conditions (8.10) are adopted to construct an expanded and stitched frequency-space domain as Figure 8.1(b) for radar operations. Alternatively, for a certain range resolution, a refined angle resolution (narrowed 3-dB beamwidth) can be realized at the expense of more LWA channels deployed.

To demonstrate the effectiveness of the proposed solution for stitching the frequency-space domain and thus enhancing the received spectrum bandwidth, one, two, and three LWA channels among a N-channel ($N \geq 3$) LWA array are used to calculate the total received power spectrum toward different AoTs, respectively. All of these LWAs are modeled with the same beam-scanning rates of 5°/GHz and a Gaussian radiation pattern with the 3- and 6-dB beamwidths of 8.5° and 12°, respectively. The carrier frequency f_c is assumed to be 35 GHz, which is also the broadside frequency of the reference LWA numbered as LWA_i. Note that the LWA_i is the central LWA among the N-channel LWA array and the subscript i is an integer constant that is most close to (N+1)/2. Based on these parameters provided above and the stitching conditions in (8.10), the BSFs of the selected three LWAs can be expressed as

$$\begin{cases} \theta_{m(i-1)}(f) = 5(f-35)+12 = 5f-163 \\ \theta_{mi}(f) = 5(f-35) = 5f-175 \\ \theta_{m(i+1)}(f) = 5(f-35)-12 = 5f-187 \end{cases} \tag{8.14}$$

The numbering and arrangement of these LWAs is consistent with Figure 8.4(b). The normalized received power spectrums when using one, two, and three Rx LWAs, can thus be calculated according to (8.6)-(8.9) and (8.14), as plotted in Figure 8.5. It can be seen obviously that in the case of a single LWA, the received power spectrum shown in Figure 8.5(a) exhibits a Gaussian profile that relies on the AoT thanks to the natural spatially dependent filtering characteristics of LWAs. Comparatively, when using two or three LWAs following the proposed stitching conditions in (8.10), spectral and spatial stitching processes can be accomplished as shown in Figure 8.5(b) and (c), with presenting an expanded coverage area of the frequency-space domain that resembles Figure 8.1(b). This is because, for any AoTs, the received frequency components from these LWA

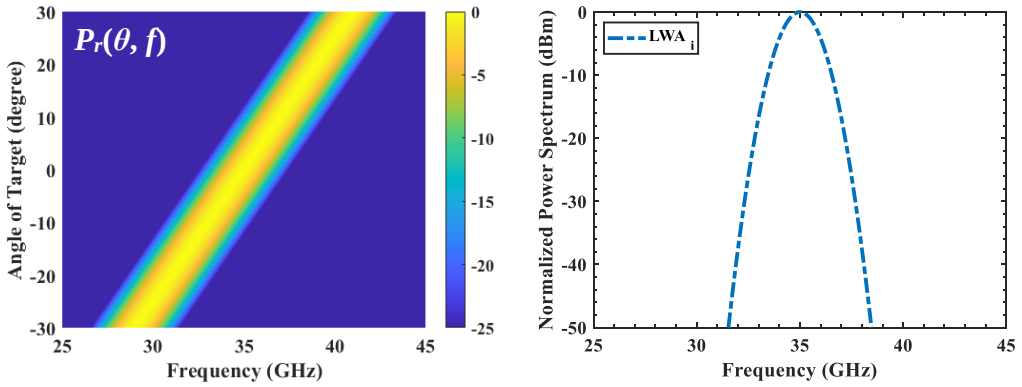

(a)

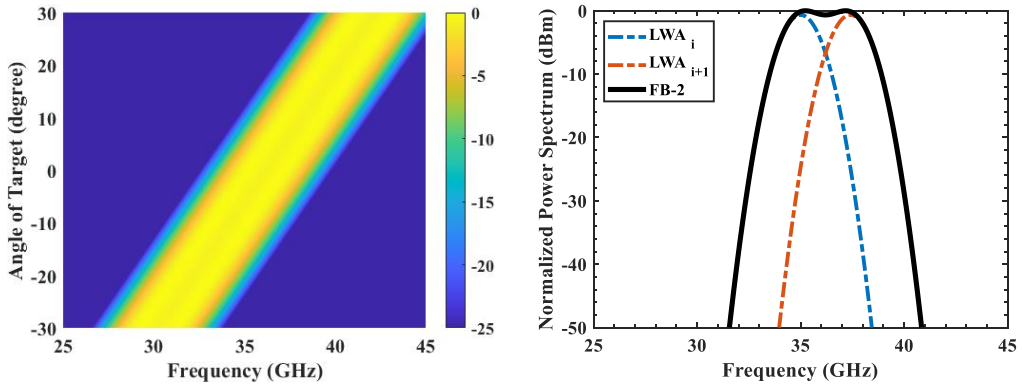

(b)

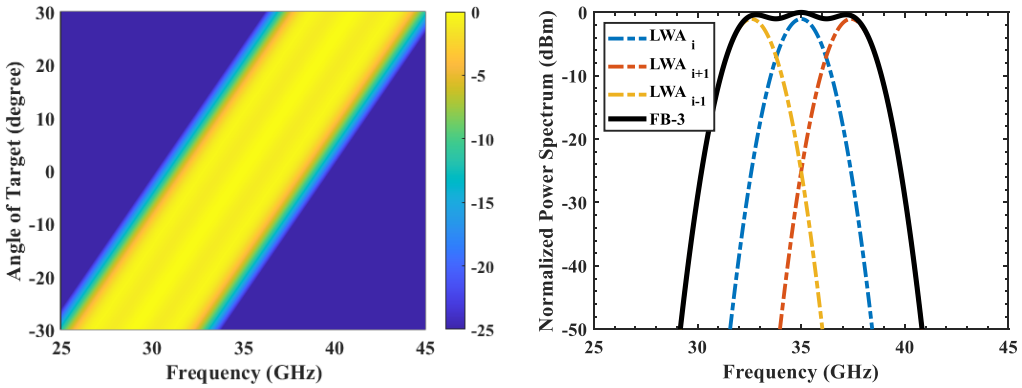

(c)

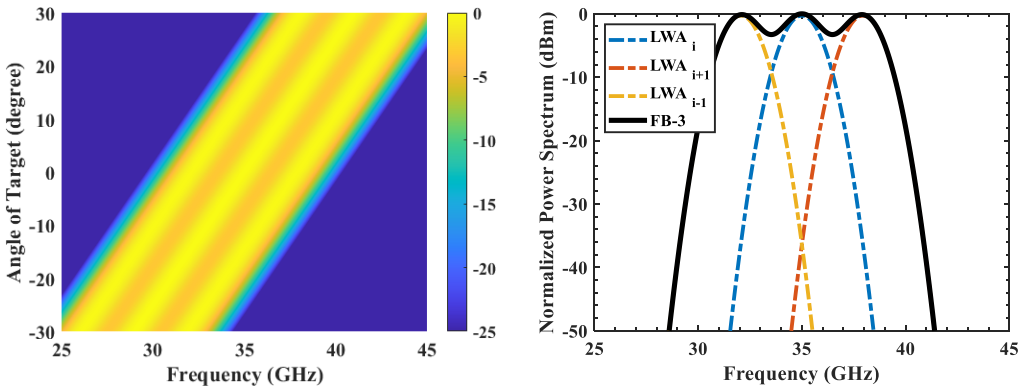

(d)

Figure 8.5 Normalized received power spectrum with respect to different number of LWA channels based on the proposed FB concept

(a) A single LWA channel; (b) FB-based two LWA channels (i.e., "FB-2") under 6-dB overlap criterion; (c) FB-based three LWA channels (i.e., "FB-3") under 6-dB overlap criterion; (d) FB-based three LWA channels under 9-dB overlap criterion. The left of each subfigure represents the received power spectrum with respect to different AoTs in the manner of heat-map, while the right is related to the special situation that the target is in the broadside direction (i.e., AoT=0)

channels would add constructively and complementarily, thereby giving rise to a widened spectrum compared to the situation of a single LWA. However, it is necessary to mention that the FB-related 6-dB criterion adopted in (8.10) are especially dedicated to obtaining a widened spectrum that particularly behaves with a relatively flat and smooth manner in the middle passband. Actually, it is not the optimum condition for a maximum achievable bandwidth. Considering that the "3-dB bandwidth" is often used as a criterion in practice to define the useful spectrum bandwidth, the summed transfer function of the FB is not necessary to behave very flat whereas suitable pits or ripples in the middle of the passband can be tolerated. That is to say, the frequency distance Δf between adjacent transfer functions shown in Figure 8.4(a) can be properly extended but not merely limited to the 6-dB criterion. For example, the overlap frequency point between two adjacent transfer functions can be relaxed to 0.354, corresponding to 9-dB stitching conditions on the analogy of (8.10). In this case, the summed transfer function or combined received spectrum would have pits or ripples that are approximately 3-dB lower than the peak, thereby maximizing the achievable frequency-space coverage and spectrum bandwidth in principle as illustrated in Figure 8.5(d). In this respect, those equations (8.10) - (8.13) should be revised accordingly using 9-dB related parameters, which are not given here for brevity. Nevertheless, it should be noted that the 6-dB associated criterion will be used by default in this chapter unless otherwise stated.

On the other hand, bear in mind that an antenna is a reciprocal component with respect to its Tx and Rx functionalities [16]. Examining the received power spectrum from those LWA channels for demonstrating the frequency-space stitching phenomenon in radar operations, as we have just conducted above, actually corresponds to the characterization of an antenna's Rx functionality. Nevertheless, the desirable frequency-space stitching illustrated in Figure 8.1(b) can also be observed from the Tx functionality of the FB-based LWA array thanks to the reciprocal theorem; this is equivalent to the examination of the resultant radiation pattern of the whole array. Specifically, at a certain frequency f, radiated signals from all those LWA channels will superpose in the free-space. Considering the fact that the received power spectrum from an Rx antenna is linearly proportional to its power gain as mentioned previously, it is expected that examining the FB-based LWA array from the perspective of the radiation (i.e. Tx functionality) would also present the desirable frequency-space stitching phenomenon similar to Figure 8.5. This is unsurprisingly and clearly illustrated in Figure 8.6, which depicts the normalized radiation patterns with respect to the FB-based LWA array consisting of different number of LWA channels that

follow the 6- or 9-dB stitching conditions. Those synthesized radiation patterns shown in Figure 8.6(b)-(d) can be directly calculated using the Friis transmission theorem [16], which are not expanded here for brevity. Notably, it is this widened synthesized beam that results in a prolonged beam dwell time and thus enhanced received spectrum bandwidth for a target. Although the two perspectives of characterization (i.e., Rx and Tx functionalities of the FB-enabled LWA array), from the enhanced received spectrum bandwidth at given AoTs as shown in Figure 8.5 to the synthesized widened radiation beamwidth at given frequencies as shown in Figure 8.6, are all valid

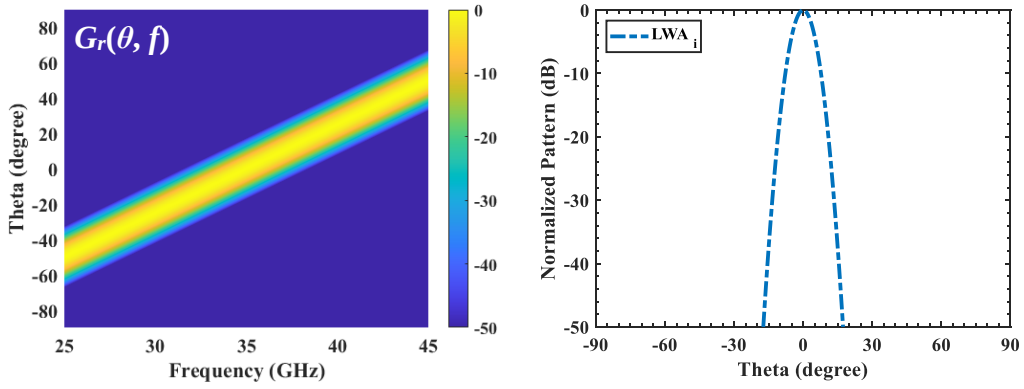

(a)

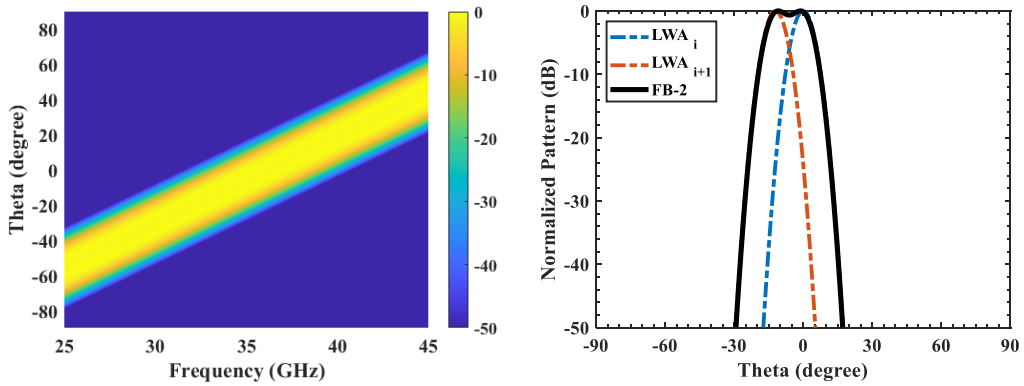

(b)

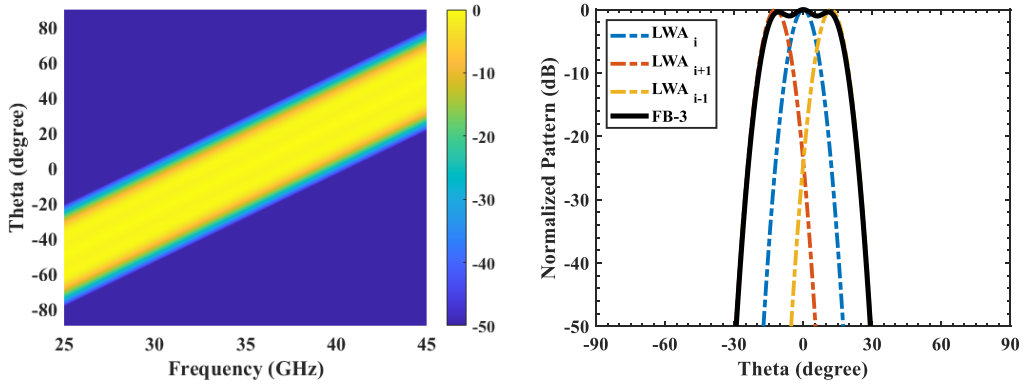

(c)

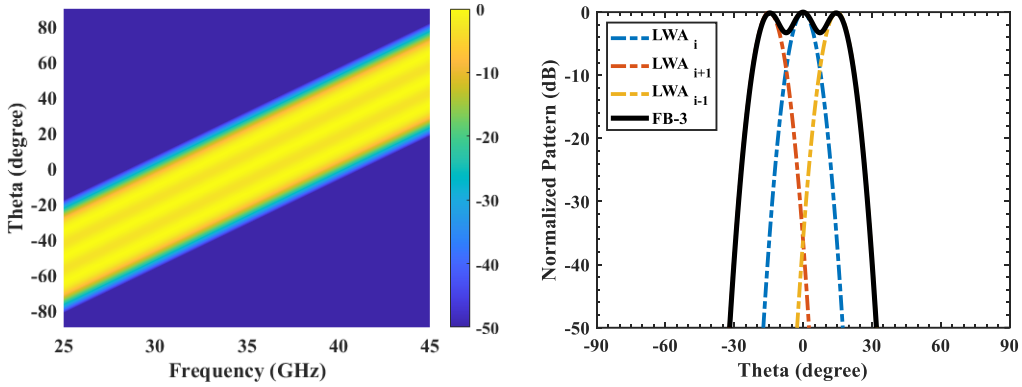

(d)

Figure 8.6 Normalized radiation patterns with respect to different number of LWAs based on the proposed FB concept

(a) A single LWA channel; (b) FB-based two LWA channels under 6-dB overlap criterion; (c) FB-based three LWA channels under 6-dB overlap criterion; (d) FB-based three LWA channels under 9-dB overlap criterion. While the left of each subfigure displays the normalized radiation pattern with respect to different frequencies in the manner of heat-map, the right is related to the case at the carrier frequency of 35 GHz

and mutually equivalent for demonstrating the frequency-space stitching effects exhibited in Figure 8.1(b), the latter is preferable and more convenient to serve as a touchstone to facilitate a practical implementation of the FB-enabled LWA array and a direct proof-of-concept, as will be shown later.

8.4 Implementation, Simulation, and Experimentation of Practical FB-Enabled LWA Array—A Direct Proof of Concept

So far, the stitching conditions for the enlarged frequency-space coverage of an LWA-driven FMCW radar as conceptually illustrated in Figure 8.1(b) has been derived. Its effectiveness has been separately examined from the perspectives of the received power spectrum and radiation power pattern of the FB-based LWA front-end, where an array of LWAs with ideal radiation performances such as linear BSF, fixed beamwidth, and constant gain were assumed. In this section, we will demonstrate how to implement a practical FB-based LWA array and then provide a direct proof of concept.

8.4.1 Generalized Design Flow for an FB-Enabled LWA Array

According to the leaky-wave theory [9][11], an LWA can be regarded as a special guiding-while-radiating lossy TL, where its radiation properties as an antenna can be easily predicted by its guided-wave characteristics as a lossy TL, i.e., the attenuation and phase constants. For a periodic LWA using the -1st-order space-harmonic to radiate, its main-beam direction (or BSF) θ_m and 3-dB beamwidth $\Delta\theta_{3dB}$ can be expressed as

$$\theta_m(f) \simeq \sin^{-1}\left(\frac{\beta_0 - \frac{2\pi}{P}}{k_0}\right),\ \Delta\theta_{3dB} \simeq \frac{0.91}{(QP/\lambda_0)\cos(\theta_m)} \tag{8.15}$$

where k_0 and λ_0 are the free-space wavenumber and wavelength, while P and Q denote the period length and quantity of unit cells, respectively. β_0 refers to the phase constant of the periodic LWA's fundamental space-harmonic, which also approximates the original phase constant of the unperturbed host TL [9][11]. For a TEM or quasi-TEM TL (e.g., microstrip line) that is used for constructing a periodic LWA, the BSF in (8.15) can be revised as

$$\theta_m(f) \simeq \sin^{-1}\left(\sqrt{\varepsilon_{eff}} - \frac{c}{P}\frac{1}{f}\right) \tag{8.16}$$

where ε_{eff} is the effective relative permittivity of the host TL. From (8.16) we can conclude that to approximately obtain an array of N LWAs with engineered BSFs and beam-crossovers that are required by the magnitude stitching condition in (8.10.1), an advisable and feasible approach is to employ a group of periodic LWAs with slightly different periods. Here, to provide an efficient design guideline and particularly, to determine the period difference of those LWA channels, we firstly designate an LWA as the reference, which is numbered as LWA_i possessing a broadside frequency of f_{bi}, period length of P_i, and unit-cell quantity of Q_i. Similar to that in Chapter 8.3, the referenced LWAi is the central one among the N-channel LWA array and the subscript i is a known integer constant that most closes to (N+1)/2. Note that at the broadside frequency fbi, the period P_i is equal to a guided-wavelength of LWA_i and the equation (8.16) is equal to zero, based on which P_i can be calculated from f_{bi} and ε_{eff}. Then, we assume our FoV of interest is close to the broadside direction. Consequently, in the vicinity of the broadside frequency f_{bi}, we may expand LWA_i's BSF at f_{bi} using Taylor Series. Keeping the first two items and neglecting higher-order ones, the BSF of

LWA_i can be approximately expressed as

$$\theta_{mi}(f) \simeq \frac{P_i \varepsilon_{eff}}{c} f - \sqrt{\varepsilon_{eff}} \tag{8.17}$$

Consider that the period difference of those LWAs is generally small and so do their broadside frequencies for the sake of obtaining well-arranged BSFs and beam-crossovers. Thus, we may approximately use the referenced LWA_i's BSF $\theta_{mi}(f)$, in terms of its various-order Taylor coefficients at f_{bi}, to expand its adjacent LWA's BSFs $\theta_{mj}(f)$ at their individual broadside frequencies f_{bj}. Here, j is a dummy variable that represents the numbering of those LWAs adjacent to the referenced LWA_i. In this case, equation (8.17) can be revised to give a generalized BSF suitable for all of these LWA channels including LWA_i, expressed as

$$\theta_{mj}(f) \simeq \frac{P_i \varepsilon_{eff}}{c} f - \frac{P_i}{P_j}\sqrt{\varepsilon_{eff}} \tag{8.18}$$

where P_j denotes the period length of the j^{th} LWA, i.e., LWA_j. When combing (8.10.1) and (8.18) together under the 6-dB design criterion, we can get

$$\begin{cases} P_j = \dfrac{\sqrt{\varepsilon_{eff}}}{(j-i)\sqrt{2}\Delta\theta_{3dB} + \sqrt{\varepsilon_{eff}}} P_i, \quad j = i, i+1, i+2, \cdots\cdots \\ \text{or} \\ P_j = \dfrac{\sqrt{\varepsilon_{eff}}}{\sqrt{\varepsilon_{eff}} - (i-j)\sqrt{2}\Delta\theta_{3dB}} P_i, \quad j = i-1, i-2, \cdots\cdots \end{cases} \tag{8.19}$$

where $\Delta\theta_{3dB}$ specifically refers to the 3-dB beamwidth of the reference LWA_i at the broadside frequency f_{bi}. Note that (8.19) only approximately works to determine the initial period values of those LWAs adjacent to the reference LWA_i, and a fine-tune process may be performed subsequently. The specific design flow of a generalized FB-enabled LWA array is summarized as:

1). Specify a reference periodic LWA with a certain broadside frequency f_{bi} (e.g., carrier frequency f_c of the chirp waveform in an FMCW radar) and 3-dB beamwidth $\Delta\theta_{3dB}$ (i.e., angle resolution $\Delta\theta$ required by an FMCW radar). In this sense, both the period length P_i and the quantity of unit cells Q_i of this reference LWA can be approximately determined from (8.15) and (8.16).

Once this reference LWA is confirmed, its beam-scanning rate S_m and group delay GD are also determined.

2). Based on the range resolution required by the radar, the quantity of LWA channels N for implementing an FB can be estimated, according to (8.13) and the beam-scanning rate of that reference LWA. Then, the period length of those adjacent LWAs around the reference LWA can be roughly calculated according to (8.19) as an initial value, while the quantities of their unit cells, at this stage, can be selected approximately to that of the reference LWA.

3). Fine-tuning processes with respect to the period length and quantity of unit cells of those neighbouring LWAs are necessary to ensure that all of these FB-related LWAs can approximately possess the designated beam-crossover and equivalent gain at the design frequency f_c to coincide with (8.10.1). This is followed by the phase alignment procedure where the initial phase difference, according to (8.10.2), can be approximately calculated by the considering the group delay and beam-scanning rate of that reference LWA as well as the designated beam-crossover condition (e.g., 6-dB criterion).

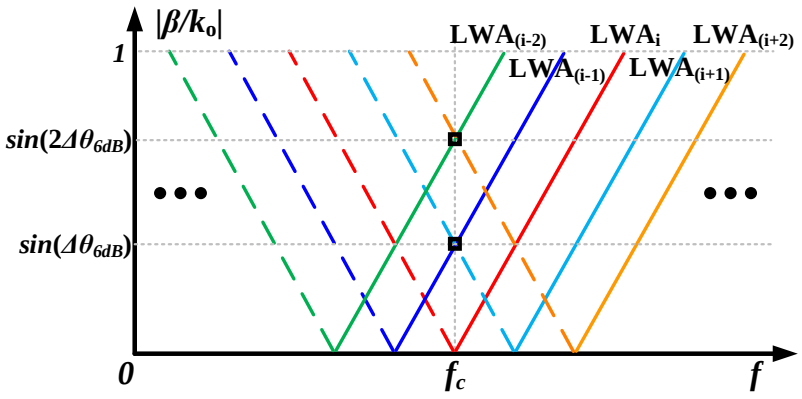

Figure 8.7 Normalized phase constant of FB-enabled LWA array

$\Delta\theta_{6dB}$ refers to 6-dB beamwidth of the referenced LWA_i at the broadside frequency f_c (i.e., f_{bi}). Dashed and solid lines represent backward and forward beam-scanning regions, respectively

Normally, for a periodic LWA, a single unit cell can be used to conveniently and accurately extract its phase constant with the aid of the Bloch-Floquet theorem [26][43]. This is an advisable step that should be conducted since we further need to use its associated dispersion diagram as a graphical

tool to facilitate the open-stopband suppression process (e.g., use some matching techniques such as delay line and quarter-wavelength transformer [15]) so that these FB-based periodic LWAs can support a continuous beam-scanning or receive signals through the broadside direction. More importantly, we can use those extracted phase constants, as conceptually illustrated in Figure 8.7, to conveniently fine-tune and determine the period lengths of those adjacent LWAs (around the reference LWA) as required by the preceding three-step design flow. For example, for the referenced LWA_{i} with a broadside frequency of $f_{bi} = f_c$ and 6-dB beamwidth of $\Delta\theta_{6dB}$, the normalized phase constants of its two most adjacent bilateral LWAs, namely $LWA_{(\mathrm{i}-1)}$ and $LWA_{(\mathrm{i}+1)}$, should pass the point of $[f_c, \sin(\Delta\theta_{6dB})]$, as shown in Figure 8.7. The remaining adjacent LWAs may be deduced by analogy with respect to their normalized phase constants.

8.4.2 Practical FB-Enabled LWA Array Using Stub-Loaded-Resonator-Based Microstrip Combline LWAs

In order to verify the proposed FB-enabled LWA array technique for the desirable frequency-space stitching behavior, we will first use the design flow formulated above to implement a practical FB-based LWA array. Consider that the proposed FB-based concept illustrated in Figure 8.4 needs that all the transfer functions of band-pass filters (or LWAs) should have equivalent bandwidths and maximum magnitudes. This can be technically translated to the fact that the candidate LWA should embrace stable radiation performances such as gain and beamwidth with frequency. Interestingly, recall that a class of multimode-resonator-related periodic LWAs proposed in our previous works [83][84] can tactfully satisfy such strict requirements about radiation behaviors imposed by the FB concept. As a result, the stub-loaded-resonator (SLR)-based microstrip combline LWA proposed in [84] is exploited here for demonstration purposes. Figure 8.8 exhibits its relevant unit cell and FB-based LWA array.

For a simple and convenient proof-of-concept without loss of generality, only two SLR-based LWAs, numbered as LWA_{i} and $LWA_{(\mathrm{i}+1)}$, are considered here. The design frequency is selected as 35 GHz, at which the first LWA (the referenced LWA_{i}) would realize the broadside radiation. The substrate adopted here is Rogers RO3035 with thickness of 0.508 mm, relative permittivity of 3.6, and loss tangent of 0.0015. The period length P_i of this referenced LWA_{i} can be determined as mentioned previously. Complete unit cell dimensions are P_i=5.16 mm, W_{mi}=0.9 mm, W_{si}=0.4mm, L_{1i}=0.6 mm, L_{2i}=1.2 mm, L_{3i}=0.3 mm, L_{di}=0.259 mm, L_{qi}=1.185 mm, and W_{qi}=0.422 mm. Notably,

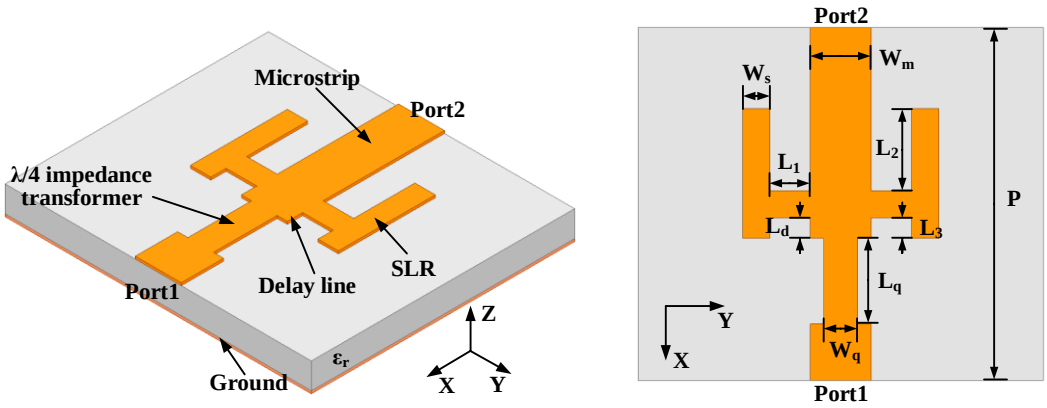

(a)

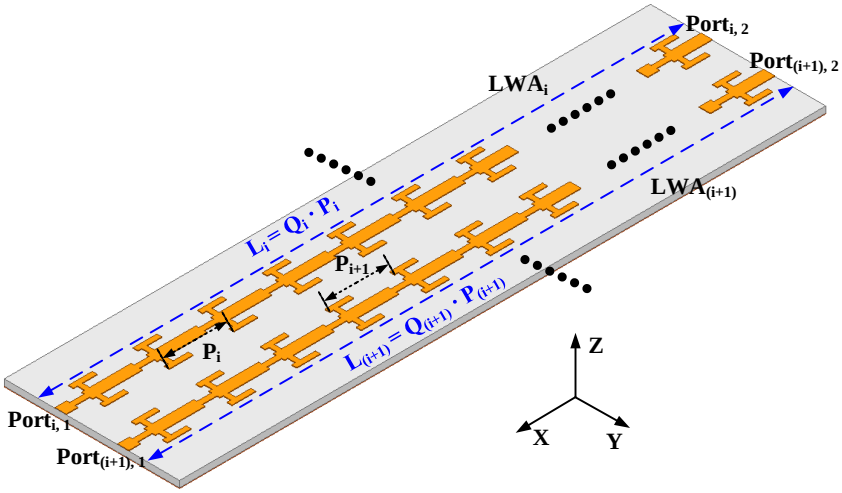

(b)

Figure 8.8 SLR-based microstrip combline LWA [84] with respect to its (a) unit cell (left: 3-D view, and right: top view), and (b) FB-enabled LWA array

instead of specifying the 3-dB beamwidth and then calculating the quantity of unit cells according to the design flow described above, we directly choose the quantity of unit cells of the LWA_i for convenience, as a result of which its 3-dB beamwidth could be determined accordingly and then used to calculate the period of $LWA_{(i+1)}$. Here, 10 unit-cells are cascaded to form an effective leaky-wave radiation for the LWA_i while the remaining power is absorbed by a matching-load termination. The simulated $|S_{11}|$ and $|S_{21}|$ of this reference LWA_i can be found in Figure 8.9(a), showing that a good impedance matching without open-stopband together with an effective radiation is realized. The normalized radiation pattern of the LWAi at the design frequency of 35 GHz is plotted in

Figure 8.9(b), with the 3- and 6-dB beamwidths of 8.5° and 12°, respectively. It should be noted that for a conservative design, 6-dB related criterion as mentioned previously is selected here. The period length of the second LWA, i.e., $LWA_{(i+1)}$, can be then calculated using (8.19), which is about 4.41 mm. Subsequently, we can use this result as an initial value to adjust the geometry of $LWA_{(i+1)}$'s unit cell by taking advantage of Figure 8.7, thereby resulting in the desirable beam-crossover and the suppression of open-stopband. After a fine-tuning process, unit cell dimensions of $LWA_{(i+1)}$ are determined as $P_{(i+1)}$ =4.66 mm, $Wm_{(i+1)}$=0.9 mm, $Ws_{(i+1)}$=0.4mm, $L1_{(i+1)}$=0.58 mm, $L2_{(i+1)}$=1.16 mm, $L3_{(i+1)}$=0.28 mm, $Ld_{(i+1)}$=0.082 mm, $Lq_{(i+1)}$=0.934 mm, and $Wq_{(i+1)}$=0.529 mm. 11 unit-cells are cascaded to establish the $LWA_{(i+1)}$ so as to realize an equivalent gain compared to that of LWA_i at the design frequency of 35 GHz. The simulated *S*-parameters and normalized radiation

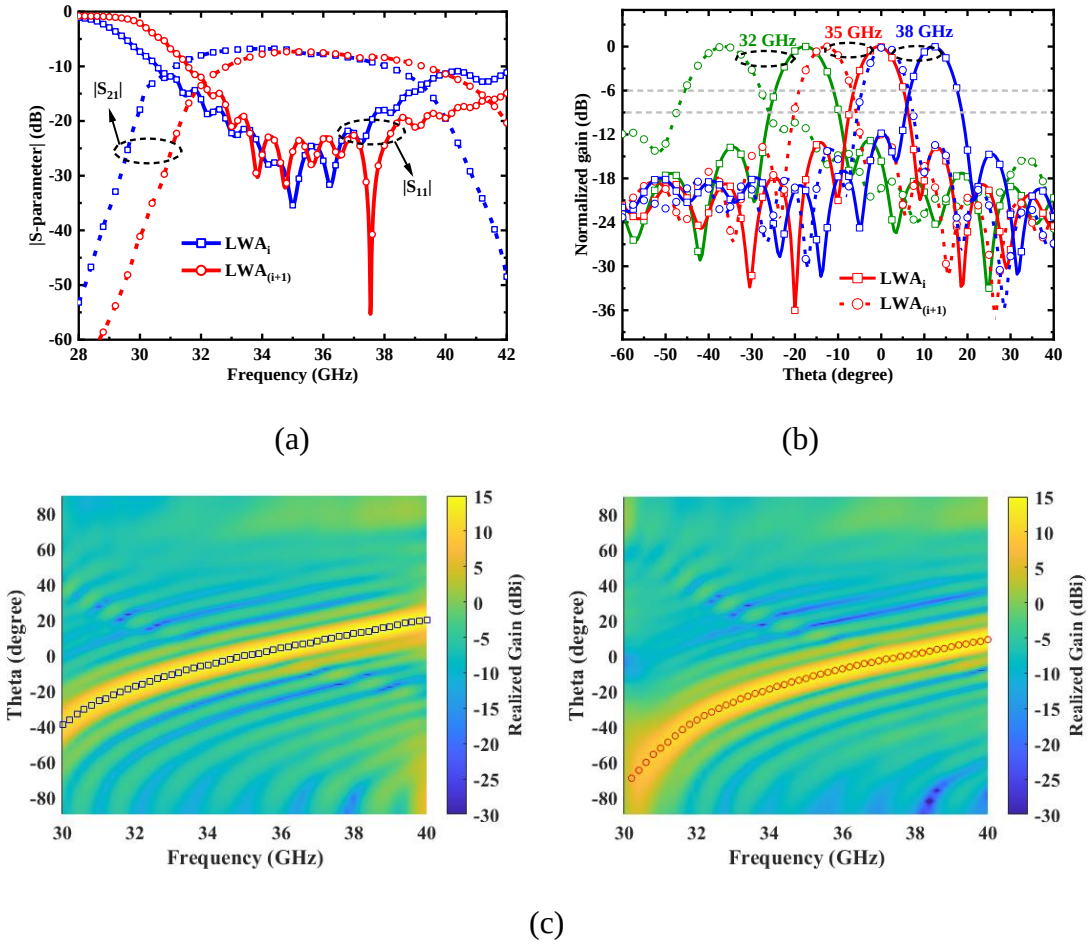

Figure 8.9 Simulated electrical behaviors of two LWAs

(a) *S*-parameters. (b) Normalized radiation patterns. (c) Main-beam directions and 2-D realized gain patterns (left: LWA_i; right: $LWA_{(i+1)}$)

patterns at 35 GHz of the $LWA_{(i+1)}$ are also plotted in Figure 8.9(a) and (b), respectively. Notably, the desirable 6-dB beam-crossover is realized by the two LWAs at the design frequency of 35 GHz. What's more, the beam-crossover of the two LWAs is sandwiched between 6- and 9-dB over the frequency range from 32-38 GHz, as also shown in Figure 8.9(b). This implies that a synthesized widened radiation beam could be realized and scanned with frequency (similar to Figure 8.6), thereby paving the way for obtaining an enhanced spectrum bandwidth towards certain AoTs within the FoV (similar to Figure 8.5). The simulated 2-D realized gain patterns (versus frequency

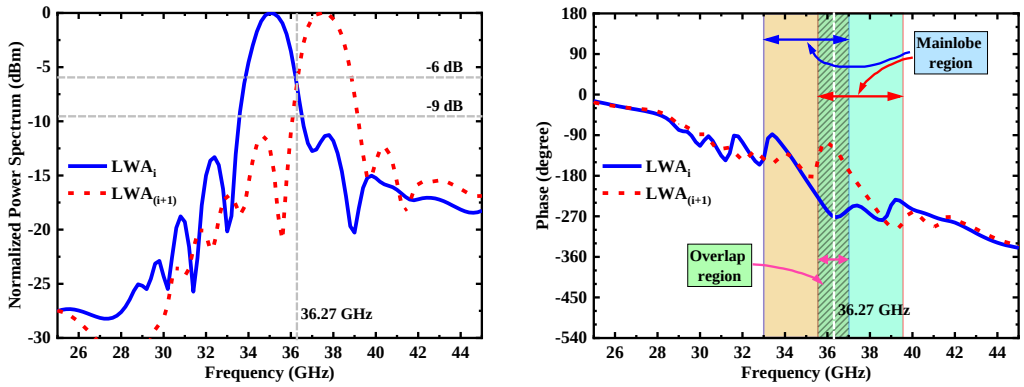

(a)

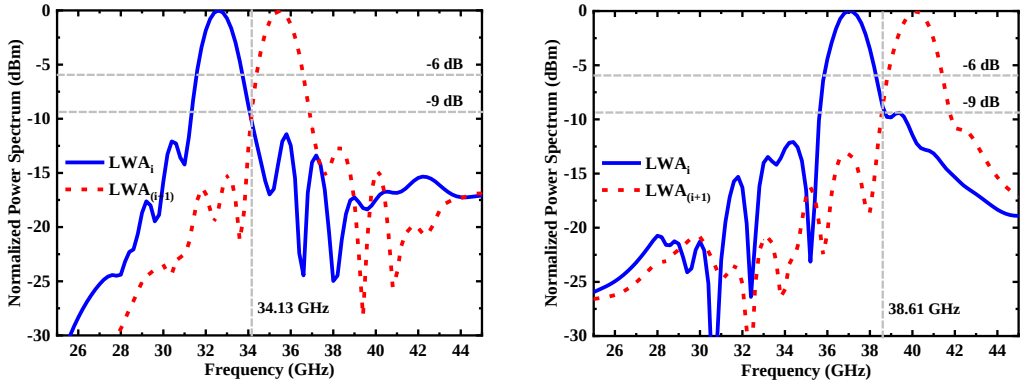

(b) (c)

Figure 8.10 Normalized received power spectrum of the two LWAs with respect to different incidence angles of a wideband uniform plane-wave

(a) 0°; (b) -10°; (c) 10°. Negative/positive angles refer to the backward/forward beam-scanning regions, respectively. In (a), the right subfigure displays the phase spectrum of received signals from the two LWAs at the broadside direction (0°)

and angle) of the two LWAs, together with their BSFs, are plotted in Figure 8.9(c). A beam-scanning rate of about 5°/GHz over the frequency region of 32-40 GHz is obtained for the two LWAs. Figure 8.10 exhibits the normalized received power spectrums of the two LWAs when they are illuminated by a wideband uniform plane-wave with the phase center (or zero-phase point) located at the antenna surface. When the incident angles of the plane-wave change from -10° (backward) to 10° (forward), the center frequency and passband of the received power spectrum shows an increasing trend for each LWA, as expected. More importantly, the two received power spectrums approximately overlap at the designate 6-dB frequency point when the incidence angle is 0°, which is consistent with Figure 8.5(b), thereby manifesting the effectiveness of the developed design flow. Also note that the spectrum crossover is still lower than 9-dB when the incident angles deviate from the broadside direction to ±10°, thereby implying that a widened spectrum with a reasonable pit or ripple could be realized within such a FoV if the two received spectrum could be added coherently. Note that this requires a phase alignment process between the two LWA channels, as described before. As shown in the right subfigure of Figure 8.10(a), the received phase spectrums of the two LWAs within their overlapped main-lobe frequency region (i.e., passband) possess a fixed phase difference of about $\Delta\varphi \approx 160^{\circ}$, which is similar to the situation displayed in Figure 8.4(a). The group delay of two LWAs in their main-lobe passbands is about $GD \approx 0.198$ ns, corresponding to a slope of about 71°/GHz for their phase spectrums. Considering that the reference LWA_i has a beam-scanning rate of about 5°/GHz and 6-dB beamwidth of about 12°, the required phase difference, according to (8.10.2), can be theoretically calculated as 170.4°. Both the simulated and calculated values of the phase difference are in a reasonable agreement. Notably, such a fixed phase spectrum difference between the two adjacent LWA channels can be compensated or calibrated out in either the digital domain by the DSP module or the RF analog domain by simply introducing a delay line on the second LWA (thanks to the relative narrowband property of the overlapped passband spectrum) as will be shown later. In this sense, the two output spectrums from the FB-based LWA array can be coherently superposed, thereby giving rise to a stitched frequency-space domain exhibiting an enhanced received spectrum bandwidth towards given AoTs within the FoV.

8.4.3 Simulation and Experimentation of the Proposed FB-Enabled LWA Array

Bear in mind that our eventual goal is to collect all the received signals from those FB-related LWA

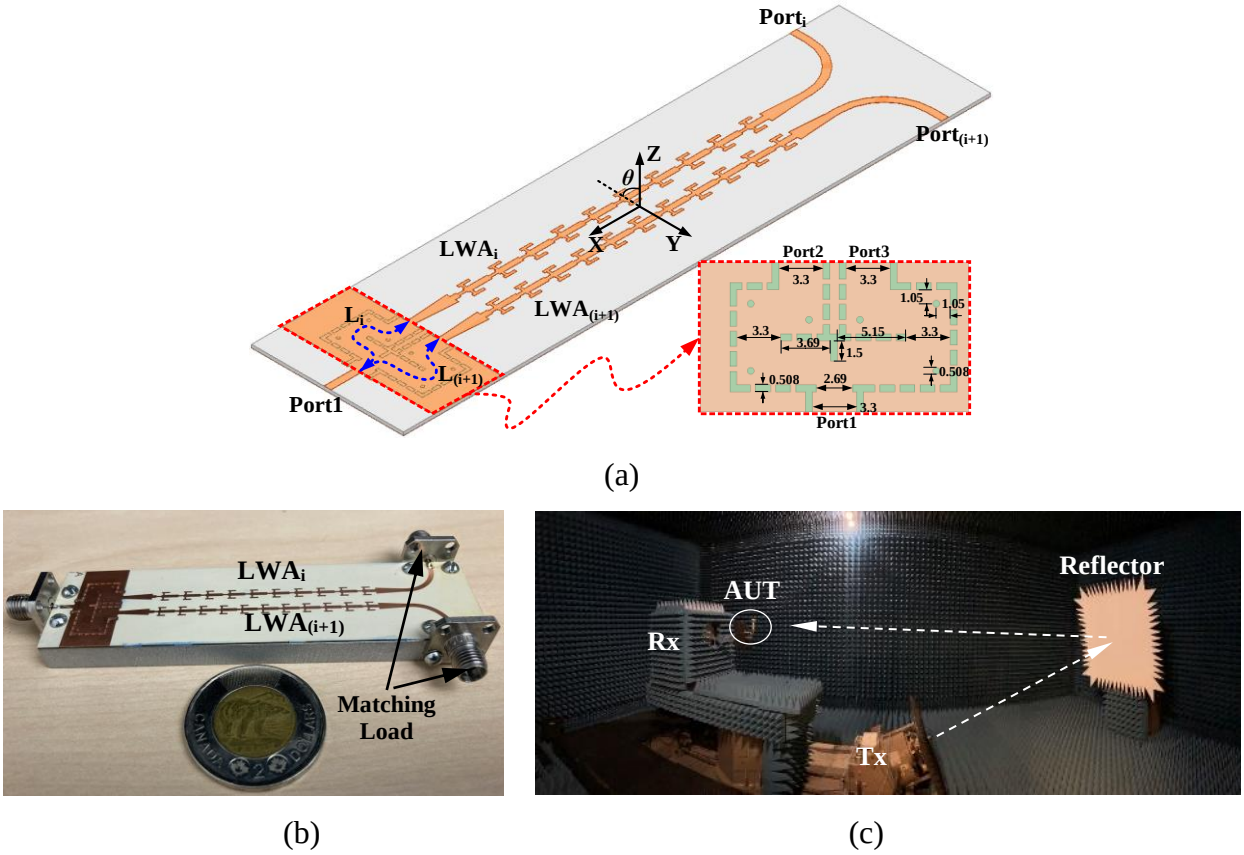

Figure 8.11 Final configuration of the proposed FB-based LWA array consisting of two SLR-based microstrip combline LWAs and a two-way SIW power divider

(a) Simulated model. (b) Fabricated prototype. (c) Measurement setup in Compact Antenna Test Range (CATR). All the parameters in (a) are in millimeters

channels so as to realize a stitched frequency-space domain coverage for radar operations. Consider that the combination process for the received signals from those *N* LWA channels in either the digital or analog domain is equivalent to the radiation pattern synthesis of an *N*-element antenna array in the free-space thanks to the fact that an antenna is reciprocal with respect to its Rx and Tx modes. Consequently, for a convenient demonstration and easy understanding of the FB-enabled LWA array technique, the antenna's Tx mode in the form of free-space signal superposition is still selected here to facilitate design and demonstration. This is just as what we have conducted to design each LWA channel in the last subsection. The proposed two SLR-based microstrip combline LWAs are connected to a two-way SIW power divider as depicted in Figure 8.11(a), and the entity

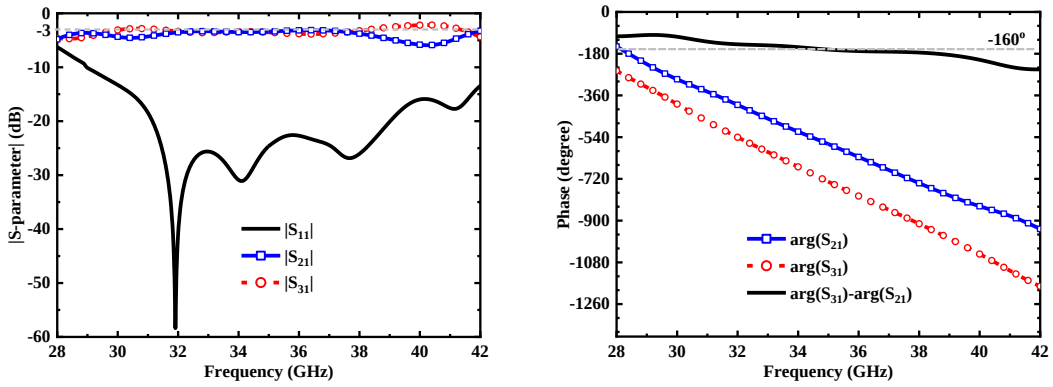

(a) (b)

Figure 8.12 Simulated S-parameters of the proposed two-way SIW power divider

(a) Magnitude. (b) Phase

can be treated as a Tx two-element LWA array. Simulated *S*-parameters in terms of the magnitude and phase frequency responses of the power divider are plotted in Figure 8.12(a) and (b), respectively. It can be seen that the magnitude imbalance is less than 0.5 dB with the frequency range of 32-38 GHz. To compensate the phase difference required by the two LWA channels so that their received spectrums can be coherently stitched as explained above, the power divider's two branches are properly adjusted and optimized with respect to their path lengths [i.e., L_i and $L_{(i+1)}$, as shown in Figure 8.11(a)], where the initial path length difference can be easily determined according to the phase difference depicted in Figure 8.9(a), i.e., $\Delta\varphi \approx 160^o$. Notably, from the perspective of the Tx functionality of an antenna, this phase compensation process between the two LWA channels is significant to ensure that the relative phases of their radiated fields in the free-space are approximately equal in the overlapped main-beam spatial region, thereby enabling their radiated fields to superpose coherently and forming a widened radiation pattern similar to Figure 8.6.

There are three ports in the proposed array, with the common port (Port1) fed with power while the other two, i.e., $Port_i$ and $Port_{(i+1)}$ terminated with matching loads. The simulated $|S_{11}|$ of the array can be found in Figure 8.13(a), with a good impedance matching realized. Simulated radiation patterns at 32 GHz, 35 GHz, and 38 GHz are plotted in Figure 8.13(b), respectively, which obviously shows that stitched and widened radiation patterns (i.e., spatial stitching process) are realized when compared to the results of two individual LWAs shown in Figure 8.9(b). This mainly

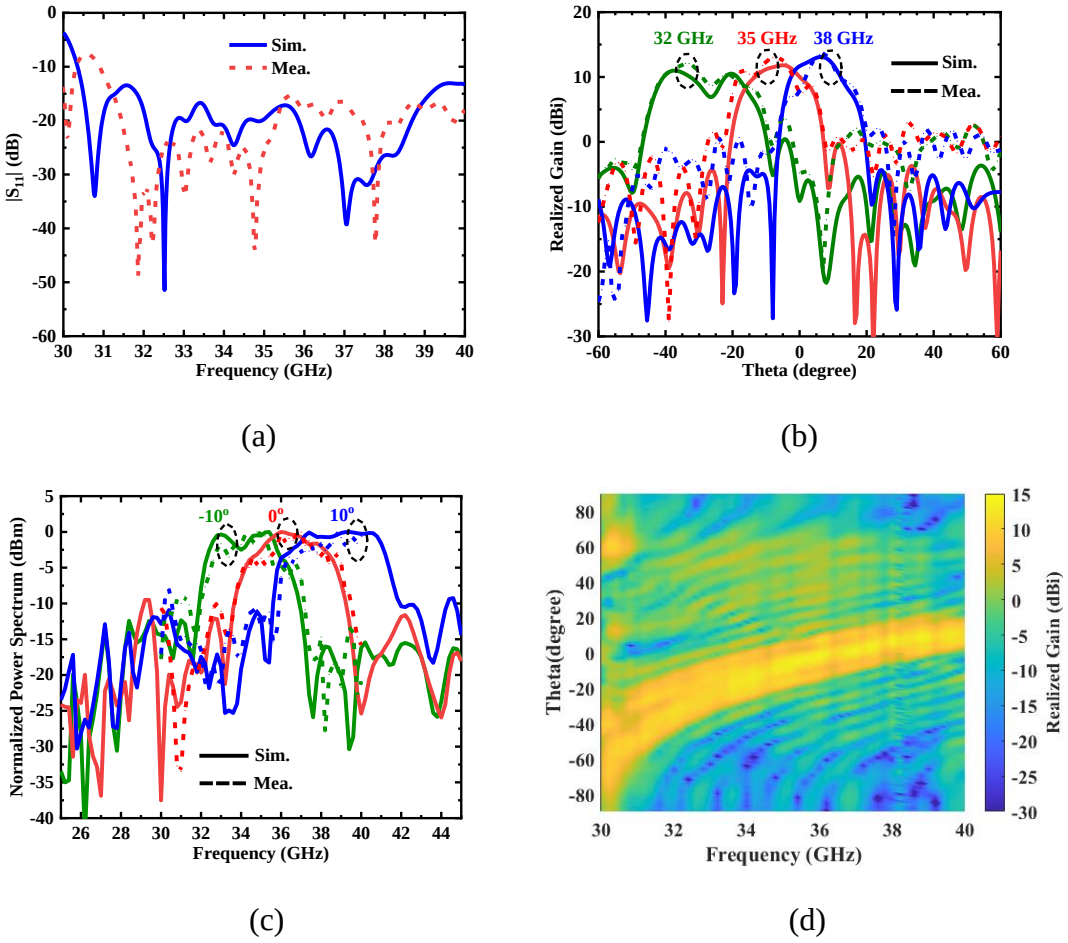

Figure 8.13 Simulated and measured results of the proposed two-element FB-based LWA array (a) $|S_{11}|$. (b) Realized gain pattern at different frequencies. (c) Normalized power spectrum towards different AoTs. (d) Realized gain as a function of both angle and frequency (only measured results). The measured results in (c) are actually the measured realized gain frequency responses

comes from that the beam-crossover between the two LWAs is kept within a reasonable level between the 6- and 9-dB conditions even though their beams are scanned with frequency, and that the required phase alignment process between the two LWAs has been successfully satisfied. Notably, from these we can rationally speculate that the desirable spectral stitching phenomenon and widened output spectrum would be found when the proposed FB-enabled LWA array operates in the Rx mode. To justify this, the proposed array is impinged by a wideband uniform plane-wave from different spatial angles, and simulated results in terms of the received normalized power

spectrums are depicted in Figure 8.13(c). As speculated, the proposed array can receive and output a stitched and approximately double-wide spectrum bandwidth compared to the situations of two individual LWAs shown in Figure 8.10 and similar as the results of Figure 8.5(b). There are two aspects that should be noticed before the experimental demonstration of the proposed design concept. Firstly, consider that the measurement setup of a typical microwave anechoic chamber is always comprised by a Tx-Rx chain, e.g., the Compact Antenna Test Range (CATR) shown in Figure 8.11(c), in which the radiation measurement of an antenna is realized by repeatedly transmitting and receiving a wideband chirp signal against different spatial angles [16]. This is actually what we need for our experimentation. Secondly, note that the total received power spectrum of the FB-based array is linearly proportional to the frequency response of the array's power gain, as described previously in Chapter 8.3. As a consequence, there is an easy and convenient approach to experimentally verify the proposed FB-enabled array technique: just use the configured setup in a microwave anechoic chamber for experimentation and the measured frequency response of the realized gain at a certain angle can be used to represent the practically received power spectrum from the FB-enabled array. The fabricated prototype of the proposed array is shown in Figure 8.11(b). Its measured $|S_{11}|$ and radiation patterns are plotted in Figure 8.13 (a) and (b), respectively. These measured results are in a reasonably good agreement with the simulated counterparts, and both demonstrate the desirable spatial stitching phenomenon. The realized gain frequency responses at several angles, which are used to represent the received power spectrums toward relevant AoTs, are plotted in Figure 8.13(c). Limited to the *Ka*-band measurement setup, only the measured results within 30-40 GHz are recorded and presented. It can be seen that the measured results of realized gain frequency responses reasonably agree with the simulated received power spectrums, thereby justifying the effectiveness of this simplified experimentation as well as the spectral stitching effects. The measured 2-D realized gain pattern of the proposed array is plotted in Figure 8.13(d), exhibiting an obvious expanded frequency-space area when compared to Figure 8.9(c).

8.5 Conclusion

In this chapter, an array technique of LWAs on the basis of the FB concept has been proposed and investigated for potential radar applications. Different from those traditional fixed-beam-antennas-based beam-scanning schemes [as shown in Figure 8.1(a)] including the mechanical beam-

scanning, multi-beam, passive/active phased array, and even full-digital phased array, the proposed scheme makes a combined use of the natural frequency-based beam-scanning inherently owned by LWAs and the FB concept to realize stitched frequency-space domain coverage for radar detections [as shown in Figure 8.1(b)]. Specifically, an array of LWA channels should be deployed, where the FB-related magnitude and phase stitching conditions in the form of the BSFs, beam-crossovers, and phase alignments should be simultaneously satisfied for those LWA channels. A detailed design flow regarding a generalized FB-enabled LWA array has been developed to facilitate a practical implementation, on which a two-channel SLR-based microstrip combline LWA array has been modeled, fabricated, and experimented for a direct proof-of-concept. Simulated and measured results are in a reasonably good agreement and both demonstrate the stitched spectral and spatial behaviors. The proposed LWA array-based scheme compared to the prevailing phased array scheme is distinct: it is the angle resolution rather than the range resolution that is put into the first priority for radar detection. As a consequence, the proposed one may be a potential candidate solution to be deployed in current and future FMCW radars for some scenarios that need a good angle resolution while moderate range resolution.

CHAPTER 9 GENERAL DISCUSSION

As a good candidate for serving beam-scanning scenarios as required by high-performance radar and/or modern communication systems, LWAs have received lots of interests among researchers from all over the world and from the last century to the present, thanks to the fact that their unique frequency-driven beam-scanning enable them to be a potential and low-cost and low-complexity substitute for the costly and complicated phased array antennas. Moreover, they can also be exploited for a wide variety of practical system applications that make use of their frequency-space mapping characteristics as described in Chapter 2.3. The design and development of various kinds of LWAs featuring multifarious functionalities/electrical characteristics and the exploration of possible system-level applications prove to be of critical significance for current and future wireless technologies (e.g., 6G and THz systems) that are demanded to provide ever-increasing high-quality and diversified services to users. To this end, this thesis has proposed several leaky-wave concepts and techniques for developing LWAs with elegant functionalities/electrical behaviors such as low SLL and cross-polarization, stable radiation, rapid beam-scanning, and filtering characteristics. More importantly, this thesis also furnishes a potential frontend antenna array technique enabling LWAs to be used for wideband operation in radar sensing and/or communication systems. It is necessary to note that those proposed design concepts and techniques are in a general manner and they can be effectively translated to lower and higher frequencies depending on application requirements. It is believed that most of readers and antenna designers can benefit more or less from these works.

Specifically, when talking about low SLL and low cross-polarization radiation behaviors, the proposed work in Chapter 3 tactfully combines the benefits of a TE_{20} mode SIW and a meandering long slot LWA. The odd-symmetry of E-fields distribution of the TE_{20} mode SIW is artfully used to design an LWA consisting of two evenly-symmetrical meandering long slots etched on the top surface of the SIW to simultaneously realize both low side-lobe and low cross-polarization. The beauty of symmetry has been vividly exhibited and used. Also note that the TE_{20} mode SIW has several advantages compared to its TE_{10} mode counterpart, such as higher performance stability, higher fabrication tolerance, lower fabrication cost, etc. Following this thread, other higher-order SIWs can also be used to design such long-slot LWAs with such desired radiation behaviors. For

example, we can use TE_{40}, TE_{60}, and TE_{80} to design such LWAs, if a narrower cross-sectional radiation pattern and higher gain are required in addition to low cross-polarization and SLL performances. However, another thing we should note is that in the proposed work in Chapter 3, the phase constant along the slot aperture has not been compensated and it is not kept the same along the slot aperture. This means that radiation from every point of the radiating line-sources is not well-aligned, thereby resulting in a slightly deteriorated radiation pattern and SLL. This slight drawback can be eliminated by a delicate control of the sidewall distance of the SIW along the slot aperture direction. The rapid beam-scanning characteristic is another functionality we want to realize for LWAs. To this end, the loading effects of RDs have been explored to increase the dispersion or beam-scanning rate of LWAs, as described in Chapter 4. Although the demonstrated example in this chapter is simply based on the use of a short period of unit-cells and a long transverse slot with a sharp inductive reactance, the shunt capacitive susceptance can also be exploited to increase the dispersion sensitivity and thus the beam-scanning rate of LWAs. Meanwhile, to have a more rapid beam-scanning rate, slow-wave TLs in the form of meandering lines can also be used, not to mention the traditional approach of using a large permittivity material filling the host TLs. As a further development of LWAs which may provide more functionalities in addition to the desirable rapid beam-scanning behavior, the concept of RBPF is proposed and investigated in Chapter 5 for developing a class of multifunctional filtering LWAs which exhibit simultaneous rapid beam-scanning and filtering characteristics. Meanwhile, using this concept both filtering/dispersion and radiation tasks can be independently managed by different modules for this class of multifunctional LWAs, thereby exhibiting a large degree of design freedom for LWAs and enabling LWAs with the potential and feasibility of independently controlling the attenuation and phase constants. In should be noted that the functionality of rapid beam-scanning is always accompanied with a large loss due to the large GDD (group delay dispersion); this is the price that has to be paid by this class of LWAs. Thus, to implement this class of LWAs, low-loss materials should be employed. A significant contribution of this thesis is the work described in Chapter 6, in which an interesting LWA technique based on the MMR concept is proposed to realize stable radiation properties (i.e., stable radiation efficiency and gain) for LWAs. Compared with traditional periodic LWAs characterized by SMR behaviors and suffered from monotonic changing radiation, the proposed LWAs are comprised of MMR-based RDs and feature stable radiation properties over the entire frequency band of operation. A distinct difference regarding applications of the MMR

concept is observed from resonant antennas/filters with wide/multi-band performances to non-resonant LWAs with radiation stability. Using this concept, a bridge can be constructed between the resonant (standing-wave) and non-resonant (travelling-wave) antenna domains, and a deeper understanding of LWAs may be obtained by general readers. As a further development of the MMR design concept, a class of single-layered multifunctional LWAs with flexibly engineered radiation and filtering characteristics are proposed and demonstrated in Chapter 7. RDs exhibiting MMR performances while particularly possessing flexible model-control capability are exploited to accomplish such design freedoms and multifunctionalities of LWAs. It should be noted that the use of the MMR concept to design LWAs is largely generalized and more mature in this place. However, note that the MMR-based RD should have coherent radiation behaviors when the resonance status changes from one to the others over the frequency of leaky-wave operation. Typically, since three consecutive resonances of the RD are simultaneously used for such a development, all the three modes should share the same polarization directions and similar radiation patterns. For example, the TM_{10} and TM_{01} mode of a rectangular patch antenna cannot be part of these modes of the MMR-based RD for LWA developments since they have different polarization status. Meanwhile, since the TM_{20} mode of a rectangular patch antenna has a conical radiation pattern which is different from the broadside radiation possessed by the related TM_{10} mode, the two modes are also not suitable for developing such an MMR-related RD. Also note that the proposed MMR design rules mainly depend on the manipulation of resonance frequency locations while without considering the Q-factor in each resonance. In practical cases, such two bilateral modes in MMR-based RDs normally have different shapes and Q-values. Thus, slight adjustment and tuning of modes' frequencies is necessary and more common to ensure that the related LWAs can eventually embrace stable radiation performances over the frequency of interest. Interestingly, an MMR-based RD with the flexible mode-control capability can facilitate this process. Although the above mentioned LWAs in this thesis work and most of other LWAs in the open literature are capable of providing a wide impedance bandwidth, their radiation bandwidth is comparatively rather narrow due to their natural frequency-scanned beams. Therefore, for possible practical wideband system applications, a front-end array technique of LWAs on the basis of an FB concept is proposed in Chapter 8. The proposed FB-enabled LWA array technique may be potentially deployed in shifterless radar systems, as a complementary solution to the current phased array architecture.

CHAPTER 10 CONCLUSION AND RECOMMENDATIONS

10.1 Conclusion

As a special kind of structures that feature both wave radiation and wave guidance behaviors, the LWA has been in the spotlight of our RF/microwave communities since its inception, and the continuous research, exploration, and utilization of LWAs have prospered more than 80 years. With the rapid development of wireless technologies and the persistent pursuit of exploring the unknown, the LWA communities will continue to flourish through the efforts of numerous researchers from all over the world. This Ph. D. thesis is mainly dedicated to the exploration of planar functional LWAs in terms of novel leaky-wave concepts and techniques that enable LWAs to furnish desirable functionalities and electrical behaviors. Meanwhile, towards some system applications that need to use wideband signal waveforms, the role and virtues of LWAs are compromised due to the unique spatially narrow-band filtering or frequency-driven beam-scanning nature of LWAs. To this end, a promising LWA array technique based on the FB concept has been proposed and investigated, especially for wideband shifterless radar sensing system applications. Specific contribution of this Ph. D. thesis is described as follows.

In chapter 3, longitudinally slotted TE_{20} mode-driven SIW LWAs with low side-lobe and low cross-polarization have been proposed and demonstrated for millimeter-wave applications. Two types of LWAs differed by the meandering direction of the long slots have been developed and demonstrated. The proposed antennas can combine the advantages of SIW higher-order modes and long slot LWAs and they may be a good candidate to develop an array in millimeter-wave systems for practical applications, e.g., a planar array with two-dimensional hybrid phase-frequency beam-scanning (pencil beam) for FMCW radars.

In chapter 4, a quasi-uniform transversely slotted SIW LWA featuring rapid beam-scanning and its hexagonal array have been proposed and investigated for millimeter-wave systems. General approaches for improving LWA-based frequency beam-scanning rate have been discussed initially, followed by the specific approaches that make use of loading effects of radiating discontinuities to increase the frequency sensitivity of phase constant of LWAs. The proposed SIW LWA is simply based on the use of a long transverse slot with a sharp inductive reactance and a short period of unit cells. For practical system applications, the proposed LWA is tapered to have a low SLL, and

a hexagonal array consisting of six proposed LWAs is developed to provide an omnidirectional coverage in the azimuth plane while remaining the rapid frequency-driven beam-scanning in the elevation plane. The proposed antenna will be a good candidate to be applied for prospective millimeter-wave systems such as autonomous driving and flying.

In chapter 5, a class of quasi-uniform 1-D multifunctional LWAs simultaneously possessing both rapid beam-scanning and frequency-selective characteristics based on the RBPF concept have been proposed, studied, and demonstrated. Two kinds of susceptance-complementary non-radiative discontinuities, namely the NRLSP and iris that can be easily realized in SIW technology, are respectively exploited to construct EBG periodic structures exhibiting flexible bandpass and dispersion behaviors, upon which radiative discontinuities (i.e., TSs) are deliberately introduced for implementing LWAs with controllable radiation leakage. Guided-wave characteristics in terms of dispersion and frequency-selectivity behaviors of the proposed periodic SIW bandpass filters have been investigated by resorting to group delay, complex propagation constants and Bloch impedance. Besides, the relationship between the GDD and beam-scanning properties of an LWA is established, by which the filter theory can be borrowed for designing LWAs with flexible beam-scanning behaviors. For demonstration purposes, two RBPF-based LWAs are developed with both filtering and rapid beam-scanning characteristics confirmed by both simulated and measured results, thereby validating the correctness and effectiveness of the RBPF concept in the design of such a class of multifunctional LWAs. As a complementary implementation, the RBPF concept with constant group delay may be potentially explored for LWAs possessing fixed beam with frequency.

In chapter 6, a class of 1-D periodic LWAs based on the MMR concept have been proposed, studied and demonstrated. Compared with traditional periodic LWAs characterized by SMR behaviors and suffered from monotonic changing radiation, the proposed LWAs are comprised of MMR-based unit cells and feature stable radiation properties over the entire frequency band of operation. A distinct difference regarding applications of the MMR concept is observed from resonant antennas/filters with wide/multi-band performances to non-resonant LWAs with radiation stability. Two kinds of typical MMR-based radiator, MED and ACPA, are exploited to construct unit cells for demonstration purposes. A detailed design procedure has been provided for this class of LWAs to facilitate their practical implementation. It is interesting to mention that the proposed design concept is simple and straightforward. Based on this, a large variety of wide/multi-band resonant

antennas can be borrowed and implemented directly on various transmission line technologies (e.g., microstrip line, CPS, and CPW) for the design and development of periodic LWAs with stable radiation.

In chapter 7, a class of single-layered multifunctional LWAs exhibiting flexibly engineered radiation and filtering characteristics, with the aid of mode-control principle, have been systematically explored and developed for microwave and millimeter-wave applications. It is demonstrated that by properly controlling the modal behaviors of the RD, the related LWAs can be freely tailored with respect to its attenuation constant while simultaneously maintaining radiation stability and possessing filtering behaviors. Aimed for different system-integration platforms, both microstrip and SIW transmission-line technologies are separately employed to implement LWAs whose RDs possess flexible mode-control capabilities. In addition to those desirable electrical performances as mentioned above, the proposed LWAs also have some merits from the perspective of industrial practicability, e.g., good design flexibilities and versatilities, single-layer, low-cost, easy fabrication/integration.

In chapter 8, an array technique of LWAs on the basis of the FB concept has been proposed and investigated for potential radar applications. Different from those traditional fixed-beam-antennas-based beam-scanning schemes including the mechanical beam-scanning, multi-beam, passive/active phased array, and even full-digital phased array, the proposed scheme makes a combined use of the natural frequency-based beam-scanning inherently owned by LWAs and the FB concept to realize stitched frequency-space domain coverage for radar detections. Specifically, an array of LWA channels should be deployed, where the FB-related magnitude and phase stitching conditions in the form of the BSFs, beam-crossovers, and phase alignments should be simultaneously satisfied for those LWA channels. A detailed design flow regarding a generalized FB-enabled LWA array has been developed to facilitate a practical implementation, on which a two-channel SLR-based microstrip combline LWA array has been modeled, fabricated, and experimented for a direct proof-of-concept. Simulated and measured results are in a reasonably good agreement and both demonstrate the stitched spectral and spatial behaviors. The proposed LWA array-based scheme compared to the prevailing phased array scheme is distinct: it is the angle resolution rather than the range resolution that is put into the first priority for radar detection. As a consequence, the proposed one may be a potential candidate solution to be deployed in current and

future FMCW radars for some scenarios that need a good angle resolution while moderate range resolution.

10.2 Recommendation for Future Work

Although this Ph. D. thesis has attempted to realize some desirable functionalities and electrical performances for LWAs with the aid of novel leaky-wave concepts and techniques, and some efforts have to invested to tackle or relieve the dilemma that the natural frequency-scanning of LWAs is not suitable for some wideband system applications such as wideband radar sensing, more researches and explorations are still required to enrich the LWA technical aspects, including the proposal of new concept and techniques for the design of multifunctional LWAs and practical system applications of LWAs. To this end, some future works will be dedicated to the following aspects:

1). How to combine several functionalities together to design multifunctional LWAs? Although this thesis has tried to combine the filtering capability and rapid beam-scanning into a single LWA using the RBPF concept, more functionalities such as those mentioned in Chapter 2.2.4 can be integrated simultaneously into an LWA. For example, how to design a periodic LWA with open-stopband suppression (i.e., continuous beam-scanning from backward to forward through the broadside directions) while simultaneously providing stable radiation behaviors and good filtering characteristics? In this case, we may use our developed MMR concept to control the leakage rate for radiation stability, the two-port filtering antenna techniques proposed in Chapter 5 for the desired filtering capability, and the open-stopband techniques introduced in Chapter 2.2.4 for the continuous beam-scanning including the broadside radiation. Although this would be more challenging, it is useful and practical for real-word system applications.

2). Although the rapid beam-scanning property of LWAs has been investigated in this thesis, how to systematically develop a class of LWAs without frequency beam-scanning (or called “beam-squinting” that would be more proper in this place) would also be interesting. Thanks to the travelling-wave nature, LWAs are generally characterized with wide impedance bandwidth. However, their natural frequency beam-scanning renders them suffering from narrow radiation bandwidth towards a specific direction. If special concepts and techniques can be exploited to design LWAs with both wide impedance and radiation bandwidth, those narrow-band-natured

conventional standing-wave array (e.g., series-fed patch array or slotted waveguide array) can be substituted. In this case, wideband system applications such as communications and radars can benefit from such truly wideband LWAs.

3). In addition to designing wideband LWAs without beam-scanning, one can also use those frequency-scanning LWAs for wideband system applications if the FB array technique proposed in Chapter 8 of this thesis can be considered. However, the content and demonstration described in that chapter is just a direct proof-of-concept from the perspective of antenna front-end without integrating the proposed LWA array technique into a practical radar sensing system. Also, only two LWA channels are considered from the perspective of convenience of demonstration. Therefore, to be more practical, a larger array will be developed and the system setup together with radar signal processing architecture will be constructed and conducted to further demonstrate this FB-based array technique.

REFERENCES

[1] M. I. Skolnik, *Introduction to Radar Systems*, 3rd ed, New York, NY, USA: McGraw-Hill, 2001.

[2] M. A. Richards, J. A. Scheer, and W. A. Holm, *Principles of Modern Radar*. Edison, NJ, USA: SciTech, 2010

[3] https://commons.wikimedia.org/wiki/File:Swingate_transmitting_towers_-_original_configuration_1936.jpg

[4] https://www.pxfuel.com/en/free-photo-xvlmv

[5] https://www.pxfuel.com/en/free-photo-xnnhf

[6] https://www.pxfuel.com/en/free-photo-xpqsd

[7] https://pixabay.com/photos/radio-telescope-radio-telescope-5381220/

[8] https://nara.getarchive.net/media/the-cobra-judy-phased-array-radar-system-on-the-missile-range-instrumentation-d23c58

[9] A. A. Oliner and D. R. Jackson, "Leaky-wave antennas" in *Antenna Engineering Handbook*, 4th ed., J. Volakis, Ed. New York: McGraw-Hill, 2007.

[10] Y. J. Guo and R. W. Ziolkowski, *Advanced Antenna Array Engineering for 6G and Beyond Wireless Communications*, Wiley-IEEE Press, 2021.

[11] D. R. Jackson and A. A. Oliner, "Leaky-wave antennas," in *Modern Antenna Handbook*, C. A. Balanis, Ed. Hoboken, NJ, USA: Wiley, 2008.

[12] https://www.pxfuel.com/en/free-photo-eemna

[13] W. W. Hansen, "Radiating electromagnetic waveguide," U.S. Patent 2 402 622, 1940.

[14] J. Liu, D. R. Jackson, and Y. Long, "Substrate integrated waveguide (SIW) leaky-wave antenna with transverse slots," *IEEE Trans. Antennas Propag.*, vol. 60, no. 1, pp. 20-29, Jan. 2012.

[15] J. T. Willianm, P. Baccarelli, S. Paulotto, and D. R. Jackson, "1-D combline leaky-wave antenna with the open stopband suppressed:design considerations and comparisons with measurements," *IEEE Trans. Antennas Propag.*, vol. 61, no. 9, pp. 4184-4492, 2013.

[16] C. Balanis, *Antenna Theory: Analysis and Design*, 4th ed. Hoboken, NJ, USA: John Wiley & Sons, 2016.

[17] R. E. Collin, *Foundations for Microwave Engineering*, 2nd ed. New York: McGraw-Hill, 1992.

[18] D. M. Pozar, *Microwave Engineering*, 3rd ed. Hoboken, NJ, USA: Wiley, 2004.

[19] G. S. Scharp, “Continuous slot antennas,” U. S. patent 4328502, May, 1982.

[20] F. Whetten and C. A. Balanis, “Meandering long slot leaky-wave antennas,” *IEEE Trans. Antennas Propag*., vol. 39, no. 11, pp. 1553-1559, Nov. 1991.

[21] A. R. Mallahzadeh, and M. H. Amini, “Design of a leaky-wave long slot antenna using ridge waveguide,” *IET Microw. Antennas Propag*., vol. 8, no. 10, pp. 714-718, 2014.

[22] F. Frezza, M. Guglielmi, and P. Lampariello, “Millimeter-wave leaky-wave antennas based on slitted asymmetric ridge waveguide,” *IEE Proc. Microw. Antennas Propag*., vol. 141, no. 3, pp. 175-180, Jun. 1994.

[23] C. D. Nallo, F. Frezza, A. Galli, and P. Lampariello, “Theoretical and experimental investigations on the 'stepped' leaky-wave antennas,” in the *digest of IEEE International Symposium Antennas and Propagation Society,* Montreal, QC, Canada, 1997.

[24] N. Javanbakht, M. S. Majedi, and A. R. Attari, “Thinned array inspired quasi-uniform leaky-wave antenna with low side-lobe level,” *IEEE Antennas Wireless Propag. Lett*., vol. 16, pp. 2992-2995, 2017.

[25] A. Sutinjo, M. Okoniewski, and R. H. Johnston, “Suppression of the slot-mode radiation in a slitted waveguide using periodic slot perturbations,” *IEEE Antennas Wireless Propag. Lett*., vol. 8, pp. 550-553, 2009.

[26] Y.-W. Wu, Z. Jiang, and Z.-C. Hao, “A 400-GHz low cost planar leaky-wave antenna with low sidelobe level and low cross-polarization level,” *IEEE Trans. THz Sci. Technol.*, vol. 10, no. 4, pp. 427– 430, Jul. 2020.

[27] W. Menzel, “A new traveling-wave antenna in microstrip,” *Archiv fur Elek-tronik und Ubertragungstechnik (AEU)*, vol. 33, no. 4, pp. 137-140, Apr. 1979.

[28] D. Xie, L. Zhu, and X. Zhang, “An EH_0-mode microstrip leaky-wave antenna with periodic loading of shorting pins,” *IEEE Trans. Antennas Propag*., vol. 65, no. 7, pp. 3419-3426, Jul. 2017.

[29] J. Liu, Y. Li, and Y. Long, “Design of periodic shorting-vias for suppressing the fundamental mode in microstrip leaky-wave antennas,” *IEEE Trans. Antennas Propag*., vol. 63, no. 10, pp. 4297-4304, Oct. 2015.

[30] Y.-L. Lyu et al, “Periodic leaky-wave antenna based on complementary pair of radiation elements,” *IEEE Trans. Antennas Propag*., vol. 66, no. 9, pp. 4503-4515, Sep. 2018.

[31] Y.-L. Lyu et al, “Leaky-wave antenna with alternately loaded complementary radiation elements,” *IEEE Antennas Wireless Propag. Lett*., vol. 17, pp. 679-683, Apr. 2018.

[32] S. Paulotto, P. Baccarelli, F. Frezza, and D. R. Jackson, “A novel technique for open-stopband suppression in 1-D periodic printed leaky-wave antennas,” *IEEE Trans. Antennas Propag*., vol. 57, no. 7, pp. 1894-1906, Jul, 2009.

[33] D. K. Karmokar, K. P. Esselle, and T. S. Bird, “Wideband microstrip leaky-wave antennas with two symmetrical side beams for simultaneous dual-beam scanning,” *IEEE Trans. Antennas Propag.*, vol. 64, no. 4, pp. 1262-1269, Apr. 2016.

[34] Y. Li, Q. Xue, E. K.-N. Yung, Y. Long, “The periodic half-width microstrip leaky-wave antenna with a backward to forward scanning capability,” *IEEE Trans. Antennas Propag.*, vol. 58, no. 3, pp. 963-966, Mar. 2010.

[35] G.-F. Cheng, and C.-K. C. Tzuang, “A differentially excited coupled half-width microstrip leaky EH1 mode antenna,” *IEEE Trans. Antennas Propag.*, vol. 61, no. 12, pp. 5885-5892, Dec. 2013.

[36] A. Lai, C. Caloz, and T. Itoh, “Composite right/left-handed transmission line metamaterials,” *IEEE Microwave. Magazine,* vol. 5, no. 3, pp. 34-50, Sep., 2004.

[37] M. A. Antoniades, and G. V. Eleftheriades, “A CPS leaky-wave antenna with reduced beam squinting using NRI-TL metamaterials,” *IEEE Trans. Antennas Propag*., vol. 56, no. 3, pp. 708-721, Mar. 2008.

[38] N. Yang, C. Caloz, and K. Wu, “Full-space scanning periodic phase reversal leaky-wave antenna,” *IEEE Trans. Microw. Theory Techn*., vol. 58, no. 10, pp. 2619-2632, Oct. 2010.

[39] Y.-J. Chi, and F.-C. Chen, “CRLH leaky wave antenna based on ACPS technology with 180^{o} horizontal plane scanning capability,” *IEEE Trans. Antennas Propag*., vol. 61, no. 2, pp. 571-577, Feb. 2013.

[40] A. Grbic, G. V. Eleftheriades, "Leaky CPW-based slot antenna arrays for millimeter-wave applications", *IEEE Trans. Antennas Propag*., vol. 50, no. 11, pp. 1494-1504, Nov. 2002.

[41] A. Mehdipour, and G. V. Eleftheriades, “Leaky-wave antennas using negative-refractive-index transmission-line metamaterial supercells,” *IEEE Trans. Antennas Propag*., vol. 62, no. 8, pp. 3929-3942, Aug. 2014.

[42] J. Xu, W. Hong, H. Tang, Z. Kuai, K. Wu, "Half-mode substrate integrated waveguide (HMSIW) leaky-wave antenna for millimeter-wave applications," *IEEE Antennas Wireless Propag. Lett.*, vol. 7, pp. 85-88, 2008.

[43] F. Xu, K. Wu, and X. Zhang, "Periodic leaky-wave antenna for millimeter wave applications based on substrate integrated waveguide," *IEEE Trans. Antennas Propag.*, vol. 58, no. 2, pp. 340-347, Feb. 2010.

[44] Y. J. Chen, W. Hong, and K. Wu, "Millimeter-wave half mode substrate integrated waveguide frequency scanning antenna with quadri-polarization," *IEEE Trans. Antennas Propag.*, vol. 58, no. 6, pp. 1848-1855, Jun. 2010.

[45] Y. J. Chen, W. Hong, K. Wu, and Y. Fan, "Millimeter-wave substrate integrated waveguide long slot leaky-wave antennas and two dimensional multibeam applications," *IEEE Trans. Antennas Propag.*, vol. 59, no. 1, pp. 40-47, Jan. 2011.

[46] A. Mallahzadeh and S. Mohammad-Ali-Nezhad, "Long slot ridged SIW leaky wave antenna design using transverse equivalent technique," *IEEE Trans. Antennas Propag.*, vol. 62, no. 11, pp. 5445–5452, Nov. 2014.

[47] A. J. Martinez-Ros, M. Bozzi, and M. Pasian, "Double-sided SIW leaky-wave antenna with increased directivity in the E-plane," *IEEE Trans. Antennas Propag.*, vol. 66, no. 6, pp. 3130–3135, Jun. 2018.

[48] A. J. Martinez-Ros, J. L. Gomez-Tornero, and G. Goussetis, "Planar leaky-wave antenna with flexible control of the complex propagation constant," *IEEE Trans. Antennas Propag.*, vol. 60, no. 3, pp. 1625–1630, Mar. 2012.

[49] M. Ettorre, R. Sauleau, and L. L. Coq, "Multi-beam multi-layer leaky-wave SIW pillbox antennas for millimeter-wave applications," *IEEE Trans. Antennas Propag.*, vol. 59, no. 4, pp. 1093–1110, Apr. 2011.

[50] Y. Geng, et al, "High-efficiency leaky-wave antenna array with sidelobe suppression and multibeam generation," *IEEE Antennas Wireless Propag. Lett.*, vol. 16, pp. 2787-2790, 2017.

[51] Y.-L, Lyu, et al, "Leaky-wave antennas based on noncutoff substrate integrated waveguide supporting beam scanning from backward to forward," *IEEE Trans. Antennas Propag.*, vol. 64, no. 6, pp. 2155–2164, Jun. 2016.

[52] Y. Dong, and T. Itoh, "Composite right/left-handed substrate integrated waveguide and half mode substrate integrated waveguide leaky-wave structures," *IEEE Trans. Antennas Propag*., vol. 59, no. 3, pp. 767-775, Mar. 2011.

[53] Y. Dong, and T. Itoh, "Substrate integrated composite right-/left-handed leaky-wave structure for polarization-flexible antenna application," *IEEE Trans. Antennas Propag*., vol. 64, no. 6, pp. 2155–2164, Jun. 2016.

[54] J. Liu, X. Tang, Y. Li, and Y. Long, "Substrate integrated waveguide leaky-wave antenna with H-shaped slots," *IEEE Trans. Antennas Propag*., vol. 60, no. 8, pp. 3962–3967, Aug. 2012.

[55] Y. Geng, J. Wang, Y. Li, Z. Li, M. Chen, and Z. Zhang, "New design of beam-formed leaky-wave antenna based on substrate integrated waveguide in a confined space," *IEEE Trans. Antennas Propag*., vol. 66, no. 11, pp. 6334–6339, Nov. 2018.

[56] W. Zhou, J. Liu, and Y. Long, "Investigation of shorting vias for suppressing the open stopband in an SIW periodic leaky-wave structure," *IEEE Trans. Antennas Propag*., vol. 66, no. 6, pp. 2936-2945, Jun. 2018.

[57] D. K. Karmokar et al, "Substrate integrated waveguide-based periodic backward-to-forward scanning leaky-wave antenna with low cross-polarization," *IEEE Trans. Antennas Propag*., vol. 66, no. 8, pp. 3846-3856, Aug. 2018.

[58] K.-M. Mak, K.-K. So, H.-W. Lai, and K.-M. Luk, "A magnetoelectric dipole leaky-wave antenna for millimeter-wave application," *IEEE Trans. Antennas Propag*., vol. 65, no. 12, pp. 6395-6402, Dec. 2017.

[59] R. Ranjan, and J. Ghosh, "SIW-based leaky-wave antenna supporting wide range of beam scanning through broadside," *IEEE Antennas Wireless Propag. Lett*., vol. 18, no. 4, pp. 606-610, Apr. 2019.

[60] T. Lou, X.-X. Yang, H. Qiu, Q. Luo, and S. Gao, "Low-cost electrical beam-scanning leaky-wave antenna based on bent corrugated substrate integrated waveguide," *IEEE Antennas Wireless Propag. Lett*., vol. 18, no. 2, pp. 353-357, Feb. 2019.

[61] D. Zheng, Y.-L. Lyu, and K. Wu, "Longitudinally slotted SIW leaky-wave antenna for low cross-polarization millimeter-wave applications," *IEEE Trans. Antennas Propag*., vol. 68, no. 2, pp. 656-664, Feb. 2020.

[62] N. B.-Makou, K. Wu, and A. A. Kishk, “Single-layer substrate-integrated broadside leaky long-slot array antennas with embedded reflectors for 5G systems,” ,” *IEEE Trans. Antennas Propag*., vol. 67, no. 12, pp. 7331-7339, Dec. 2019.

[63] M. R. Rahimi, M. S. Sharawi, and K. Wu, “Higher-order space harmonics in substrate integrated waveguide leaky-wave antennas,” *IEEE Trans. Antennas Propag*., vol. 69, no. 8, pp. 4332-4346, Aug. 2021.

[64] J. Liu, and J. Liang, “Gain enhancement of transversely slotted substrate integrated waveguide leaky-wave antennas based on higher modes,” *IEEE Trans. Antennas Propag*., vol. 69, no. 8, pp. 4423-4438, Aug. 2021.

[65] N. Javanbakht, R. E. Amaya, J. Shaker, and B. Syrett, “Side-lobe level reduction of half-mode substrate integrated waveguide leaky-wave antenna,” *IEEE Trans. Antennas Propag*., vol. 69, no. 6, pp. 3572-3577, Jun. 2021.

[66] J. Y. Yin et al, “Frequency-controlled broad-angle beam scanning of patch array fed by spoof surface plasmon polaritons,” *IEEE Trans. Antennas Propag*., vol. 64, no. 12, pp. 5181-5189, Dec. 2016.

[67] Q. L. Zhang, Q. Zhang, and Y. Chen, “Spoof surface plasmon polariton leaky-wave antennas using periodically loaded patches above PEC and AMC ground planes,” *IEEE Antennas Wireless Propag. Lett*., vol. 16, pp. 3014-3017, 2017.

[68] D. Wei, J. Li, J. Yang, Y. Qi, and G. Yang, “Wide-scanning-angle leaky-wave array antenna based on microstrip SSPPs-TL,” *IEEE Antennas Wireless Propag. Lett*., vol. 17, no. 8, pp. 1566-1570, Aug. 2018.

[69] S.-D. Xu, D.-F. Guan, Q. Zhang, P. You, S. Ge, X.-X. Hou, Z.-B. Yang, and S.-W. Yong, “A wide-angle narrowband leaky-wave antenna based on substrate integrated waveguide-spoof surface plasmon polariton structure,” *IEEE Antennas Wireless Propag. Lett*., vol. 18, no. 7, pp. 1386-1389, Jul. 2019.

[70] W. Feng, Y. Feng, L.-S. Wu, Y. Shi, X. Y. Zhou, and W. Che, “A novel leaky-wave endfire filtering antenna based on spoof surface plasmon polariton,” *IEEE Trans Plasma Science,* vol. 48, no. 9, pp. 3061-3066, Sept. 2020.

[71] H.-W. Yu, Y.-C. Jiao, C. Zhang, Z.-B. Weng, “Dual-linearly polarized leaky-wave patch array with low cross-polarization levels using symmetrical spoof surface plasmon polariton lines,” *IEEE Trans. Antennas Propag*., vol. 69, no. 3, pp. 1781-1786, Mar. 2021.

[72] K. Rudramuni, K. Kandasamy, Q. Zhang, X.-L. Tang, A. Kandwal, P. K. T. Rajanna, and H. Liu, "Goubau-line leaky-wave antenna for wide-angle beam scanning from backfire to endfire," *IEEE Antennas Wireless Propag. Lett*., vol. 17, no. 8, pp. 1571-1574, Aug. 2018.

[73] G. S. Kong, H. F. Ma, B. G. Cai, and T. J. Cui, "Continuous leaky-wave scanning using periodically modulated spoof plasmonic waveguide," *Sci. Rep.* 6, 29600 (2016)

[74] D. S.-Escuderos, M. F.-Bataller, J. I. Herranz, and M. C.-Fabres, "Periodic leaky-wave antenna on planar goubau line at millimeter-wave frequencies," *IEEE Antennas Wireless Propag. Lett*., vol. 12, pp. 1006-1009, 2013.

[75] L. Liu, M. Chen, J. Cai, X. Yin, and L. Zhu, "Single-beam leaky-wave antenna with lateral continuous scanning functionality based on spoof surface plasmon transmission line," *IEEE Access*, vol. 7, pp. 25225-25231, 2019.

[76] S. Ge, Q. Zhang, C.-Y. Chiu, Y. Chen, and R. D. Murch, "Single-side-scanning surface waveguide leaky-wave antenna using spoof surface plasmon excitation," *IEEE Access*, vol. 6, pp. 66020-66029, 2018.

[77] M. Vukomanovic, J.-L. V.-Roy, O. Q.-Teruel, E. R.-Iglesias, Z. Sipus, "Gap waveguide leaky-wave antenna," *IEEE Trans. Antennas Propag*., vol. 64, no. 5, pp. 2055-2060, May. 2016.

[78] L. Wang, J. L. G.-Tornero, E. R.-Igles, O. Q.-Teruel, "Low-dispersive leaky-wave antenna integrated in groove gap waveguide technology," *IEEE Trans. Antennas Propag*., vol. 66, no. 11, pp. 5727-5736, Nov. 2018.

[79] S. Wang, Z. Li, B. Wei, S. Liu, and J. Wang, "A *Ka*-band circularly polarized fixed-frequency beam-scanning leaky-wave antenna based on groove gap waveguide with consistent high gains," *IEEE Trans. Antennas Propag*., vol. 69, no. 4, pp. 1959-1969, Apr. 2021.

[80] J. Cao, H. Wang, S. Tao, S. Mou, and Y. Guo, "Highly integrated beam scanning groove gap waveguide leaky wave antenna array," *IEEE Trans. Antennas Propag*., vol. 69, no. 8, pp. 5112-5117, Aug. 2021.

[81] N. Memeletzoglou, E. R.-Iglesias, "Holey metasurface prism for the reduction of the dispersion of gap waveguide leaky-wave antennas", *IEEE Antennas and Wireless Propagation Letters*, vol. 18, no. 12, pp. 2582-2586, 2019.

[82] N. Memeletzoglou, E. R.-Iglesias, "Array of stacked leaky-wave antennas in groove gap waveguide technology", *Sci. Rep.* 11, 2260 (2021).

[83] D. Zheng, and K. Wu, "Leaky-wave antenna featuring stable radiation based on multi-mode resonator (MMR) concept," *IEEE Trans. Antennas Propag*., vol. 68, no. 3, pp. 2016-2030, Mar. 2020.

[84] D. Zheng, and K. Wu, "Multifunctional leaky-wave antenna with tailored radiation and filtering characteristics based on flexible mode-control principle", *IEEE Open Journal of Antennas Propag*., vol. 2, pp. 858-869, 2021.

[85] Y. Geng, et al, "High-efficiency leaky-wave antenna array with sidelobe suppression and multibeam generation," *IEEE Antennas Wireless Propag. Lett*., vol. 16, pp. 2787-2790, 2017.

[86] H. V. Nguyen, A. Parsa, and C. Caloz, "Power-recycling feedback system for maximization of leaky-wave antennas radiation efficiency," *IEEE Trans. Microwave Theory Tech*., vol. 58, no. 7, pp:1641-1650, Jul. 2010.

[87] T. R. Cameron, A. T. Sutinjo, and M. Okoniewski, "A circularly polarized broadside radiating "herringbone" array design with the leaky-wave approach," *IEEE Antennas Wireless Propag. Lett*., vol. 9, pp. 826-829, 2010.

[88] H. Lee, J. H. Choi, C. –T. M. Wu, and T. Itoh, "A compact single radiator CRLH-inspired circularly polarized leaky-wave antenna based on substrate-integrated waveguide," *IEEE Trans. Antennas Propag.*, vol. 63, no. 10, pp. 4566-4572, Oct, 2015.

[89] P. Chen, W. Hong, Z. Kuai, and J. Xu, "A substrate integrated waveguide circularly polarized slot radiator and its linear array," *IEEE Antennas Wireless Propag. Lett*., vol. 8, pp. 120-123, 2009.

[90] X. Lv, W. Cao, Z. Zeng, and S. Shi, "A circularly polarized frequency beam scanning antenna fed by microstrip spoof SPP transmission line," *IEEE Antennas Wireless Propag. Lett*., vol. 17, no. 7, pp. 1329-1333, Jul. 2018.

[91] Q. Zhang, Q. Zhang, and Y. Chen, "High-efficiency circularly polarized leaky-wave antenna fed by spoof surface plasmon polaritons," *IET Micro. Antennas Propag*., vol. 12, no. 10, pp. 1639-1644, 2018.

[92] Y. Zhang, H. Liu, C. Meng, Y. Lin, Y. Zhang, E. Forsberg, and S. He, "A broadband high-gain circularly polarized wide beam scanning leaky-wave antenna," *IEEE Access*, vol. 8, pp. 171091-171099, 2020.

[93] M. M. Sabahi, A. A. Heidari, and M. Movahhedi, "A compact CRLH circularly polarized leaky-wave antenna based on substrate integrated waveguide," *IEEE Trans. Antennas Propag.*, vol. 66, no. 9, pp. 4407-4414, Sept, 2018.

[94] A. P. Saghati, M. M. Mirsalehi, and M. H. Neshati, "A HMSIW circularly polarized leaky-wave antenna with backward, broadside, and forward radiation," *IEEE Antennas Wireless Propag. Lett*., vol. 13, pp. 451-454, 2014.

[95] M. H. Rahmani, and D. Deslandes, "Backward to forward scanning periodic leaky-wave antenna with wide scanning range," *IEEE Trans. Antennas Propag.*, vol. 65, no. 7, pp. 3326-3335, Jul, 2017.

[96] A. Zandamela, A. A.-Bassam, and D. Heberling, "Circularly polarized periodic leaky-wave antenna based on dielectric image line for millimeter-wave radar applications," *IEEE Antennas Wireless Propag. Lett*., vol. 20, no. 6, pp. 938-942, Jun. 2021.

[97] Y.-L. Lyu, F.-Y. Meng, G.-H. Yang, D. Erni, Q. Wu, and K. Wu, "Periodic SIW leaky-wave antenna with large circularly polarized beam scanning range," *IEEE Antennas Wireless Propag. Lett*., vol. 16, pp. 2493-2496, 2017.

[98] Y. Hou, Y. Li, Z. Zhang, and Z. Feng, "High-gain leaky-wave endfire antenna based on Hansen-Woodyard condition," *IEEE Antennas Wireless Propag. Lett*., vol. 18, no. 10, pp. 2155-2159, Oct. 2019.

[99] Y. Hou, Y. Li, Z. Zhang, and Z. Feng, "Narrow-width periodic leaky-wave antenna array for endfire radiation based on Hansen-Woodyard condition," *IEEE Trans. Antennas Propag.*, vol. 66, no. 11, pp. 6393-6396, Nov. 2018.

[100] P. Liu, H. Feng, Y. Li, and Z. Zhang, "Low-profile endfire leaky-wave antenna with air media," *IEEE Antennas Wireless Propag. Lett*., vol. 66, no. 3, pp. 1086-1092, Mar. 2018.

[101] S. Ge, Q. Zhang, A. K. Rashid, G. Zhang, C.-Y. Chiu, and R. Murch, "Analysis of asymmetrically corrugated goubau-line antenna for endfire radiation," *IEEE Trans. Antennas Propag.*, vol. 67, no. 11, pp. 7133-7138, Nov. 2019.

[102] L. Sun, Y. Hou, Y. Li, Z. Zhang, and Z. Feng, "An open cavity leaky-wave antenna with vertical-polarization endfire radiation," *IEEE Trans. Antennas Propag.*, vol. 67, no. 5, pp. 3455-3460, May. 2019.

[103] L. Sun, P. Liu, Y. Li, L. Chang, K. Wei, and Z. Zhang, “Metal strip endfire antenna based on TE1 leaky-wave mode,” *IEEE Trans. Antennas Propag.*, vol. 68, no. 8, pp. 5916-5923, Aug. 2020.

[104] Y. Hou, Y. Li, Z. Zhang, and Z. Feng, “A broadband and high-gain endfire antenna array fed by air-substrate parallel strip line,” *IEEE Trans. Antennas Propag.*, vol. 67, no. 8, pp. 5717-5722, Aug. 2019.

[105] C.-J. Wang, C. F. Jou, and J.-J. Wu, “A novel two-beam scanning active leaky-wave antenna,” *IEEE Trans. Antennas Propag.*, vol. 47, no. 8, pp. 1314-1317, Aug. 1999.

[106] T.-L. Chen, and Y.-D. Lin, “Dual-beam microstrip leaky-wave array excited by aperture-coupling method,” *IEEE Trans. Antennas Propag.*, vol. 51, no. 9, pp. 2496-2498, Sep. 2003.

[107] Y. Li, Q. Xue, E. K.-N. Yung, and Y. Long, “Fixed-frequency dual-beam scanning microstrip leaky-wave antenna,” *IEEE Antennas Wireless Propag. Lett*., vol. 6, pp. 444-446, 2007.

[108] Y. Li, Q. Xue, E. K.-N. Yung, and Y. Long, “Dual-beam steering microstrip leaky-wave antenna with fixed operating frequency,” *IEEE Trans. Antennas Propag.*, vol. 56, no. 1, pp. 248-252, Jan. 2008.

[109] C. H. Zhang, J. Ren, X. Du, and Y. Yin, “Dual-beam leaky-wave antenna based on dual-mode spoof surface plasmon polaritons,” *IEEE Antennas Wireless Propag. Lett*., *early access*

[110] Z. L. Ma, K. B. No, C. H. Chan, and L. J. Jiang, “A novel supercell-based dielectric grating dual-beam leaky-wave antenna for 60 GHz applications,” *IEEE Trans. Antennas Propag.*, vol. 64, no. 12, pp. 5521-5526, Dec. 2016.

[111] Z. L. Ma, and L. J. Jiang, “One-dimensional triple periodic dual-beam microstrip leaky-wave antenna,” *IEEE Antennas Wireless Propag. Lett*., vol. 14, pp. 390-393, 2014.

[112] Y. Hou, Y. Li, Z. Zhang, and Z. Feng, “Dual-beam periodic leaky-wave antenna with reduced beam squinting,” *IEEE Antennas Wireless Propag. Lett*., vol. 18, no. 12, pp. 2533-2537, Dec. 2019.

[113] M. Movahhedi, M. Karimipour, and N. Komjani, “Multibeam bidirectional wideband/wide-scanning-angle holographic leaky-wave antenna,” *IEEE Antennas Wireless Propag. Lett*., vol. 18, no. 7, pp. 1507-1511, Jul. 2019.

[114] A. Sarkar, D. A. Pham, and S. Lim, “Tunable higher order mode-based dual-beam CRLH microstrip leaky-wave antenna for V-band backward-broadside-forward radiation coverage,” *IEEE Trans. Antennas Propag.*, vol. 68, no. 10, pp. 6912-6922, Oct. 2020.

[115] Y. Geng, J. Wang, Y. Li. Z. Li, M. Chen, and Z. Zhang, "High-efficiency leaky-wave antenna array with sidelobe suppression and multibeam generation," *IEEE Antennas Wireless Propag. Lett*., vol. 16, pp. 2787-2790, 2017.

[116] J. Liu, D. R. Jackson, Y. Li, C. Zhang, and Y. Long, "Investigation of SIW leaky-wave antenna for endfire-radiation with narrow beam and sidelobe suppression," *IEEE Trans. Antennas Propag*., vol. 62, no. 9, pp. 4489-4497, Sep. 2014.

[117] Z. Li, J. Wang, M. Chen, and Z. Zhang, "New approach of radiation pattern control for leaky-wave antennas based on the effective radiation sections," *IEEE Trans. Antennas Propag*., vol. 63, no. 7, pp. 2867-2878, Jul. 2015.

[118] P. F. Kou, and Y. J. Chen, "*Ka*-band low-sidelobe-level slot array leaky-wave antenna based on substrate integrated nonradiative dielectric waveguide," *IEEE Antennas Wireless Propag. Lett*., vol. 16, pp. 3075-3078, 2017.

[119] M. T. Mu, and Y. J. Chen, "Low sidelobe level short leaky-wave antenna based on single-layer PCB-based substrate integrated image guide," *IEEE Trans. Antennas Propag*., vol. 17, no. 8, pp. 1519-1523, Aug. 2018.

[120] Z. Li, J. Wang, Z. Zhang, and M. Chen, "Far field computation of the travelling wave structures and a new approach for suppressing the sidelobe levels," *IEEE Trans. Antennas Propag*., vol. 61, no. 4, pp. 2308-2312, Apr. 2013.

[121] A.-R. Kiani, F. Geran, S. M. Hashemi, and K. Forooraghi, "A presentation of a mathematical formula to design of a quasi-uniform leaky-wave antenna with ultralow sidelobe level," *IEEE Antennas Wireless Propag. Lett*., vol. 18, no. 5, pp. 901-905, May. 2019.

[122] D.-J. Wei, J. Li, J. Liu, G. Yang, and W. Zhang, "Dual-band substrate-integrated waveguide leaky-wave antenna with a simple feeding way," *IEEE Antennas Wireless Propag. Lett*., vol. 18, no. 4, pp. 591-595, Apr. 2019.

[123] T. Kodera, and C. Caloz, "Dual-band full-space scanning leaky-wave antenna based on ferrite-loaded open waveguide," *IEEE Antennas Wireless Propag. Lett*., vol. 8, pp. 1202-1205, 2009.

[124] J. Machac, M. Polivka, K. Zemlyakov, "A dual band leaky-wave antenna on a CRLH substrate integrated waveguide," *IEEE Trans. Antennas Propag*., vol. 61, no. 7, pp. 3876-3879, Jul. 2013.

[125] R. B. V. B. Simorangkir, and Y. Lee, "A planar dual-band periodic leaky-wave antenna based on a mu-negative (MNG) transmission line," *IEEE Trans. Antennas Propag*., vol. 63, no. 5, pp. 2370-2374, May. 2015.

[126] D. K. Karmokar, and K. P. Esselle, "Periodic U-slot-loaded dual-band half-width microstrip leaky-wave antennas for forward and backward beam scanning," *IEEE Trans. Antennas Propag*., vol. 63, no. 12, pp. 5372-5381, Dec. 2015.

[127] Y. Li, and J. Wang, "Dual-band leaky-wave antenna based on dual-mode composite microstrip line for microwave and millimeter-wave applications," *IEEE Trans. Antennas Propag*., vol. 66, no. 4, pp. 1660-1668, Apr. 2018.

[128] Q. Zhang, Q. Zhang, H. Liu, and C. H. Chan, "Dual-band and dual-polarized leaky-wave antennas based on slotted SIW," *IEEE Antennas Wireless Propag. Lett*., vol. 18, no. 3, pp. 507-511, Mar. 2019.

[129] M. Wang, H. F. Ma, W. X. Tang, H. C. Zhang, W. X. Jiang, and T. J. Cui, "A dual-band electronic-scanning leaky-wave antenna based on a corrugated microstrip line," *IEEE Trans. Antennas Propag*., vol. 67, no. 5, pp. 3433-3438, May. 2019.

[130] K. Rudramuni, B. Majumder, P. K. T. Rajanna, K. Kandasamy, and Q. Zhang, "Dual-band asymmetric leaky-wave antennas for circular polarization and simultaneous dual beam scanning," *IEEE Trans. Antennas Propag*., vol. 69, no. 4, pp. 1843-1852, Apr. 2021.

[131] C. D. Bui, N. N.-Trong, T. K. Nguyen, "A planar dual-band and dual-sense circularly polarized microstrip patch leaky-wave antenna," *IEEE Antennas Wireless Propag. Lett*., vol. 19, no. 12, pp. 2162-2166, Dec. 2020.

[132] A. Sakar, A. H. Naqvi, and S. Lim, "(40 to 65) GHz higher order mode microstrip-based dual band dual beam tunable leaky-wave antenna for millimeter wave applications," *IEEE Trans. Antennas Propag*., vol. 68, no. 11, pp. 7255-7265, Nov. 2020.

[133] D. K. Karmokar, Y. J. Guo, P.-Y. Qin, K. P. Esselle, and T. S. Bird, "Forward to backward beam-scanning tri-band leaky-wave antenna," *IEEE Antennas Wireless Propag. Lett*., vol. 16, pp. 1891-1894, 2017.

[134] Y. Geng, J. Wang, Z. Li, Y. Li, M. Chen, and Z. Zhang, "Dual-beam and tri-band SIW leaky-wave antenna with wide beam scanning range including broadside direction," *IEEE Access*, vol. 7, pp. 176361-176368, 2019.

[135] S. S. Haghighi, A.-A. Heidari, and M. Movahhedi, “A three-band substrate integrated waveguide leaky-wave antenna based on composite right/left-handed structure,” *IEEE Trans. Antennas Propag*., vol. 63, no. 10, pp. 4578-4582, Oct. 2015.

[136] L. Chiu, W. Hong, and Z. Kuai, “Substrate integrated waveguide slot array antenna with enhanced scanning range for automotive application,” in *IEEE Asia Pacific Microwave conference*, Singapore, 2009.

[137] S. Ma et al, “Liquid crystal leaky-wave antennas with dispersion sensitivity enhancement,” *IEEE Trans. Compon., Packag., Manuf. Technol*., vol. 7, no. 5, pp. 792-801, May. 2017.

[138] L. Cui, W. Wu, and D.-G, Fang, “Printed frequency beam-scanning antenna with flat gain and low sidelobe levels,” *IEEE Antennas Wireless Propag. Lett*., vol. 12, pp. 292-295, 2013.

[139] W. Cao, Z. Chen, W. Hong, B. Zhang, and A. Liu, “A beam-scanning leaky-wave slot antenna with enhanced scanning angle range and flat gain characteristic using composite phase-shifting transmission line,” *IEEE Trans. Antennas Propag*., vol. 62, no. 11, pp. 5871-5875, Nov. 2014.

[140] N. Boskovic, B. Jokanovic, and M. Radovanovic, “Printed frequency scanning antenna arrays with enhanced frequency sensitivity and sidelobe suppression,” *IEEE Trans. Antennas Propag*., vol. 65, no. 4, pp. 1757-1764, Apr. 2017.

[141] D. Zheng, Y.-L. Lyu, and K. Wu, “A quasi-uniform transversely slotted SIW leaky-wave structure with enhanced beam-scanning rate for millimeter-wave applications,” in *IEEE MTT-S Int. Microw. Symp. Dig*., Boston, MA, USA, Jun. 2019, pp. 885–888.

[142] D. Zheng, Y.-L. Lyu, and K. Wu, “Transversely slotted SIW leaky-wave antenna featuring rapid beam-scanning for millimeter-wave applications,” *IEEE Trans. Antennas Propag*., vol. 68, no. 6, pp. 4172-4185, Jun. 2020.

[143] D. Zheng and K. Wu, “Multifunctional filtering leaky-wave antenna exhibiting simultaneous rapid beam-scanning and frequency-selective characteristics based on radiative bandpass filter concept,” *IEEE Trans. Antennas Propag*., vol. 68, no. 8, pp. 5842-5854, Aug., 2020.

[144] D.-F. Guan, Q. Zhang, P. You, Z. B. Yang, and S. Q. Yong, “Scanning rate enhancement of leaky-wave antennas using slow-wave substrate integrated waveguide structure,” *IEEE Trans. Antennas Propag*., vol. 66, no. 7, pp. 3747-3757, Jul. 2018.

[145] D. Xie and L. Zhu, “Microstrip leaky-wave antennas with nonuniform periodical loading of shorting pins for enhanced frequency sensitivity,” *IEEE Trans. Antennas Propag*., vol. 66, no. 7, pp. 3337–3345, Jul. 2018.

[146] S.-D. Xu et al, “A wide-angle narrowband leaky-wave antenna based on substrate integrated waveguide-spoof surface plasmon polariton structure,” *IEEE Antennas Wireless Propag. Lett*., vol. 18, no. 7, pp. 1386-1389, Jul. 2019.

[147] M. G.-Vigueras, J. L. G.-Tornero, G. Goussetis, A. R. Weily, and Y. J. Guo, “Enhancing frequency-scanning response of leaky-wave antennas using high-impedance surfaces,” *IEEE Antennas Wireless Propag. Lett*., vol. 10, pp. 7-10, 2011.

[148] G. Zhang, Q. Zhang, S. Ge, Y. Chen, and R. D. Murch, “High scanning-rate leaky-wave antenna using complementary microstrip-slot stubs,” *IEEE Trans. Antennas Propag*., vol. 67, no. 5, pp. 2913-2922, May. 2019.

[149] G. Zhang, Q. Zhang, Y. Chen, and R. D. Murch, “High-scanning-rate and wide-angle leaky-wave antennas based on glide-symmetry goubau line”, *IEEE Trans. Antennas Propag*, vol. 68, no. 4, pp. 2531-2540, 2020.

[150] J. Zhong, A. K. Rashid, and Q. Zhang, “45° linearly polarized and circularly polarized high-scanning-rate leaky-wave antennas based on slotted substrate integrated waveguide”, *IEEE Access*, vol. 8, pp. 82162-82172, 2020.

[151] Jianfeng Chen, Wei Yuan, Wen Xuan Tang, Lei Wang, and Qiang Cheng, Tie Jun Cui, “Linearly sweeping leaky-wave antenna with high scanning rate”, *IEEE Trans. Antennas Propag*, vol. 69, no. 6, pp. 3214-3223, 2021.

[152] D. Ma, J. Zhong, S. Shen, A. Dubey, C. Zhang, Q. Zhang, and R. D. Murch, "Single-shot frequency-diverse near-field imaging using high-scanning-rate leaky-wave antenna", *IEEE Trans. Microw. Theory Techn.*, vol. 69, no. 7, pp. 3399-3412, 2021.

[153] A. J. Mackay, and G. V. Eleftheriades, “Meandered and dispersion-enhanced planar leaky-wave antenna with fast beam scanning”, *IEEE Antennas Wireless Propag. Lett.*,, vol. 20, no. 8, pp. 1596-1600, 2021.

[154] Y. You, Y. Lu, Y. Wang, J. Xu, J. Huang, and W. Hong, "Enhanced pencil-beam scanning CTS leaky-wave antenna based on meander delay line", *IEEE Antennas Wireless Propag. Lett.*,, vol. 20, no. 9, pp. 1760-1764, 2021.

[155] S. Xiao, Z. Shao, M. Fujise, and B.-Z. Wang, “Pattern reconfigurable leaky-wave antenna design by FDTD method and Floquet’s theorem,” *IEEE Trans. Antennas Propag*, vol. 53, no. 5, pp. 1845-1848, May. 2005.

[156] R. O. Ouedraogo, E. J. Rothwell, and B. J. Gresstis, “A reconfigurable microstrip leaky-wave antenna with broadly steerable beam,” *IEEE Trans. Antennas Propag*, vol. 59, no. 8, pp. 3080-2083, Aug. 2011.

[157] J. Li, M. He, C. Wu, and C. Zhang, “Radiation-pattern-reconfigurable Graphene leaky-wave antenna at Terahertz band based on dielectric grating structure,” *IEEE Antennas Wireless Propag. Lett.,*, vol. 16, pp. 1771-1775, 2017.

[158] Z. Hu, Z. Shen, and W. Wu, “Reconfigurable leaky-wave antenna based on periodic water grating,” *IEEE Antennas Wireless Propag. Lett.,*, vol. 13, pp. 134-137, 2014.

[159] D. K. Karmokar, K. P. Esselle, and S. G. Hay, “Fixed-frequency beam steering of microstrip leaky-wave antennas using binary switches,” *IEEE Trans. Antennas Propag*, vol. 64, no. 6, pp. 2146-2154, Jun. 2016.

[160] M. Li, M.-C. Tang, and S. Xiao, “Design of a LP, RHCP, and LHCP polarization-reconfigurable holographic antenna,” *IEEE Access*, vol. 7, pp. 82776-82784, 2019.

[161] Y. Geng, J. Wang, Y. Li, Z. Li, M. Chen, and Z. Zhan, “Radiation pattern-reconfigurable leaky-wave antenna for fixed-frequency beam steering based on substrate-integrated waveguide,” *IEEE Antennas Wireless Propag. Lett.*, vol. 18, no. 2, pp. 387-391, Feb. 2019.

[162] S.-L. Chen, D. K. Karmokar, P.-Y. Qin, R. W. Ziolkowski, and Y. J. Guo, “Polarization-reconfigurable leaky-wave antenna with continuous beam-scanning through broadside,” *IEEE Trans. Antennas Propag*, vol. 68, no. 1, pp. 121-133, Jan. 2020.

[163] A. Suntives, and S. V. Hum, “A fixed-frequency beam-steerable half-mode substrate integrated waveguide leaky-wave antenna,” *IEEE Trans. Antennas Propag*, vol. 60, no. 5, pp. 2540-2544, May. 2012.

[164] Z. Li, Y. J. Guo, S.-L. Chen, and J. Wang, “A period-reconfigurable leaky-wave antenna with fixed-frequency and wide-angle beam scanning,” *IEEE Trans. Antennas Propag*, vol. 67, no. 6, pp. 3720-3732, Jun. 2019.

[165] A. Neto, S. Bruni, G. Gerini and M. Sabbadini, “The leaky lens: A broad-band fixed-beam leaky-wave antenna”, *IEEE Trans. Antennas Propag*., vol. 53, no. 10, pp. 3240-3246, Oct. 2005.

[166] H. Mirzaei and G. V. Eleftheriades, “Arbitrary-angle squint-free beamforming in series-fed antenna arrays using non-foster elements synthesized by negative-group-delay networks”, *IEEE Trans. Antennas Propag*., vol. 63, no. 5, pp. 1997-2010, May 2015.

[167] A. Mehdipour, J. W. Wong and G. V. Eleftheriades, “Beam-squinting reduction of leaky-wave antennas using huygens metasurfaces”, *IEEE Trans. Antennas Propag.*, vol. 63, no. 3, pp. 978-992, Mar. 2015.

[168] K. M. Kossifos and M. A. Antoniades, "A NRI-TL metamaterial leaky-wave antenna radiating at broadside with zero beam-squinting", *IEEE Antennas Wireless Propag. Lett.,* vol. 17, no. 12, pp. 2223-2227, Dec. 2018.

[169] L. Wang, J. L. Gómez-Tornero and O. Quevedo-Teruel, "Substrate integrated waveguide leaky-wave antenna with wide bandwidth via prism coupling", *IEEE Trans. Microw. Theory Techn.*, vol. 66, no. 6, pp. 3110-3118, Jun. 2018.

[170] O. Zetterstrom, E. Pucci, P. Padilla, L. Wang, and O. Q.-Teruel, “Low-dispersive leaky-wave antennas for mmWave point-to-point high-throughout communications,” *IEEE Trans. Antennas Propag*, vol. 68, no. 3, pp. 1322-1331, Mar. 2020

[171] J. Chen, W. Yuan, C. Zhang, W. X. Tang, L. Wang, Q. Cheng, T. J. Cui, “Wideband leaky-wave antennas loaded with gradient metasurface for fixed-beam radiations with customized tilting angles”, *IEEE Trans. Antennas Propag*, vol. 68, no. 1, pp. 161-170, 2020.

[172] Q. Chen, O. Zetterstrom, E. Pucci, A. P.-Caballero, P. Padilla, O. Q.-Teruel, “Glide-symmetric holey leaky-wave antenna with low dispersion for 60 GHz point-to-point communications”, *IEEE Trans. Antennas Propag*, vol. 68, no. 3, pp. 1925-1936, 2020.

[173] R.-T. Hong, J. Shi, D.-F. Guan, X. Huang, W. Cao, Z.-P. Qian, “Air-filled substrate integrated waveguide leaky-wave antenna with wideband and fixed-beam characteristics”, *IEEE Trans. Antennas Propag*, vol. 68, no. 10, pp. 7184-7189, 2020.

[174] F. Yang, and Y. R.-Samii, *Electromagnetic Band Gap Structures in Antenna Engineering*, Cambridge University Press, 2009.

[175] H. Paaso, A. Mammela, D. Patron, and K. R. Dandekar, “Modified MUSIC algorithm for DOA estimation using CRLH leaky-wave antennas,” in *8th International Conference on Cognitive Radio Oriented Wireless Networks*, Washington, DC, USA.

[176] H. Paaso, N. Gulati, D. Patron, A. Hakkarainen, J. Werner, K. P. Dandekar, M. Valkama, and A. Mammela, “DoA estimation using compact CRLH leaky-wave antennas: novel algorithms and measured performance,” *IEEE Trans. Antennas Propag*, vol. 65, no. 9, pp. 4836-4849, Sept. 2017.

[177] D. Patron, H. Paaso, A. Mammela, D. Piazza, and K. R. Dandekar, “Improved design of a CRLH leaky-wave antenna and its application for DOA estimation,” in *2013 IEEE-APS Topical Conference on Antennas and Propagation in Wireless Communications (APWC)*, Turin, Italy.

[178] B. Husain, M. Steeg, and A. Stohr, “Estimating direction-of-arrival in a 5G hot-spot scenario using a 60 GHz leaky-wave antenna,” in 2017 *IEEE International Conference on Microwaves, Antennas, Communications and Electronic Systems (COMCAS)*, Tel-Aviv, Israel.

[179] X. Yu, and H. Xin, “Direction of arrival estimation utilizing incident angle dependent spectra,”

[180] C.-T. M. Wu, “A real-time multiple target detecting scheme based on microwave metamaterials,” in *IEEE European Microwave Conference (EuMC)*, Pairs, France, 2015.

[181] S. Abielmona, H. V. Nguyen, and C. Caloz, “Analog direction of arrival estimation using an electronically-scanned CRLH leaky-wave antenna,” *IEEE Trans. Antennas Propag*, vol. 59, no. 4, pp. 1408-1412, Apr. 2011.

[182] M. K. Emara, D. J. King, H. V. Nguyen, S. Abielmona, and S. Gupta, “Millimeter-wave slot array antenna front-end for amplitude-only direction finding,” *IEEE Trans. Antennas Propag*, vol. 68, no. 7, pp. 5365-5374, Jul. 2020.

[183] M. P.-Garcia, D. C.-Rebenaque, and J. L. G.-Tornero, “Frequency-scanned monopulse pattern synthesis using leaky-wave antennas for enhanced power-based direction-of-arrival estimation,” *IEEE Trans. Antennas Propag*, vol. 67, no. 11, pp. 7071-7086, Nov. 2019.

[184] S. Gupta, S. Abielmona, and C. Caloz, “Microwave analog real-time spectrum analyzer (RTSA) based on the spectral-spatial decomposition property of leaky-wave structures,” *IEEE Trans. Microw. Theory Techn.*, vol. 57, no. 12, pp. 2989-2999, Dec. 2009.

[185] D. J. King, M. K. Emara, and S. Gupta, “Millimeter-wave integrated side-fire leaky-wave antenna and its application as a spectrum analyzer,” *IEEE Trans. Antennas Propag*, vol. 69, no. 9, pp. 5401-5412, Sep. 2021.

[186] M. K. Emara, and S. Gupta, “Multi-port leaky-wave antennas as real-time analog spectral decomposers,” in 2020 *14th European Conference on Antennas and Propagation (EuCAP)*, Copenhagen, Denmark.

[187] S. Gupta, H. V. Nguyen, T. Kodera, S. Abielmona, and C. Caloz, “CRLH leaky-wave antenna based frequency division duplexing transceiver yes,” in 2009 *Asia Pacific Microwave Conference*, Singapore.

[188] T. Kodera, and C. Caloz, “Integrated leaky-wave antenna-duplexer/diplexer using CRLH uniform ferrite-loaded open waveguide,” *IEEE Trans. Antennas Propag*, vol. 58, no. 8, pp. 2508-2514, Aug. 2010.

[189] N. J. Karl, R. W. Mckinney, Y. Monnai, R. Mendis, and D. M. Mittleman, “Frequency-division multiplexing in the terahertz range using a leaky-wave antenna,” *Nature Photon* 9, 717–720 (2015).

[190] J. Ma, N. J. Karl, S. Bretin, G. Ducournau, and D. M. Mittleman, “Frequency-division multiplexer and demultiplexer for terahertz wireless links,” *Nat Commun* 8, 729 (2017).

[191] M. K. Emara, and S. Gupta, “Integrated multi-port leaky-wave antenna multiplexer/demultiplexer system for millimeter-wave communication,” *IEEE Trans. Antennas Propag*, vol. 69, no. 9, pp. 5244-5256, Sep. 2021.

[192] K.-L. Chan and S. R. Judah, “A beam-scanning frequency modulated continuous wave radar,” *IEEE Trans. Instrum. Meas*., vol. 47, no. 5, pp. 1223–1227, Oct. 1998.

[193] A. Hommes, A. Shoykhetbrod, and N. Pohl, “A fast tracking 60 GHz radar using a frequency scanning antenna,” in Proc. 39th *Int. Conf. Infr., Millim., THz. Waves (IRMMW-THz)*, 2014, pp. 1–2.

[194] A. Shoykhetbrod, T. Geibig, A. Hommes, R. Herschel, and N. Pohl, “Concept for a fast tracking 60 GHz 3D-radar using frequency scanning antennas,” in 41st *International Conference on Infrared, Millimeter, and Terahertz waves (IRMMW-THz)*, 2016.

[195] M. Steeg, A. A. Assad, and A. Stöhr, "Simultaneous DoA estimation and ranging of multiple objects using an FMCW radar with 60 GHz leaky-wave antennas", in 43rd *International Conference on Infrared, Millimeter, and Terahertz waves (IRMMW-THz)*, 2018.

[196] H. Matsumoto, I. Watanabe, A. Kasamatsu, and Y. Monnai, “Integrated terahertz radar based on leaky-wave coherence tomography,” *Nat. Electron.* 3, 122–129 (2020).

[197] Z. Sun, K. Ren, Q. Chen, J. Bai, and Y. Fu, “3D radar imaging based on frequency-scanned antenna,” *IEICE Electronics Express*, vol. 14, no. 12, pp. 1-10, 2017.

[198] K. Murano, I. Watanabe, A. Kasamatsu, S. Suzuki, M. Asada, W. Withayachumnankul, T. Tanaka, and Y. Monnai, “Low-profile terahertz radar based on broadband leaky-wave beam steering,” *IEEE Trans. THz Sci. Technol.*, vol. 7, no. 1, pp. 60– 69, Jan. 2017.

[199] Y. Alvarez et al, “Submillimeter-wave frequency scanning system for imaging applications,” *IEEE Trans. Antennas Propag*, vol. 61, no. 11, pp. 5689-5696, Nov. 2013.

[200] S. Li, C. Li, W. Liu, Z. Sun, S. Lang, Z. Lu, X. Zhang, and G. Fang, "Study of terahertz superresolution imaging scheme with real-time capability based on frequency scanning antenna," *IEEE Trans. THz Sci. Technol.,* vol. 6, no. 3, pp. 451– 463, May. 2016.

[201] Y. Amarasinghe, R. Mendis, and D. M. Mittleman, "Real-time object tracking using a leaky THz waveguide," *Opt. Express*, vol. 28, no. 12, pp. 17997-18005, 2020.

[202] K. Murata et al, "See-through detection and 3D reconstruction using terahertz leaky-wave radar based on sparse signal processing," *J. Infrared Milli. THz Waves*, vol. 39, pp. 210-221, 2018.

[203] Y. Yuan, C. Lu, A. Y.-K. Chan, C.-H. Tseng, and C.-T. M. Wu, "Multi-target concurrent vital sign and location detection using metamaterial-integrated self-injection-locked quadrature radar sensor," *IEEE Trans. Microw. Theory Techn.*, vol. 67, no. 12, pp. 5429-5437, Dec. 2019.

[204] C. Lu, Y. Yuan, C.-H. Tseng, and C.-T. M. Wu, "Multi-target continuous-wave vital sign radar using 24 GHz metamaterial leaky-wave antennas," in 2019 *IEEE MTT-S International Microwave Biomedical Conference (IMBioC)*, Nanjing, China.

[205] J. L. Gómez-Tornero, A. T. Martínez, D. C. Rebenaque, M. Gugliemi, and A. Álvarez-Melcón, "Design of tapered leaky-wave antennas in hybrid waveguide-planar technology for millimeter waveband applications," *IEEE Trans. Antennas Propag*., vol. 53, no. 8, pp. 2563-2577, Aug. 2005.

[206] J. L. Gómez-Tornero, G. Goussetis, A. P. Feresidis, and A. Á. Melcón, "Control of leaky-mode propagation and radiation properties in hybrid dielectric-waveguide printed-circuit technology: Experimental results," *IEEE Trans. Antennas Propag.*, vol. 54, no. 11, pp. 3383-3390, Nov. 2006.

[207] P. Wu, J. Liu, and Q. Xue, "Wideband excitation technology of TE20 mode substrate integrated waveguide (SIW) and its applications," *IEEE Trans. Microw. Theory Techn*., vol. 63, no. 6, pp. 1863-1874, Jun. 2015.

[208] P. Wu, S. Liao, and Q. Xue, "Wideband excitations of higher-order mode substrate integrated waveguide and their applications to antenna array design," *IEEE Trans. Antennas Propag*., vol. 65, no. 8, pp. 4038-4047, Aug. 2017.

[209] Y. J. Chen, W. Hong, and K. Wu, "Design of a monopulse antenna using a dual V-type linearly tapered slot antenna (DVLTSA)," *IEEE Trans. Antennas Propag*., vol. 56, no. 9, pp. 2903-2909, Sep. 2008.

[210] F. Xu and K. Wu, "Understanding leaky-wave structure—A special form of guided-wave structures," *IEEE Microw. Mag*., vol. 14, no. 5, pp. 87–96, Jul./Aug. 2013.

[211] W. Menzel and A. Moebius, "Antenna concepts for millimeter-wave automotive radar sensors," *Proc. IEEE*, vol. 100, no. 7, pp. 2372–2379, Jul. 2012.

[212] B.-H. Ku et al., "A 77–81 GHz 16-element phased-array receiver with ±50◦ beam-scanning for advanced automotive radars," *IEEE Trans. Microw. Theory Techn*., vol. 62, no. 11, pp. 2823–2832, Nov. 2014.

[213] J. Xu, Z. N. Chen, and X. Qing, "CPW center-fed single-layer SIW slot antenna array for automotive radars," *IEEE Trans. Antennas Propag*., vol. 62, no. 9, pp. 4528–4536, Sep. 2014.

[214] J. Xu, W. Hong, H. Zhang, G. Wang, Y. Yu, and Z. H. Jiang, "An array antenna for both long- and medium-range 77 GHz automotive radar applications," *IEEE Trans. Antennas Propag*., vol. 65, no. 12, pp. 7207–7216, Dec. 2017.

[215] F. Parment, A. Ghiotto, T.-P. Vuong, J.-M. Duchamp, and K. Wu, "Air-filled substrate integrated waveguide for low-loss and high powerhandling millimeter-wave substrate integrated circuits," *IEEE Trans. Microw. Theory Techn*., vol. 63, no. 4, pp. 1228–1238, Apr. 2015.

[216] J. Liu, Q. Xue, H. Wong, H. W. Lai, and Y. Long, "Design and analysis of a low-profile and broadband microstrip monopolar patch antenna," *IEEE Trans. Antennas Propag*., vol. 61, no. 1, pp. 11–18, Jan. 2013.

[217] Y.-J. Chen and R.-B. Wu, "A wide-band multiport planar power-divider design using matched sectorial components in radial arrangement," *IEEE Trans. Microw. Theory Techn*., vol. 46, no. 8, pp. 1072–1078, 1998.

[218] F.-R, Yang, Y. Qian, R. Coccioli, and T. Itoh, "A novel low-loss slow-wave microstrip structure," *IEEE Microwave Guided Wave Lett*., vol. 8, no. 11, pp. 372–374, Nov. 1998.

[219] C.-K. Wu, H.-S. Wu, and C.-K. C. Tzuang, "Electric-magnetic-electric slow-wave microstrip line and bandpass filter of compressed size," *IEEE Trans. Microwave Theory Tech*., vol. 50, no. 8, pp. 1996–2004, Aug. 2003.

[220] H. Jin, K. Wang, J. Guo, S. Ding, and K. Wu, "Slow-wave effect of substrate integrated waveguide patterned with microstrip polyline," *IEEE Trans. Microw. Theory Techn*., vol. 64, no. 6, pp. 1717–1726, Jun. 2016.

[221] I. Rumsey, M. P.-May, and P. K. Kelly, “Photonic bandgap structures used as filters in microstrip circuits,” *IEEE Microwave Guided Wave Lett*., vol. 8, no. 10, pp. 336–338, Oct. 1998.

[222] V. Radisic, Y. Qian, R. Coccioli, and T. Itoh, “Novel 2-D photonic bandgap structure for microstrip lines,” *IEEE Microwave Guided Wave Lett*., vol. 8, no. 2, pp. 69–71, Feb. 1998.

[223] N. C. Karmakar, and M. N. Mollah, “Investigations into nonuniform photonic-bandgap microstripline low-pass filters,” *IEEE Trans. Microwave Theory Tech*., vol. 51, no. 2, pp. 564–572, Feb. 2003.

[224] S.-G. Mao, and M.-Y. Chen, “Propagation characteristics of finite-width conductor-backed coplanar waveguides with periodic electromagnetics bandgap cells,” *IEEE Trans. Microwave Theory Tech*., vol. 50, no. 11, pp. 2624–2628, Nov. 2002.

[225] L. Zhu, “Guided-wave characteristics of periodic coplanar waveguides with inductive loading—unit-length transmission parameters,” *IEEE Trans. Microwave Theory Tech*., vol. 51, no. 10, pp. 2133–2138, Oct. 2003.

[226] T.-Y. Yun and K. Chang, “Uniplanar one-dimensional photonic-bandgap structures and resonators,” *IEEE Trans. Microwave Theory Tech*., vol. 49, no.3, pp. 549–553, Mar. 2001.

[227] Y. L. Zhang, W. Hong, K. Wu, J. X. Chen, and H. J. Tang, “Novel substrate integrated waveguide cavity filter with defected ground structure,” *IEEE Trans. Microwave Theory Tech.*, vol. 53, no. 4, pp. 1280–1287, Apr. 2005.

[228] Z.-C. Hao, W. Hong, J.-X. Chen, X.-P. Chen, and K. Wu, “Compact super-wide bandpass substrate integrated waveguide (SIW) filters,” *IEEE Trans. Microwave Theory Tech*., vol. 53, no. 9, pp. 2968–2977, Sep. 2005.

[229] D. Deslandes and K. Wu, “Single-substrate integration techniques of planar circuit and waveguide filters,” *IEEE Trans. Microwave Theory Tech*., vol. 51, no. 2, pp. 593–596, Feb. 2003.

[230] F. Parment, A. Ghiotto, T.-P. Vuong, J.-Marc, and K. Wu, “Low-loss air-filled substrate integrated waveguide (SIW) bandpass filter with inductive posts,” in 45th *IEEE European Microwave Conference (EuMC)*, Paris, France, Sep. 2019.

[231] C.-K. Lin and S.-J. Chung, “Synthesis and design of a new printed filtering antenna,” *IEEE Trans. Microwave Theory Tech*., vol. 59, no. 11, pp. 1036–1042, Mar. 2011.

[232] H. Chu, J.-X. Chen, S. Luo, and Y.-X. Guo, “A millimeter-wave filtering monopulse antenna array based on substrate integrated waveguide technology,” *IEEE Trans. Antennas Propag*., vol. 64, no. 1, pp. 316-312, Jan. 2016.

[233] Y. Zhang, X. Y. Zhang, L. H. Ye, and Y. M. Pan, “Dual-band base station array using filtering antenna elements for mutual coupling suppression,” *IEEE Trans. Antennas Propag*., vol. 64, no. 8, pp. 3423–3430, Aug. 2016.

[234] C.-X. Mao, S. Gao, Y. Wang, F. Qin, and Q.-X. Chu, “Multimode resonator-fed dual-polarized antenna array with enhanced bandwidth and selectivity,” *IEEE Trans. Antennas Propag.*, vol. 63, no. 12, pp. 5492–5499, Dec. 2015.

[235] F.-C. Chen, J.-F. Chen, Q.-X. Chu, and M. J. Lancaster, “X-band waveguide filtering antenna array with nonuniform feed structure,” *IEEE Trans. Antennas Propag*., vol. 65, no. 12, pp. 4843–4850, Dec. 2017.

[236] F. Queudet, B. Froppier, Y. Mahe, and S. Toutain, “Study of a leaky waveguide for the design of a filtering antennas,” in 33rd *IEEE European Microwave Conference (EuMC)*, Munich, Germany, Oct. 2003.

[237] M. H. Rahmani and Dominic Deslandes, “Circularly polarized periodic leaky-wave antenna with filtering capability,” *IET Microw. Antennas Propag*.,vol. 12, no. 11, pp. 1811-1815, May. 2018.

[238] J. S. Hong and M. J. Lancaster, *Microstrip Filters for RF/Microwave Applications*. New York: Wiley, 2001.

[239] N. Marcuvitz, Waveguide Handbook, ser. MIT Rad. Lab.. New York: McGraw-Hill, 1951.

[240] T. Zhao, D. R. Jackson, J. T. Williams, H.-Y. D. Yang, and A. Oliner, “2-D periodic leaky-wave antennas—part I: metal patch design,” *IEEE Trans. Antennas Propag*., vol. 53, no. 11, pp. 3505–3514, Nov. 2005.

[241] T. Zhao, D. R. Jackson, and J. T. Williams, “2-D periodic leaky-wave antennas—part II: slot design,” *IEEE Trans. Antennas Propag*., vol. 53, no. 11, pp. 3515–3524, Nov. 2005.

[242] T. Zhao, D. R. Jackson, and J. T. Williams, “General formulas for 2D leaky wave antennas,” *IEEE Trans. Antennas Propag*., vol. 53, no. 11, pp. 3525–3533, Nov. 2005.

[243] C. Mateo-Segura, G. Goussetis, and A. P. Feresidis, “Sub-wavelength profile 2-D leaky-wave antennas with two periodic layers”, *IEEE Trans. Antennas Propag*., vol. 59, pp.416- 424, Feb. 2011.

[244] C. Mateo-Segura, A. P. Feresidis, and G. Goussetis, "Broadband leaky-wave antennas with double-layer PRS: analysis and design," in *5th Proc. EuCAP*, pp. 2102-2105, Apr. 2011.

[245] C. Mateo-Segura, A. P. Feresidis, and G. Goussetis, "Bandwidth enhancement of 2-D leaky-wave antennas with double-layer periodic surfaces," *IEEE Trans. Antennas Propag*., vol. 62, no. 2, pp.586- 593, Feb. 2014.

[246] D. Zheng and Q.-X. Chu, "A multimode wideband ±45º dual-polarized antenna with embedded loops," *IEEE Antennas and Wireless Propag. Lett*., vol. 16, pp. 633-636, 2017.

[247] D. Zheng and Q.-X. Chu, "A wideband dual-polarized antenna with two independently controllable resonant modes and its array for base-station applications*," IEEE Antennas and Wireless Propag. Lett*., vol. 16, pp. 2014-2017, 2017.

[248] N.-W. Liu, L. Zhu, W.-W. Choi, and X. Zhang, "A low-profile aperture-coupled microstrip antenna with enhanced bandwidth under dual resonance," *IEEE Trans. Antennas Propag*., vol. 65, no. 3, pp. 1055-1062, Mar. 2017.

[249] W. C. Mok, S. H. Wong, K. M. Luk, and K. F. Lee, "Single-layer single-patch dual-band and triple-band patch antennas," *IEEE Trans. Antennas Propag*., vol. 61, no. 8, pp. 4341-4344, Aug. 2013.

[250] S. X. Ta, H. Choo, I. Park, and R. W. Ziolkowski, "Multi-band, wide-beam, circularly polarized, crossed, asymmetric barbed dipole antennas for GPS applications," *IEEE Trans. Antennas Propag*., vol. 61, no. 11, pp. 5771-5775, Nov. 2013.

[251] A. A. Deshmukh, and K. P. Ray, "Multi-band configurations of stub-loaded slotted rectangular microstrip antennas," *IEEE Antennas Propag. Magazine*, vol. 52, no. 1, pp. 89-103, Feb. 2010.

[252] L. Zhu, S. Sun, and W. Menzel, "Ultra-wideband (UWB) bandpass filters using multiple-mode resonator," *IEEE Microw. Wireless Compon. Lett*., vol. 15, no. 11, pp. 796-798, 2005.

[253] H. Wang, Q.-X. Chu, and J.-Q. Gong, "A compact wideband microstrip filter using folded multiple-mode resonator," *IEEE Microw. Wireless Compon. Lett*., vol. 15, no. 11, pp. 796-798, 2005.

[254] X.-P. Chen, K. Wu, and Z.-L. Li, "Dual-band and triple-band substrate integrated waveguide filters with chebyshev and quasi-elliptic responses," *IEEE Trans. Microw. Theory Techn*., vol. 55, no. 12, pp. 2569-2578, Dec. 2007.

[255] H.-W. Wu, and R.-Y. Yang, "A new quad-band bandpass filter using asymmetric stepped impedance resonators," *IEEE Microw. Wireless Compon. Lett*., vol. 21, no. 4, pp. 203-205, Apr. 2011.

[256] K. M. Luk, and H. Wong, "A new wideband unidirectional antenna element." *Int. J. Microw. Opt. Technol*., vol. 1, no. 1, pp. 35-44, Jun. 2006.

[257] K. M. Luk and B. Q. Wu, "The magnetoelectric dipole—a wideband antenna for base stations in mobile communications," *Proc. IEEE*, vol. 100, no. 7, pp. 2297-2307, Jul. 2012.

[258] S. D. Targonski, R. B. Waterhouse, and D. M. Pozar, "Design of wide-band aperture-stacked patch microstrip antennas," *IEEE Trans. Antennas Propag*., vol. 46, no. 9, pp. 1245-1251, Sep. 1998.

[259] R. Garg, P. Bhartia, I. Bahl, and A. Ittipiboon, *Microstrip Antenna Design Handbook*, Artech House, 2001.

[260] J. R. James and A. Henderson, "A critical review of millimeter planar arrays for military applications," *Military Microwaves Conf*., London, England, October 20–22, 1982.

[261] L. Chettri, and R. Bera, 'A comprehensive survey on Internet of Things (IoT) toward 5G wireless systems,' *IEEE Internet of Things Journal*, vol. 7, no. 1, pp. 16-32, Jan. 2020.

[262] R. Lu, L. Zhang, J. Ni, and Y. Fang, "5G vehicle-to-everything services: gearing up for security and privacy," *Proc. IEEE*, vol. 108, no. 2, pp. 378-389, Feb. 2020.

[263] H. Zhou, W. Xu, J. Chen, and W. Wang, "Evolutionary V2X technologies toward the internet of vehicles: challenges and opportunities," *Proc. IEEE*, vol. 108, no. 2, pp. 308-323, Feb. 2020.

[264] W. M. A.-Wahab, and S. S.-Naeini, "Wide-bandwidth 60-GHz aperture-coupled microstrip patch antennas (MPAs) fed by substrate integrated waveguide (SIW)," *IEEE Antennas and Wireless Propag. Lett.*, vol. 10, pp. 1003-1005, 2011.

[265] A. Karar et al, "Broadbanding of substrate integrated waveguide based slotted array antenna using dual slot configuration," in 4th *International Conference on Opto-Electrics and Applied Optics*, 2017.

[266] Q. Liao, and L. Wang, "Switchable bidirectional/unidirectional LWA array based on half-mode substrate integrated waveguide," *IEEE Antennas and Wireless Propag. Lett*., vol. 19, no. 7, pp. 1261-1265, Jul. 2020.

[267] W.-J. Lu and L. Zhu, "Wideband stub-loaded slotline antennas under multi-mode resonance operation," *IEEE Trans. Antennas Propag*., vol. 63, no. 2, pp. 818-828, Feb. 2015.

[268] X. Y. Zhang, J.-X. Chen, Q. Xue, and S.-M. Li, "Dual-band bandpass filters using stub-loaded resonators," *IEEE Microw. Wireless Compon. Lett*., vol. 17, no. 8, pp. 583-585, Aug. 2007.

[269] H. L. V. Trees, *Optimum Array Processing: Part IV of Detection, Estimation, and Modulation Theory*, New York, NY, USA: John Wiley & Sons, 2002.

[270] A. W. Rudge, "Multiple-beam antennas: offset reflectors with offset feeds," *IEEE Trans. Antennas Propag*., vol. 23, no. 3, pp. 317–322, May 1975.

[271] K. S. Rao, G. A. Morin, M. Q. Tang, S. Richard, and K. K. Chan, "Development of a 45 GHz multiple-beam antenna for military satellite communications," *IEEE Trans. Antennas Propag*., vol. 43, no. 10, pp. 1036–1047, Oct. 1995.

[272] T. P. Nguyen, C. Pichot, C. Migliaccio, and W. Menzel, "Study of folded reflector multibeam antenna with dielectric rods as primary source," *IEEE Antennas Propag. Lett*., vol. 8, pp. 786–789, Jul. 2009.

[273] Z. H. Jiang, M. D. Gregory, and D. H. Werner, "Broadband high directivity multibeam emission through transformation optics-enabled metamaterial lenses," *IEEE Trans. Antennas Propag*., vol. 60, no. 11, pp. 5063–5074, Nov. 2012.

[274] C. Metz et al., "Fully integrated automotive radar sensor with versatile resolution," *IEEE Trans. Microw. Theory Techn*., vol. 49, no. 12, pp. 2560–2566, Dec. 2001.

[275] Y. J. Cheng et al., "Substrate integrated waveguide (SIW) Rotman lens and its Ka-band multibeam array antenna applications," *IEEE Trans. Antennas Propag*., vol. 56, no. 8, pp. 2504–2513, Aug. 2008.

[276] P. Chen et al., "A multibeam antenna based on substrate integrated waveguide technology for MIMO wireless communications," *IEEE Trans. Antennas Propag*., vol. 57, no. 6, pp. 1813–1821, Jun. 2009.

[277] R. J. Mailloux, *Phased Array Antenna Handbook*, 3rd ed., Norwood, MA: Artech House, 2018.

[278] J. Hirokawa and M. Ando, "Single-layer feed waveguide consisting of posts for plane TEM wave excitation in parallel plates," *IEEE Trans. Antennas Propag*., vol. 46, no. 5, pp. 625–630, May. 1998.

[279] L. Yan, W. Hong, G. Hua, J. Chen, K. Wu, and T. J. Cui, "Simulation and experiment on SIW slot array antennas," *IEEE Microw. Wireless Compon. Lett*., vol. 14, no. 9, pp. 446–448, Sept. 2004.

[280] S. Sugawa, K. Sakakibara, N. Kikuma, and H. Hirayama, “Low-sidelobe design of microstrip comb-line antenna using stub-integrated radiating elements in the millimeter-wave band,” *IEEE Trans. Antennas Propag*., vol. 60, no. 10, pp. 4699-4709, Oct. 2012.

[281] F. Schwering and S. T. Peng, “Design of dielectric grating antennas for millimeter wave applications,” *IEEE Trans. Microw. Theory Techn*., vol. 31, no. 2, pp. 199–209, Feb. 1983.

[282] F. J. Harris, *Multirate Signal Processing for Communication Systems*, Upper Saddle River, NJ, USA: Prentice Hall PTR, 2004.

[283] M. Jankiraman, *FMCW Radar Design*, Norwood, MA, USA: Artech House, 2018.

[284] https://www.ti.com/sensors/mmwave-radar/automotive/products.html

[285] S. Chen, B. Liu, C. Feng, C. V.-Gonzalez, and C. Wellington, “3D point cloud processing and learning for automotive driving: impacting map creation, localization, and perception,” *IEEE Signal Processing Magaz*., vol. 38, no. 1, pp. 68-86, Jan. 2021.

APPENDIX A LIST OF PUBLICATIONS

Published journal papers:

[J1] **D. Zheng**, and K. Wu, "Multifunctional leaky-wave antenna with tailored radiation and filtering characteristics based on flexible mode-control principle", *IEEE Open Journal of Antennas Propaga.*, vol. 2, pp. 858-869, 2021.

[J2] **D. Zheng**, and K. Wu, "Multifunctional filtering leaky-wave antenna exhibiting simultaneous rapid beam-scanning and frequency-selective characteristics based on radiative bandpass filter concept", *IEEE Antennas Propaga.*, vol. 68, no. 8, pp. 5842-5854, Aug. 2020.

[J3] **D. Zheng**, Y.-L. Lyu, and K. Wu, "Transversely slotted SIW leaky-wave antenna featuring rapid beam-scanning for millimeter-wave applications", *IEEE Antennas Propaga.*, vol. 68, no. 6, pp. 4172-4185, Jun. 2020.

[J4] **D. Zheng**, and K. Wu, "Leaky-wave antenna featuring stable radiation based on multimode resonator (MMR) concept," *IEEE Trans. Antennas Propag.*, vol. 68, no. 3, pp. 2016-2030, Mar. 2020.

[J5] **D. Zheng**, Y.-L. Lyu, and K. Wu, "Longitudinally slotted SIW leaky-wave antenna for low-cross polarization millimeter-wave applications," *IEEE Trans. Antennas Propag.*, vol. 68, no. 2, pp. 656-664, Feb. 2020.

Journal papers to be submitted:

[J6] **D. Zheng**, and K. Wu, "Filter-Bank-enabled leaky-wave antenna array technique for radar applications in stitched frequency-space domain", *IEEE Trans. Antennas Propag.*

Conference papers:

[C1] **D. Zheng**, and K. Wu, "Generalized design considerations of leaky-wave antennas based on multi-mode resonator (MMR) concept", in *IEEE Antennas and Propagation Society International Symposium (APS/URSI)*, Singapore, 2021.

[C2] **D. Zheng**, and K. Wu, "Substrate integrated waveguide leaky-wave antennas with tailored characteristics for millimeter-wave applications", in *IEEE 50th European Microwave Conference (EuMC)*, Utrecht, Netherlands, 2021.

[C3] **D. Zheng**, and K. Wu, "Filtering leaky-wave antennas: composition principles, design considerations, and multifunction characteristics", in *IEEE Antennas and Propagation Society International Symposium (APS/URSI)*, Montreal, Canada, 2020.

[C4] **D. Zheng**, and K. Wu, "Radiating discontinuity in leaky-wave antenna: a role in complex propagation constant engineering", in *IEEE Antennas and Propagation Society International Symposium (APS/URSI)*, Montreal, Canada, 2020.

[C5] **D. Zheng**, Y.-L. Lyu, and K. Wu, "A quasi-uniform transversely slotted SIW leaky-wave structure with enhanced beam-scanning rate for millimeter-wave applications", in *IEEE MTT-S International Microwave Symposium (IMS)*, Boston, USA, 2019.

Patents:

[P1] **D. Zheng** and K. Wu, "Filter-bank-enabled leaky-wave antenna array technique for radar sensing systems in stitched frequency-space domain", US patent in processing